THE EFFECT OF DIET ON THE CELLULAR RESPONSE TO A SMALL FOCAL ISCHEMIC STROKE

by © Kathleen E. Fifield

A thesis submitted to the
School of Graduate Studies in partial fulfillment of the
requirements for the degree of
Doctor of Philosophy

Division of Biomedical Sciences, Faculty of Medicine
Memorial University of Newfoundland

October 2021
St. John's Newfoundland and Labrador

ABSTRACT

Overwhelming evidence demonstrates that diet-induced obesity increases the risk of ischemic stroke. Furthermore, obesity is associated with worse neurological outcomes following overt ischemic strokes. The majority of strokes seen clinically; however, are covert, small strokes that often evade detection. How obesity impacts the cellular response to covert strokes is unclear. Furthermore, whether obesity alters the cellular response within the infarct core or penumbra is not known. To address these issues, I developed a mouse model of diet-induced obesity by feeding mice a high fat diet (HFD) for twelve weeks. Intra-cortical injections of Endothelin-1, a vasoconstrictor was used to induce a focal ischemic stroke that is representative of covert strokes observed in the clinic. To distinguish the ischemic core from the penumbra, an intra-cardiac injection of a dextran-linked fluorochrome was given at the time of euthanasia to label perfused blood vessels. Quantification of the number of labelled blood vessels per area allowed post mortem distinction of the infarct core from the penumbra in brain sections. Using this technique the cellular responses were examined in each region following stroke. The results show that: (1) prolonged high fat diet worsens stroke outcomes following small covert strokes; (2) cellular responses within the core and penumbra are distinct with the majority of neurons dying in the core by 4 hours. Neurons in the penumbra can survive up to 72 hours post-stroke despite extensive blood brain barrier (BBB) breakdown, leukocyte infiltration and astrogliosis; (3) acute administration of docosahexanoic acid (DHA) post-stroke ameliorates BBB disruption at 24 hours post-stroke in both diet groups, but its efficacy is attenuated in high-fat diet fed mice. In summary, diet-induced obesity exacerbates covert-like stroke injuries by worsening the cellular responses in the varying

levels of perfusion across the infarct, while DHA may be a viable treatment for covert strokes.

GENERAL SUMMARY

Ischemic stroke is a vascular disease with diet-induced obesity being a major risk factor. Covert strokes are small focal strokes that produce subtle deficits and are more common than overt strokes. However, the effect of high fat diet (HFD) on brain tissue after these small focal strokes occurs is not well known. This thesis examines what happens to different cells within the brain following high fat diet in small strokes that mimic covert stroke. Stroke induces death of brain tissue where blood flow is interrupted, termed the ischemic core. Surrounding this core is the penumbra, where most brain cells are still alive but are vulnerable to further damage. To determine the effect of a high fat diet on stroke, brain cells within the ischemic core and penumbra were examined in mice following a 12-week high fat diet feeding regimen. The damage to brain cells was also examined at intervals throughout the acute 24 hours following stroke to determine which brain cells were affected and the timeline of their injury. Finally, DHA, an omega-3 fatty acid was injected following stroke to determine whether it was neuroprotective. The results show that: (1) prolonged high fat diet causes worse outcomes after stroke resulting in more inflammation and larger strokes, (2) the cellular responses within the core and penumbra are distinct and differentially affect neuron survival (3) administration of DHA reduces BBB breakdown; however, this effect is reduced with HFD. We show that high fat diets can worsen responses within the ischemic brain. Furthermore, DHA treatment can potentially ameliorate stroke damage when given at early time points post-stroke. Taken together, this thesis demonstrates the impact of prolonged high fat diet on small strokes that mimic covert stroke.

ACKNOWLEDGMENTS

I would like to acknowledge my supervisor Dr. Jacqueline Vanderluit for her support and mentorship throughout the PhD program. Her guidance has created the confidence within me to pursue my goals and future endeavours. I would like to thank my supervisory committee Dr. Michiru Hirasawa and Dr. Xihua Chen for their support and supervision in completion of my graduate work. A special thank you to Dr. Craig Moore and Dr. Matt Parsons for their aid and direction. I would like to acknowledge both past and present lab members of the Vanderluit lab: Robert Flemmer, Joanna Raman-Nair, Brittany Geizer, Brian Roome, Lauren Fogarty and Robert Bartlett. I would like to acknowledge Todd Rowe, Lisa Fang and Dylan Galloway for their help with experiments. A special thank you to Samantha Carew, Abhinaba Ghosh, Bandhan Mukherjee and Victoria Linehan for their support and friendship. I would like to acknowledge my financial support: NSERC, CIHR, the Keith Griffiths family (Keith Griffiths Memorial Heart and Stroke Foundation Graduate Scholarship), the Colman family (Colman award) and Dean M. Ian Bowmer (Graduate Travel Award). I would like to thank Research and Graduate Studies, in particular Amy Carroll and Rhonda Roebotham, and the Academic graduate studies assistant Deborah Parrot. Finally, I would like to acknowledge my family, Heather and Randy Benoit and Amanda Fifield for their unwavering support and guidance and my partner Stephen Murphy for his encouragement throughout the years.

This thesis is dedicated to my beloved father Peter Fifield who passed from cardiovascular disease in 2017. I know he is proud of his daughter.

Table of Contents

ABSTRACT....2

GENERAL SUMMARY....4

ACKNOWLEDGMENTS....5

LIST OF TABLES....13

LIST OF FIGURES....14

LIST OF ABBREVIATIONS....16

LIST OF APPENDENCIES....24

CHAPTER 1

INTRODUCTION AND OVERVIEW....25

1.1 Overview....26

1.1.1 Incidence and Risk Factors of Stroke....26

1.1.2 Classification of Stroke....27

1.1.3 Clinical Progression of Ischemic Stroke from Acute to Chronic....31

1.2 The Neurovascular Unit: Maintaining Homeostasis within the Brain....37

1.2.1 Cell types that comprise the neurovascular unit and their function....37

1.2.2 Blood brain barrier: protection of the central nervous system....40

1.3 Cascade of cellular events following ischemic stroke....43

1.3.1 Progression of Cellular Events within Minutes to Hours following Acute Ischemic Stroke....45

1.3.2 Cell degeneration and death: necrosis, apoptosis and autophagy....47

1.3.3 Glial response and inflammation....50

1.3.4 Neurogenesis and neural circuit reorganization post-stroke 55

1.4 Animal models of ischemic stroke 56

1.4.1 Current rodent models of stroke 58

1.4.2 Translating to the clinic 62

1.5 Dietary influences on ischemic stroke 63

1.5.1 The good fats versus the bad fats 64

1.5.2 Diet-induced obesity and the effects on the brain 65

1.5.3 Stroke studies examining diet-induced obesity in rodent models 67

1.5.4 The effect of omega-3 following ischemic stroke 69

1.6 Rationale and Hypothesis 70

CHAPTER 2

PROLONGED HIGH FAT DIET WORSENS THE CELLULAR RESPONSE TO A SMALL, COVERT-LIKE ISCHEMIC STROKE 72

CO-AUTHORSHIP STATEMENT 73

2.1 Introduction 74

2.2 Methods 77

2.2.1 Mice 77

2.2.2 In vivo stroke experiments 77

2.2.3 Behavioural testing 79

2.2.4 Tissue processing 80

2.2.5 Cresyl violet staining 81

2.2.6 Infarct volume calculation and targeting the anterior forelimb motor cortex 82
2.2.7 Immunohistochemistry 85
2.2.8 Immunofluorescence with Fluoro-Jade C staining 86
2.2.9 Microscopy, Cell Counts and Densitometry 87
2.2.10 Characterization of Perfusion regions 88
2.2.11 In vitro blood vessel constriction experiment 90
2.2.12 Western blot 91
2.2.12.1 Protein extraction 91
2.2.12.2 Determining protein concentration 91
2.2.12.3 Electrophoresis and western blot procedures 92
2.2.13 Statistical analysis 95
2.3 Results 95
2.3.1 An increase in body mass and adipose tissue is seen following 12 weeks of HFD. 95
2.3.2 Worse stroke outcomes are observed in HFD-fed mice following a focal ischemic stroke. 96
2.3.3 HFD leads to a smaller blood vessel lumen of penetrating arterioles within the cortex. 100
2.3.4 HFD did not increase inflammatory markers within the basilar artery. 103
2.3.5 HFD causes a greater infiltration of macrophages into the infarct. 105
2.3.6 Increased astrogliosis is observed within the cortex of the infarcted hemisphere. 108

2.3.7 Relationship between the perfusion deficit and the infarct. 111

2.3.8 Astrogliosis and neuroinflammation within the infarcted cortex. 114

2.3.9 High-fat diet results in reduced survival of neurons within the hypo-perfused cortex. 117

2.4 Discussion 120

2.4.1 Diet-induced obesity is established after 12 weeks of HFD feeding 121

2.4.2 Prolonged HFD exacerbates small, covert-like strokes 122

2.4.3 HFD causes narrowing of brain arterioles 123

2.4.4 HFD induces a greater inflammatory response following stroke 124

2.4.5 A distinct cellular composition is observed within the perfusion regions 125

2.5 Conclusions 125

CHAPTER 3

RAPID DEGENERATION OF NEURONS IN THE PENUMBRA REGION FOLLOWING A SMALL, FOCAL ISCHEMIC STROKE. 127

CO-AUTHORSHIP STATEMENT 128

3.1 Introduction 129

3.2 Methods 131

3.2.1 Animals 131

3.2.2 Surgical procedures 132

3.2.3 Tissue processing 133

3.2.4 Infarct volume calculation 133

3.2.5 Immunohistochemistry 134

3.2.6 Fluoro-Jade C staining 135
3.2.7 Microscopy, cell counting and densitometry analysis.....136
3.2.8 Characterization of Perfusion Regions.....137
3.2.9 Statistical analysis 140
3.3 Results.....140
3.3.1 Infarct volume is stable in the acute 72 h post-stroke period. 140
3.3.2 Dextran labelling of blood vessels reveals the number of open blood vessels perfusing the brain. 143
3.3.3 Breakdown of the blood brain barrier is observed at 24 h post-stroke. 147
3.3.4 Astrocyte reactivity is significantly elevated by 24 h post-stroke.....150
3.3.5 An increase in microglia/macrophages is observed at 24 h post-stroke with distinct localization within the infarct. 153
3.3.6 The majority of neuronal cell death occurs within the first 4 h post-stroke.....158
3.4 Discussion 166
3.4.1 Extensive BBB breakdown occurs during the acute post-stroke period. 167
3.4.2 Glial activation coincides with BBB breakdown 169
3.4.3 Neuron survival is significantly reduced within 4 hours post-stroke.....170
3.4.4 Surviving neurons undergo extensive degeneration from 4 to 24 hours post-stroke 171
3.5 Conclusions.....175
CHAPTER 4
DOCOSAHEXAENOIC ACID ATTENUATES BLOOD BRAIN BARRIER

DISRUPTION WITHIN THE CORTEX OF LEAN MICE FOLLOWING ACUTE ISCHEMIC STROKE. 177
CO-AUTHORSHIP STATEMENT 178
4.1 Introduction 179
4.2 Methods 182
4.2.1 Experimental design 182
4.2.2 Focal ischemic stroke surgical procedures 183
4.2.3 Tissue processing for histology and immunohistochemistry 184
4.2.4 Cresyl Violet histology 184
4.2.5 Infarct volume and non-perfused region calculation 185
4.2.6 Immunohistochemistry 185
4.2.7 Fluoro Jade C staining 186
4.2.8 Microscopy and cytometric analysis 187
4.2.9 Statistical Analysis 188
4.3 Results 189
4.3.1 A significant increase in weight is observed following 12 weeks of high fat diet feeding. 189
4.3.2 The effect of post-stroke DHA treatment on infarct volume following acute focal ischemic stroke. 190
4.3.3 DHA treatment reduced BBB breakdown however, this effect was reduced with HFD feeding. 192
4.3.4 DHA alters the inflammatory response within the acute ischemic brain. 199

4.3.5 Acute DHA treatment promotes neuron survival within the core but not in the penumbra. 206

4.4 Discussion 210

4.4.1 The effect of HFD and DHA on infarct size at 24 hours post-stroke 210

4.4.2 DHA reduces BBB breakdown at 24 hours post-stroke 212

4.4.3 DHA reduces inflammation within the ischemic brain 213

4.4.4 DHA does not affect the immediate survival of neurons in the penumbra 215

4.5 Conclusions 217

CHAPTER 5

DISCUSSION 218

5.1 The impact of diet on infarct volume 219

5.2 Vascular responses and injury of the BBB 221

5.3 Distinction of the ischemic core from the penumbra 223

5.4 Glial Response and inflammation 224

5.5 Neuronal survival following ischemic stroke 226

5.6 Future directions 228

5.7 Implications of findings 231

5.8 Conclusions 232

References 233

Appendix 284

Animal Ethics Approval Documentation 285

Diet Composition 286

LIST OF TABLES

Table 1.1: Classification of stroke. 30
Table 1.2: Microglia classification.....54
Table 1.3: Ischemic stroke models.....57
Table 2.1: Assessment of open blood vessels across ischemic injury at 7 days post-surgery.....89
Table 2.2: SDS page gel ingredients.....94

LIST OF FIGURES

Figure 1.1: Cerebral blood flow within the core and penumbra following ischemic stroke. 34
Figure 1.2: Cells comprising the Neurovascular Unit. 38
Figure 1.3: Cascade of events following ischemic stroke. 44
Figure 2.1: Mapping to the anterior forelimb motor cortex. 84
Figure 2.2: HFD-fed mice have larger infarct volumes post-stroke. 99
Figure 2.3: HFD results in a smaller blood vessel lumen of penetrating arterioles within the cerebral cortex. 102
Figure 2.4: Inflammatory markers VCAM-1 and COX-2 did not increase significantly within the basilar artery following prolonged HFD. 104
Figure 2.5: HFD increases the macrophage response within the mouse cortex following a focal ischemic stroke. 107
Figure 2.6: Increased astrogliosis is observed within the infarcted hemisphere. 110
Figure 2.7: Regions of perfusion deficit across the injured cortex following either intra-cortical injections of saline or ET-1. 113
Figure 2.8: Distinct localization of microglia/macrophages and astrocytes within the infarcted hemisphere. 116
Figure 2.9: HFD reduced the number of surviving neurons within the hypo-perfused region. 119
.....142
Figure 3.1: Endothelin-1 creates a small focal ischemic stroke that is stable over time. 142
Figure 3.2: Endothelin-1 focal ischemic stroke produces a perfusion deficit that can be visualized with fluorescent labelled dextran. 145
Figure 3.3: Blood brain barrier breakdown is observed as a leakage of dextran-conjugated Oregon Green into the brain parenchyma at 24 h and 72 h post-stroke. 149
Figure 3.4: An increase in astrogliosis is observed at 24 h post-stroke. 152
Figure 3.5: A significant increase in the microglia/macrophage response begins at 24 h post stroke and continues to increase up to 72 h. 154

Figure 3.6: An increase in phagocytosis is observed from 24 to 72 h post-stroke with a distinct localization of immune cells within the infarct. 157
Figure 3.7: Extensive neuron degeneration is observed across the infarct during the initial 72 h post-stroke. 159
Figure 3.8: Neuronal loss occurs within the first 4 h post stroke. 162
Figure 3.9: Degeneration of axons and dendrites occurs throughout the acute 24 h post-stroke period. 165
Figure 3.10: Comparison of the acute cellular responses to an ischemic stroke between the non-perfused infarct core and hypo-perfused penumbra region. 174
Figure 3.11: Distinct cellular responses are observed within the core, hypo-perfused penumbra and perfused region. 176
Figure 4.1: The effect of acute post-stroke DHA treatment on infarct size. 191
Figure 4.2: DHA treatment attenuated BBB breakdown. 194
Figure 4.3: Albumin extravasation within the cortex 24 hours following a focal ischemic stroke. 196
Figure 4.4: Infiltration of neutrophils within the infarct was reduced with DHA treatment. 198
Figure 4.5: DHA reduced cyclooxygenase-2 expression within the infarct. 200
Figure 4.6: HFD led to an increase in microglia and macrophages within the infarct at 24 hours post-stroke. 202
Figure 4.7: Macrophage/microglia location within the infarct following acute ischemic stroke. 205
Figure 4.8: Effect of DHA on neuron survival within the ischemic core and penumbra. 207
Figure 4.9: DHA treatment does not rescue neuron degeneration. 209
Figure 5.1: Summary of main findings. 220

LIST OF ABBREVIATIONS

AA- Arachidonic acid

AC3- Active Caspase 3

ACSF- Artificial cerebral spinal fluid

AF- Atrial fibrillation

AMPARs- α-amino-3-hydroxy-5-methyl-4-isoxazolepropionic acid receptor

ANOVA- Analysis of variance

AP- Anterior-posterior

ApoE- Apolipoprotein E

AQ-4- Aquaporin-4

Arg1- Arginase-1

ARRIVE- Animal Research: Reporting of *In Vivo* Experiments

ATP- Adenosine triphosphate

ATPase- Adenosine triphosphatase

A.U.- Arbitrary units

BAK- B-cell lymphoma-2 antagonist killer

BBB- Blood brain barrier

BCL-2- B-cell lymphoma 2

BDNF- Brain-derived neurotrophic factor

BM- Basement membrane

BMI- Body mass index

BPB- Bromophenol Blue

BV- Blood vessel

C57BL/6J- C57 black 6 J

Ca^{2+}- Calcium

$CaCl_2$- Calcium chloride

Cat. #- Catalog number

CBF- Cerebral blood flow

CBV- Cerebral blood volume

CCA- Common carotid artery

CCL- CC chemokine ligand

CD- Cluster of differentiation

Cl^- - Chloride

CNS- Central nervous system

CO_2- Carbon dioxide

COX-1- Cyclooxygenase-1

COX-2- Cyclooxygenase-2

CT- Computed tomography

CXCL- CXC chemokine ligand

Da- Dalton

DAB- Diaminobenzidine

DAMPs- Damage associated molecular patterns

ddH2O- Double-distilled water

DHA- Docosahexaenoic Acid

DNA- DeoxyriboNucleic Acid

DTT- dithiothreitol

DV- Dorsal-ventral

DWI- Diffusion weighted imaging

EGFP- Enhanced green fluorescent protein

EGTA- ethylene glycol tetraacetic acid

EPA- Eicosapentaenoic acid

EtOH- Ethanol

ET-1- Endothelin-1

EVT- Endovascular thrombectomy

FJC- Fluoro-Jade C

g- Grams

GABA- γ-aminobutyric acid

GFAP- Glial fibrillary acidic protein

GLAST- Glutamate aspartate transporter 1

GLT-1- Glutamate transporter 1

GPR120- G protein-coupled receptor 120

GFP- Green fluorescent protein

h- Hours

H_2O_2- Hydrogen peroxide

HCl- Hydrochloric acid

HEPES- N-2-hydroxyethylpiperazine-N-ethanesulfonic acid

HFD- High fat diet

H-P- hypo-perfused

HRP- horseradish peroxidase

Iba-1- Ionized calcium binding adaptor molecule 1

ICAM-1- Intercellular adhesion molecule-1

ICH- Intracerebral haemorrhage

i.c.v.- Intracerebroventricular

IgG- Immunoglobulin G

IKKβ- Inhibitor of nuclear factor kappa-B kinase subunit beta

IL-10- Interleukin-10

IL-1β- Interleukin 1 beta

iNOS- inducible nitric oxide synthase

i.p.- Intraperitoneal

i.v.- Intravenous

K^+- Potassium

KCl- Potassium chloride

kDa- kilodalton

kg- Kilogram

$KMnO_4$- Potassium permanganate

LC3-II- Light-chain 3 II

LPS- Lipopolysaccharide

Ly6G- Ly6 complex locus G

mA- Milliampere

3-MA- 3-Methyladenine

MAP-2- Microtubule-associated protein 2

MCA- Middle cerebral artery

MCAO- Middle cerebral artery occlusion

MCHR1- Melanin-concentrating hormone receptor 1

MCP-1- Monocyte chemoattractant protein-1

mg- Milligram

$MgCl_2$- Magnesium chloride

mGluR- Metabotropic glutamate receptors

Min- Minute

ML- Medial-lateral

ml- Milliliter

mm- Millimetre

mM- Millimolar

MMPs- Matrix metalloproteinases

MR CLEAN- Multicenter randomized clinical trial of endovascular treatment for acute ischemic stroke in the Netherlands

MRI- Magnetic Resonance imaging

mRNA- Messenger Ribonucleic Acid

MR RESCUE- Mechanical Retrieval and Recanalization of Stroke Clots Using Embolectomy

Na^+- Sodium

NaCl- Sodium chloride

NaF- Sodium fluoride

$NaHCO_3$- Sodium bicarbonate

Na_2HPO_4- Disodium phosphate

NaH_2PO_4- Monosodium phosphate

$NaVO_4$- Sodium orthovanadate

NPD1- Neuroprotectant D1

NeuN- Neuronal nuclei

NF-κB- Nuclear factor kappa-light-chain-enhancer of activated B cells

nM- Nanomolar

nm- Nanometer

NMDA- N-methyl-D-aspartate

NO- Nitric oxide

N-P- Non-perfused

n-3 PUFAs- polyunsaturated fatty acids

NVU- Neurovascular unit

O_2- Oxygen

OGD- Oxygen-glucose deprivation

P- Perfused

PBS- Phosphate Buffered Saline

PECAM-1- platelet endothelial cell adhesion molecule 1

PFA- paraformaldehyde

PGE2- Prostaglandin E2

pH- Power of hydrogen

PMSF- Phenylmethylsulfonyl fluoride

PWI- Perfusion weighted imaging

ROI- Region of interest

ROS- Reactive oxygen species

Rpm- Rotations per minute

SAH- Subarachnoid haemorrhagic

SBI- Silent brain infarction

s.c.- Subcutaneous

SD- Standard deviation

SDS- Sodium Dodecyl Sulfate

SDS-PAGE- Sodium Dodecyl Sulfate Polyacrylamide Gel Electrophoresis

Shh- Sonic Hedgehog

SVZ- Subventricular zone

TGF-β- Transforming growth factor beta

TIA- Transient ischemic attack

TJ- Tight junction

TMEM119- Trans-membrane protein 119

TNF- Tumor necrosis factor

tPA- Tissue plasminogen activator

TPBS- Tween-20 Phosphate Buffered Saline

TUNEL- Terminal deoxynucleotidyl transferase dUTP nick end labeling

UV- Ultraviolet

V- Volts

VCAM-1- Vascular Cell Adhesion Molecule 1

Vim- Vimentin

v/v- Volume per volume

w/v- Weight per volume

µg- Microgram

µl- Microliter

µm- Micron

^{o}C- degrees Celsius

∑- Sum

LIST OF APPENDENCIES

Animal Ethics Approval……...285

Diet composition…….….286

CHAPTER 1

INTRODUCTION AND OVERVIEW

1.1 Overview

Ischemic stroke remains one of the most preventable cardiovascular diseases. Covert stroke, in which neurological deficits are subtle, occur frequently in patients with cardiovascular disease and can increase the risk of overt stroke (Gupta et al., 2016; Vermeer et al., 2007). A major risk factor for ischemic stroke is diet-induced obesity that results in a decline in vascular health (Dorrance et al., 2014). There is a definitive link between unhealthy diets that induce obesity and increased risk of ischemic stroke. However, the manner in which diet-induced obesity modulates ischemic injury following small covert strokes remains unclear. This thesis examines (1) the impact of diet on post-stroke outcome at the cellular level following a small, focal ischemic stroke (2) the cellular response in the acute post-stroke period and (3) the impact of docosahexaenoic acid, an omega-3 fatty acid, administration in the post-stroke period on the acute cellular response.

1.1.1 Incidence and Risk Factors of Stroke

Stroke is a neurovascular event that causes permanent disability and is the third leading cause of death in Canada, with approximately 62,000 strokes per year (Coutts et al., 2015). Of those 62,000 strokes that occur, approximately 1200 to 1400 strokes occur in Newfoundland and Labrador annually, which is the highest incident compared to any other province (StatisticsCanada, 2008). Although approximately 80% of individuals survive a stroke, the majority of people live with long-term disability. There are approximately 405,000 individuals in Canada living with the consequences of stroke that have permanent disability (Krueger et al., 2015). This number is set to double in Canada

over the next 20 years. For those admitted to the hospital, 40% will be readmitted for another cardiovascular event such as heart attack or stroke (Heart&Stroke, 2019). Furthermore, the recurrence rate of stroke is 5 to 25% within 1 year and 20 to 40% within 5 years (Donkor, 2018). The increasing rate of stroke in the population reiterates the importance of researching new therapeutic interventions.

The risk factors for developing stroke include cardiovascular health risks such as high blood pressure, high blood cholesterol and irregular heartbeat such as atrial fibrillation (AF) (Benjamin et al., 2019). Hypertension is the most prevalent risk factor accounting for 35% to 50% of stroke risk (Meschia et al., 2014). Furthermore, those individuals that experience AF are 5 times more likely to develop stroke (Ganjehei et al., 2011). Diet-induced obesity is a major risk factor for developing ischemic stroke (Meschia et al., 2014). A previous meta-analysis from 25 studies showed that compared to individuals that are normal weight, ischemic stroke risk increased by 22% in overweight individuals and increased by 64% in obese individuals (Strazzullo et al., 2010). There is a linear positive relationship between body mass index (BMI) and stroke risk so that for every 1 unit increase in BMI, stroke risk increases approximately 5% (Kernan et al., 2013). These reports indicate that there is a clear link between diet-induced obesity and stroke risk. However, the effect of diet-induced obesity on the cellular, structural and functional damage caused by stroke remains unclear.

1.1.2 Classification of Stroke

There are two main types of stroke that can occur within the brain namely haemorrhagic and ischemic (Table 1.1). Haemorrhagic stroke occurs in approximately

15% of the population, whereas ischemic stroke is more prevalent occurring in approximately 85% of stroke patients (Smith, 2011). Haemorrhagic stroke occurs when there is rupture of a blood vessel resulting in bleeding within the brain or bleeding between the dura and arachnoid within the subarachnoid space (Grysiewicz et al., 2008). These are termed intracerebral haemorrhage (ICH) and subarachnoid haemorrhagic (SAH), respectively (Table 1.1). Individuals with the highest risk for ICH are those with hypertension and over the age of 55. SAH most commonly occurs when an aneurysm ruptures or there is a vascular malformation such as an arteriovenous malformation that results in haemorrhage (Grysiewicz et al., 2008). Treatment for haemorrhagic stroke includes minimizing bleeding within the brain and reducing intracranial pressure through surgical removal of part of the skull.

Ischemic stroke commonly occurs with the occlusion of a blood vessel within the brain. A transient ischemic attack (TIA) or ministroke typically occurs when there is temporary occlusion of a blood vessel with rapidly presenting clinical symptoms that completely resolve within 24 hours (Nadarajan et al., 2014) (Table 1.1). However, TIA is a predictor of ischemic stroke with the short-term risk increasing from 3% to 10% at 2 days, 5% at 7 days, and 9% to 17% at 90 days following a TIA (Gupta et al., 2014). Large-artery atherosclerosis occurs when there is >50% stenosis of a brain artery resulting in an athero-thrombotic stroke (Adams et al., 1993) (Table 1.1). A cardioembolic stroke occurs when a brain artery is occluded by an embolus originating from the heart (Adams et al., 1993) (Table 1.1). Small-artery occlusion arises when small vessels are obstructed resulting in subtle dysfunction within the affected brain area. This stroke subtype also includes lacunar infarction, which occurs when the small penetrating arteries that supply

blood to the brain's deeper structures, such as the thalamus or basal ganglia, are blocked (Regenhardt et al., 2019) (Table 1.1).

Covert stroke is the most common form of ischemic stroke outnumbering overt strokes 5:1 ("Mind the Connection: Preventing stroke and dementia," 2016). These covert strokes or silent brain infarctions do not present with overt neurological deficits as observed with overt stroke (Vermeer et al., 2007) (Table 1.1). The subtle deficits may include reduced physical function, such as visual, arm and leg disturbances, and cognitive deficits that often are unnoticed (Vermeer et al., 2007). These deficits depend on where the covert stroke is located in the brain. The challenge with diagnosing covert stroke is that these strokes are identified with brain imaging, namely noncontrast Computed Tomography (CT) scan, and most patients typically will not receive a CT scan of the brain until they present with a major cerebrovascular event (Birenbaum et al., 2011; Fanning et al., 2014). Although only subtle deficits are observed, covert strokes increase the risk of overt ischemic stroke by greater than 3-fold and are an indication of declining cardiovascular health (Gupta et al., 2016; Vermeer et al., 2003). Despite the prevalence and health implication of this form of stroke, preclinical research has focussed on overt stroke models, less is known about the cellular response to a covert stroke. To fill this knowledge gap, this thesis focuses on the acute cellular responses using a small focal ischemic stroke model that has similarities with covert strokes.

Table 1.1: Classification of stroke.

Classification	Types	Cause	Rate
Haemorrhagic Stroke	Intracerebral haemorrhage	Hypertension.	Accounts for 10-20% of all strokes, 15.9 per 100 000 per year (Sacco et al., 2009)
	Subarachnoid haemorrhagic	Rupture of aneurysm or presence of vascular malformation.	Between 5 and 10 per 100 000 per year (Linn et al., 1996).
Ischemic Stroke	Athero-thrombotic stroke	Large-artery atherosclerosis with >50% stenosis or artery.	Accounts for 20% of all strokes (Leys, 2001).
	Cardioembolic stroke	Blood clot travels to the brain to occlude blood vessel.	Accounts for 15 to 30% of ischemic strokes (Gorelick, 2004)
	Lacunar stroke	Small penetrating arteries that supply blood to the brain's deeper structures are blocked.	Between 12.7–19.0 per 100,000 population per year (Bejot et al., 2008).
	Silent brain infarction (Covert stroke)	Lack clinically overt symptoms. Caused by general cardiovascular disease.	Outnumber overt strokes 5:1 ("Mind the Connection: Preventing stroke and dementia," 2016).
Transient ischemic attack		Temporary occlusion of a blood vessel. Symptoms completely resolve within 24 hours.	Approximately 500,000 TIAs occur each year (Gorelick, 2004)

1.1.3 Clinical Progression of Ischemic Stroke from Acute to Chronic

All cells depend on blood flow for oxygen (O_2) and glucose and the removal of waste and carbon dioxide (CO_2). Normal cerebral blood flow (CBF) is maintained at approximately 50 ml per 100 g of brain tissue per minute and its disruption greatly impacts cell survival (Cipolla, 2009; Phillips & Whisnant, 1992). Following the initial occlusion of a blood vessel within the brain, there is an immediate reduction in CBF. If CBF is reduced to less than 20% of baseline CBF (< 10 ml/100g/min), brain tissue will significantly deplete their energy stores of adenosine triphosphate (ATP), as well as oxygen and waste products will accumulate. This results in necrotic cell death within the centre of the infarct, defined as the ischemic core. Cells that undergo necrotic cell death cannot be rescued (Moskowitz et al., 2010) (Fig 1.1). Surrounding the infarct core is the penumbra where CBF is reduced to 20% to 40% of baseline CBF (10- 18 ml/100g/min). Within the penumbra, viable brain cells exist; however, energy metabolism is insufficient to maintain active signaling resulting in synaptic failure (Astrup et al., 1981; Hofmeijer & van Putten, 2012) (Fig 1.1). With continued occlusion of the blood vessel, the cells within the penumbra die and the ischemic core expands (Moskowitz et al., 2010).

Studies examining the penumbra post-stroke using various imaging modalities such as CT and Magnetic Resonance imaging (MRI) scans show a reduction of the penumbra with a corresponding expansion of the infarct within the 24-hour acute period (Davis & Donnan, 2014). Using diffusion-weighted MRI, Lansberg and colleagues (2001) demonstrated that lesion volume increased significantly up to 72 hours post-stroke then gradually reduced up to 25 days (Lansberg et al., 2001). Imaging techniques such as

diffusion weighted imaging (DWI) and perfusion weighted imaging (PWI) can be used to visualize ischemic stroke progression. Using these combined imaging techniques, a DWI/PWI mismatch can be obtained. Several studies have used this DWI/PWI mismatch as a measure of the penumbra to ischemic core ratio indicating the amount of salvageable brain tissue (Albers et al., 2006; Leigh et al., 2018; Schlaug et al., 1999). Although there is controversy over whether or not this mismatch accurately defines the penumbra, there is evidence to show that the penumbra may still exist out to 24 hours post-stroke, albeit much smaller in size (Ebinger et al., 2009; Leigh et al., 2018). Therefore, the cells in the penumbra are in a vulnerable state during the acute post-stroke period, with decreasing potential for rescue as the ischemic injury progresses. Surviving brain tissue adjacent to the border of the infarct, termed the peri-infarct cortex, can undergo remodelling provided that sufficient blood flow is present (Murphy & Corbett, 2009).

Beyond the acute post-stroke (< 24 hours) into the sub-acute period (>24 hours to weeks), some stroke survivors exhibit spontaneous recovery even without therapeutic intervention (Bernhardt et al., 2017; Birenbaum et al., 2011). Angiogenesis within the peri-infarct has been observed by 4 to 7 days post-stroke resulting in an increase in microvessel density (Hatakeyama et al., 2020; Martin et al., 2012). This increase in microvessel density is associated with neuronal remodeling and functional improvement (Hatakeyama et al., 2020). Within one to four weeks post-stroke, neural plasticity occurs within the peri-infarct and new axonal projections form resulting in remapping of neuronal connections (Murphy & Corbett, 2009). It is within this period that rehabilitation is critical (Bernhardt et al., 2017; Biernaskie et al., 2004). Despite such promising endogenous recovery that could occur, it is contingent on the brain tissue surviving the

initial ischemic insult. Therefore, therapeutic intervention within the acute post-stroke period remains crucial for optimal restoration of function.

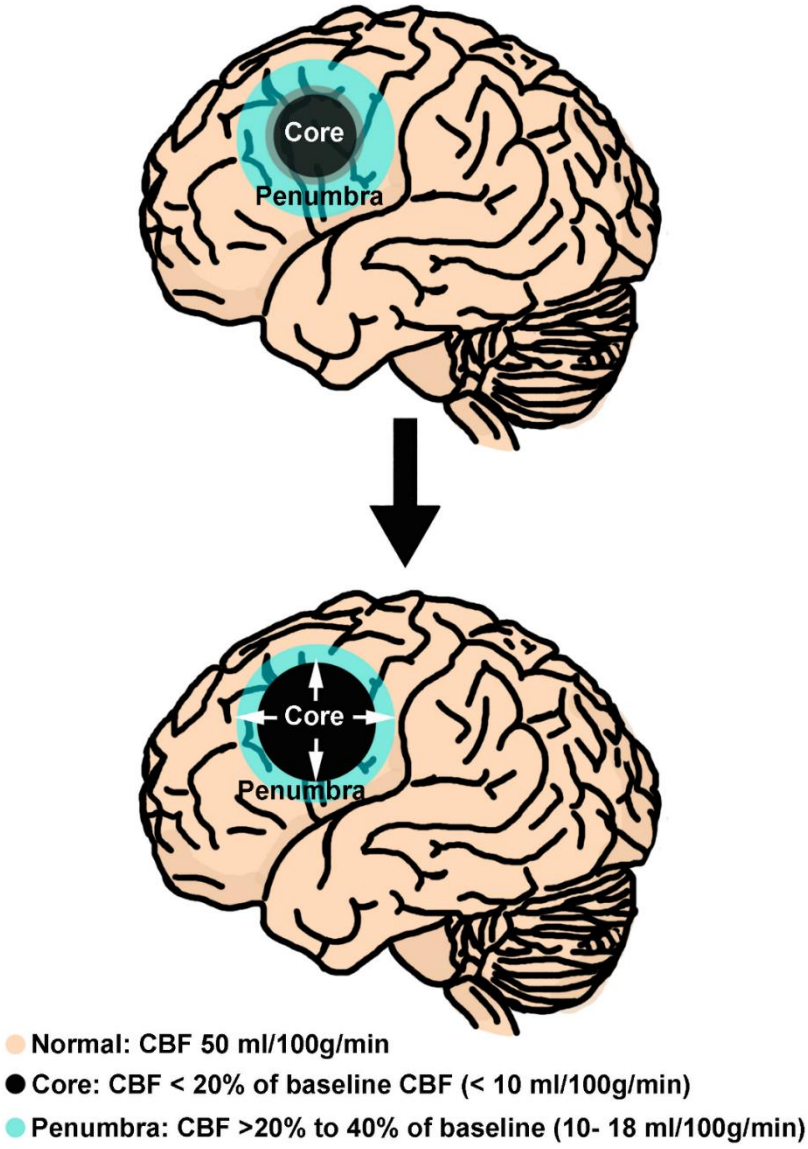

Figure 1.1: Cerebral blood flow within the core and penumbra following ischemic stroke.

Following ischemic stroke, there is an immediate reduction in cerebral blood flow (CBF) from 50 ml/100g/min to less than 10 ml/100g/min delineating the ischemic core. Surrounding the ischemic core is the penumbra, with a CBF of greater than 10 to 18 ml/100g/min. Over time, the ischemic core expands and the penumbral region is reduced. This is an original figure. Peach= Normal CBF, Black= Ischemic core, Blue= Penumbra

1.1.4 Rescuing the Penumbra: Emphasis on Acute Post-stroke Intervention

Clinical treatments for ischemic stroke focus on immediate recanalization of the occluded blood vessel within the brain which need to be applied within the acute hours post-stroke. Other than physiotherapy, there are no other treatments beyond the acute post-stroke period. Over the last decades, intravenous application of tissue Plasminogen Activator (tPA) has been the primary treatment intervention for acute ischemic stroke. tPA catalyzes the conversion of the proenzyme plasminogen to plasmin, a serine protease, which ultimately leads to lysis of the clot (Loscalzo & Braunwald, 1988). While effective, this treatment is applied to only a fraction of stroke patients. Due to the risk of haemorrhage, the time frame for using tPA is limited to 4.5 hours post-stroke resulting in <10% of stroke patients receiving this treatment (Nadeau et al., 2005). Patients are excluded from tPA intervention based on medical history that increase the risk of brain haemorrhage, including severe hypertension, prior history of diabetes and greater than 80 years old (Powers et al., 2015). Furthermore, tPA can directly damage cells (Abu Fanne et al., 2010; Chevilley et al., 2015; Nicole et al., 2001; Wang et al., 2003; Yamashita et al., 2009). Although tPA has been an effective thrombolytic agent, its limitations require that new therapeutic interventions be developed.

Over the past decade, endovascular thrombectomy (EVT) has become a promising intervention for ischemic stroke. EVT physically removes the clot from brain arterioles significantly improving stroke outcome (Nogueira et al., 2018). In 2014, a multicenter randomized clinical trial of endovascular treatment for acute ischemic stroke in the Netherlands (MR CLEAN) examined the use of EVT as a treatment for acute ischemic

stroke (Berkhemer et al., 2015; Fransen et al., 2014). Patients that received intraarterial treatment and EVT within 6 hours had more favourable functional outcomes and reduced infarct volumes on CT scan compared to those that only received tPA (Berkhemer et al., 2015). Another prominent EVT trial, Mechanical Retrieval and Recanalization of Stroke Clots Using Embolectomy (MR RESCUE) trial, examined mechanical embolectomy in stroke patients across 22 sites in North America (Kidwell et al., 2013). Despite the use of mechanical embolectomy in patients with a discernable penumbra, there were no significant benefits in comparison to standard care (Kidwell et al., 2013). This may have been due to the delay of EVT intervention at 8 hours post-stroke, which is longer than previous EVT trials (Furlan et al., 1999; Kidwell et al., 2013; Smith et al., 2005). Although EVT advances stroke therapy, the timeline for EVT is still limited with the greatest benefit between 2 to 7.3 hours (Saver et al., 2016).

Several studies have suggested expanding the use of thrombolytics and/or EVT use beyond 4.5 hours and 6 hours, respectively, to rescue the penumbra (Albers, 1999; Murata et al., 2008; Pena et al., 2017; Tan et al., 2015). Although evidence suggests that the penumbra may still exist out to 24 hours post-stroke, it is unknown how much of the penumbra can be salvaged within this time frame. Furthermore, the increased risk of haemorrhagic transformation with delayed thrombolytic therapies such as tPA may cause more damage than recovery (Jickling et al., 2014). Therefore, it is imperative that stroke research continues to investigate cellular targets with therapeutic potential within the acute post-stroke period.

1.2 The Neurovascular Unit: Maintaining Homeostasis within the Brain

Homeostasis within the brain is maintained at the level of the neurovascular unit (NVU) that includes neurons, astrocytes and endothelial cells and their interactions among one another (Fig. 1.2). These cell-cell interactions are essential for proper brain function and are the basis of disease when interactions are lost (Moskowitz et al., 2010). The most notable function of the NVU involves the process of neurovascular coupling, in which neuron activity initiates vascular responses to affect blood flow to an active region in the brain and maintaining the BBB (Daneman, 2015; Iadecola, 2017; LeDoux et al., 1983). Disruption to both of these functions occur post-stroke, which is detrimental to brain homeostasis.

1.2.1 Cell types that comprise the neurovascular unit and their function

The concept of the NVU emerged in 2001 to describe the relationship between the brain and its vasculature (Iadecola, 2017). Prior to this, the cells of the brain and the cerebral vascular were considered two distinct entities and their interactions were not commonly studied (Iadecola, 2017). It is now well recognized that the dysfunction of the NVU is the focus of stroke pathology. The NVU consists of neurons, astrocytes, microglia, endothelial cells that compose blood vessels, pericytes, vascular smooth muscle cells and extracellular matrix (Iadecola, 2017; Shabir et al., 2018) (Fig. 1.2).

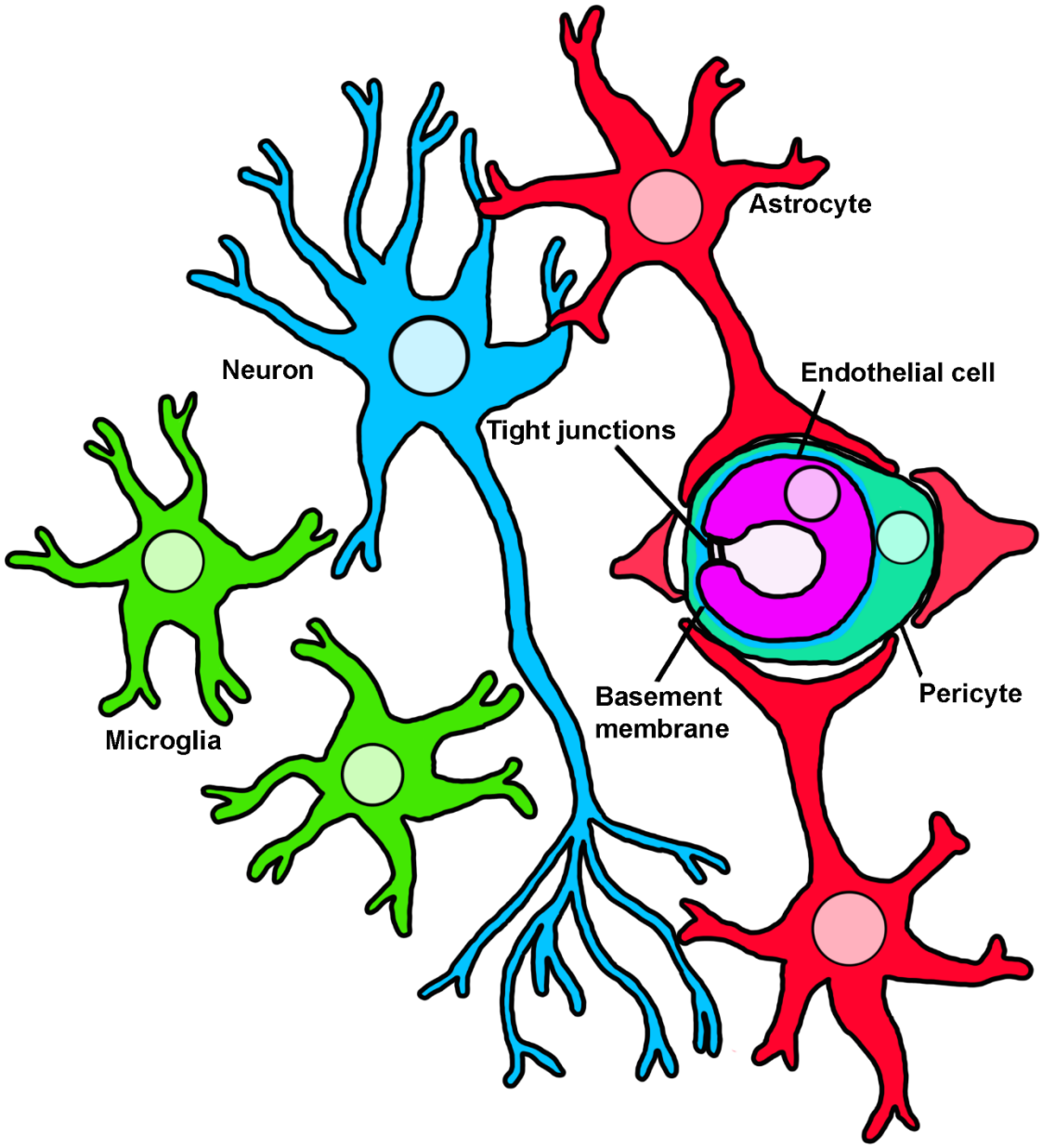

Figure 1.2: Cells comprising the Neurovascular Unit.

The Neurovascular Unit (NVU) within the brain is comprised of several interacting cells including neurons, astrocytes, microglia, pericytes and endothelial cells. Tight junctions between vascular endothelial cells form the blood brain barrier. Dysfunction of the NVU following ischemic stroke can lead to disruption of homeostatic functioning of the brain. This is an original figure.

One of the most important roles of the NVU is the interaction between neurons and cerebral blood vessels termed neurovascular coupling. With neurovascular coupling, neuron activity initiates a release of vasoactive mediators that act on local blood vessels causing a vascular response and ultimately a change in CBF (Iadecola, 2017; LeDoux et al., 1983). This coupling is achieved either directly through an interneuron or indirectly via astrocytes (Shabir et al., 2018). Neurovascular coupling through astrocytes involves the release of vasoactive mediators at astrocyte endfeet that wrap around blood vessels causing either vasodilation or vasoconstriction. These vasoactive mediators directly act on the smooth muscle cells of blood vessels (Gordon et al., 2007; Zonta et al., 2003). During ischemic stroke, excess extracellular glutamate induces an increase in astrocyte intracellular Ca^{2+} leading to a wave of Ca^{2+} throughout the astrocyte networks (Cornell-Bell et al., 1990; Seidel et al., 2016). This Ca^{2+} wave has been associated with spreading depolarizations typically observed following ischemic stroke (Peters et al., 2003; Seidel et al., 2016). Although the mechanism by which astrocyte Ca^{2+} waves propagate spreading depolarization and alter CBF is not fully understood, studies suggest it occurs through Prostaglandin E2 (PGE2) mediated vasodilation in a low O_2 environment (Gordon et al., 2011; Seidel et al., 2016). Thus, neurons and astrocytes together regulate the blood flow via cell-cell interactions within the NVU.

Astrocytes influence the neuronal functions by supplying energy substrates to neurons and regulating neurotransmitter availability. The brain consumes the highest amount of energy accounting for 20% of oxygen use and 25% of glucose use in comparison to the rest of the body (Belanger et al., 2011). To meet this high energy demand, the rate of oxidative metabolism in neurons is high using lactate and glucose as

energy substrates (Belanger et al., 2011). Astrocytes are crucial for providing lactate to neurons through the astrocyte-neuron lactate shuttle (Falkowska et al., 2015). Astrocytes convert glucose to pyruvate which is then converted to lactate and shuttled to neurons via monocarboxylate transporters. Neurons convert lactate to pyruvate for energy use. Astrocytes also recycle glutamate following synaptic release from neurons and convert this to glutamine where it is then shuttled back to neurons and converted to glutamate (Barros et al., 2018; Mangia et al., 2012). Following ischemic stroke, the reduction in CBF leads to reduced oxygen and glucose availability that cannot meet the high energy demand of neurons. As a significant quantity of energy is required for cells to maintain their membrane potential, any loss in energy supply results in membrane depolarization leading to excess release of neurotransmitters from neurons. An increase in extracellular glutamate causes over activation of NMDA receptors mediating an influx of intracellular Ca^{2+} and activation of cell death pathways, leading to apoptosis or necrosis of the cell (Lo, 2008; Szydlowska & Tymianski, 2010). Thus, astrocyte's inability to remove excess glutamate and to provide energy substrates to neurons contributes to the initiation of neuronal cell death through excitotoxicity.

1.2.2 Blood brain barrier: protection of the central nervous system

The BBB regulates the movement of molecules from the peripheral circulation into the central nervous system (Daneman & Prat, 2015). This is accomplished by tight junction (TJ) proteins located between endothelial cells that limit paracellular transport. Although TJs between endothelial cells are the primary barrier between the blood stream and brain parenchyma, other cells and cellular components regulate the BBB including

pericytes, astrocytes, basement membrane (BM) and extracellular matrix (Jiang et al., 2018).

Following ischemic stroke, the BBB is compromised resulting in increased permeability for peripheral molecules and immune cells to enter the brain (Jiang et al., 2018). This is due not only to endothelial and TJ protein damage but also damage to other cell types such as pericytes and astrocytes that help maintain the BBB. Within hours post-stroke, significantly reduced blood flow causes damage and swelling of vascular endothelial cells and detachment of the BM that provides structural support (Kwon et al., 2009; Sandoval & Witt, 2008). Furthermore, TJ protein complexes become disrupted when damage occurs to endothelial cells. TJ proteins are redistributed intracellularly via endocytosis, reducing the presence of these proteins between endothelial cells, which leads to an increase in permeability of molecules across the BBB. Previous studies have shown that TJ proteins remain intact up to 6 hours post-stroke with TJ disruption occurring at a much later time between 48 to 58 hours post-stroke (Keaney & Campbell, 2015; Knowland et al., 2014). This is accompanied with delayed leakage of immunoglobulin G (IgG) within the brain (Knowland et al., 2014). This demonstrates that TJ are redistributed and reduced following stroke which leads to diminished BBB integrity.

Brain edema causes major disruption to the BBB. Edema includes cytotoxic edema that is caused by accumulation of fluid and Na^+ intracellularly leading to swelling of cells and vasogenic edema due to extracellular fluid accumulation (Liang et al., 2007). Cytotoxic edema of endothelial cells, neurons and astrocytes occurs within minutes of stroke onset as a result of ATP depletion followed by an influx of extracellular ions, such

as Na^+ and Cl^-, changing the ionic gradient and allowing an influx of water into the cell leading to necrotic cell death (Liang et al., 2007). Vasogenic edema occurs within hours post-stroke and is an indicator of vascular injury (Simard et al., 2006; Stokum et al., 2016). This vascular injury causes significant disruption of the BBB allowing peripheral molecules to enter the brain.

Injury to the vasculature also damages astrocytes and pericytes resulting in further BBB disruption. Kwon and colleagues showed that astrocyte endfeet partially detach from the BM surrounding endothelial cells within 4 hours following middle cerebral artery occlusion (MCAO) and contact is completely lost by 48 hours post-stroke (Kwon et al., 2009). This astrocyte-BM detachment is due to the opening of aquaporin-4 (AQ-4) water channels in astrocyte endfeet resulting in a rapid influx of water and swelling of the endfeet within 1 hour following MCAO (Kwon et al., 2009; Winkler et al., 2020). This rapid increase in water within astrocytes causes cytotoxic edema and leads to rupture of the astrocyte plasma membrane and the subsequent extracellular accumulation of fluid within the brain parenchyma by 16 hours post-stroke (Kwon et al., 2009).

The totality of these events causes major disruption of the BBB, leakage of peripheral molecules, such as albumin, and leukocyte infiltration into the brain. Previous studies visualized this leakage using dyes and fluorescent tracers of different molecular weights (Durukan et al., 2009). It was previously reported that there is a biphasic opening of the BBB with leakage occurring within hours post-stroke, followed by a refractory period, and opening a second time between 5 to 72 hours (Belayev et al., 1996; Kuroiwa et al., 1985; Sandoval & Witt, 2008; Witt et al., 2008). However, more recent studies show that the BBB remains open. Using transient 90-minute MCAO, Strbian and

colleagues found leakage of the smaller gadolinium molecule (590 Da) and the larger Evans Blue albumin (75.8 kDa) both as early as 25 minutes following reperfusion and leakage was observed out to 3 to 5 weeks post-stroke (Strbian et al., 2008). Therefore, BBB disruption can continue for weeks beyond the initial insult.

Furthermore, leukocyte infiltration within the brain is an indicator of significant BBB breakdown. Neutrophils have been shown to infiltrate the brain within 6 to 48 hours following transient MCAO and 12 to 72 hours following permanent MCAO (Zhang et al., 1994). Matrix metalloproteinases (MMPs) released from neutrophils, in particular MMP-9, causes further damage to endothelial cells and extracellular matrix degradation leading to TJ disruption (Stokum et al., 2016). BBB breakdown leading to leukocyte infiltration within the brain has been well defined in stroke models that produce large infarcts such as MCAO. However, this injury is not well characterized in smaller focal strokes.

1.3 Cascade of cellular events following ischemic stroke

Following the initial occlusion of a blood vessel within the brain, there is a cascade of cellular events that causes the expansion of the ischemic core and reduction of the penumbra (Moskowitz et al., 2010). These events occur within hours to days post-stroke and can cause secondary damage beyond the initial insult (Fig. 1.3).

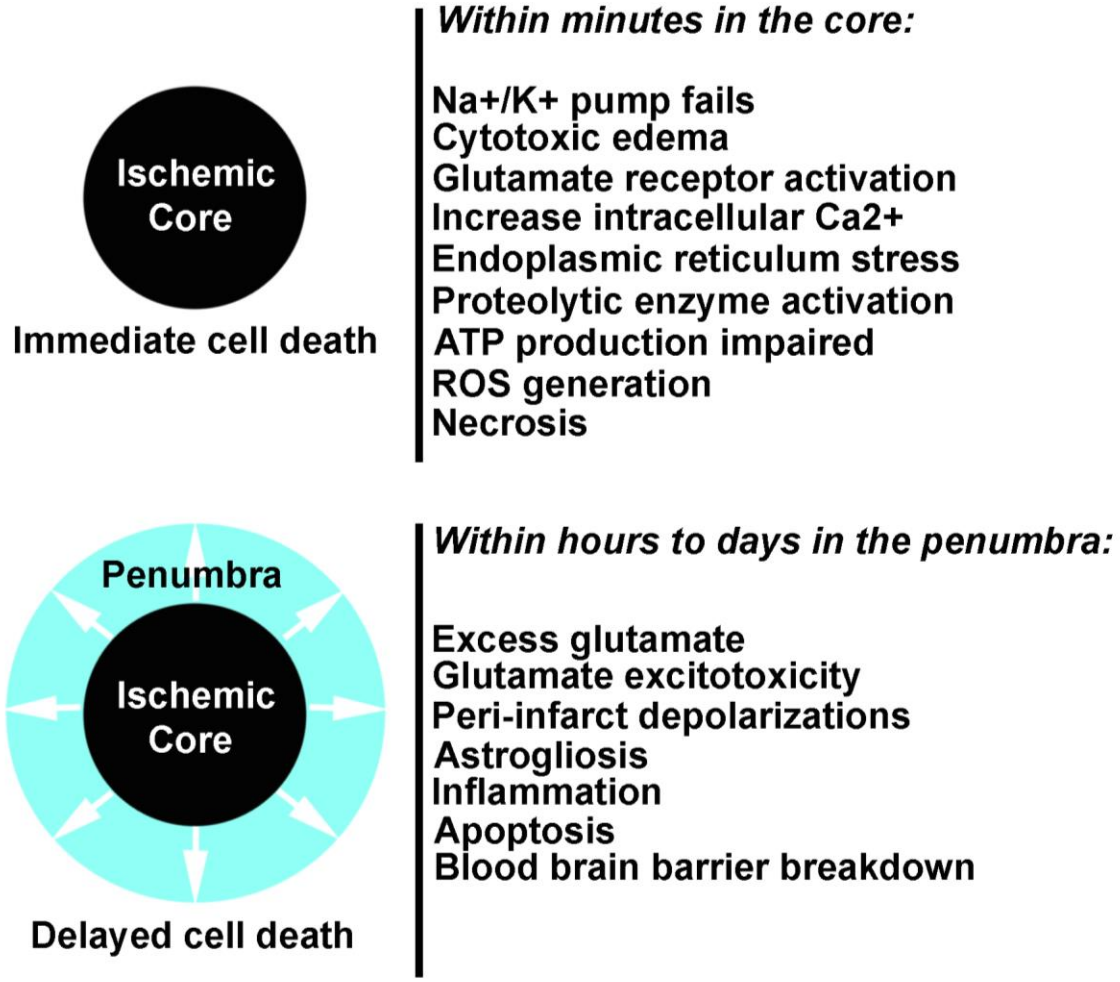

Figure 1.3: Cascade of events following ischemic stroke.

Following ischemic stroke, there is a cascade of cellular events that cause the ischemic core to expand and reduce the size of the penumbra. Within the ischemic core there is immediate cell death as a result of energy failure and impaired ATP production. However, within the penumbra there is delayed cell death with the potential to reduce ischemic injury and salvage brain tissue. Cells within the penumbra are susceptible to ischemic death due to secondary damage, such as astrogliosis, inflammation and blood brain barrier breakdown. White arrows represent expansion of the ischemic core. This is an original figure.

1.3.1 Progression of Cellular Events within Minutes to Hours following Acute Ischemic Stroke

As described in section 1.1.3, the immediate reduction of CBF following occlusion of a blood vessel occurs in both the ischemic core and surrounding penumbra. The ischemic core is characterized as having a CBF of less than 10 ml/100g/min indicating reduced oxygen, glucose supply and ATP production (Moskowitz et al., 2010). This energy supply is insufficient to maintain ionic gradients necessary to maintain membrane potential as the Na^+/potassium (K^+) pump fails (Huang et al., 2015). Na^+ and chloride (Cl^-) ions enter the cell bringing with them an influx of water which causes cytotoxic edema (Liang et al., 2007). This cytotoxic edema can potentially cause the cell to rupture and die. Simultaneously, extracellular accumulation of K^+ and glutamate initiate depolarizations of neurons within the area. This anoxic depolarization occurs within minutes of stroke onset within the core and spreads to the penumbra for a duration of 6 to 8 hours post-stroke (Kunz et al., 2010). Increases in intracellular Ca^{2+} due to failure of Ca^{2+} pumps, activation of voltage-gated Ca^{2+} channels and glutamate receptor activation causes a surplus of Ca^{2+} (Sekerdag et al., 2018). Excess Ca^{2+} activates proteolytic enzymes within the cell leading to damage to the cell membrane, cytoskeleton, microtubules and mitochondria (Artal-Sanz & Tavernarakis, 2005; Fern & Moller, 2000). Furthermore, Ca^{2+} overload produces reactive oxygen species (ROS) leading to oxidative stress which in turn damages intracellular components of the cell such as mitochondria and DNA. Mitochondria are also a source of ROS producing oxygen free radicals. These events cause immediate cell death in the core that is not reversible.

Within the penumbra, where the CBF is between 10 and 18 ml/100g/min, cells survive; however, energy metabolism is not sufficient to maintain optimal function and cellular processes are impaired (Astrup et al., 1981; Moskowitz et al., 2010). Neurons within the penumbra will depolarize as a result of an imbalance of ionic gradients and excess extracellular K^+ and excitatory amino acids such as glutamate. However, unlike neurons in the core, neurons in the penumbra can repolarize to depolarize again. This results in a wave of peri-infarct depolarizations increasing infarct size (Dirnagl et al., 1999). With continued neuronal depolarization, these injured neurons become electrically silent due to insufficient energy to repolarize their membranes. This loss of electrical activity of neurons results in spreading depression (Cozzolino et al., 2018). Furthermore, the accumulation of extracellular glutamate released from presynaptic neurons can lead to excitotoxicity. Astrocytes remove excess extracellular K^+ and glutamate through the glutamate aspartate transporter 1 (GLAST) and glutamate transporter 1 (GLT-1); however, these transporters are reduced following ischemic stroke and glutamate reuptake is impaired (Barreto et al., 2011). As a result, excess extracellular glutamate can activate ionotropic glutamate receptors on post-synaptic neurons (Szydlowska & Tymianski, 2010). This activation causes an increase in intracellular Ca^{2+} and activation of cell death pathways. Furthermore, excess extracellular glutamate can cause continuous depolarization of neurons in the penumbra, thereby perpetuating the influx of Ca^{2+} within the cell (Sekerdag et al., 2018). The overall result is excitotoxicity of the cell. Unlike the ischemic core in which cell death is immediate, cells in the penumbra can survive and damage can be reversed if reperfusion is reinstated in time.

1.3.2 Cell degeneration and death: necrosis, apoptosis and autophagy

Cells within the ischemic brain can undergo immediate cell death, such as with necrosis, or delayed death, as with apoptosis (Moskowitz et al., 2010). Following stroke, neurons within the ischemic core are particularly vulnerable to necrosis while neurons within the penumbra predominantly undergo apoptosis (Wei et al., 2004; Yuan, 2009).

Necrosis involves physical damage to the cell causing rupture to the cell membrane (Edinger & Thompson, 2004). This can be due to cytotoxic edema where the cell swells to the point of rupture and/or activation of ROS and proteolytic enzymes that degrade the cell membrane. Once the membrane ruptures, intracellular contents spill into the brain parenchyma causing a robust inflammatory response (Edinger & Thompson, 2004). The morphology of cells undergoing necrosis is distinct with clear cytoplasmic vacuolation and membrane rupture (Edinger & Thompson, 2004). Necrosis occurs during the initial ischemic injury and cannot be reversed.

Apoptosis is a programmed cell death that is activated by intracellular stressors, such as a surplus of intracellular Ca^{2+}, or extracellular ligands that activate membrane receptors. Both pathways lead to mitochondrial damage (Sekerdag et al., 2018). Unlike cells undergoing necrosis, apoptotic cells do not initiate an inflammatory response. The nucleus shrinks and the chromatin condenses while the plasma membrane remains intact (Wei et al., 2004). The role of apoptosis in cell death following stroke is underscored by the study showing that genetic deletion of Caspase 3 reduced infarct volume more than 50% in comparison to wild-type/heterozygote controls 24 hours post-stroke (Dojo Soeandy et al., 2019). This indicates that apoptosis contributes to delayed injury hours beyond the initial ischemic insult. Previous studies have observed delayed apoptosis of

both astrocytes and neurons following ischemic stroke in rodents (Dojo Soeandy et al., 2019; Xu & Zhang, 2011). Using ET-1-induced ischemic stroke, Soeandy and colleagues show that greater than 90% of apoptotic cells were neurons within the ischemic region and less than 5% were astrocytes, at 24 hours post-stroke (Dojo Soeandy et al., 2019). This is not surprising as astrocytes have been shown to be more resilient to cell death in comparison to neurons (Barreto et al., 2011). Overall, apoptosis is a delayed form of cell death that occurs following ischemic stroke.

In healthy neurons, autophagy is a "self-eating" intracellular process that clears damaged organelles and cellular components. Briefly, phagophores form the autophagosome, which fuses with a lysosome to then form the autolysosome. These autolysosomes contain enzymes that can degrade damaged organelles, such as mitochondria, and protein aggregates so that cellular homeostasis can be maintained, acting as a pro-survival mechanism (Hou et al., 2019; Kim et al., 2018). Accumulating evidence has shown that autophagy contributes to the degeneration of neurons post-stroke (Yang et al., 2013). Indeed, the beading and swelling of axons and dendrites that occurs within hours post-stroke has been suggested to be due to accumulation of autophagosomes for clearance of organelles (Yang et al., 2013). Excessive autophagy can lead to degeneration of the cell and cell death (Kim et al., 2018; Yang et al., 2013). Furthermore, inhibition of autophagy has been shown to reduce stroke injury following permanent MCAO in mice (Wei et al., 2013). This suggests that excessive autophagy may play a role in delayed cell death and degeneration induced by stroke.

Following acute ischemic stroke, surviving neurons within the penumbra undergo pathological changes, including degeneration of dendritic processes and spines that may

limit postsynaptic potentials (Brown et al., 2008). This degeneration occurs within minutes in the ischemic core, but is delayed in the penumbra. Axonal damage has also been observed following ET-1 induced MCAO (Gresle et al., 2006). Swollen axons were observed at 6 hours, by 72 hours axons appeared bulbous and there was a progressive loss of the axonal marker SMI-312 in the penumbra (Gresle et al., 2006). These axons appeared fragmented and had increased immunopositivity for amyloid precursor protein, which is an indicator of axonal injury. Degeneration of dendrites and axons within the ischemic region is observed days beyond ET-1 induced stroke (Nguemeni et al., 2015). Although neuron degeneration as demonstrated with Fluoro-Jade C staining peaked at 24 hours, the neuronal cell bodies were still present out to 7 days post-stroke (Nguemeni et al., 2015). These studies indicate that neurons within the penumbra are in a precarious state and, even though death is delayed, degeneration can occur days beyond the initial insult.

Damage to neuronal structures, including dendrites and the soma, can be reversed up to a point, depending on the duration of ischemia (Zhu et al., 2017). Using bilateral common carotid artery ligation, Zhu and colleagues subjected mice to 20 min, 1, 3 or 6 hours of ischemia and imaged neuron structures from 1 hour up to 6 hours following reperfusion. Imaging following 6 hours of reperfusion revealed a reversal of dendritic blebbing when ischemia was induced for 20 min or 1 hour; however, this reversal was reduced when the ischemia was induced for 3 hours and non-existent when induced for 6 hours (Zhu et al., 2017). Additionally, nuclear chromatin margination and karyopyknosis, or chromatin condensation, developed in neurons at 6 hours post-stroke, indicating irreversible damage to the cell (Zhu et al., 2017). These studies suggest that surviving

neurons within the penumbra have a limited time frame for rescue during the acute post-stroke period.

1.3.3 Glial response and inflammation

Ischemic injury induces a robust glial response including activation of both astrocytes and microglia that can recruit peripheral immune cells to the site of injury (Pekny et al., 2014). One of the most prominent responses of astrocytes to injury is astrocyte reactivity or astrogliosis wherein a scar is formed surrounding the ischemic region (Sofroniew, 2015). In the healthy brain, astrocyte endfeet form the glia limitans as a means of separating the CNS from peripheral tissues as well as maintaining the BBB (Quintana, 2017; Sofroniew, 2015).

Following stroke, activated astrocytes become hypertrophic and increase the expression of intermediate filaments, such as glial fibrillary acidic protein (GFAP) and vimentin (Vim), to form a barrier preventing the further spread of peripheral leukocytes within the brain. This barrier is both beneficial and detrimental to recovery. The astrocytic barrier is beneficial by isolating leukocytes from entering the brain; however, it is also detrimental as astrogliosis can amplify the inflammatory response and prevent axonal growth and repair (Sofroniew, 2015; Su et al., 2010). Within hours following stroke, reactive astrocytes release pro-inflammatory cytokines and chemokines, such as tumor necrosis factor alpha (TNF-α), interleukin 1 beta (IL-1β), monocyte chemoattractant protein-1 (MCP-1) and CXC chemokine ligand (CXCL) (Sofroniew, 2015). These pro-inflammatory signals recruit leukocytes such as neutrophils and monocytes that aggravate the ischemic injury. Furthermore, reactive astrocytes have been

shown to inhibit neurite outgrowth *in vitro* (Berretta et al., 2016). In contrast, inhibition of astrogliosis by pharmacological application or genetic deletion of GFAP or vimentin has been shown to exacerbate ischemic injury (de Pablo et al., 2013; Li et al., 2008). This suggests that astrocytes lacking intermediate filaments are less protective in preventing neuron death. Astrogliosis, therefore prevents further ischemic damage.

Within the healthy brain, "resting" microglia survey the brain parenchyma and phagocytize cellular debris and apoptotic cells (Chen & Trapp, 2016; Xing et al., 2012). Microglial processes extend to neuronal synapses to remodel synaptic terminals (Wake et al., 2009). Microglia also play a role in BBB maintenance, vascular remodeling and angiogenesis (Dudvarski Stankovic et al., 2016). The cross-talk between microglia and other cells, such as neurons, endothelial cells and astrocytes is essential to maintain homeostasis within the brain.

Following ischemic stroke, microglia change from the resting state (M0) into an activated state: M1, classical activation state or M2, alternative activation state (Xing et al., 2012; Zhou et al., 2017) (Table 1.2). This coincides with a change in microglial morphology going from several ramified processes to an ameboid shape. The M1 and M2 activation states are not distinct classifications but rather a continuum between two states (Patel et al., 2013; Xing et al., 2012). Within minutes to hours post-stroke, M1 microglia produce pro-inflammatory mediators including TNF-α, IL-1β, CXCL, MMPs, reactive oxygen species and reactive nitrogen species such as NO (Patel et al., 2013). In contrast, M2 microglia release anti-inflammatory mediators for resolution of inflammation and phagocytising debris, including Transforming growth factor beta (TGF-β), IL-10, and Arginase-1 (Arg1) that reduces NO production (Patel et al., 2013). Activated microglia

with an ameboid (M1) morphology expressing IL-1β have been observed at 16 and 24 hours following permanent MCAO within the infarct (Mabuchi et al., 2000). M1 mRNA expression has also been shown to increase from 3 days to 14 days following MCAO (Hu et al., 2012). In contrast, M2 mRNA expression is present at 1 day, peaks at 3 to 5 days and decreases at 7 days post-stroke (Hu et al., 2012). This study indicates that the M1 microglial phenotype remains out to 14 days post-stroke; while the M2 phenotype subsides beyond 7 days.

There is a bidirectional relationship between injured cells within the brain and activated microglia. For example, reactive astrocytes can activate and recruit microglia to the insult and activated microglia in turn can induce astrocytes to become reactive (Liddelow et al., 2017; Pekny et al., 2014). Injured cells can release several factors including damage associated molecular patterns (DAMPs), cytokines, ATP and ROS, to recruit and activate microglia (Davalos et al., 2005; Ma et al., 2017). Hu and colleagues showed that microglia switched to the M1 phenotype when exposed for 48 hours to conditioned media from neurons that underwent 60 minutes of OGD (Hu et al., 2012). This demonstrates that ischemic neurons release factors that induce the M1 phenotype. However, M1 microglia co-cultured with ischemic neurons reduce neuron survival while M2 microglia appeared to be neuroprotective. This is consistent with previous studies showing that the pro-inflammatory M1 phenotype can exacerbate ischemic injury leading to increased neuron death and BBB breakdown (Chen et al., 2019; Yang et al., 2015; Zheng et al., 2019). Furthermore, switching the M1 phenotype to M2 may be a neuroprotective strategy to reduce ischemic injury (Zheng et al., 2019). These studies

indicate that microglia activation, whether pro- or anti-inflammatory, can have a profound effect on stroke outcome.

Table 1.2: Microglia classification

Phenotype	Markers	Indication
M0- Resting	Iba-1, F4/80	Survey local microenvironment to maintain homeostasis Several processes present
M1- Classical activation	Iba-1 (upregulated), iNOS, CD11b, CD16, CD32, and CD86	Produces pro-inflammatory mediators TNF-α, IL-1β, IL-6, CCL2, CXCL, MMPs. Produces reactive oxygen and nitrogen species Low level of phagocytoses
M2- Alternative activation	Iba-1 (upregulated), CD206, Arg1, CCL22, Ym1/2, IL-10, and TGF-β.	Produces anti-inflammatory mediators TGF-β, IL-10, and Arg1 Release trophic factors Tissue repair High level of phagocytoses Resolution of inflammation

1.3.4 Neurogenesis and neural circuit reorganization post-stroke

Beyond the acute post-stroke period, there is partial repair of the neurovascular unit followed by reorganization of neuronal circuits. Preclinical stroke models have shown that ischemic stroke can induce both neurogenesis and angiogenesis in an effort to repair the damaged brain (Moskowitz et al., 2010). There are two neurogenic niches located within the adult human brain important for neurogenesis, including the subgranular zone of the dentate gyrus and the subventricular zone (SVZ) of the lateral ventricles (van Strien et al., 2011). In the healthy adult brain, the SVZ contains neural progenitor cells that differentiate into neurons following migration to their target sites. For instance, neuroblasts within the SVZ will migrate to the olfactory bulb via the rostral migratory stream and differentiate into interneurons. Following ischemic stroke, these neuroblasts within the SVZ will migrate to the site of injury and differentiate into neurons (Moskowitz et al., 2010). However, 80% of newly generated neurons die (Arvidsson et al., 2002). Furthermore, it is unclear if those neurons that survive can function and integrate into the neural circuitry (Kannangara et al., 2018). Pharmacological strategies are being developed to stimulate neurogenesis and increase integration of neurons into neural circuits post-stroke (Marques et al., 2019).

Following stroke, brain plasticity occurs through a remapping of damaged neural circuits to adjacent healthy cortex or contralateral cortex (Murphy & Corbett, 2009; Nudo, 2003). Within hours to one-week post-stroke, neurons in the peri-infarct show reduced electrical activity, while those in the core die. One to 4 weeks post-stroke, growth factors, such as brain derived neurotrophic factor (BDNF), promote axonal projections to adjacent cortical areas and new synapses via synaptogenesis are formed (Murphy &

Corbett, 2009). These neurons become excitable and connections are strengthened. From 4 to 8 weeks, synaptic connections are refined and cortical regions adjacent to the peri-infarct now have circuits that were damaged within that peri-infarct. For example, connections from peri-infarct neurons within the forelimb somatosensory cortex will be integrated in the adjacent hindlimb somatosensory cortex (Murphy & Corbett, 2009). Studies have shown a reorganization of the contralateral cortex during functional recovery post-stroke (Buetefisch, 2015; Takatsuru et al., 2009). Takatsuru and colleagues showed remodelling and new neuronal circuits within the somatosensory cortex contralateral to the site of stroke induced injury in the ipsilateral somatosensory cortex (Takatsuru et al., 2009). Interestingly, stroke increased neuronal activity and dendritic spines within the contralateral cortex at 2 days and 1 week post-stroke, respectively (Takatsuru et al., 2009). This study suggests that remodeling of neuronal circuits occurs within the contralateral hemisphere following recovery from ischemic stroke. Overall, remapping and reorganization or neuronal circuits both adjacent to the infarct and within the contralateral cortex can promote functional recovery.

1.4 Animal models of ischemic stroke

There are numerous preclinical models of ischemic stroke in rodents. The majority of stroke models focus on blocking blood flow in large arteries or smaller arterioles. There are advantages and disadvantages with each model as to how accurately the injury replicates clinical stroke (Table 1.3).

Table 1.3: Ischemic stroke models.

Ischemic Stroke Model	Advantage	Disadvantage	Range of infarct size
MCAO (Permanent and transient MCAO)	Control of reperfusion Large penumbra	Produces large infarcts Produces progressive edema Sensitive to stroke duration	21-45% of hemisphere (Carmichael, 2005)
Embolic Stroke model	Testing of thrombolytics	Produces variable infarct size Partial reperfusion due to break down of clot	16.6-40% of hemisphere (Overgaard et al., 2010)
Vessel Occlusion (2-VO, 4-VO)	Mimics global ischemia such as malignant stroke or brain death following cardiac arrest	High variability Can induce seizures High mortality rate Invasive procedure	Large range with significant infarct size (Deng & Xu, 2009; Pontarelli et al., 2012)
Photothrombosis model	Precise occlusion of artery Reduced variability of infarct size	Produces rapid cytotoxic and vasogenic edema Early BBB breakdown Small penumbra	Smaller in size, Range from 1 to 1.5 mm^3 depending on duration of illumination (Clarkson et al., 2013)
Endothelin-1 model	Low mortality Gradual reperfusion Direct ET-1 application causing focal stroke	Species difference in ET-1 receptor expression Direct effect of ET-1 on brain cells such as astrocytes and neurons	Smaller in size from 1.43 to 40 mm^3, depending on concentration of ET-1 and brain area (Fifield & Vanderluit, 2020; Nguemeni et al., 2015)

1.4.1 Current rodent models of stroke

Several rodent ischemic stroke models use the introduction of a suture or ligation of a brain artery to induce stroke. The most widely used model is MCAO where an intraluminal suture permanently or temporarily occludes the MCA (Guan et al., 2012). This is accomplished by introducing the suture within either the internal or external carotid artery and advancing it to the MCA until blood flow is blocked (Fluri et al., 2015). The suture can be left permanently in place or removed to allow reperfusion of tissues typically following a duration of 60-, 90- or 120-minutes post-stroke (Fluri et al., 2015; Sommer, 2017). The vasoactive peptide ET-1 can also be injected adjacent to the MCA to constrict the artery and induce stroke (Biernaskie et al., 2001). The advantages of using MCAO as a stroke model include the ability to control the timing of reperfusion and the robust presence of a penumbra. Furthermore, occlusion of the MCA accounts for 70% of thromboembolic infarcts observed in the clinic (Fluri et al., 2015). The MCAO model results in significantly large infarcts in both mice and rats with progressive edema that mimics malignant stroke in the clinic (Carmichael, 2005). The majority of strokes are typically small with a range of 4.5 to 14% of the hemisphere being infarcted (Carmichael, 2005). In comparison, MCAO results in infarct sizes ranging from 21 to 45% of the affected hemisphere. Therefore, this model mimics a less common malignant stroke which can damage approximately 39 to 47% of the affected hemisphere, resulting in an 80% mortality rate (Simard et al., 2011). This model is also sensitive to the duration of stroke with a difference of 15 to 30 minutes resulting in a 6-fold increase in infarct volume in mice (McColl et al., 2004). As an alternative technique, the craniectomy model involves surgically removing the skull to expose the MCA for ligation (Fluri et al., 2015).

This technique allows for direct occlusion of the artery, however; there is a risk of damaging the brain during the craniectomy (Fluri et al., 2015). Although the size of an MCAO infarct in mice is not representative of the typical strokes observed in the clinic, the MCAO model does allow multiple brain regions to be examined following stroke, including the cortex and deeper cortical structures (Carmichael, 2005).

An alternative model is the embolic stroke model that involves introducing microspheres or a thrombin clot into the artery for occlusion. The clot is prepared using autologous blood advanced to the MCA via the internal carotid artery or thrombin can be directly injected into the MCA which can be difficult to access (Zhang et al., 2015). This model allows for testing of thrombolytics such as tPA in its effectiveness in breaking down the clot. However, the embolic stroke model produces infarcts of variable sizes depending on the blood vessel that is occluded (McCabe et al., 2018). The clot can break up spontaneously and occlude arteries beyond the MCA resulting in multiple smaller focal infarcts (McCabe et al., 2018). Furthermore, this would only partially occlude the MCA allowing for partial perfusion. The variability of infarct size using the embolic stroke model makes it difficult to reproduce and compare across studies.

Global ischemia can be achieved using the 2- or 4-vessel occlusion model (2-VO, 4-VO). The 2-VO model involves bilateral occlusion of the common carotid arteries (CCA), whereas the 4-VO model involves occlusion of four vessels including both CCAs and both vertebral arteries (Pontarelli et al., 2012; Schmidt-Kastner et al., 1989). The 4-VO model produces a large ischemic injury that mimics malignant stroke or brain death following cardiac arrest (Deng & Xu, 2009). There are several disadvantages of this model including variability in the brain areas that undergo ischemia which can include the

forebrain and hippocampus (Pontarelli et al., 2012). Furthermore, the surgeries for 4-VO are invasive requiring two days to complete (Deng & Xu, 2009). This model can also induce seizures and has a high mortality rate (Deng & Xu, 2009). Therefore, the 2-VO or 4-VO model is not an ideal ischemic stroke model.

The photothrombosis model uses intravenous injection of a photoactive dye, such as Rose Bengal and light activation of this dye to induce reactive oxygen radicals, such as superoxide formation causing endothelial injury (Fluri et al., 2015; McCabe et al., 2018; Uzdensky, 2018). A portion of the skull/bone is partially removed or thinned for the light illumination to reach the cortex. The injury to endothelial cells consequently activates platelets leading to their aggregation and thrombi formation (Watson et al., 1985). The photothrombotic stroke produces small focal infarcts by illuminating a specific wavelength of light directly on a specific blood vessel. Therefore, occlusion of the artery is precise reducing variability of infarct size among animals (Sommer, 2017). The smaller infarcts produced can range from 1.0 mm^3 to 1.5 mm^3 depending on the duration of light exposure (Clarkson et al., 2013). This technique produces cortical strokes; however, creating strokes in deeper structures is challenging as the depth of illumination through the tissue is limited. Furthermore, it has been reported that this model produces rapid cytotoxic and vasogenic edema leading to early BBB breakdown not typically observed in acute stroke in the clinic (Fluri et al., 2015; Lee et al., 1996). The penumbra region produced using this model is small in comparison to other stroke models such as MCAO (Fluri et al., 2015). The lack of a penumbra does not make this the ideal model to study tissue recovery in the acute post-stroke period.

The ET-1 ischemic stroke model produces a focal ischemic stroke by application of the vasoactive peptide ET-1 that causes vasoconstriction of arteries. Two endothelin receptors, ET-A and ET-B, are expressed on vascular smooth muscle cells and arteries. ET-A receptors cause vasoconstriction when bound, whereas ET-B receptors cause vasodilation through the release of nitric oxide (Verhaar et al., 1998). When applied, ET-1 causes significant reduction in CBF within 1 hour (60% reduction) and continues up to 3 hours (40% reduction) with gradual reperfusion occurring from 16 to 48 hours post-injection (Biernaskie et al., 2001; Fuxe et al., 1992; Hughes et al., 2003; Windle et al., 2006). An advantage of this model is gradual reperfusion of the ischemic injury which mimics clinical stroke. This gradual reperfusion reduces shear stress injury to the vascular endothelium typically observed in models such as transient MCAO where reperfusion is abrupt (Xu et al., 2018). Furthermore, the ET-1 stroke model produces focal infarcts with the presence of a substantial penumbral region that has the potential to be rescued (McCabe et al., 2018). Despite its increasing use, there are limitations when using the ET-1 model to induce ischemic stroke. ET-1 can be applied directly on the MCA or injected into the brain to cause local vasoconstriction of blood vessels around the injection site (Roome et al., 2014; Windle et al., 2006). Intra-cortical injection directly into the brain causes mechanical damage due to drilling of the skull and the injection itself which cannot be avoided. Another disadvantage is that the ET-1 peptide binds to ET-A and B receptors that are expressed on numerous brain cells including endothelial vascular cells, smooth muscle cells of blood vessels, astrocytes, neurons and microglia (Hughes et al., 2003). This can modify glia and neuron responses by activating endothelin receptors on these cells (Uesugi et al., 1996; Uesugi et al., 1998). Endothelin receptor expression is

different in rat and mouse tissues which can affect vasoconstriction and infarct progression between animals. For instance, the maximal constrictor response of the aorta to ET-1 was 11 ± 2.6% in mice compared to 93 ± 7% in rats (Wiley & Davenport, 2004). Rats have a higher expression of ET-A and infarcts are easily replicated. Mice express higher levels of ET-B than ET-A. To generate a consistent infarct, the concentration of ET-1 injected is increased and multiple (2-3) injections are required. This causes more mechanical damage than the single injection in the rat**.** Despite these limitations, ET-1 induced stroke produces focal infarcts that are representative of those observed in the clinic. The size of the strokes produced can be controlled with minimal variability. The ET-1 ischemic stroke model is used in this thesis to produce a small focal ischemic stroke within the cortex of mice.

1.4.2 Translating to the clinic

There are challenges of translating results from animal stroke models to therapies in the clinic. Over the last decade, basic science research has explored new therapeutic interventions in animal models of stroke; however, the overwhelming majority of treatments have failed to pass clinical trials yielding neutral or negative results (Jickling & Sharp, 2015). With over 1000 therapeutic agents tested using animal stroke models and 114 of these agents tested in acute stroke patients, only tPA has been found to be an effective treatment post-stroke (O'Collins et al., 2006).

Preclinical studies have failed to address stroke as a co-morbid neurovascular disease using healthy lean rodents as subjects (Haley & Lawrence, 2016). Decline in cardiovascular health that arises with age, unhealthy diets and lack of exercise can have a

profound effect on stroke outcome and this is not typically addressed in preclinical studies (Haley & Lawrence, 2016; Xu et al., 2019). For instance, rodents do not suffer from aging diseases as they have a lifespan of 2 to 3 years; whereas, stroke generally occurs in older humans (mean age 69 years) (Kissela et al., 2012). As well, some animal models induce massive ischemic damage to the brain that does not mimic typical strokes observed in the clinic (Carmichael, 2005). These models, such as MCAO, mimic malignant stroke in which recovery is poor. Furthermore, it is increasingly difficult to compare across studies with the use of so many stroke models and their modifications. Stroke models that use permanent occlusion can yield significantly different results in comparison to those that induce reperfusion with varying reperfusion times post-stroke. It is imperative to use a reproducible stroke model that most closely reflects the characteristics of clinical stroke. Therefore, in this thesis the ET-1 stroke model was chosen that produces small and consistent strokes representative of clinical stroke.

1.5 Dietary influences on ischemic stroke

Accumulating evidence has demonstrated that diet-induced obesity is an independent risk factor of ischemic stroke (Kernan et al., 2013; Meschia et al., 2014). Obesity has general adverse effects on the central nervous system (CNS) and periphery with increases in inflammation and vascular dysfunction (Asghar & Sheikh, 2017; Csige et al., 2018; Guillemot-Legris & Muccioli, 2017). Furthermore, previous studies have demonstrated that diet-induced obesity can exacerbate ischemic stroke leading to larger infarcts (Haley & Lawrence, 2016). However, the effect of diet-induced obesity on

cellular changes and their time course after small strokes that mimic covert stroke remain unclear.

1.5.1 The good fats versus the bad fats

The type of ingested fat can have a profound effect on modulating health and disease, especially inflammation and cardiovascular function (Jain et al., 2015; Teng et al., 2014). Saturated fatty acids and polyunsaturated fatty acids, such as omega-6 have been shown to be pro-inflammatory causing low-grade inflammation. These 'bad' fats are observed in the typical western diet and lead to increased white adipose tissue. Saturated fatty acids can bind to toll-like receptors and activate expression of inhibitor of nuclear factor kappa-B kinase subunit beta (IKKβ) and nuclear factor kappa-light-chain-enhancer of activated B cells (NF-κB) generating an inflammatory response (Schaeffler et al., 2009; Teng et al., 2014). Furthermore, omega-6, also known as linoleic acid, is a precursor for arachidonic acid, which can generate eicosanoids (Teng et al., 2014). These eicosanoids, which include prostaglandins, thromboxanes and leukotrienes, are mediators of pro-inflammatory cytokines (Innes & Calder, 2018).

In contrast, omega-3 is a 'good fat' that is anti-inflammatory (Teng et al., 2014). Two examples of omega-3 fats, eicosapentaenoic acid (EPA) and docosahexaenoic acid (DHA) reduce the production of pro-inflammatory mediators through binding to the receptor G protein-coupled receptor 120 (GPR120) that in turn, inhibits NF-κB signalling (Teng et al., 2014). Furthermore, both EPA and DHA reduce the expression of adhesion molecules on blood vessels thereby limiting leukocyte interactions with endothelial cells (Baker et al., 2018). The vascular response to ischemic injury causes an increase in the

expression of adhesion molecules on endothelial cells (Yilmaz & Granger, 2008). This causes the circulating leukocytes to slow down and stick to the wall. The longer the leukocyte adheres to the blood vessel wall, the greater the incidence of the leukocyte penetrating the wall and entering the brain (Yilmaz & Granger, 2008). Therefore, reducing the expression of adhesion molecules on endothelial cells limits leukocyte adhesion and infiltration into the brain. The increased expression of adhesion molecules on endothelial cells, such as intercellular adhesion molecule-1 (ICAM-1) and Vascular Cell Adhesion Molecule 1 (VCAM-1) also occurs in the development of atherosclerosis, and can be reduced with omega-3 diet or supplements (Baker et al., 2018; Fotis et al., 2012). Omega-3 has been shown to improve cardiovascular function as the metabolites of omega-3 dilate coronary arterioles (Ye et al., 2002). Overall, the type of fat can modify inflammatory and cardiovascular processes and be either detrimental to neurovascular health or prevent neurovascular disease.

1.5.2 Diet-induced obesity and the effects on the brain

One of the main effects of prolonged high-fat diet is an increase in neuroinflammation within the brain. This is due in part to an increase in inflammation caused by the high-fat diet itself and excessive peripheral adipose tissue. High-fat diet increases circulating fatty acids that can activate the immune system via toll-like receptors, producing pro-inflammatory cytokines and chemokines such as TNF-α, IL-1β and CCL2 (Guillemot-Legris & Muccioli, 2017). These circulating pro-inflammatory mediators can act on endothelial cells or cross the BBB activating neuroinflammation within the brain. This could occur early and within 24 hours of HFD feeding in rats without an increase in adipose tissue, and is characterized by increased mRNA expression

of pro-inflammatory cytokines TNF-α, IL-1β and IL-6 and an increased number of microglia in the hypothalamus (Thaler et al., 2012). This demonstrates that HFD itself can induce inflammation within the brain even in the absence of weight gain. In addition, prolonged high-fat diet causes adipocytes to become hypertrophic and release pro-inflammatory adipokines, such as leptin, adiponectin, IL-6 and TNF-α (Arnoldussen et al., 2014). These adipokines can cross the BBB to impair synaptic plasticity, neurogenesis, and cognitive function in the obese brain (Arnoldussen et al., 2014; Pickering et al., 2005). Furthermore, macrophages that reside within adipose tissue will become activated and switch from M2 to the pro-inflammatory M1 polarization (Guillemot-Legris & Muccioli, 2017). This chronic low-grade inflammation has been shown to induce cognitive deficits and learning and memory impairments (Arnoldussen et al., 2014; Cordner & Tamashiro, 2015). Overall, chronic high-fat diet feeding can lead to persistent inflammation within the brain and periphery.

Diet-induced obesity can alter cerebrovascular function leading to reduced cerebral blood perfusion with the brain (Ayata et al., 2013; Dorrance et al., 2014). This can be attributed to disruption of vasomotor activity and reduced intraluminal diameter of large cerebral arteries (Ayata et al., 2013; Deutsch et al., 2009; Li et al., 2013). Prolonged HFD impairs resting CBF and neurovascular coupling within the brain, which may be due to impaired autoregulation of cerebral vascular tone (Li et al., 2013). Previous studies have also shown that cerebral blood vessels are narrower and stiffer with chronic HFD (Deng et al., 2014; Deutsch et al., 2009). Vascular remodeling that occurs with chronic HFD feeding can affect cerebrovascular function within the brain. The effects of HFD on

inflammation and the vasculature can make the brain more susceptible to injury following ischemic stroke.

1.5.3 Stroke studies examining diet-induced obesity in rodent models

Previous studies have shown that diet-induced obesity can exacerbate ischemic stroke causing larger strokes within the brain (Cao et al., 2015; Herz et al., 2015; Maysami et al., 2015). These studies showed that the duration of both HFD feeding and artery occlusion can affect the severity of the ischemic insult. Diet-induced obesity has also been shown to alter inflammation and increase the severity of the ischemic injury (Maysami et al., 2015; Terao et al., 2008). HFD fed mice showed increased expression of chemokines CCL3 and CXCL-1 within the ischemic brain 24 hours following 30 minute MCAO (Maysami et al., 2015). This was associated with an increase in neutrophil infiltration in the brain. Increases in CXCL chemokines can recruit neutrophils and this is mediated by expression of CXCR-2 specific to neutrophils (Stadtmann & Zarbock, 2012). Previous studies have also shown an upregulation of adhesion molecules ICAM-1 and VCAM-1 within cerebral blood vessels with HFD and western diet (Cao et al., 2015; Herz et al., 2014; Herz et al., 2015). These adhesion molecules mediate infiltration of neutrophils and other leukocytes into the ischemic brain (Gonzalez-Amaro et al., 1998). Once in the brain, neutrophils can worsen ischemic stroke through oxidative stress by producing enzymes such as iNOS, NADPH oxidase and myeloperoxidase which can directly damage cells and the vasculature (Beray-Berthat et al., 2003; Herz et al., 2015; Sun et al., 2018). Overall, this demonstrates that chronic inflammation associated with prolonged HFD can worsen ischemic stroke outcomes.

Studies have shown that diet-induced obesity can disrupt the BBB leading to increased permeability within the ischemic brain (Deng et al., 2014; Maysami et al., 2015; McColl et al., 2010; Terao et al., 2008). Rats/mice fed HFD for 6 months, had a 5% increase in IgG extravasation into the brain than chow fed rat/mice at 24 hours following a 20 minute MCAO (Maysami et al., 2015). This increase in IgG extravasation within the brain was also observed in mice following 10 weeks of HFD and a longer 90 minute MCAO (Deng et al., 2014). Interestingly the increase in IgG extravasation was mouse strain specific with a 5% increase observed in CD1 mice and 10% increase in C57BL/6J mice, which are more prone to obesity (Deng et al., 2014). The IgG extravasation is mediated by matrix metalloproteinase (MMP) activity. MMP are endopeptidases that can degrade the basement membrane of cerebral blood vessels and impair the integrity of the BBB (Yang et al., 2019). Genetic ablation of MMP-9 attenuated the IgG extravasation observed in wild type mice fed HFD (Deng et al., 2014). Indeed, studies have shown an increase in MMP activity, such as MMP-9 and MMP-2 in obese rodents (Deutsch et al., 2009; McColl et al., 2010). Cycolooxygenase-2 (COX-2) has also been implicated in BBB breakdown post-stroke and HFD increases COX-2 expression mainly in monocytes/macrophages (Lee et al., 2001; Zhang et al., 2005). Metabolism of arachidonic acid via COX-2 generates ROS and prostanoids that leads to a pro-inflammatory environment within the brain (Smith et al., 2000). Increases in circulating COX-2, in turn causes increased damage resulting in larger infarct volumes (Dhungana et al., 2013; Zhang et al., 2005). COX-2 disrupts the BBB after ischemic stroke due to ROS generation and proinflammatory mediators (Candelario-Jalil et al., 2007; Frankowski et al., 2015). Interestingly, inhibition of COX-2 reduces MMP-3/MMP-9 activity

demonstrating a link between PGE2 signaling and MMP mediated disruption post-stroke (Frankowski et al., 2015). Overall, prolonged HFD exacerbates BBB disruption which is mediated through increases in both COX-2 and MMP activity.

1.5.4 The effect of omega-3 following ischemic stroke

Omega-3 polyunsaturated fatty acids, such as DHA can have a protective effect on the ischemic brain (Belayev et al., 2009; Eady et al., 2012). Numerous studies have shown that Omega-3s reduce inflammation and oxidative stress post-stroke, which attenuates BBB breakdown and reduces infarct volume (Belayev et al., 2018; Chang et al., 2013; Hong et al., 2015; Shi et al., 2016). For instance, pre-treatment of DHA for 3 days prior to a permanent MCAO reduced mRNA expression of pro-inflammatory cytokines TNF-α, IL-1β and IL-6. This DHA treatment reduced infarct volume approximately 15% in comparison to controls given a saline injection (Chang et al., 2013). Furthermore, post-treatment of DHA at 3 hours following an MCAO reduced Evans Blue extravasation by 30% at 6 hours, 48% at 24 hours and 38% at 72 hours post-stroke (Hong et al., 2015). DHA's neuroprotective effect was also observed in rodents fed a DHA rich diet prior to the stroke (Lalancette-Hebert et al., 2011; Luo et al., 2018; Zhang et al., 2014). Previously, it was shown that 3 months of a DHA enriched diet significantly reduced levels of COX-2 and IL-1β within the brains of mice (Lalancette-Hebert et al., 2011). The efficacy of DHA in reducing ischemic damage depends on its mode of administration, the dose of DHA injected and whether it is applied prior to stroke or afterward (Belayev et al., 2009; Pu et al., 2016). DHA i.p. injections (10 mg/kg) combined with an Omega-3 rich diet significantly reduced brain atrophy, while each

treatment alone was insufficient (Pu et al., 2016). Belayev and colleagues showed that a low to medium range of DHA doses (3.5 to 35 mg/kg) given 3 hours following 60 minute MCAO all significantly improved neurological scores at 24 hours to 7 days post-stroke (Belayev et al., 2009). In contrast, a higher DHA dose (70 mg/kg) did not improve these scores. The time at which DHA is introduced can also affect post-stroke outcomes, (i.e. as a pre-treatment or post-treatment). A pre-treatment study showed that 3 weeks of fish oil supplement containing 60% DHA reduced the size of cerebral microinfarcts 7 days following penetrating arteriole occlusion (Luo et al., 2018). The majority of DHA studies have been performed using the MCAO model which produces larger infarcts. It is unknown whether application of DHA in the acute post-stroke period can affect the ischemic response to a small stroke, which will be explored in this thesis.

1.6 Rationale and Hypothesis

Previous studies have shown the detrimental effects of diet-induced obesity on post-stroke outcomes (Asghar & Sheikh, 2017; Sorop et al., 2017). However, the effect of diet-induced obesity on the cellular responses following smaller focal strokes is not as well understood and will be explored in this thesis. Few studies have examined the cellular response in relation to the level of blood perfusion in the affected brain tissue in the context of HFD. Thus, the distinct cellular responses that occur within the ischemic core and penumbra overtime is unclear. Healthy fats such as omega-3 have been shown to reduce injury following ischemic stroke in rodents (Lalancette-Hebert et al., 2011). However, the potential use of healthy fats as a treatment following acute ischemic stroke in lean and obese mice has yet to be explored. Studies have neglected the influence of

diet-induced obesity on the cellular events following acute ischemic stroke. This is a critical gap in knowledge, as it is within this acute post-stroke period that the penumbra has the greatest potential for rescue thereby minimizing further neurological damage. Therefore, this thesis will focus on the progression of stroke within the penumbra during the acute period.

Hypothesis: High fat diet is known to exacerbate the injury response to ischemic strokes. Here, I hypothesize that prolonged high fat diet negatively impacts the brain and vasculature such that it also exacerbates the injury response to a very small covert-like ischemic stroke. This damage will be observed early within the acute and sub-acute period post-stroke. I will assess the impact of prolonged high fat diet on the cellular response within both the infarct core and the penumbra.

To address this hypothesis, I have the following three objectives:

Objective #1: Assess the impact of high fat diet-induced obesity on the cellular responses during the sub-acute period following a covert-like stroke (Chapter 2).

Objective #2: Characterize the cellular response within the ischemic core and penumbra during the acute post-stroke period (Chapter 3).

Objective #3: Assess the effect of post-stroke DHA application on the acute cellular to stroke in diet-induced obese mice and lean controls (Chapter 4).

CHAPTER 2

PROLONGED HIGH FAT DIET WORSENS THE CELLULAR RESPONSE TO A SMALL, COVERT-LIKE ISCHEMIC STROKE

CO-AUTHORSHIP STATEMENT

I, Kathleen Fifield, designed the experiments with my supervisor Dr. Jacqueline Vanderluit. For chapter 2, I performed all experiments and made all figures with edits from my supervisor. Todd Rowe aided in brain dissections for *in vitro* blood vessel constriction experiments. Joanna Raman-Nair completed part of the quantification for the *in vitro* blood vessel constriction experiment presented in Fig. 2.3. Both Dr. Michiru Hirasawa and Dr. Jacqueline Vanderluit edited writing for publication. This study is currently published: Fifield, K., E., Rowe, T., M., Raman Nair, J., Hirasawa, M., Vanderluit, J., L. (2019). Prolonged high-fat diet worsens the cellular response to a covert-like ischemic stroke. *Neuroscience*, *406*: 637-652.

2.1 Introduction

Diet-induced obesity is linked to an increased risk of developing cardiovascular diseases such as ischemic stroke. Among those who experience a stroke, obese individuals experience more complications, longer hospitalization stays, and have less functional improvement than lean individuals (Kalichman et al., 2016; Razinia et al., 2007; Yaegashi et al., 2005). Preclinical studies have similarly demonstrated that diet-induced obesity in rodents results in larger infarcts and more severe behavioral deficits (Haley & Lawrence, 2016). However, it is unclear how diet-induced obesity affects the cellular response to a focal ischemic stroke to cause larger infarcts with worse outcomes. With the increasing incidences of obesity and stroke in both aging and youth populations in the western world, there is a need to better understand the impact of obesity on strokes and their outcomes.

The most common form of stroke is ischemic stroke which accounts for 85% of all strokes (Smith, 2011). Ischemic stroke is caused by the occlusion of a cerebral blood vessel where the resulting infarct size depends on the size of the blood vessel that is occluded. Overt strokes occur in large arteries and cause significant damage to the brain with obvious physical and mental deficits. Covert strokes occur in smaller arteries or arterioles and result in small infarcts with subtle deficits that are often only diagnosed with brain imaging (Longstreth, 2005). The incidence of covert strokes to overt strokes is 5:1 indicating that the majority of strokes are very small ("Mind the Connection: Preventing stroke and dementia," 2016). Despite this, the majority of pre-clinical stroke research has utilized middle cerebral artery occlusion (MCAO), which models overt strokes. Occluding the middle cerebral artery causes extensive damage in both cortical

and striatal regions within the brain leading to extensive edema, a robust inflammatory response and a large ischemic core with a progressively expanding infarct (Carmichael, 2005). These large infarcts are not reflective of strokes more commonly seen in the clinic in which patients survive. Animal models of clinically relevant, smaller strokes are necessary to examine the impact of diet-induced obesity on the cellular response to stroke. One model of a very small stroke with a minimal ischemic core in mice can be induced by intra-cortical microinjections of the vasoactive peptide ET-1, which induces a robust constriction of blood vessels localized around the injection site (Roome et al., 2014).

Occlusion of cerebral blood vessels to less than 20% of total CBF results in a non-perfused region producing an ischemic core where cell death is immediate and untreatable (Bandera et al., 2006; Moskowitz et al., 2010). Surrounding the core is the penumbra with an area of CBF of >20% to <40% in which cells may survive but are susceptible to further damage if blood flow is not reinstated in a timely manner. Maintaining the health of brain tissue in this susceptible region may prevent expansion of the infarct during the sub-acute period following stroke. It is largely unknown whether pre-existing conditions such as obesity or prolonged consumption of a HFD affects the sensitivity of the brain to further damage within this susceptible region.

At the cellular level, the loss of blood flow during ischemic stroke disrupts cell-cell interactions within the neurovascular unit consisting of neurons, astrocytes, microglia and vascular endothelial cells, which are essential for forming the BBB and for the exchange of nutrients between the blood and the brain (Daneman & Prat, 2015). Ischemia causes injury to vascular endothelial cells resulting in a breakdown of the BBB and the

invasion of immune cells from the blood, and the subsequent activation of astrocytes and microglia. Astrocytes upregulate the expression of GFAP and migrate to form a glial scar around the injury to protect neurons outside the injury from invading immune cells and exposure to pro-inflammatory molecules (Barreto et al., 2011). Microglia change from a resting, highly ramified cell to an amoeboid-shaped cell that phagocytose debris within the injury (Patel et al., 2013). In the acute phase post-stroke, microglia release pro-inflammatory molecules that cause further destruction within the injury; however, as the injury resolves, microglia switch to producing anti-inflammatory molecules that are beneficial to the surviving cells (Liu et al., 2016). Obesity is associated with chronic low-grade inflammation that is believed to be the cause of the increased release of inflammatory mediators and immune cell infiltration into the brain following MCAO (Cao et al., 2015; Denes et al., 2010; Deng et al., 2014; Maysami et al., 2015; Terao et al., 2008). Whether obesity affects the cellular response within the neurovascular unit in a covert stroke model still needs to be explored.

The aim of this study was to examine the impact of a chronic HFD on the behavioral and cellular response to a clinically relevant, small, focal ischemic injury. The Vanderluit lab has previously shown that ET-1 injections targeted to the anterior forelimb motor cortex results in a reproducible, small infarct with measurable behavioral deficits (Roome et al., 2014). Furthermore, injections outside of the target area of the anterior forelimb motor cortex do not elicit behavioral deficits. This model therefore, allows for a direct functional assessment of a well-localized focal ischemia that may be comparable to covert strokes (Roome et al., 2014). Following intra-cortical injections of ET-1 or saline, dextran-conjugated Texas Red was used to label perfused blood vessels and explore the

effect of diet-induced obesity on the cellular response in the non-perfused core, the hypo-perfused surround and the perfused region around the infarct. This study demonstrates that prolonged HFD significantly exacerbates the response to a small covert-sized stroke by worsening the cellular response within and around the infarct with different levels of blood perfusion.

2.2 Methods

2.2.1 Mice

A total of 59 male C57BL/6 mice (Charles River Laboratories, QC, Canada) were used in this study. C57BL/6 mice were used in this study because they are more susceptible to HFD-induced increases in body weight and adipose tissue in comparison to other mouse strains (Chu et al., 2017). 39 mice were used for *in vivo* stroke experiments, 16 mice were used for *in vitro* blood vessel constriction experiments and 4 untreated naïve mice were used to assess endogenous numbers of microglia. Animal experiments were conducted in compliance with the ARRIVE (Animal Research: Reporting of *In Vivo* Experiments) guidelines (Kilkenny et al., 2010). Experimental procedures were approved by Memorial University of Newfoundland's Institutional Animal Care Committee adhering to the Canadian Council on Animal Care guidelines.

2.2.2 In vivo stroke experiments

Mice were single housed and maintained on a 12:12 hour light-dark cycle. 39 mice were fed either standard rodent chow (Chow) (14% fat; Lab Diets, MO, USA, Prolab RMH 3000, Cat. # 0001495) or HFD (60% fat; Research Diets, NJ, USA, Cat. #

D12492) starting at 4 weeks of age until euthanasia. Food and water were provided *ad libitum*. Mice were weighed once a week at the same time of day. After twelve weeks, mice were assigned to one of four groups: (i) Chow+Saline; (ii) HFD+Saline; (iii) Chow+Endothelin-1 (ET-1); and (iv) HFD+ET-1.

Stereotaxic surgery was performed under isofluorane anaesthesia using an isoflurane vaporizer (Harvard Apparatus, Cat. # 340471). A subcutaneous (s.c.) injection of Buprenorphine (0.02 mg/kg, Temgesic, Animal Resources Centre, Montreal, QC), an analgesic, was given immediately following anaesthesia. A mouse stereotaxic instrument (David Kopf Instruments, Tujunga, CA, USA, Cat. # 308019R) was used to conduct the surgery. An Ideal Microdrill (Cellpoint Scientific, Gaithersburg, MD, USA, Cat. # 67-1000) was used to drill a hole in the skull at each coordinate. A pulled glass pipette attached to a 5 µl Hamilton syringe (Hamilton Co, Reno, NV, USA, Cat. # 7633-01) was used for injections and flow rate was controlled using a syringe pump (Fusion 100, Chemyx Co, Stafford, Tx, USA). Two intra-cortical injections were made into the anterior forelimb cortex at the following coordinates relative to bregma: (i) +0.2 anterior-posterior (AP), +1.5 medial-lateral (ML), -1.0 dorsal-ventral (DV) and (ii) +1.0 AP, +1.5 ML, -1.0 DV. For each injection site, 1µl of saline (0.9% Saline) or 1 µl of ET-1 (2 µg/µl, Cedarlane, Cat. # 05-23-3800) was injected over a 5-minute period at a rate of 0.2 µl/min. Following each injection, the pipette was left in place for 5 minutes to avoid backflow when removed. Injections of saline were used to control for both the damage due to the needle injury and the injection volume. Body temperature was monitored with a rectal probe and maintained at 37.0ºC ± 0.5ºC (TC Data Logger Thermometer, Omega

Engineering Inc., Stamford, CT, USA, Cat. # HH127). Following surgery, mice were placed in their home cage on top of a heating pad to prevent hypothermia for a minimum of 2 hours. The animal's wellness was monitored and recorded twice a day until euthanasia. This included monitoring body weight, appetite, hydration and piloerection. Body weight was recorded and the minimal allowable body weight loss was 20% from baseline. Mice were euthanized if greater than 20% weight was lost (n=0).

Criterion for inclusion into the study required that the injury/infarct was located within the anterior forelimb motor cortex as described in Section 2.2.6. Ten mice were excluded from the study for failure to meet this criterion. In addition, one mouse died one day post-surgery and two mice were excluded due to surgical complications leaving a total of 26 mice in the *in vivo* stroke experiments. The number of mice per group was as follows: Chow+Saline n=5; HFD+Saline n=7; Chow+ET-1 n=6; and HFD+ET-1 n=8.

2.2.3 Behavioural testing

Behavioural deficits were assessed during the light cycle using the cylinder test, which assesses forelimb motor deficits (Roome & Vanderluit, 2015). The mouse was placed in a transparent plexiglass cylinder (94 mm diameter) that was placed on a transparent table, so that behaviour could be filmed from below using a digital Sony Handycam (Sony, North York, Ontario, Canada, Cat. # DCR-SR42). Filming took place for a minimum of 5 minutes or until the mouse reared and touched the cylinder wall a minimum of 20 times. Cylinder testing was conducted one day before surgery to establish a baseline of behavior and at 1 day and 7 days post-surgery. "Paw-dragging behaviour" was assessed using VLC media player (https://www.videolan.org/vlc/index.html). Paw

dragging was assessed by examining the dragging of the affected limb when the mouse reared in the cylinder, made contact with the wall and subsequently dragged its paw towards its center or down in a vertical direction (Roome et al, 2014; Roome & Vanderluit 2015). For each forelimb paw, the number of total paw drags against the cylinder wall was counted and presented as a percent of the total number of paw touches. Counts were performed on the affected and unaffected limbs (contralateral and ipsilateral to the intra-cortical injections, respectively). All counts were performed blind to treatment and time post-surgery. Four HFD-fed mice were inactive and did not explore the cylinder resulting in their exclusion from the behavioral analysis. Therefore, the number of mice per group for behavioral analysis was as follows: Chow+Saline *n=5*, HFD+Saline *n=6*, Chow+ET-1 *n=6*, HFD+ET-1 *n=5*.

2.2.4 Tissue processing

At 7 days post-surgery, mice were injected intra-peritoneally with Euthanyl (250 mg/ml sodium pentobarbital, Vetoquinol, Cat. # IEUS001). Once mice became unresponsive and while the heart was still beating, 250 µl dextran-conjugated Texas Red (1 µg/µl dissolved in 0.9% saline, Invitrogen, Cat. # D1864) was injected into the left ventricle. The dextran was allowed to circulate within the mouse vascular system for approximately 2 minutes before dissection occurred (Grade et al., 2013). Brains were then dissected and blocked using a 1 mm coronal acrylic brain matrix so that the anterior and posterior portions of the brain, not including the stroke region, were discarded. This was to ensure greater diffusion for preservation throughout the blocked part that contained the stroke. The brain region containing the infarct was fixed in 4% w/v paraformaldehyde in

phosphate buffered saline (1XPBS; 137 mM NaCl, 2.7 mM KCl, 10 mM Na_2HPO_4, 1.8 mM KH_2PO_4), pH 7.4 overnight at 4 ^oC for two consecutive days. Brain sections were then cryoprotected in increasing concentrations of sucrose (12%, 16% and 22% w/v) in 1X PBS, pH 7.4 over three days and then embedded in Tissue-Tek O.C.T. (Sakura Finetek, CA, USA, Cat. # 4583) and frozen in isopentane cooled in dry ice. At the time of dissection, the epididymal, retroperitoneal and perirenal fat pads were extracted and the combined weight was used as a measure of adiposity.

Frozen brains were sectioned using a cryostat microtome (Micron HM 520 Cryostat, Fisher scientific, PA, USA, Cat. # 12-550-15). Serial coronal sections throughout the rostral to caudal brain were collected on Superfrost Plus microscope slides (Fisher Scientific, PA, USA, Cat. # 12-550-15) until the entire infarct was collected. Serial sections were collected across sets of 6 slides, such that the sections on each slide represented sections 140 µm apart. The sixth slide of every set was used for Cresyl violet histology and the other slides were stored at -80 ^oC until immunohistochemical processing.

2.2.5 Cresyl violet staining

Cresyl violet staining was conducted on representative slides throughout the rostral to caudal extent of the infarct. Slides were placed on a slide warmer at 37 ^oC for 20 minutes then placed in 0.1% w/v Cresyl Violet solution (3.1 mM Cresyl Violet acetate (Sigma, Cat. # C-1791), 40 mM glacial acetic acid, 325 mM NaOAc adjusted to pH 5.2 and filtered) for 30 minutes. Slides were then dehydrated in increasing concentrations of ethanol (EtOH) (50%, 75%, 90%, 95% and three times in 100% ethanol) for 30 seconds

each. Slides were then placed in isopropanol for 30 seconds and toluene two times for 1 minute each. Slides were coverslipped using Permount (Fisher Chemical, NJ, USA, Cat. # SP15-500) and Fisherbrand Microscope Cover Glass (Fisher Scientific, NH, USA, Cat. # 12545C).

2.2.6 Infarct volume calculation and targeting the anterior forelimb motor cortex

Cresyl violet-stained coronal brain sections from the rostral to caudal extent of the injury were used to measure infarct volumes and then corrected for edema (Roome et al., 2014). Sets of slides that contained every tenth section and therefore were 140 µm apart were used for this measurement. Each section was photographed with a Zeiss Stemi-2000C dissecting microscope with an attached Zeiss Axiocam Mrm Rev3 camera. The area of the ipsilateral cortex containing the infarct and the contralateral cortex were measured using the outline tool in AxioVision v4.8 software. The area of the infarct was calculated by subtracting the healthy ipsilateral cortex from the healthy contralateral cortex.

Infarct volume=∑ [(healthy contralateral cortical area-healthy ipsilateral cortical area) x 14 µm] x 10 (interval between sections)

Infarct volume was corrected for edema by applying an average edema scaling factor per each infarct that was defined as the ratio between the ipsilateral cortex area to the contralateral cortex area. This ratio was measured for each section and then averaged to obtain an edema scaling factor for each mouse:

Edema scaling factor= [∑ (ipsilateral cortical area/contralateral cortical area)]/number of sections

The corrected infarct volume was calculated by multiplying the infarct volume measurement by the average edema scaling factor (Belayver et al., 2005; Langdon et al., 2010). Two animals were removed from infarct volume calculations due to incomplete sectioning of the injury. Infarct volume was measured in the following number of animals per treatment group (Chow+Saline n=5, HFD+Saline n=6, Chow+ET-1 n=6, HFD+ET-1 n=7).

The location of each infarct was mapped and only infarcts that were located within the anterior forelimb motor cortex and considered "on-target" were included in the study (Roome et al., 2014). The depth of the infarct was measured from the pia to the corpus callosum in 250 µm intervals medial to lateral and presented as the percent depth of damage. For example, if the injury extended entirely from the pia to the corpus callosum this would indicate 100% damage. This was calculated across the injury anterior-posterior at 140 µm intervals. From this, the center of the infarct (most damage) could be determined and then mapped using a map of the forelimb motor cortex and mouse brain atlas (Franklin & Paxinos, 2008; Tennant et al., 2011). Infarcts that were primarily contained with the anterior portion of the forelimb motor cortex were considered "on target" and included in the study (Fig 2.1). Those infarcts that were not centred in this area were considered "off target" and excluded from analysis (n=10).

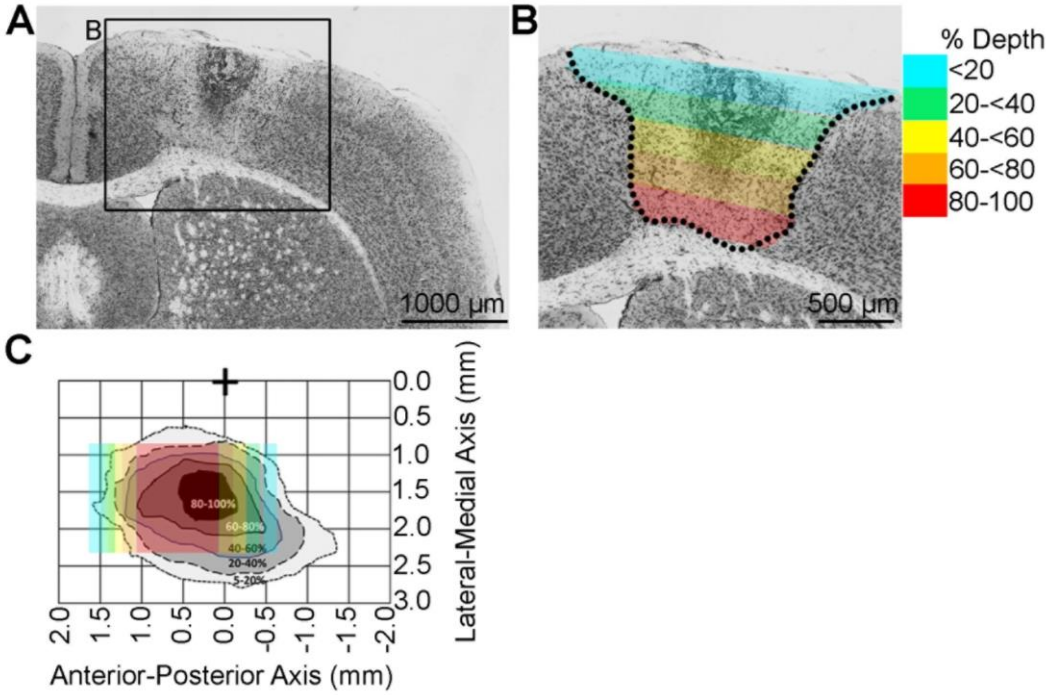

Figure 2.1: Mapping to the anterior forelimb motor cortex.

(A) Low magnification image depicting coronal brain section with infarct. (B) Higher magnification shows the infarct within cortex. Dotted lines outline injury. Infarct damage was represented as % depth of damage so that 100% damage extended from the pia to the corpus callosum. This damage was then mapped to the anterior forelimb motor cortex. (C) Map of the forelimb motor cortex. Blocks overlaying the map indicate the depth of damage so that red blocks are 80% to 100% depth and are concentrated over the anterior portion of the forelimb motor cortex. If the greatest damage (80% to 100%) of the infarct did not overlay within this region, those infarcts were considered “off target” are excluded from the study.

2.2.7 Immunohistochemistry

Immunohistochemistry was completed on brain sections containing the center of the infarct. Primary antibodies to the following antigens were used: CD68 (1:400, AbD Serotec, Cat. # MCA1957, RRID: AB_322219), COX-2 (1:200, Cayman Chemical, Cat. # 160126, RRID: AB_327872), glial fibrillary acidic protein (GFAP,1:400, Dako, Cat. # Z0334, RRID: AB_10013382), ionized calcium binding adaptor molecule-1 (Iba-1, 1:1000, Wako Chemicals, Cat. # 019-19741, RRID: AB_839504), neuronal nuclei (NeuN,1:100, Millipore, Cat. # MAB-377, RRID: AB_2298772), platelet endothelial cell adhesion molecule-1 (PECAM-1, 1:200, BD Biosciences, Cat. # 550274, RRID: AB_393571), TMEM119 (1:100, Abcam, Cat. # ab209064, RRID: AB_2728083) and VCAM-1 (1:200, Abcam, Cat. # ab134047, RRID: AB_2721053). Sections for NeuN immunofluorescence underwent a 3-minute acetone pre-treatment. Slides were incubated with primary antibodies overnight in a humidity chamber at room temperature. The next day, after washes the slides were incubated with the appropriate secondary antibody for one hour in a humidity chamber at room temperature in the dark. For fluorescent immunohistochemical detection, the following secondary antibodies were used: anti-mouse Alexa Fluor 488 antibody (1:200, Invitrogen, Cat. # A21202, RRID: AB_2535788), anti-rabbit Alexa Fluor 488 antibody (1:200, Invitrogen, Cat. # A21206, RRID: AB_2535792) or anti-rat Alexa Fluor 488 antibody (1:200, Invitrogen, Cat. # A21208, RRID: AB_2535794) followed by Hoechst (0.05 mg/ml dissolved in 1XPBS, Bisbenzimide H33258, Sigma Chemical Co., Cat. # 1155) staining to label nuclei. An anti-rabbit DyLight 649 antibody (1:200, Jackson ImmunoResearch, Cat. # 111496144) was used for double immunohistochemistry to detect antibodies to CD68. Slides were

coverslipped with 1:3 glycerol:1x PBS solution and nail polish was used to seal the coverslips. For enzymatic immunohistochemical detection, the secondary antibody, anti-rabbit IgG (H+L)-HRP conjugate (1:200, Bio-Rad Inc., Cat. #170-6515, RRID: AB_11125142) was used. The 3,3'-Diaminobenzidine (DAB) reaction was performed according to manufacturer's instructions (Cedarlane, Cat. # SK-4100, RRID: AB_2336382). The substrate working solution was prepared by adding the following to 5 ml of tap water: 84 µl of Buffer stock solution, 100 µl of DAB stock solution, 80 µl of H_2O_2 solution and 80 µl of Nickel solution. Four drops (approximately 100 µl) of this solution was placed on each section and developed in the dark. Brain sections were rinsed in H_2O then dehydrated by transferring slides through a series of increasing concentrations of ethanol solutions (50%, 75%, 90%, 95% and three times in 100% EtOH 30 seconds each) followed by isopropanol and toluene before coverslipping with Permount (Fisher Scientific, Cat. # SP15-500).

2.2.8 Immunofluorescence with Fluoro-Jade C staining

Immunofluorescence with antibodies against NeuN was performed as described followed by Fluoro-Jade C (Millipore Sigma, Cat. # AG325) staining to examine degenerating neurons within the infarct. For Fluoro-Jade C staining, slides were pre-treated in 1% w/v sodium hydroxide in 80% EtOH for 5 min, followed by 70% EtOH for 2 min and washed in water for 2 min followed by 0.06% w/v potassium permanganate ($KMnO_4$), for 4 min and washed in water for 2 min. Slides were then stained in 0.0001% v/v Fluoro-Jade C solution diluted in 0.001% v/v acetic acid (pH 4.5) for 10 min and

rinsed in tap water. After drying overnight on a slide warmer at 37 ºC, slides were then coverslipped with DPEX (Cedarlane, Cat. # 13514).

2.2.9 Microscopy, Cell Counts and Densitometry

Images were photographed on a Zeiss Imager.Z1 upright microscope (5x, 10x and 20x objectives) or a Zeiss Stemi-2000C dissecting microscope with a ZeissAxiocam Mrm Rev3 camera (Carl Zeiss, Germany) and analysed using Zeiss AxioVision v4.8 software. Whole brain images (Figure 2.7 A,C) were photographed using a Cytation 5 cell imaging multi-mode reader (Biotek, VT, USA). Figures were compiled using Adobe Photoshop C2 (San Jose, CA, USA) and contrast and brightness were adjusted equally for all images.

Cell counting and densitometry analyses were performed on two to three 14 µm-thick coronal sections per mouse spaced at 140 µm intervals using ImageJ software (http://rsbweb.nih.gov/ij/). Iba-1+ cells were counted in three separate boxed areas (200 µm X 200 µm) per section around the infarct border and within the contralateral hemisphere. CD68+, TMEM119+ and double-labelled (CD68+ and TMEM119+) cells were counted within the infarct core (200 µm X 200 µm in two boxed areas per section). For naïve animals, TMEM119+ cells were counted within two boxed areas (200 µm X 200 µm) per section with 3 sections per animal. GFAP densitometry analysis was performed on five separate boxed areas (100 µm x 100 µm) at each distance from the infarct border: 0, 200 and 800 µm per section in 3 sections per animal. The Rodbard optical density calibration in ImageJ was used for densitometry analysis. The relative density of staining in each area was calculated by subtracting the background density in an area void of GFAP staining from that of the area of interest and then dividing by the

background density. NeuN+ cells were counted in three separate boxed areas (200 µm x 200 µm) per section, 3 sections per animal, within the non-perfused, hypo-perfused and perfused regions at equal depths of 500 µm from the pial surface. Fluoro-Jade C+ cells and double-labelled (Fluoro-Jade C+ and NeuN+) cells were counted in two separate boxed areas (200 µm x 200 µm) per section, 3 sections per animal, in the hypo-perfused region.

2.2.10 Characterization of Perfusion regions

To assess the number of blood vessels perfusing the brain following stroke, dextran-labelled Texas Red was injected prior to euthanasia to label blood vessels that were open and not occluded. Note that the term "perfused" is used to indicate brain regions with open blood vessels and not as a direct measurement of blood flow. Three regions of perfusion (non-perfused, hypo-perfused, and perfused) were operationally defined based on the number of dextran-conjugated Texas Red-labelled blood vessels present within a 200 µm x 200 µm boxed area (Fig. 2.7 B-D, Table 2.1). Sampling for the perfused region was performed in the contralateral cortex, where a consistent density of >10 Texas-Red labelled blood vessels per area was counted across acute time points post-stroke (data not shown). The hypo-perfused region was defined as an area with 6 to 10 perfused blood vessels per area, whereas the non-perfused region had ≤5 labelled blood vessels. For each animal, these three regions were defined, and for each level of perfusion the number of labelled blood vessels in three boxed areas was averaged.

Table 2.1: Assessment of open blood vessels across ischemic injury at 7 days post-surgery.

Number of blood vessels (BV)	Non-perfused Region ≤ 5 BV	Hypo-perfused Region > 5 - ≤ 10 BV	Perfused Region > 10 BV
Chow+Saline	3.8 ± 1.1	-	14.2 ± 2.0
HFD+Saline	3.8 ± 1.1	-	15.2 ± 1.3
Chow+ET-1	2.4 ± 1.0	8.9 ± 0.6	14.9 ± 1.3
HFD+ET-1	2.3 ± 0.8	8.7 ± 0.3	15.1 ± 1.6

Three regions with different levels of perfusion within the injured and contralateral cortex (perfused region) were operationally defined based on the number of perfused blood vessels (BV). Dextran-conjugated Texas Red+ blood vessels were counted within a 200 µm X 200 µm boxed area at 7 days post-surgery (Chow+Saline *n*=5; HFD+Saline *n*=7; Chow+ET-1 *n*=6; HFD+ET-1 *n*=8). Data are expressed as mean ±SD.

2.2.11 In vitro blood vessel constriction experiment

Blood vessel constriction within the cortex was assessed in brain slices *in vitro* by applying vasoconstrictors. Mice fed either Chow or HFD were deeply anaesthetized with an intra-peritoneal injection of Euthanyl. Once mice became non-responsive, dextran-conjugated Texas Red was injected into the heart to label perfused blood vessels. Brains were dissected and coronal brain sections 250 µm thick were collected using a vibratome. Slices were maintained in ice-cold artificial cerebral spinal fluid (ACSF) comprised of the following: 126 mM NaCl, 2.5 mM KCl, 1.2 mM NaH_2PO_4, 1.2 mM $MgCl_2$, 2 mM $CaCl_2$, 25 mM $NaHCO_3$, and 10 mM glucose, continuously bubbled with O_2 (95%) and CO_2 (5%). Brain slices were individually incubated in ACSF for a 10 minute-baseline and then ET-1 was applied at a final concentration of either 5 or 10 nM for an additional 20 minutes. Following incubation, brain slices were immediately transferred to 4% PFA overnight for fixation. For the high K+ condition, after the 10-minute ACSF incubation brain slices were transferred to high K+ ACSF comprised of the following: 8.5 mM NaCl, 120 mM KCl, 6.3 mM $Na_2H_2PO_4$ and 1.2 mM $MgCl_2$, for 5 minutes and then transferred to 4% PFA for fixation. For ACSF control condition, brain slices were incubated in ACSF for 30 minutes.

Blood vessels were imaged at a depth of 500 µm from the cortical surface using a Zeiss Imager.Z1 upright microscope and the lumen width of dextran-conjugated Texas Red+ blood vessels were measured. For each blood vessel, the average lumen width was quantified by measuring five different points along the blood vessel within a length of 50 µm. Ten penetrating arterioles were measured per animal.

2.2.12 Western blot

2.2.12.1 Protein extraction

Basilar arteries were dissected from mice fed either Chow or HFD for 12 weeks and immediately frozen in dry ice. To extract protein, arteries were homogenized with a sonicator in lysis buffer containing protease inhibitors (20 mM N-2-hydroxyethylpiperazine-N-ethanesulfonic acid (HEPES) at pH 7.4, 50 mM β- glycerol phosphate, 2 mM ethylene glycol tetraacetic acid (EGTA), 1 mM dithiothreitol (DTT), 10 mM NaF, 1 mM $NaVO_4$, 1% Triton x-100, 10 % glycerol, 200 µg/ml phenylmethylsulfonyl fluoride (PMSF)) incubated on ice for 2 to 3 minutes and homogenized again. Following breakdown of the tissue, lysates were centrifuged at 2000 rpm (4^oC) for 5 minutes using an Eppendorf Centrifuge (Hamburg, Germany, Cat. # 4417R) and the supernatant was collected in microcentrifuge tubes.

2.2.12.2 Determining protein concentration

Protein concentration of the extracted sample was determined using a Bio-Rad protein determination assay kit (Bio-Rad, Cat. # 500-0006). The extracted protein sample was diluted in duplicates to 1:5, 1:10 and 1:15 dilution using lysis buffer and 5 µl of each of these diluted samples were added to 795 µl of ddH2O. The Bio-Rad Protein Assay reagent (BioRad, CA, USA, Cat. # 500-0006) (200 µl) was added to each diluted sample and incubated for 15 minutes at room temperature for colour formation to occur. Absorbance was read at 595 nm using a Thermo Scientific Genesys 10 UV Scanning spectrophotometer (WI, USA). These sample absorbances were compared to a standard

curve using Bovine Serum Albumin (Sigma, MO, USA, Cat. # B4287) with a concentration from 0 to 7.5 µg/ml, using the following formula:

$$Sample\ concentration\ [\mu g/\mu l] = \frac{Average\ sample\ absorbance}{Volume\ of\ sample\ (\mu l) * slope} * Dilution\ factor$$

2.2.12.3 Electrophoresis and western blot procedures

Samples were first prepared by adding 20 µl of lysis buffer then adding 5 µl of 5X loading buffer (250 mM Tris-HCl (pH 6.8), 0.5 M DTT, 10% Sodium Dodecyl Sulfate (SDS; Invitrogen, CA, USA, Cat. # 15525-017), 0.5% Bromophenol Blue (BPB; Fisher Scientific, NJ, USA, Cat. # B392-5), 50% Glycerol) followed by boiling the samples for 5 minutes. The samples were loaded in the 10% gel and run in the electrophoresis apparatus (Bio-Rad Mini-PROTEAN Tetra Cell, CA, USA, Cat. # 1658003) powered by a BioRad PowerPac Basic Power Supply (BioRad, CA, USA, Cat. # 1645050). A pre-stained protein ladder (Bio-Rad Precision Plus Protein Standards Kaleidoscope, CA, USA, Cat. # 161-0375 Rev B) was used as a molecular weight marker. Gels were run in a running buffer (50 mM Tris, 150 mM glycine, 3.5 mM SDS) at 80 V until the samples passed through the stacking gel portion and entered the separating gel, at which point the voltage was increased to 110 V. Following separation of the bands, the samples were transferred onto a nitrocellulose membrane using a transfer apparatus (Bio-Rad Mini Trans Blot Cell, BioRad, CA, USA, Cat. # 1703930). The transfer of proteins from gel to membrane was completed in transfer buffer (25 mM Tris, 150 mM glycine, 20% v/v methanol) at 290 mA.

Following transfer, the membrane was washed in Tween-20 Phosphate Buffered Saline (TPBS; 5 mM NaH_2PO_4, 20 mM Na_2HPO_4, 154 mM NaCl, 0.1% Tween 20) and then blocked with 5% v/v skim milk in TPBS for 1 hour at room temperature. The blot was then incubated with primary antibodies against COX-2 (1:1000, Cayman Chemical, Cat. # 160126, RRID: AB_327872), VCAM-1 (1:1000, Abcam, Cat. # ab134047, RRID: AB_2721053) and β-actin (1:2500, Sigma, Cat. # A5316, RRID: AB_476743) overnight at 4 ^oC on a platform rocker. Following washes with 0.5% skim milk in TPBS, the membrane was incubated with the secondary antibody IgG (H+L)-HRP conjugate (1:2000, Goat anti-Rabbit IgG HRP conjugate, BioRad, CA, USA, Cat. # 1706515) for 1 hour. Bands were visualized using the enhanced chemiluminescence substrate kit (Perkin Elmer, Lot. # 203-13261) and imaged on an ImageQuant LAS 4000 biomolecular imager (GE Healthcare Life Sciences, Product # 28955810). Blot images were analyzed using ImageJ (http://rsbweb.nih.gov/ij/) and the ratio of the optical density of the interested protein to the loading control protein, actin, was quantified and expressed as arbitrary units (A.U.).

Table 2.2: SDS page gel ingredients.

Ingredients	Separating Gel (10%)	Stacking Gel (4%)
ddH_2O	7.0 ml	4.05 ml
0.5 M Tris, 1.5 M glycine (pH 8.8)	4.0 ml	-
0.5 M Tris-HCl (pH 6.8)	-	1.4 ml
10% SDS	0.8 ml	0.4 ml
50% glycerol	2.0 ml	1.0 ml
40% arcylamide, 0.25% bisacrylamide	5.0 ml (filtered)	1.25 ml (filtered)
Ammonium persulphate	30 mg in 1 ml ddH_2O	25 mg in 1 ml ddH_2O
TEMED	0.02 ml	0.01 ml
Total Volume (ml)	20 ml	10 ml

2.2.13 Statistical analysis

All counts and measurements were performed blind. Data are expressed as mean ± standard deviation (SD) and analyzed by Graph Pad Prism V software (GraphPad Software Inc., La Jolla, CA, USA). Data was tested for normal distributions with the D'Agostino and Pearson omnibus normality test. A two-way repeated measures ANOVA was used to analyze weekly increases in body weight and paw drags (Figs. 2.2 A, E, F) and GFAP density at different distances from the infarct (Figs. 2.7 B-D). Main effects were followed up with multiple group comparisons using Bonferroni post hoc analysis. A two-way ANOVA was used to analyze changes in body weight post-surgery, fat pad weight, injury volume, blood vessel lumen width, Iba1+ cells, and NeuN+ cells. When significant main effects occurred, multiple group comparisons were performed with Bonferroni post hoc analysis. Body weight at 12 weeks, blood vessel lumen width in perfused tissue, CD68+ cells, CD68+ only cells, NeuN+ cells and Fluoro-Jade C+ with NeuN+ cells in the hypo-perfused region were analyzed using the two-tailed unpaired t-tests followed by an F-test to test for equal variances (Figs. 2.2 B, 2.5 D,F, 2.10 D,E). A t-test was used to analyze COX-2 and VCAM-1 protein levels following western blot procedures (Fig. 2.4). Significance level for all analyses was determined at $p < 0.05$.

2.3 Results

2.3.1 An increase in body mass and adipose tissue is seen following 12 weeks of HFD.

Starting at the time of weaning, mice were placed on either a HFD or Chow diet for 12 weeks. Weekly increases in body weight were recorded for Chow-fed and HFD-fed

groups (Fig. 2.2 A). There was an increase in body weight over time [$F(11,24) = 127.5$, $p<0.001$] and the interaction between diet and time was significant [$F(11,24) = 11.69$, $p<0.0001$]. Mice on the HFD gained significantly more weight than Chow-fed mice at 10 weeks, ($p<0.05$) and from 11 to 12 weeks, ($p<0.01$, $p<0.001$). At twelve weeks, mice underwent surgery and received either two injections of saline (control) or ET-1 into the anterior portion of the forelimb motor cortex (Roome et al., 2014). On the day of surgery, HFD-fed mice were approximately 10 grams heavier than Chow-fed mice (Fig. 2.2 B, $t(24) = 5.203$, $p<0.001$). Mice in both diet groups lost weight post-surgery. Diet but not surgical treatment (Saline vs ET-1) had a significant effect on this weight loss [$F(1,15) = 19.87$, $p<0.001$] as HFD-fed mice lost significantly more weight than Chow-fed mice following intra-cortical injections of either saline ($p<0.05$) or ET-1 ($p<0.01$) (Fig. 2.2 C). There was no difference in the amount of weight loss between saline and ET-1 injections. Despite a greater weight loss over the one-week post-surgery in HFD-fed animals, diet significantly affected the size of the epididymal, retroperitoneal and perirenal fat pads [$F(1,15) = 61.02$, $p<0.0001$], as both HFD+Saline and HFD+ET-1 mice had significantly more adipose tissue than their Chow-fed counterparts at the time of euthanasia (Fig. 2.2 D, $p<0.001$). These results demonstrate that 12 weeks of HFD causes significant increases in overall body mass and adipose tissue.

2.3.2 Worse stroke outcomes are observed in HFD-fed mice following a focal ischemic stroke.

It has been previously shown that due to the small size of ET-1 induced infarcts in mice, the standard forelimb asymmetry analysis of the cylinder test was not sensitive

enough to detect forelimb motor deficits (Roome et al., 2014; Schallert et al., 2000). Instead, these strokes resulted in mice performing a paw-dragging behavior of the affected limb when exploring the cylinder, which is a more sensitive measure of the subtle deficits elicited by these small infarcts (Roome & Vanderluit, 2015). This novel sensitive test was used to determine whether diet-induced obesity resulted in more severe behavioral deficits post-stroke. The percentage of paw-drags to total cylinder touches was quantified as a measure of forelimb motor deficit for the affected and unaffected forelimbs. Treatment [$F(3,18)=13.63$, $p<0.001$], time [$F(2,18)=47.10$, $p<0.0001$] and the interaction between treatment and time [$F(6,18)=9.555$, $p<0.0001$] all impacted paw dragging by the affected limb. Chow+Saline and HFD+Saline mice did not have significant behavioral deficits of the affected limb at 1- or 7-days post-surgery. In contrast, Chow+ET-1 mice performed significantly more paw drags than either Chow+Saline or HFD+Saline mice at 1 day ($p<0.05$) and 7 days ($p<0.001$) post-surgery. Similarly, HFD+ET-1 mice performed more paw drags than either Chow+Saline or HFD+Saline mice at both 1 and 7 days ($p<0.001$) post-surgery. HFD+ET-1 mice performed more paw drags than Chow+ET-1 mice at 1-day post-stroke ($p<0.001$); however, by 7-days these deficits were not significantly different from Chow+ET-1 mice (Fig. 2.2 E). There were no significant behavioral deficits measured in the unaffected limb across the different treatment groups (Fig. 2.2 F). These results show that ET-1 induced strokes cause significantly worse behavioral deficits of the affected paw than saline-injected controls and this deficit was exacerbated by HFD only in the acute period at 1-day post-surgery.

Next, it was questioned whether HFD affected injury size in the cortex following ET-1 or saline injections. At 7-days post-surgery, damage to brain tissue in the motor cortex was observed in mice that received either saline or ET-1 injections. The saline injections caused tissue damage which can be attributed to mechanical damage of the needle poke and damage associated with the injection volume of 1 µl at each site. The size of the injuries were influenced by both diet [$F(1,20)=4.518$, $p<0.05$] and injection type [$F(1,20)=19.69$, $p<0.001$]. Intra-cortical ET-1-induced strokes resulted in larger injuries than those caused by injections of saline (Fig. 2.2 G, H). Further, HFD+ET-1 mice had significantly larger infarcts than Chow+ET-1 mice (Fig. 2.2 G, $p<0.05$). Thus, 12 weeks of HFD significantly exacerbates the ET-1 induced infarct volumes within the cortex, but not the injuries caused by saline injections.

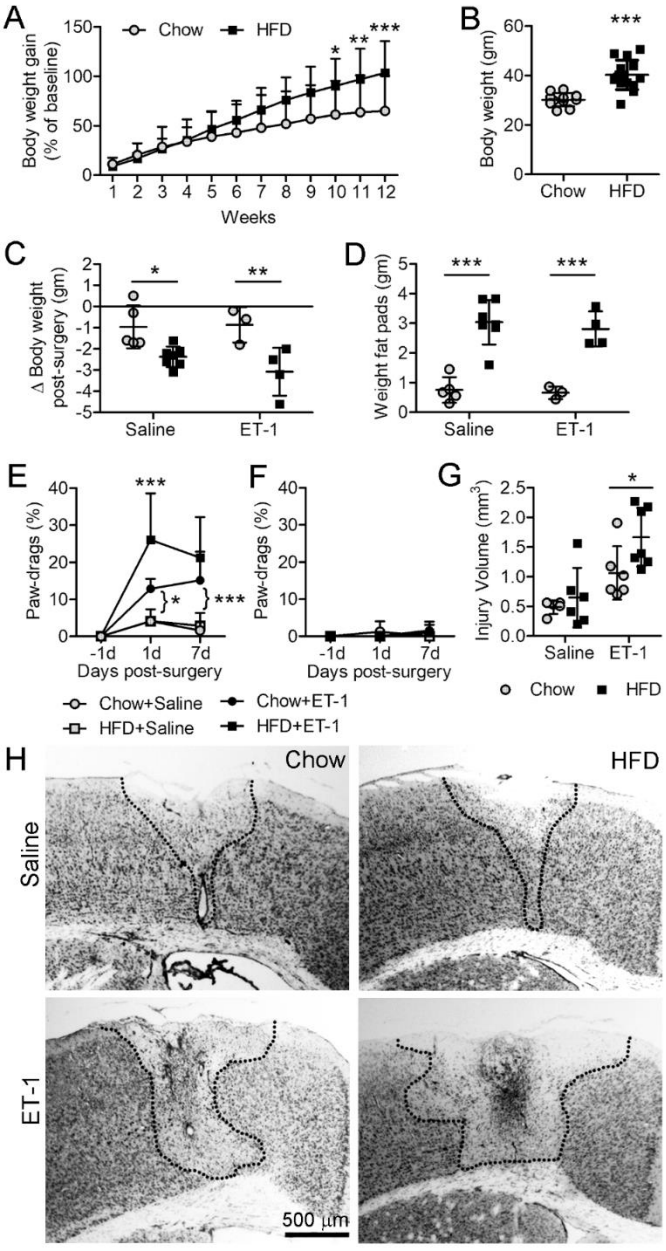

Figure 2.2: HFD-fed mice have larger infarct volumes post-stroke.

(A) Mice were weighed weekly over the 12 weeks prior to surgery and the percent body weight gain from baseline was recorded (Chow *n*=11, HFD *n*=15). In comparison to Chow-fed mice, a significant increase in percent weight gain was observed from 10 to 12 weeks in HFD-fed mice. (B) On the day of surgery, HFD-fed mice (filled squares, n=15)

weighed significantly more than Chow-fed controls (open circles, *n*=11). (C) Over the one-week period post-surgery, HFD-fed mice lost significantly more weight than Chow-fed controls in both the Saline and ET-1 groups (Chow+Saline *n*=5, Chow+ET-1 *n*=3, HFD+Saline *n*=7, HFD+ET-1 *n*=4). (D) At 7-days post-surgery, HFD-fed mice in both the Saline and ET-1 groups had significantly larger fat pads than Chow-fed mice (Chow+Saline *n*=5, Chow+ET-1 *n*=3, HFD+Saline *n*=7, HFD+ET-1 *n*=4). (E) Chow and HFD-fed mice that received an ET-1-induced stroke displayed significantly more paw-dragging of the affected limb at 1- and 7-days post-stroke than saline injected counterparts. Paw-dragging behaviour was increased in HFD+ET-1 mice at 1-day post-stroke in comparison to all other treatment groups, however by 7-days it was comparable to Chow+ET-1 mice (Chow+Saline *n=5*, Chow+ET-1 *n=6*, HFD+Saline *n=6*, HFD+ET-1 *n=5*). (F) Behavioral deficits were not observed in the unaffected limb. (G) Comparison of injury volumes for ET-1 and saline injuries in HFD and Chow-fed mice at 7-days post-surgery (Chow+Saline *n*=5, Chow+ET-1 *n*=6, HFD+Saline *n*=6, HFD+ET-1 *n*=7). (H) Cresyl violet staining of representative brain sections through the injury sites from HFD and Chow-fed mice. Outlines show area of the injured cortex. Data are expressed as mean ± SD. **p<0.05, **p<0.01, ***p<0.001*.

2.3.3 HFD leads to a smaller blood vessel lumen of penetrating arterioles within the cortex.

The larger infarcts observed in the HFD+ET-1 mice may be attributed to a difference in the contractility of the cerebrovasculature caused by HFD and/or ET-1. To determine whether 12 weeks of HFD affected the arterioles within the brain, the luminal width of arterioles that penetrate into the forebrain cortex were measured at the same depth as the intra-cortical injections of ET-1 and saline were performed *in vivo*. In transcardially-fixed brain sections, arterioles from Chow-fed mice had a luminal width of 4.5 ± 0.1 µm (*n*=5), whereas arterioles in HFD-fed mice were significantly narrower at

3.8 ± 0.1 µm (n=7) (t(10)=5.403, $p<0.001$). Next, to assess whether HFD would also change the contractility of these cerebral arterioles in response to ET-1, brain slices from Chow and HFD-fed mice were incubated with the vasoconstrictor ET-1 or a high concentration of KCl and the lumen width of penetrating cerebral arterioles was measured (Fig. 2.3 A). A two-way repeated measures ANOVA revealed that treatment [F(3,42)= 40.38, $p<0.001$] and the interaction between treatment and diet [F(3,42)= 3.626, $p<0.05$] affected blood vessel constriction. At basal conditions (30 min ACSF), HFD-fed mice had significantly narrower arterioles than Chow-fed mice consistent with the results found in perfusion-fixed brains (Fig. 2.3 B, $p<0.01$). Differences in the luminal widths of the penetrating arterioles in these brain slices and those in our fixed brain sections may be attributed to contraction of the tissue during the dehydration process for cryoprotection. Application of KCl (120 mM) or two different concentrations of ET-1 (5 nM or 10 nM) resulted in constriction of arterioles in both Chow and HFD groups. The final lumen widths in the presence of high KCl or ET-1 were not significantly different between groups despite the difference in baseline widths (Fig. 2.3 B). When normalized to the baseline luminal widths (30 min ACSF), it was found that arterioles in HFD-fed mice constricted significantly less when incubated with 10 nM ET-1 than those in Chow-fed controls (Fig. 2.3 C, t(13) = 2.638), $p<0.05$). Overall, these results show that under HFD conditions, the penetrating arterioles within the cerebral cortex are narrower and may have a reduced response to additional vasoconstrictors.

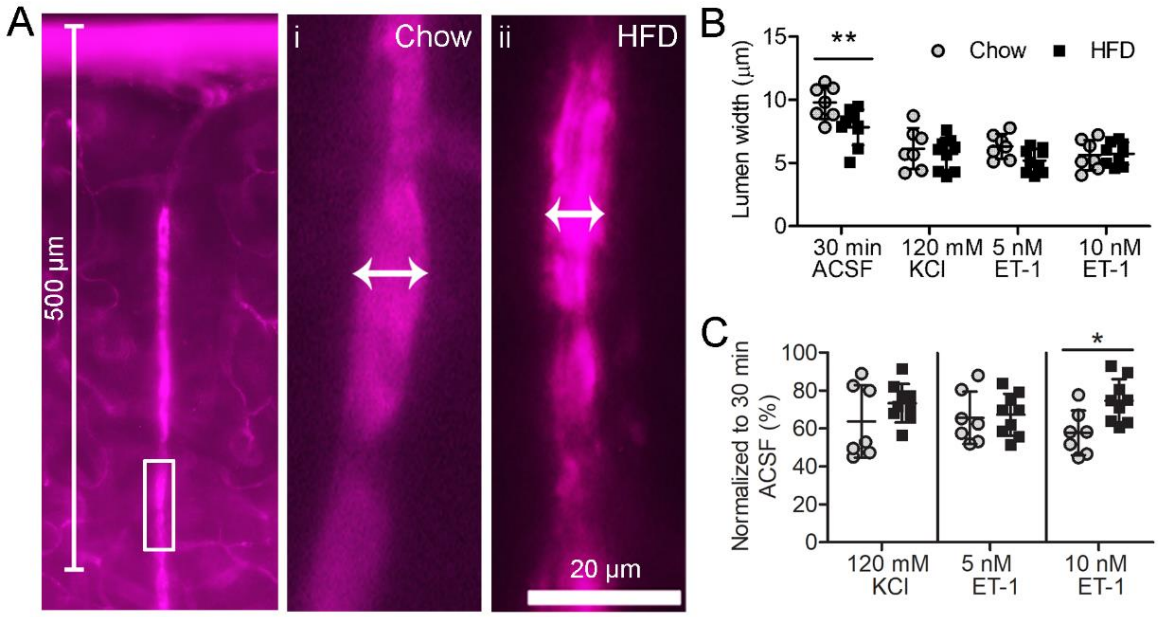

Figure 2.3: HFD results in a smaller blood vessel lumen of penetrating arterioles within the cerebral cortex.

(A) Representative images of dextran-conjugated Texas Red-labeled blood vessel within the cerebral cortex following 30 min incubation in ACSF. Measurements were taken in arterioles approximately 500 µm below the surface of the cortex. (i, ii) Higher magnification of measured arterioles. (ii) Arteriole in boxed region in A. Arrow indicates arteriole lumen width that was measured for analysis. (B) Quantification of lumen widths of cerebral arterioles in brain slices from Chow and HFD animals incubated with 30 min ACSF, 120 mM KCl, 5 nM ET-1 or 10 nM ET-1. (C) Lumen width measurements normalized to the untreated condition (30 min ACSF incubation) (Chow n=7, HFD n=9). Data are expressed as mean ± SD. *$p<0.05$, **$p<0.01$.

2.3.4 HFD did not increase inflammatory markers within the basilar artery.

Inflammation within the basilar artery was examined in Chow and HFD mice. The basilar arteries were dissected following euthanization and sectioned for immunohistochemistry or processed for western blot to determine VCAM-1 (Chow n=7; HFD n=7) and COX-2 (Chow n=7; HFD n=6) protein levels. Both VCAM-1 and COX-2 positive immunofluorescence was observed within the basilar arteries, which was also co-labelled with the dextran-conjugated fluorochrome (Fig. 2.4 A, B). Western blot analysis revealed that VCAM-1 was not significantly elevated within the basilar arteries following 12 weeks of HFD (Fig. 2.4 C, D, $t(12)=1.614$, $p>0.05$). Furthermore, there was not a significant increase in overall COX-2 protein expression within the basilar artery of HFD fed mice in comparison to chow controls (Fig. 2.4 C, F, $t(11)=1.786$, $p>0.05$). This suggests that overall protein expression of VCAM-1 and COX-2 inflammatory markers was not significantly elevated in the large basilar arteries of HFD mice in comparison to chow-fed controls.

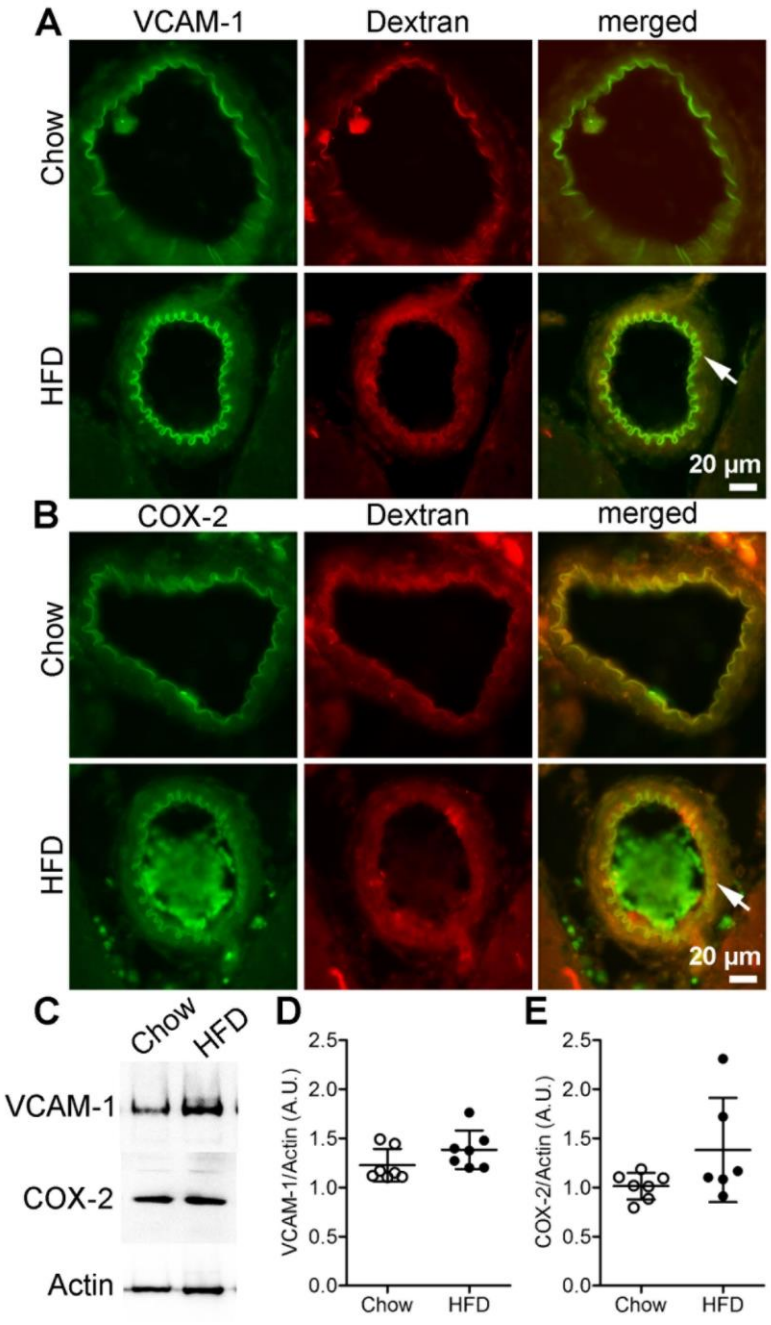

Figure 2.4: Inflammatory markers VCAM-1 and COX-2 did not increase significantly within the basilar artery following prolonged HFD.

Representative images showing cross section of the basilar artery in Chow and HFD mice. (A) Immunohistochemistry shows VCAM-1 within the basilar artery with dextran

labelling the lumen of the blood vessel. Arrow indicates VCAM-1+ fluorescence. (B) Images show COX-2 immunofluorescence within the basilar artery of Chow and HFD mice. Arrow indicates COX-2+ fluorescence. (C) Representative western blots for VCAM-1, COX-2 and Actin protein expression within Chow and HFD basilar arteries. (D) Quantification of VCAM-1 relative to Actin expressed as arbitrary units (A.U.) (Chow *n=7*, HFD *n=7*). (E) Quantification of COX-2 relative to Actin expressed as A.U. (Chow *n=7*, HFD *n=6*). Data are expressed as means ± SD.

2.3.5 HFD causes a greater infiltration of macrophages into the infarct.

The immune response has been shown to be a contributing factor to HFD-induced increases in stroke severity in MCAO stroke models (Dhungana et al., 2013; Herz et al., 2015; Maysami et al., 2015). To determine whether HFD also modulates the immune response to a small ischemic stroke, microglia and macrophages within the ipsilateral (injured) and contralateral (uninjured) cortex were examined using Iba-1, a marker for myeloid cells (Fig. 2.5 A). A two-way ANOVA revealed that treatment [$F(1,22) = 80.40$, $p<0.0001$] and the interaction between diet and treatment [$F(1,22) = 14.15$, $p<0.01$] affected the number of microglia and macrophages within the injured cortex. HFD+ET-1 mice had significantly more microglia/macrophages within their ipsilateral cortices than Chow+ET-1 (Fig. 2.5 B, $p<0.01$). In addition, Iba-1 immunopositive cells surrounding the infarct core in HFD+ET-1 mice appeared to have more complex processes compared to all other treatment groups (Fig. 2.5 A, iv). Within the contralateral cortex, Iba-1 expression appeared to be higher in microglia from HFD+ET-1 mice compared to all other treatments (Fig. 2.5 A, iv'). In the Saline-injected control mice, no diet effect was observed in the number of Iba-1+ cells within the core of the injury (Fig. 2.5 B). This is

consistent with previous research which shows no increase microglia or macrophages within the cortices of HFD-fed animals (Guillemot-Legris et al., 2016).

To distinguish the resident microglia population from the invading macrophage population, double-immunolabelling was performed with an anti-TMEM119 antibody, a marker specific for microglia combined with an anti-CD68 antibody, a marker expressed in macrophages and upregulated in activated microglia (Chistiakov et al., 2017). Cell counts were performed within a 200 µm by 200 µm area in the core of the infarct, where cells that were double-labelled for CD68+ and TMEM119+ were identified as microglia whereas, cells that were only CD68+ were determined to be macrophages (Fig. 2.5 C). Quantification of the total number of CD68+ cells revealed a two-fold increase within the infarct core of HFD+ET-1 mice compared to Chow+ET-1 mice (Fig. 2.5 D, $t(12) = 4.788$, $p<0.001$). Furthermore, in comparison to the number of TMEM119+ microglia in naïve mice (8.8 ± 0.7 cells), Chow+ET-1 mice appeared to have a two-fold increase in microglia [$F(2,17) = 10.94$, $p<0.01$] whereas, no change was observed within the infarct core in HFD+ET-1 mice (Fig. 2.5 E). The majority of CD68+ cells in both Chow+ET-1 and HFD+ET-1 mice were immunonegative for TMEM119, indicating that these cells were likely macrophages. In HFD+ET-1 mice, there were significantly more cells that were CD68+ only than in Chow+ET-1 mice (F, $t(12) = 5.983$, $p<0.0001$) (Fig. 2.5). Taken together, these results suggest that diet influences the type of immune cells that respond to the ischemic stroke. In chow conditions, microglia are the main cell population that responds to ischemia, while in HFD conditions a greater number of macrophages infiltrate into the infarct.

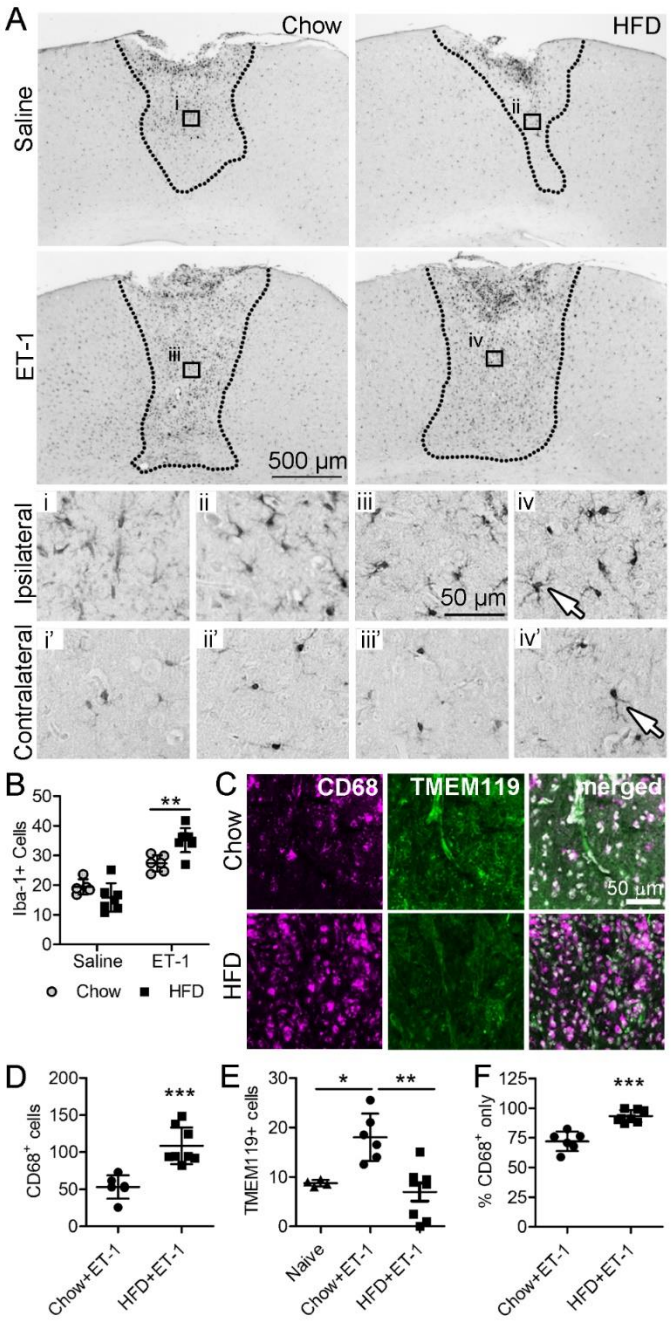

Figure 2.5: HFD increases the macrophage response within the mouse cortex following a focal ischemic stroke.

(A) Immunohistochemistry for Iba-1 showing microglia/macrophages following saline or ET-1 intracortical injections in mice fed Chow or HFD. Boxed regions (i- iv) are shown

at higher magnification below. (i'-iv') shows Iba-1+ microglia/macrophages within a comparable region in the cortex of the contralateral hemisphere. Arrows point to Iba-1+ microglia/macrophages. (B) Quantification of Iba-1+ cells within the ipsilateral (infarcted) hemisphere at 7 days post-stroke (Chow+Saline n=5, Chow+ET-1 n=6, HFD+Saline n=7, HFD+ET-1 n=8). (C) Double immunofluorescence for CD68, a marker of activated microglia and macrophages and TMEM119, a microglia-specific marker within the infarct core of Chow+ET-1 and HFD+ET-1 mouse brains. (D,E) Quantification of the number of cells positive for CD68 (D) and TMEM119 (E) within the infarcts of Chow+ET-1 and HFD+ET-1 mice or naïve brain. (F) The percentage of the total CD68+ cell population that are only CD68+ and negative for TMEM119 within the infarcts of Chow+ET-1 and HFD+ET-1 mice. Data are expressed as means ± SD. *$p<0.05$, ** $p<0.01$, ***$p<0.001$.

2.3.6 Increased astrogliosis is observed within the cortex of the infarcted hemisphere.

Astrogliosis was observed spreading outwards from the injuries in both saline and ET-1-treated brains. To determine the level of astrocyte activation, immunohistochemistry for GFAP was performed at 7-days post-stroke and the relative density of GFAP was compared at three sites: the border of the injuries defined as the area demarcated by the increase in GFAP expression, as well as 200 µm and 800 µm away from the border (Fig. 2.6 A). When comparing the impact of an ET-1 induced stroke injury versus saline injections on the spread of astrogliosis, the type of injection (ET-1 vs saline) [$F(1,24) = 22.68$, $p<0.0001$], the distance from the injury examined [$F(2,24) = 19.90$, $p<0.0001$] and the interaction between injection type and distance [$F(2,24) = 0.3147$, $p<0.0001$] all affected the spread of astrogliosis. In chow and HFD-fed mice combined, ET-1-induced strokes resulted in a >2-fold increase in GFAP density

compared to saline injuries at each of the three locations examined (Fig. 2.6 B, $p<0.001$). Next, the impact of diet on the spread of astrogliosis was examined following saline injections and ET-1 strokes separately. In saline-treated brains, there was an effect of distance [$F(2,10) = 12.62$, $p<0.001$] on the spread of astrogliosis (Fig. 2.6 C). In ET-1 injected mice, there was also a significant effect of distance [$F(2,12) = 10.19$, $p<0.001$] on the spread of astrogliosis. In Chow+ET-1 mice, GFAP density showed a gradual decrease from the border to 200 µm and 800 µm out. On the other hand, in HFD+ET-1 mice, GFAP density remained elevated out to 800 µm from the border (Fig. 2.6 D). This data shows a trend towards an increased spread in astrogliosis with the HFD condition. These results suggest that focal ischemia induces astrogliosis that spreads extensively around the infarct, which is modestly enhanced by HFD.

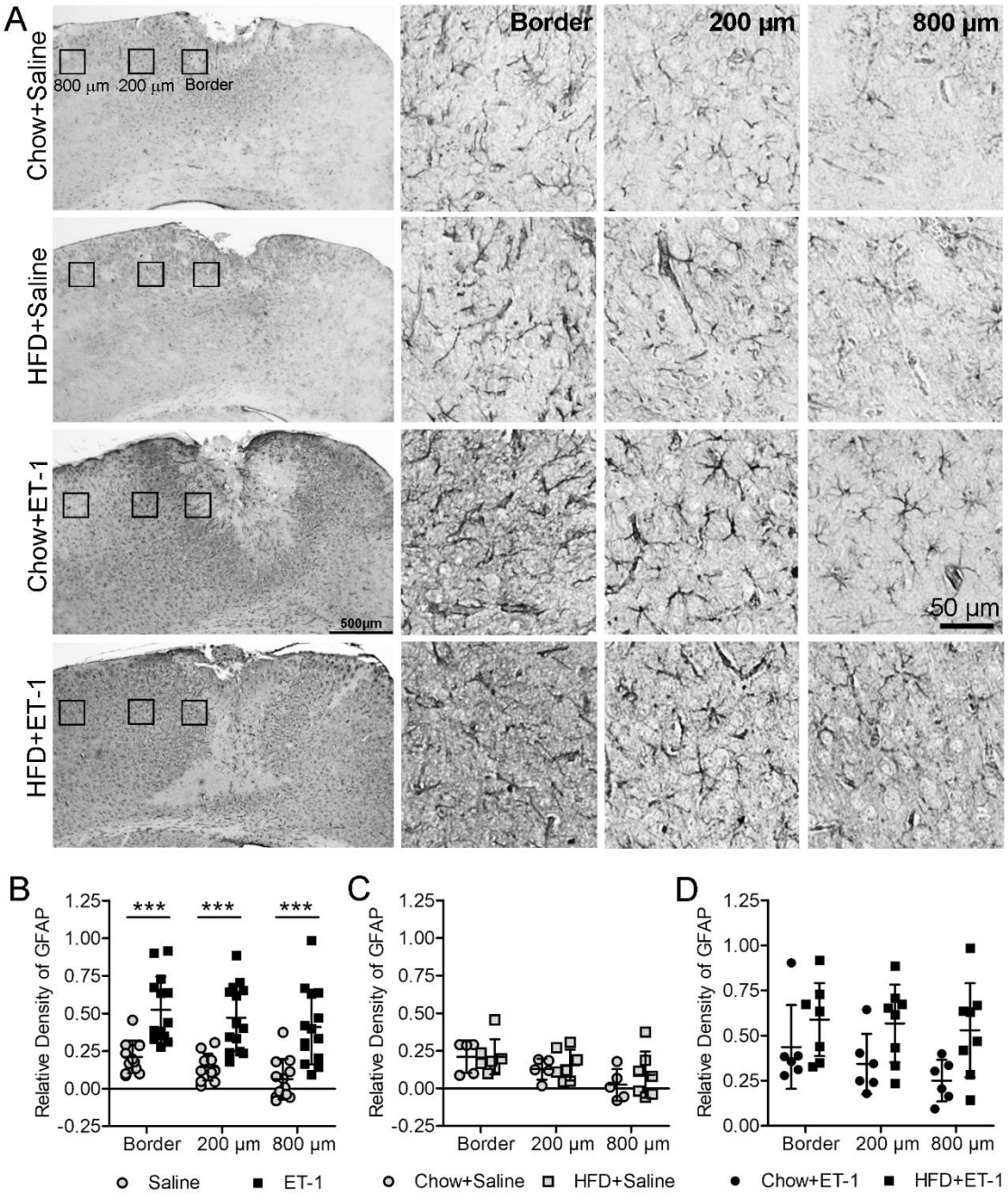

Figure 2.6: Increased astrogliosis is observed within the infarcted hemisphere.

(A) Photomicrographs depicting astrocyte reactivity within the injured cortex of Saline or ET-1 mice fed either Chow or HFD. *Left:* Boxed regions show areas of GFAP density

quantification along the border, 200 µm and 800 µm from the border of the injury. *Right:* Higher magnification of the boxed areas shows GFAP staining across the regions examined for each condition. (B) Effect of injury (saline) or stroke (ET-1) on the density of GFAP staining within the ipsilateral hemisphere in Chow and HFD-fed mice combined (Saline n=12, ET-1 n=14). (C) GFAP density following saline injections (Chow+Saline n=5, HFD+Saline n=7). (D) GFAP density following an ET-1 induced stroke (Chow+ET-1 n=6, HFD+ET-1 n=8). Data are expressed as means ± SD. ***$p<0.001$.

2.3.7 Relationship between the perfusion deficit and the infarct.

Next, to examine how the cellular response corresponded to changes in blood perfusion in and around the infarct, dextran-conjugated Texas Red was used to label blood vessels that were perfused at the time of euthanasia (Grade et al., 2013). A reduction in the number of perfused blood vessels was observed within both saline and ET-1 injuries (Fig. 2.7 A). The region of perfusion deficit overlapped with the area of cellular damage as visualized by cresyl violet histology and the transition from perfused regions to reduced perfusion corresponded with reduced cresyl violet staining (Fig. 2.7 A). The size of the regions lacking perfused blood vessels appeared different in saline versus ET-1 injuries. In saline-injected brains, the region lacking perfused blood vessels was narrow and localized to the site of the needle injury. In contrast, in ET-1 infarcted brains, the loss of perfused blood vessels at the core of the injury appeared larger, as expected (Fig. 2.7 C). Furthermore, in ET-1 treated brains, the tissue immediately surrounding the injury core appeared to have Texas-Red-labeled blood vessels but those were fewer (hypo-perfused) compared to un-injured perfused regions in the contralateral hemisphere.

Noting these different levels of perfusion observed within and surrounding the injured tissue, three regions were defined with distinct levels of blood perfusion (perfused, hypo-perfused and non-perfused) based on the number of Texas Red-filled blood vessels within a 200 µm x 200 µm area (Fig. 2.7 B-D) (Table 2.1). The perfused region was assessed by quantifying the number of labelled blood vessels in the contralateral hemisphere at the same M-L and D-V location as the infarct. The non-perfused region was synonymous with the core of the injury with ≤5 labelled blood vessels. The transition from the non-perfused core of the injury to perfused tissue appeared to be abrupt in saline-injected brains, whereas in ET-1 injected brains, the transition appeared more gradual with a region of hypo-perfusion (Fig. 2.7 B). The hypo-perfused region was defined as having 6 to 10 blood vessels within a 200 x 200 µm area. Because the hypo-perfused transition in the saline-injected brains was very narrow, it was not included in the analysis. Immunolabeling with the endothelial cell marker PECAM-1 showed the presence of blood vessels lacking perfusion in the non-perfused core of ET-1 injuries (Fig. 2.7 D).

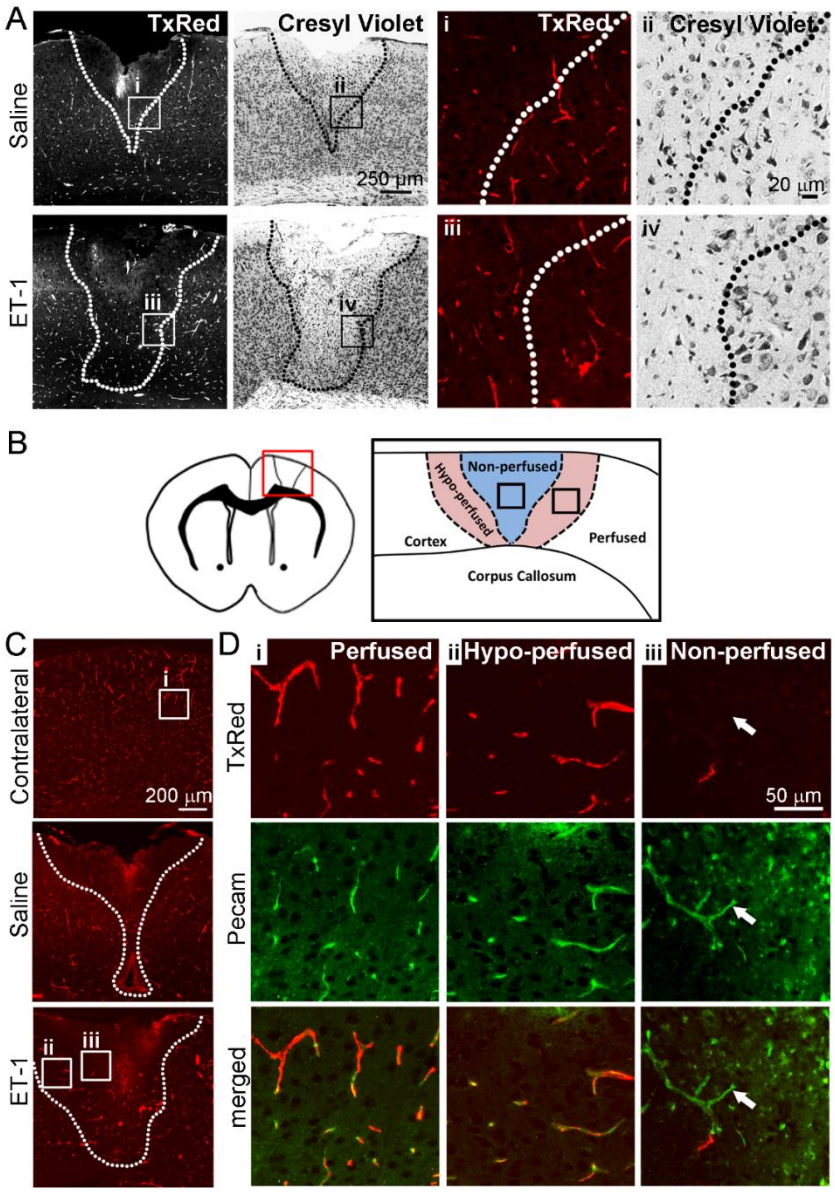

Figure 2.7: Regions of perfusion deficit across the injured cortex following either intra-cortical injections of saline or ET-1.

(A) Representative photomicrographs of coronal sections through the cortex following either intra-cortical injections of saline (physical needle damage) or ET-1 (stroke damage). Dextran-conjugated Texas Red-labelled blood vessels and cresyl violet-stain to visualize tissue histology show the region of perfusion deficit within the corresponding

injured cortices. Dotted lines outline damaged areas. Higher magnification of boxed areas (i-iv) show the transition from perfused to non-perfused regions, which correspond to the injured areas (reduced cresyl violet staining). (B) Schematic of a coronal section through the mouse brain following stroke with higher magnification of the regions of perfusion deficit. (C) Representative low magnification images of dextran-conjugated Texas Red-labelled blood vessels within the contralateral cortex (un-injured) and within the injured cortex produced by intra-cortical injections of saline or ET-1. (D) Higher magnifications of boxed areas (i-iii) in C depicting the three regions with different levels of perfusion (perfused, hypo-perfused and non-perfused). Dextran-conjugated Texas Red labels perfused blood vessels and immunohistochemistry for PECAM-1 labels vascular endothelial cells. In the non-perfused region, an example of PECAM-1+ blood vessels that are not double-labelled with Texas Red is shown (arrow), indicating that these vessels were not perfused. Each boxed area is 200 μm X 200 μm corresponding to the area in which Texas Red-labelled blood vessel counts were performed to define the level of perfusion.

2.3.8 Astrogliosis and neuroinflammation within the infarcted cortex.

Next, it was questioned how different blood perfusion levels corresponded to the location of microglia/macrophages and astrogliosis in Chow+ET-1 and HFD+ET-1 mice at 7-days post stroke. Iba1+ cells were observed within all three regions of perfusion, however; these cells were highly concentrated within the non-perfused core of the infarct (Fig. 2.8 A). The location of Iba1+ microglia and macrophages cells relative to the non-perfused core was similar in both Chow+ET-1 and HFD+ET-1 mice, although the numbers of macrophages were higher in HFD+ET-1 mice as previously shown in Fig. 2.5 F.

In contrast to the Iba1+ microglia and macrophages, there were very few GFAP+ astrocytes within the non-perfused core of the infarct (Fig. 2.8 B). Instead, more GFAP+ astrocytes were seen in the hypo-perfused region surrounding the core and extending into the perfused region around the infarct where the glial scar was forming in both Chow+ET-1 and HFD+ET-1 mice. HFD did not influence the pattern of GFAP+ astrocyte localization within the non-perfused and hypo-perfused regions; however, there was a trend showing an increased spread of astrogliosis across perfused regions in the cortex in the HFD condition (Fig. 2.6 D). These results demonstrate how microglia/macrophage cells and astrocytes adopt unique locations within and around the infarct.

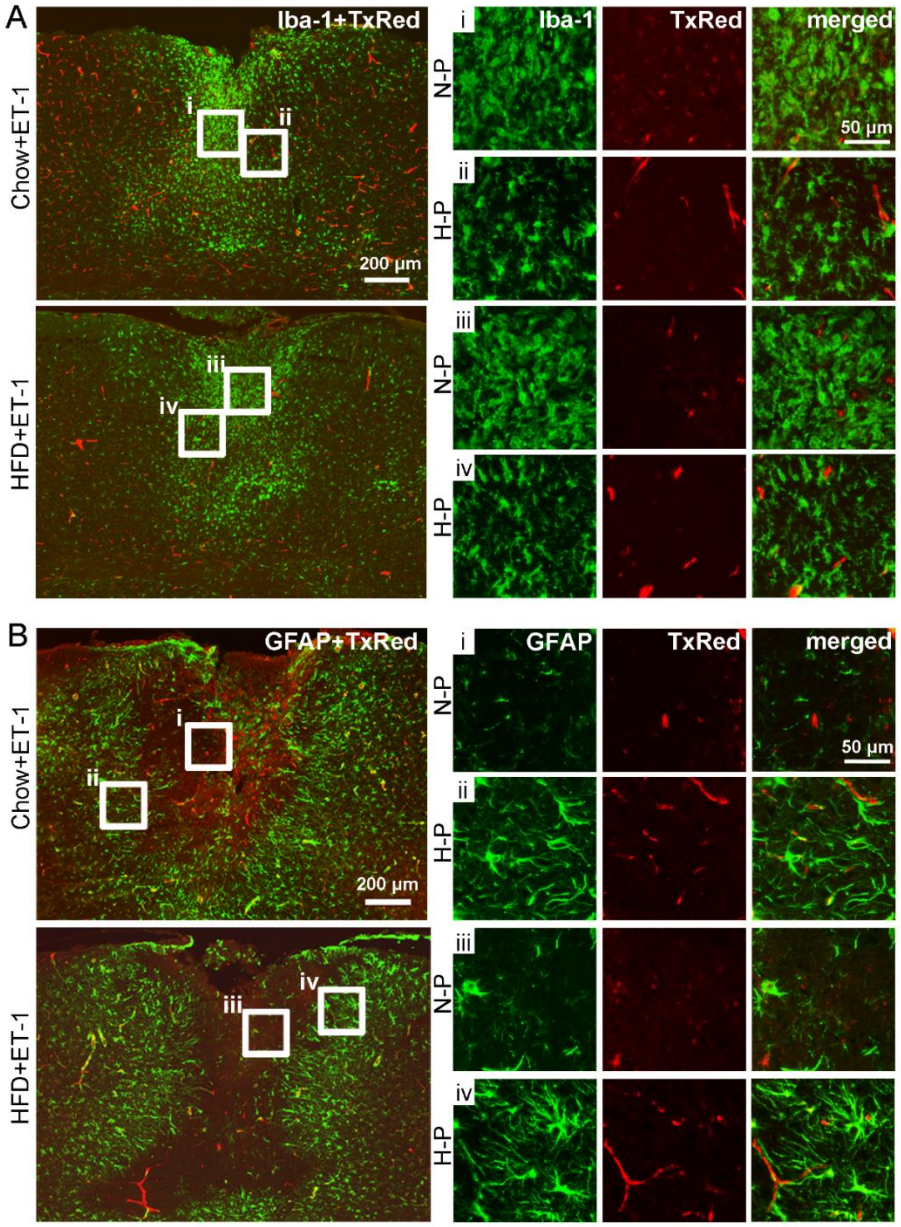

Figure 2.8: Distinct localization of microglia/macrophages and astrocytes within the infarcted hemisphere.

(A) *Left:* Representative low magnification photomicrographs showing the location of Iba-1+ microglia/macrophages within the regions of different perfusion levels across the infarct as determined by Texas-Red labelling. *Right:* Higher magnification of boxed

regions (i-iv) in A. Iba-1+ cells are shown within non-perfused (N-P) and hypo-perfused (H-P) regions of the infarcts in Chow+ET-1 (i, ii) and HFD+ET-1 (iii, iv) mice. Iba-1 microglia/macrophages are highly concentrated in non-perfused regions. (B) *Left:* Low magnification images showing the location of GFAP+ astrocytes across the regions of different perfusion levels in the infarct as determined by Texas Red. *Right:* Higher magnification of boxed regions (i-iv) in B. GFAP+ astrocytes are shown within the N-P and H-P regions of the infarcts in Chow+ET-1 (i, ii) and HFD+ET-1 (iii, iv) mice. Astrocytes are sparse in non-perfused regions while high in density in hypo-perfused regions. N-P= non-perfused, H-P= hypo-perfused

2.3.9 High-fat diet results in reduced survival of neurons within the hypo-perfused cortex.

Based on the observation that microglia/macrophages and astrogliosis increase within specific regions relative to the infarct, neuron survival was examined across regions with different levels of perfusion in Chow and HFD-fed mice. Neurons were quantified using the neuronal marker NeuN within the non-perfused and hypo-perfused regions of the ipsilateral cortex and the perfused region of the contralateral cortex. Neuron density within the perfused region of the contralateral hemisphere was similar in all conditions and was not affected by diet or treatment (Fig. 2.9 A, B). In contrast, diet had a significant effect [$F(1,22) = 52.30$, $p<0.0001$] on the number of NeuN+ neurons within the non-perfused core of the injury (Fig. 2.9 A, C, $p<0.001$). Within the hypo-perfused region, HFD+ET-1 mice had significantly fewer NeuN+ neurons in comparison to Chow+ET-1 mice (Fig. 2.9 D, two-tailed, $t(12) = 3.034$, $p<0.05$). Next, the surviving NeuN+ neurons were examined to determine whether they were healthy or dying in Chow+ET-1 and HFD+ET-1 mice. Double immunohistochemistry for active Caspase-3, a

marker of apoptotic cells and NeuN combined with Hoechst nuclear staining did not result in positive Caspase-3/NeuN staining within the infarct, indicating apoptosis was not a contributing factor to cell death at 7-days post-stroke (data not shown). In contrast, Fluoro-Jade C, a marker of degenerating neurons, labelled cells within both the non-perfused infarct core and the hypo-perfused region around the core (Fig. 2.9 F). Quantification of Fluoro-Jade C+ cells in the hypo-perfused region revealed no significant differences between diet groups with 6.1 ± 3.0 cells in Chow+ET-1 mice (n=4) versus 12.6 ± 4.4 cells in HFD+ET-1 (n=4) [t(6) = 2.43, p=0.0512]. There was a greater reduction in the number of NeuN+ neurons within the hypo-perfused region in HFD+ET-1 mice (Fig. 2.9 D). Double-labelling NeuN with Fluoro-Jade C revealed no significant difference in the number of double-labelled Fluoro-Jade C+/NeuN+ cells between HFD+ET-1 mice and Chow+ET-1 mice (Fig. 2.9 E, t(6) = 2.430, p=0.13). Although the total number of FJC+/NeuN+ neurons appeared to be the same (Chow= 5.4 vs HFD= 8.8), when compared to the total number of NeuN+ neurons in the hypo-perfused region (Chow= 37 vs HFD= 27.7), the percent of degenerating neurons is higher in the HFD condition at 32% vs 13.5% in the chow condition. Taken together, these results show that HFD increases stroke severity and the vulnerability of neurons within the hypo-perfused region to an ischemic insult

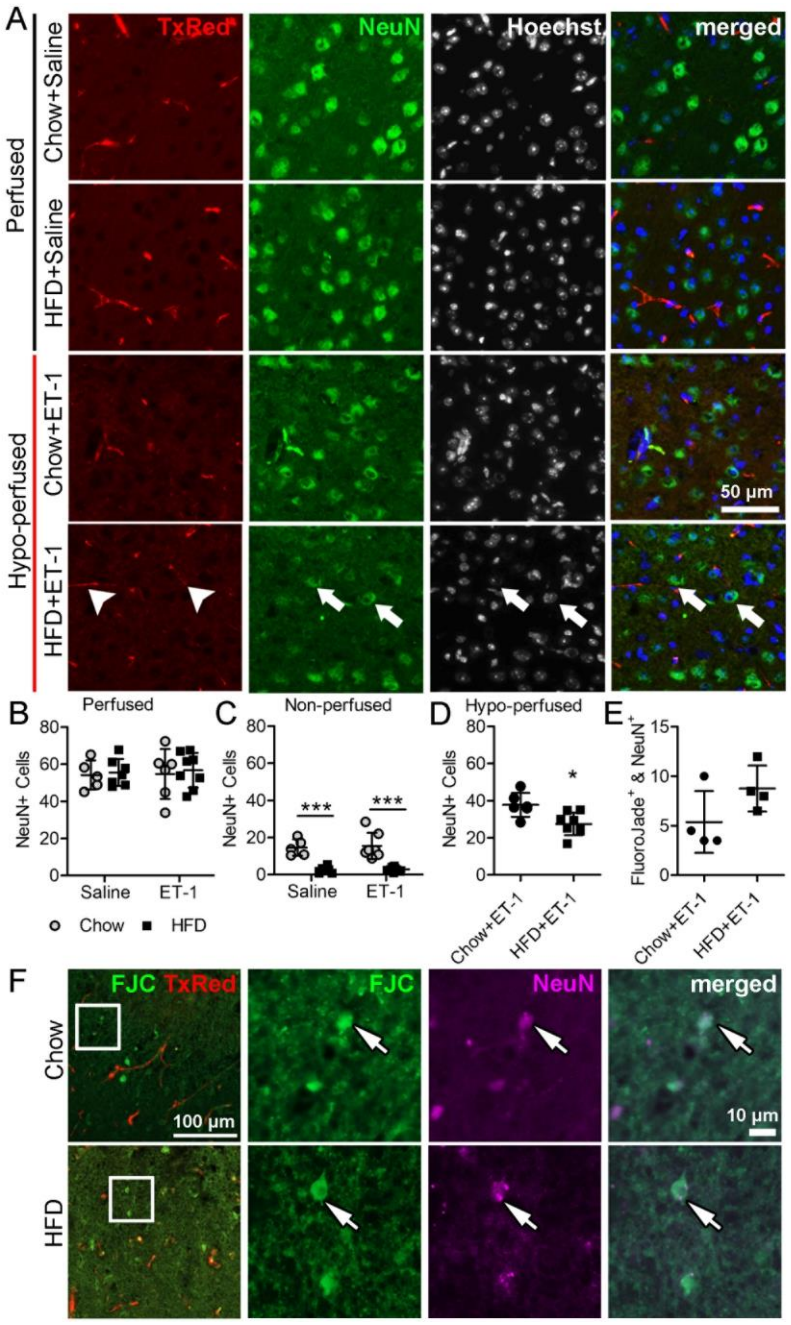

Figure 2.9: HFD reduced the number of surviving neurons within the hypo-perfused region.

(A) Representative photomicrographs of dextran-conjugated Texas Red labelled blood vessels (red), NeuN+ neurons (green) and Hoechst+ nuclei (blue) within perfused (saline) and hypo-perfused (ET-1) regions of the cortex. Arrowheads point to Texas Red+ blood vessels (red) and arrows point to neurons (green) and Hoechst+ nuclei (blue). Quantification of NeuN+ neurons in (B) perfused (contralateral cortex) and (C) non-perfused regions (200 x 200 µm) for each condition (Chow+Saline n=5, Chow+ET-1 n=6, HFD+Saline n=7, HFD+ET-1 n=8). (D) Quantification of NeuN+ neurons in the hypo-perfused region in Chow+ET-1 and HFD+ET-1 mice (Chow+ET-1 n=6, HFD+ET-1 $n=8$). Hypo-perfused regions were minimal in saline injected groups and were not analyzed. (E) The number of double-labelled Fluoro-Jade C and NeuN+ cells (degenerating neurons) within the hypo-perfused region (Chow+ET-1 n=4, HFD+ET-1 n=4). (F) Representative images of Fluoro-Jade C and NeuN+ cells within the hypo-perfused region of the infarct from Chow+ET-1 and HFD+ET-1 mice. Data are expressed as mean ± SD. *$p<0.05$, *** $p<0.001$.

2.4 Discussion

The goal of this study was to examine the impact of HFD on the sub-acute cellular response to a small, focal ischemic stroke. There are three main findings. First, that following prolonged HFD feeding, an ET-1-induced focal ischemia results in larger stroke injuries. Second, that HFD causes a narrowing of brain arterioles. Third, that the cellular response to a focal stroke is associated with the level of blood perfusion within and around the infarct, and HFD negatively and differentially impacts different cell types depending on the level of perfusion. The implications from these findings are that chronic HFD exacerbates the cellular response to a small, covert-like ischemic stroke.

2.4.1 Diet-induced obesity is established after 12 weeks of HFD feeding

Mice fed a HFD had significantly greater body mass after 12 weeks compared to those fed a Chow diet. The increase in weight was in part attributable to a three-fold increase in visceral fat pad mass demonstrating diet-induced obesity. Previous studies have shown that this mouse model displays not only obesity but also alterations in blood lipids, increases in circulating inflammatory cytokines and some components of metabolic syndrome (Haley et al., 2017; Maysami et al., 2015). Acute 3-day consumption of a 60% HFD disrupts glucose metabolism, whereas increased blood triglycerides, circulating neutrophils and macrophage infiltration into adipose tissue are observed with chronic HFD consumption (Haley et al., 2017). Chronic consumption of a HFD, therefore, has widespread effects on multiple body systems. As the present study did not control for these variables, it remains unclear whether the observed differences in stroke outcomes are due to direct effects of HFD or indirect effects resulting from obesity, inflammation and/or other metabolic disturbances.

Interestingly, at one-week post-stroke, mice fed a HFD lost more weight than Chow-fed mice irrespective of the type of injection (Saline or ET-1). This may indicate greater susceptibility to post-operative stress as a result of the increased body mass. This finding is consistent with previous studies that have shown that obese rodents have extended post-surgical recovery compared to non-obese controls (Poppendieck et al., 2013). Furthermore, clinical studies have also demonstrated that obese patients have more complications and longer hospital stays post-stroke (Ghanta et al., 2017). Thus, diet-induced obesity may adversely affect the ability to cope with the stress of surgery.

2.4.2 Prolonged HFD exacerbates small, covert-like strokes

Clinical research has described conflicting results of the impact of obesity on stroke outcomes. Commonly termed the 'obesity paradox', studies have described better outcomes and reduced mortality with obese patients. These findings have recently been challenged by the limitations of their studies including a lack of body weight measurement, selection bias, survival bias, BMI inaccuracies, and observational study design (Oesch et al., 2017). Clinical stroke research has challenges in comparing across individuals as the age, the sex, the location of the stroke, the size of the infarct and comorbidities complicate the study design. In contrast, preclinical research studies, which can control the age, the sex, the diet and the location and type of ischemic insult have shown that diet-induced obesity exacerbates stroke outcomes. Previous studies have shown that rodents fed a HFD or western diet for 1 to 6 months had larger infarcts (23% - 150% increase) and worse behavioral deficits following much larger stroke insults (Cao et al., 2015; Deng et al., 2014; Haley & Lawrence, 2017; Herz et al., 2014; Kim et al., 2014; Maysami et al., 2015; Wu et al., 2016). The majority of these studies use MCAO that results in infarcts that encompass >20% of the hemisphere and cause significant edema (Carmichael, 2005). In the current study, intra-cortical injections of ET-1 produced a very small ~1.0 mm^3 infarct, mimicking more common covert strokes. Despite the small size of these infarcts, mice fed a HFD for 12 weeks had a greater immune response, more widespread astrogliosis and a greater loss of neurons resulting in a ≥50% increase in infarct size compared to Chow-fed counterparts. Therefore, these results demonstrate that HFD feeding exacerbates the outcome of a focal ischemic insult. The results suggest that obesity also exacerbates the cellular response to very small strokes like covert strokes.

2.4.3 HFD causes narrowing of brain arterioles

The impact of HFD and obesity on blood vessels in the periphery is well documented (for review see (Gu & Xu, 2013)). HFD and obesity are associated with an increased risk of developing hypertension, which in turn, can further increase the risk of stroke (Jiang et al., 2016; Strazzullo et al., 2010). Although no significant change in systemic blood pressure was observed in a study that utilized the same animal model as the present study (C57Bl/6 mice on a HFD (60% of calories from fat) for 3 months or 6 months) (Maysami et al., 2015), HFD feeding has been shown to affect large arteries in the brain with narrowing of the middle cerebral artery and altered contractile and relaxation properties of the basilar artery (Deutsch et al., 2009; Li et al., 2013; Osmond et al., 2009). Whether HFD affects the smaller arterioles in the brain; however, is less well known. Our findings show that 12 weeks of HFD feeding caused a narrowing of the brain arterioles that penetrate into the cortex. Furthermore, the contractile response of these arterioles to application of ET-1 was reduced in HFD-fed mice, resulting in the same final luminal width as that of Chow-fed mice. Therefore, our finding suggests that the larger infarcts observed in HFD-fed mice are unlikely to be due to a greater constriction of blood vessels by ET-1. Whether the reduced basal size of the penetrating brain arterioles contributes to larger infarcts in HFD+ET-1 mice is unclear, but may explain the improved stroke outcomes with the application of angiotensin receptor blockers, which dilate blood vessels (Miyamoto et al., 2012). As HFD has pleiotropic effects throughout the body including the immune system and the vascular system, further investigation is necessary.

2.4.4 HFD induces a greater inflammatory response following stroke

Following ischemic stroke, three regions of blood perfusion could be identified within and surrounding the resulting infarct. The three regions were defined according to the number of blood vessels that were perfused and labelled with dextran-Texas Red at the time of euthanasia. Within each region, the composition of microglia/macrophages, astrocytes and neurons was found to be distinct. Furthermore, depending on the region, HFD feeding had differential effects on the cellular response. This could be seen within the non-perfused infarct core where there were few surviving neurons or astrocytes with primarily activated microglia and macrophages. This may be due to damage to blood vessels resulting in breakdown of the BBB and entry of immune cells into the brain parenchyma (Heiss, 2012). Following ET-1-induced stroke, there was a significant increase in the number of CD68+ myeloid cells largely due to enhanced infiltration of macrophages in HFD-fed mice compared to Chow-fed mice, demonstrating that HFD feeding may cause more significant breakdown of the BBB. A greater immune response has previously been demonstrated in diet-induced obese rodents with larger strokes such as MCAO (Cao et al., 2015; Dhungana et al., 2013; Herz et al., 2014; Maysami et al., 2015). Although results did not show significantly elevated levels of the adhesion molecule VCAM-1 or the inflammatory marker COX-2 in the larger basilar arteries of HFD mice, several studies have shown an increase in inflammation within blood vessels indicating an overall reduced health of the vasculature (Fotis et al., 2012; Shen et al., 2016; Zhang et al., 2005). For instance, Shen and colleagues found an increase in VCAM-1 and MCP-1 protein expression within cerebral microvessels following 3 and 6 weeks of high-cholesterol diet. (Shen et al., 2016). These studies suggest that diets high in

cholesterol/fat can elevate adhesion molecules within cerebral blood vessels, which may facilitate entry of leukocytes within the brain.

2.4.5 A distinct cellular composition is observed within the perfusion regions

The cellular composition of the hypo-perfused region surrounding the injury core was different compared to the non-perfused injury core. There were a greater number of activated astrocytes in the hypo-perfused region with increased expression of GFAP, a characteristic feature of activation. Furthermore, more surviving neurons along with fewer microglia and macrophages were observed in this region in comparison to the non-perfused core. However, HFD negatively affected the number of neurons in this hypo-perfused region, suggesting that HFD may cause neurons to be more sensitive to damage by hypo-perfusion. Finally, astrogliosis was found to spread from the injury border outward into the hypo-perfused and perfused regions. Here, the negative impact of HFD was observed as a trend towards a greater spread in astrogliosis. In previous studies, obese rodents show increased astrogliosis within the brain following larger ischemic insults such as permanent MCAO and bilateral CCA occlusion (Cheon et al., 2014; Dhungana et al., 2013; Yan et al., 2014). Thus, within each brain region with a different level of perfusion, HFD appears to exacerbate the cellular response to an ischemic stroke.

2.5 Conclusions

In summary, HFD feeding exacerbates the cellular response to a small focal ET-1 injection and this is specific to an ischemic injury and not the physical injury from fluid injection. By identifying three regions with different blood perfusion levels following ET-

1 injection, the results show that the cellular composition differs in distinct brain regions relative to the injury core. HFD negatively impacts different cell types within each region of perfusion. HFD-fed mice show an increase in macrophage infiltration and a decrease in neuron survival, with more extensive gross tissue damage and larger infarcts. Overall, the results demonstrate that the brain is more susceptible to focal ischemic damage when exposed to prolonged HFD, suggesting that diet-induced obesity may negatively influence the clinical outcomes of covert strokes.

CHAPTER 3

RAPID DEGENERATION OF NEURONS IN THE PENUMBRA REGION FOLLOWING A SMALL, FOCAL ISCHEMIC STROKE.

CO-AUTHORSHIP STATEMENT

I, Kathleen Fifield, designed the experiments with my supervisor Dr. Jacqueline Vanderluit. I performed all experiments and made all figures with edits from my supervisor. Both Dr. Michiru Hirasawa and Dr. Jacqueline Vanderluit edited writing for publication. This study is currently published: Fifield, K., E., Vanderluit, J., L. (2020). Rapid degeneration of neurons in the penumbra following a small, focal ischemic stroke. *European Journal of Neuroscience, 00*:1–19.

3.1 Introduction

Ischemic stroke is a debilitating neurovascular disease. It is the leading cause of long-term disability and the second leading cause of death globally (Benjamin et al., 2018). Ischemic stroke is caused by occlusion of a blood vessel within the brain reducing CBF to <20% resulting in an ischemic core of non-salvageable tissue (Bandera et al., 2006; Moskowitz et al., 2010). Surrounding the core is the penumbra zone, a region of hypo-perfusion (>20% - <40% CBF) where cells are injured and have the potential to be rescued. Without early reperfusion, cells within the penumbra zone die causing the ischemic core to expand (Back et al., 2004). Current therapeutic treatments are focussed on recanalization to restore blood flow and rescue these cells from death. The application of tissue Plasminogen Activator (tPA) has historically restricted the treatment window to 4.5 hours post-stroke (Lees et al., 2010). With the advent of endovascular thrombectomy, clinicians are extending the surgical treatment window to beyond 6 hours with the hopes of rescuing as many neurons as possible within the penumbra region and restoring function (Snelling et al., 2019). However, it is not clear how long injured neurons within the penumbra region can survive post-stroke. It is, therefore, imperative to understand the acute cellular response within the penumbra to provide direction for future therapeutic procedures.

The interdependence of the vasculature with the brain's neurons, macroglia, and microglia, also called the neurovascular unit (NVU), is crucial for maintaining the brain's homeostasis (Iadecola, 2017). Ischemia affects the health and survival of all cells in the NVU downstream of the blockage. Immediately following ischemic stroke, excitotoxic injury incurs death and damage of cells within the infarct (Dirnagl & Endres, 2014;

Stankowski & Gupta, 2011). Although excitotoxicity is classically associated with neuronal cell death, it also damages other cells within the NVU. For example, increased extracellular K^+ ion concentrations triggers astrocyte endfeet to dissociate from blood vessels (Kwon et al., 2009; Wang & Parpura, 2016). Loss of this glial-vascular connection disrupts the transfer of nutrients and oxygen from the blood to neurons placing them under further stress. Injured endothelial cells down-regulate junctional protein expression and increase adhesion protein expression causing immune cells like leukocytes and monocytes to adhere to the luminal surface. Injury to astrocyte endfeet in combination with endothelial cell changes results in a breakdown of the blood brain barrier (BBB) and the invasion of immune cells into the brain parenchyma (Jones et al., 2018; Matsumoto et al., 2008; Ronaldson & Davis, 2012). In the hours to days that follow, the injury expands as a result of secondary damage from inflammation and programmed cell death (Dirnagl & Endres, 2014). The inflammatory response is driven by resident microglia and invading immune cells which secrete cytokines and phagocytose cellular debris (Fumagalli et al., 2019; Ritzel et al., 2015; Woo et al., 2016). However, it remains unclear how the inflammatory responses differ between the infarct core versus the penumbra.

Accurately modelling clinical stroke has been a challenge for preclinical research and accounts for some of the failure of promising preclinical therapies to be translated to the clinic (Fluri et al., 2015). Current strategies to improve the translation of preclinical research are focussing on modelling specific components of clinical stroke. For instance, the preclinical Endothelin-1 stroke model is advantageous for modelling the penumbra, as local injections of ET-1, a vasoconstrictive peptide, induces a focal stroke with a large

penumbra (Biernaskie et al., 2001; Dirnagl & Endres, 2014; Lake et al., 2015; Lake et al., 2017; Willing, 2009; Windle et al., 2006). The ET-1 mediated local vasoconstriction is followed by gradual reperfusion that reflects the kinetics of ischemia and reperfusion in clinical stroke. In contrast, other stroke models such as middle cerebral artery occlusion by ligation or filament/thread techniques result in abrupt reperfusion (Domingo et al., 2000; Henshall et al., 1999). It has been shown that ET-1 injections targeted to the forelimb sensorimotor cortex in mice results in a reproducible ischemic stroke (Dojo Soeandy et al., 2019; Roome et al., 2014; Soylu et al., 2012). Despite an increasing use of the ET-1 model in preclinical stroke research, an understanding of the acute cellular response within the penumbra is lacking. Given the importance of the penumbra in stroke recovery, further research is needed to understand how the different cellular components of the neurovascular unit respond to an ischemic stroke.

To better understand cell survival within the penumbra, the acute cellular response within the infarct core was compared with the penumbra. The ET-1 injection model was used to induce a small, focal ischemic stroke in mice. The dextran-vascular labelling technique was used to identify the different regions of perfusion around the infarct. Analysis of the cellular response was performed from 4 to 72 hours post-stroke.

3.2 Methods

3.2.1 Animals

Fifty-nine male C57BL/6 mice between 3-6 months of age were individually housed and maintained on a 12:12 hour light-dark cycle with food and water provided *ad libitum*. Animals were randomly assigned to experimental groups and experiments were

conducted in compliance with ARRIVE (Animal Research: Reporting of *In Vivo* Experiments) guidelines (Kilkenny et al., 2010). All experiments were approved by Memorial University of Newfoundland's Animal Care Committee adhering to Canadian Council on Animal Care guidelines.

3.2.2 Surgical procedures

Stereotaxic surgery was performed under isofluorane anaesthesia as previously described in Chapter 2. Body temperature was continuously monitored during surgery with a rectal probe and maintained at 37.0 ^{o}C ± 0.5 ^{o}C using a heating pad and heat lamp. Two separate intra-cortical injections of saline for control groups (Saline) or Endothelin-1 (2 µg/µl, Cedarlane, Cat. # 05-23-3800) for experimental groups (ET-1) were injected using pulled-glass needles. Injections were targeted to the anterior forelimb motor cortex at the following coordinates relative to bregma: (i) +0.2 mm anterior-posterior (AP), +1.5 mm medial-lateral (ML), -1.0 mm dorsal-ventral (DV) and (ii) +1.0 mm AP, +1.5 mm ML, -1.0 mm DV. At each injection site, 1 µl of saline or ET-1 was injected at a rate of 0.2 µl/min with 0.5 µl released at a depth of -0.4 mm DV from the pia for 5 min and 0.5 µl at a depth of -0.6 mm DV for 5 min. The needle was left in place for 5 min at each DV location after the completed injection to avoid backflow. Following surgery, all mice received subcutaneous injections of Buprenorphine (0.02 mg/kg) and saline (1 ml of 0.9%). Mice were placed in their home cage and the cage was placed on a heating pad for approximately 2 hours to maintain stable body temperature. The animal's wellness was monitored as described in Chapter 2.

3.2.3 Tissue processing

Animals were anaesthetized with an intra-peritoneal injection of Euthanyl (250 mg/ml Sodium Pentobarbital- Vetoquinol, Cat. # IEUS001) at 2, 4, 8, 12, 24 and 72 hours following stroke or saline surgeries. An intra-cardiac injection of 250 µl dextran-conjugated Texas Red (1 µg/µl, Invitrogen, Cat. # D1864) or dextran-conjugated Oregon Green (1 µg/µl, Invitrogen, Cat. # D7173) was given when the mouse became unresponsive and while the heart was still beating. To label blood vessels that were open and perfusing the brain, the dextran-conjugated fluorochrome was allowed to circulate through the vascular system for approximately 2 minutes before dissection began (Fifield et al., 2019; Grade et al., 2013). Brains were extracted, blocked with a 1 mm coronal acrylic brain matrix, fixed in 4% paraformaldehyde and then cryoprotected in 12%, 16% and 22% w/v sucrose in 1X PBS, pH 7.4. Brains were embedded in Tissue Tek O.C.T (Thermo Fisher Scientific, Cat. # 12-730-571) and frozen in dry ice-cooled isopentane. Brains were sectioned on a Microm cryostat and 14 µm thick sections were collected on microscope slides (Thermo Fisher Scientific, Cat. # 1255015).

3.2.4 Infarct volume calculation

Infarct volume corrected for edema was calculated for each animal at 12 h, 24 h and 72 h post-surgery as previously described in Chapter 2. Coronal brain sections through the rostral to caudal extent of the injury were stained with 0.1% cresyl violet for histological analysis. A Zeiss Stemi-2000C dissecting microscope with an attached Zeiss Axiocam Mrm Rev3 camera (Carl Zeiss, Germany) was used to photograph images and infarct volumes were analysed using Zeiss AxioVision v4.8 software. Infarcts were

mapped to the anterior forelimb motor cortex as previously described in Chapter 2. To ensure that cellular quantification was completed within the same rostral to caudal region, infarcts that did not map onto the anterior forelimb motor cortex were deemed "off target" and were excluded from further analysis (n=2) (Roome et al., 2014). Injury volumes that exceeded two standard deviations above or below the mean or had excessive mechanical damage were excluded from the final analysis (n=3).

3.2.5 Immunohistochemistry

Brain sections through the center of the infarct were used for immunohistochemistry. The following primary antibodies were used for immunohistochemical analysis: rat anti-CD68 (1:400, Cedarlane, Cat. # MCA1957, RRID: AB_322219), rabbit anti-glial fibrillary acidic protein (GFAP, 1:400, Dako, Cat. # Z0334, RRID: AB_10013382), rabbit anti-ionized calcium binding adaptor molecule 1 (Iba-1, 1:1000, Wako Chemicals, Cat. # 019-19741, RRID: AB_839504), rat anti-Ly6G (1:500, BD Pharmingen, Cat. # 551459, RRID: AB_394206), mouse anti-microtubule-associated protein 2 (MAP-2, 1:200, Santa Cruz, Cat. # sc-74421, RRID: AB_1126215), mouse anti-neuronal nuclei (NeuN, 1:100, Millipore, Cat. # MAB-377, RRID: AB_2298772), rabbit anti-pan-neurofilament (SMI-312, 1:100, Biolegend, Cat. # 837904, RRID: AB_2566782), rat anti-platelet endothelial cell adhesion molecule 1 (PECAM-1, 1:200, BD Biosciences, cat#550274, RRID: AB_393571) and rabbit anti-TMEM119 (1:100, Abcam, Cat. # ab209064, RRID: AB_2728083). Immunofluorescence specifically for antibodies against NeuN underwent a 3-minute acetone pre-treatment. Slides were incubated with primary antibody overnight at room temperature and after washes with 1x

PBS slides were incubated with a secondary antibody for one hour. Secondary antibodies for fluorescent immunohistochemical detection included: goat anti-mouse Alexa Fluor 488 antibody (1:200, Invitrogen, Cat. # A21202, RRID: AB_2535788), goat anti-rat Alexa Fluor 488 antibody (1:200, Invitrogen, Cat. # A21208, RRID: AB_2535794), goat anti-rabbit Alexa Fluor 488 antibody (1:200, Invitrogen, Cat. # A21206, RRID: AB_2535792) and goat anti-rabbit DyLight 649 antibody (1:200, Jackson ImmunoResearch Lab Inc., Cat. # 111-496-144). Hoechst staining (Bisbenzimide H33258, Sigma Chemical Co., Cat. # 1155) was used to label nuclei. Slides were coverslipped with 1:3 glycerol:1x PBS solution and nail polish was applied around the coverslip. Enzymatic immunohistochemical detection was completed using the secondary antibody goat anti-rabbit immunoglobulin horseradish peroxidase conjugate (IgG (H+L)-HRP conjugate) (1:200, Bio-Rad Inc., Cat. # 170-6515, RRID: AB_11125142) followed by a 3,3'-Diaminobenzidine (DAB) reaction (Cedarlane, Cat. # SK-4100, RRID: AB_2336382) according to the manufacturer's instructions. Slides were dehydrated with increasing concentrations of ethanol followed by isopropanol and toluene and then coverslipped with Permount (Fisher Scientific, Cat. # SP15-500).

3.2.6 Fluoro-Jade C staining

Fluoro-Jade C (FJC) staining was used to detect degenerating cells within the infarct. Slides were placed in 1% sodium hydroxide in 80% ethanol for 5 min then placed in 70% ethanol for 2 min followed by a 2 min wash in water. Slides were then placed in 0.06% potassium permanganate, for 10 min and washed in water for 2 min. Following washing, slides were immersed in 0.0001% FJC working solution diluted in 0.001%

acetic acid, for 30 min and afterwards washed again in water. After drying on a slide warmer overnight at 35^{o}C, slides were cleared in Hemo-De (Fisher Scientific, Cat. # NC0174259) for 1 min and coverslipped with DPEX (Cedarlane, Cat. # 13514).

3.2.7 Microscopy, cell counting and densitometry analysis

A Zeiss Imager.Z1 upright microscope (5x, 10x, 20x and 40x objective lenses), a Zeiss Observer.Z1 inverted microscope (5x, 10x, 20x and 40x objective lenses) and a Zeiss Stemi-2000C dissecting microscope with a Zeiss Axiocam Mrm Rev3 camera (Carl Zeiss, Germany) were used to photograph tissue sections. Images were compiled using Adobe Photoshop CS2 (San Jose, CA, USA) and contrast and brightness was adjusted equally for all images. Cell counting and densitometry was performed using ImageJ software (https://imagej.nih.gov/ij/). Analyses were performed on three representative sections through the center of the injury, or for naïve animals, on sections from a comparable anterior-posterior location within the brain. Quantification obtained from three representative sections were then averaged for each animal.

For microglia/macrophage cell counts, Iba-1+ cells were counted in three separate 200 µm X 200 µm boxed areas per section within the infarct and within a similar region in the naïve brain. For astrocyte activation, densitometry analysis was performed on 5 separate 100 µm x 100 µm boxed areas around the infarct and within the naïve brain. For densitometry analysis, ImageJ was calibrated using the Rodbard optical density calibration. The density of each area was represented as relative to the background density. The calculation was as follows:

Relative density = (density of area of interest - background density)/ background density

To assess blood brain barrier breakdown, the number of blood vessels leaking dextran-conjugated fluorochrome were counted within the saline injury or ET-1 stroke at each time point. A blood vessel was considered "leaky" if a diffuse patch of dextran surrounding the vessel was equal to or greater than 15 µm in diameter. Patches of dextran not associated with a blood vessel but meeting this criterion were also included. The number of leaky blood vessels (patches of dextran) was quantified across the entire injury at 5x within a 2.4 mm^2 area (dimension 1.549 mm X 1.549 mm boxed region). Three sections were quantified per animal and the mean number of blood vessels/section/animal were represented in the graph.

Neuron survival was assessed by counting the number of NeuN+ cells in three separate 200 µm x 200 µm boxed areas. The boxes were placed at equal depths of 500 µm from the pial surface. Blood vessels were quantified within each box to determine whether it was in the non-perfused or hypo-perfused region prior to NeuN cell counts. The number of NeuN+ cells and Hoechst+ cells were quantified within both the non-perfused region and the hypo-perfused region of the infarct. Naïve counts were performed in untreated control mice. The number of intact dendrites was quantified within a 200 µm wide x 100 µm high boxed area in three sections per animal at 500 µm from the pial surface. A dendrite was considered intact if it was a minimum of 50 µm in length or longer without showing blebbing.

3.2.8 Characterization of Perfusion Regions

The regions of perfusion were operationally defined based on the number of dextran-conjugated fluorochrome-labelled blood vessels (Oregon Green or Texas Red

fluorochromes) present within a 200 µm x 200 µm area (Table 3.1) (Fifield et al., 2019). Note, that dextran labeling of the blood vessel was used to mark blood vessels that were open and perfusing blood at each time point and not as a measurement or indicator of blood flow. The number of labelled blood vessels in three sample areas were averaged per area and blood vessel 'perfusion' was assessed at 5 different time points post-stroke: 4, 8, 12, 24, and 72 hours post-stroke (n=3-5 mice per time point). To determine the number of perfused/labelled blood vessels within either the "perfused region" (contralateral cortex) or in the naïve brain (untreated, control mice), counting boxes (200 µm x 200 µm box) were placed in the cortex at approximately the same distance from midline and at comparable depths from the pial surface. Based on the blood vessel (BV) counts, three regions of perfusion were operationally defined as the non-perfused (≤ 5 BV), hypo-perfused (> 5 – 10 BV), and perfused regions (> 10 BV).

Table 3.1: Defining the regions of perfusion within the uninjured and injured cortex in the acute post-stroke period.

Condition	Time post-stroke	n	Perfused (# BV)	Hypo-perfused (# BV)	Non-perfused (# BV)
Naïve	0h	4	12.4 ±0.9		
Saline	Contralateral	19	14.5 ±1.7		
	4h	4			2.1±1.3
	8h	4			2.0±1.5
	12h	4			2.9±0.7
	24h	4			0.8±0.4
	72h	3			0.8±0.2
ET-1	Contralateral	21	14.2 ±1.4		
	4h	4		9.1±0.4	3.0±1.7
	8h	5		7.7±1.1	1.8±1.8
	12h	4		8.5±0.7	1.0±1.3
	24h	4		9.1±0.2	2.1±1.0
	72h	4		8.4±1.3	1.3±1.8
	# of blood vessels (BV)		**> 10 BV**	**> 5 - 10 BV**	**≤ 5 BV**

Regions of perfusion within the naïve, the perfused contralateral cortices and the hypo-perfused and non-perfused regions of the injured cortices were operationally defined based on the number of perfused (dextran-Texas Red labelled) blood vessels (BV) within a 200 µm X 200 µm boxed area at multiple time points post-injury. Data are expressed as mean ± SD.

3.2.9 Statistical analysis

The experimenter was blind to all conditions during data analysis. Data are expressed as mean ± SD. Data was analyzed using GraphPad Prism 5 software (La Jolla, CA, USA). For each analysis, statistical significance was determined at $p<0.05$. A two-way ANOVA was used to analyze infarct volume (Fig. 3.1 B), the number of leaky blood vessels (Fig. 3.3 C), GFAP relative density (Fig. 3.4 A), the number of Iba-1+ cells (Fig. 3.5 A) and the number of NeuN+ and Hoechst+ cells within the non-perfused core (Fig. 3.8 B,C). Significant main effects were followed by Bonferroni post hoc analysis. A one-way ANOVA was used to analyze the number of NeuN+ and Hoechst+ cells within the hypo-perfused region (Fig. 3.8 E, F) as well as the number of intact MAP2+ dendrites in this region (Fig. 3.9 C). Dunnett's post hoc analysis was completed following significant main effects. A Cohen's d analysis was completed to determine the effect size following analysis of the number of leaky blood vessels.

3.3 Results

3.3.1 Infarct volume is stable in the acute 72 h post-stroke period.

Infarct volumes were examined at 12, 24 and 72 hours following ischemic stroke or saline surgeries (Fig. 3.1). The injury sizes were affected by the type of injection [$F(1,17)=26.62$, $p<0.05$] with ET-1 induced infarcts consistently two-fold larger than injuries from saline injections (Fig. 3.1 B). The saline injections caused tissue damage, which can be attributed to mechanical damage of the needle poke and damage associated with the injection volume of 1 µl at each of the two injection sites. The overall injury

sizes did not change significantly over the 72 hours post surgery in both ET-1 induced infarcts and saline injuries.

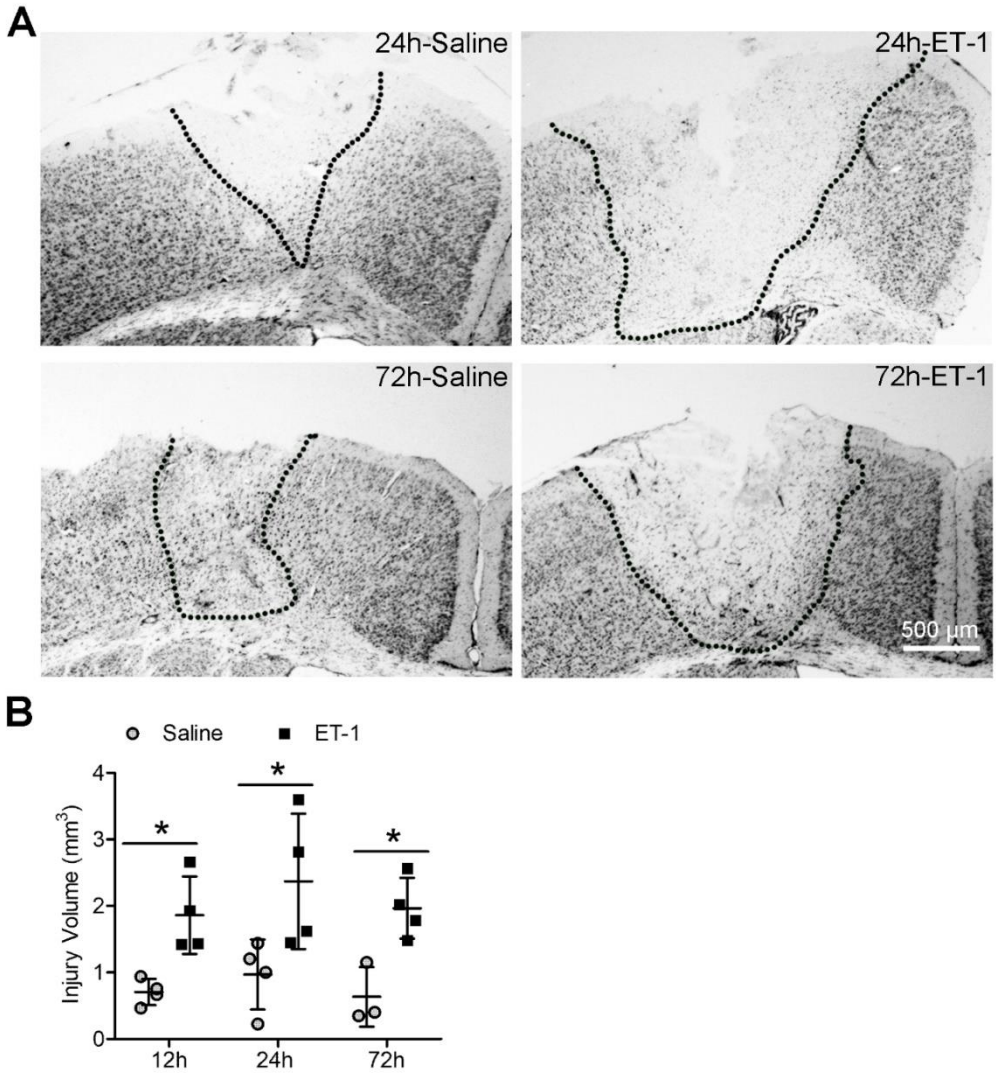

Figure 3.1: Endothelin-1 creates a small focal ischemic stroke that is stable over time.

(A) Cresyl violet staining of the cortex following intra-cortical injections of saline or ET-1 at 24 h and 72 h post-stroke. Dotted lines outline the damaged cortex. (B) Quantification of infarct volumes for saline and stroke injuries at multiple time points post-stroke (two-way ANOVA and Bonferroni post hoc, 12 h: *n*=4 Saline, *n*=4 ET-1; 24 h: *n*=4 Saline, *n*=4 ET-1; 72 h: *n*=3 Saline, *n*=4 ET-1). Data are expressed as mean +/- SD. *$p<0.05$.

3.3.2 Dextran labelling of blood vessels reveals the number of open blood vessels perfusing the brain.

To label open blood vessels, an intra-cardiac injection of dextran-conjugated to a fluorochrome (Oregon Green or Texas Red) was given prior to euthanasia. The dextran-conjugated fluorochrome circulates in the blood and adheres to the blood vessel walls allowing post-fixation analysis of open/perfused blood vessels (Fig. 3.2). At 2 h post-stroke, a lack of dextran-Oregon Green labelled blood vessels within the core of the infarct indicated there were no open blood vessels perfusing the infarct core at the time of euthanasia (Fig. 3.2 A). In contrast, numerous Oregon Green labelled blood vessels were observed in the contralateral cortex indicating blood vessels were open and perfused in the healthy cortex. Higher magnification of the border of the infarct revealed a transition zone between a "perfused region", with numerous Oregon Green labelled blood vessels to a "non-perfused region" void of labelled blood vessels (Fig. 3.2 B). The transition zone contained fewer labelled blood vessels than the perfused regions and was accordingly termed the "hypo-perfused region" (Fig. 3.2 B, C).

To detect the presence of perfused versus non-perfused blood vessels, dextran-labelling of blood vessels was combined with immunostaining for CD31 (PECAM-1), a marker of endothelial cells. In the non-perfused region, PECAM-1 positive (PECAM-1+) blood vessels were detected; however, they were not labelled with dextran-Oregon Green confirming they were not perfused. Blood vessels in the perfused region around the infarct and in the contralateral hemisphere were all double labelled with PECAM-1 and dextran-Oregon Green indicating vessels were perfused. In these normal perfused regions, the dextran labeling was found to obscure the PECAM-1+ immunostaining signal when

both channels were combined. In contrast, in the hypo-perfused region, blood vessels double-labelled with PECAM-1+ and dextran-Oregon Green+ were observed, which may be indicative of reduced levels of perfusion (Fig. 3.2 D, E). These findings demonstrate that blood vessels within the infarct core were not perfused at the time of euthanasia.

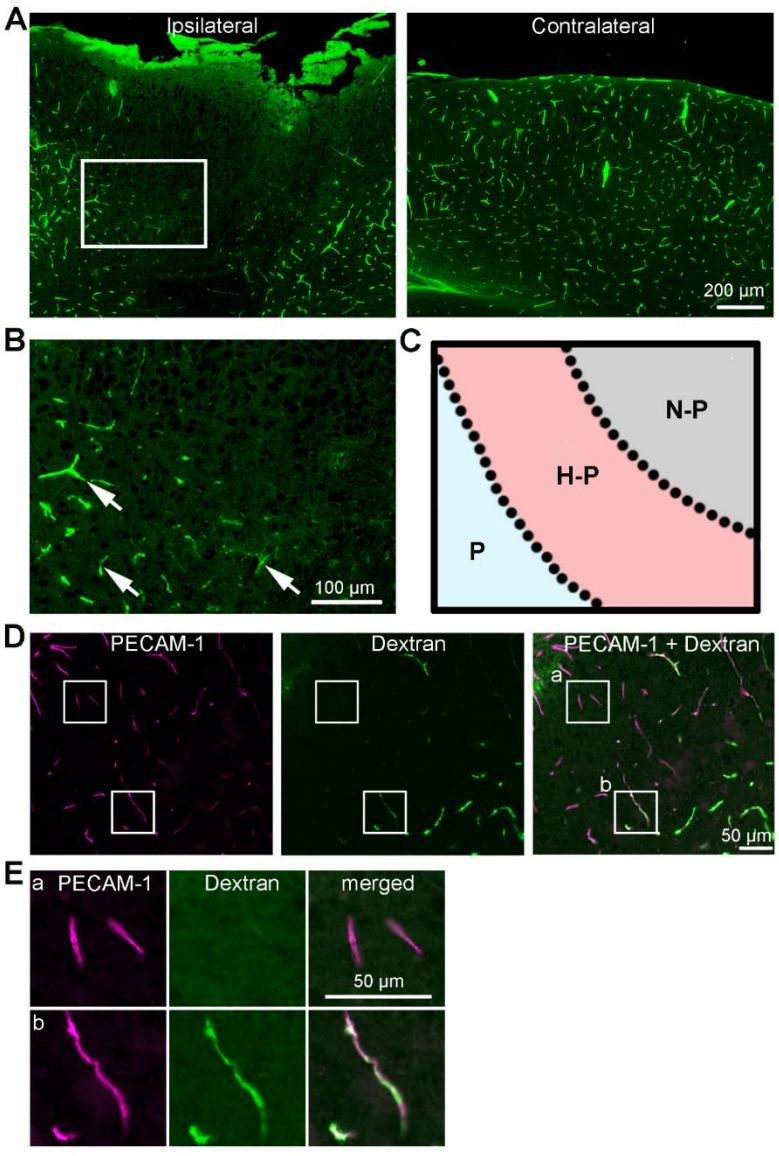

Figure 3.2: Endothelin-1 focal ischemic stroke produces a perfusion deficit that can be visualized with fluorescent labelled dextran.

(A) Low magnification images of the ipsilateral cortex injected with ET-1 and contralateral cortex showing dextran-conjugated Oregon Green labelled blood vessels at 2 h post-stroke. Labelled blood vessels are not observed within the infarct core. (B) Higher magnification of the boxed area in panel A showing the transition from perfused to non-perfused blood vessels around the perimeter of the infarct. Arrows point to perfused blood

vessels. (C) Schematic of the three different regions of perfusion around the infarct shown in B, reflecting the differences in the density of perfused (dextran-labelled) blood vessels. N-P= non-perfused core, H-P= hypo-perfused region, P= perfused region. (D) At 2 h post-stroke, immunostaining with antibodies to the endothelial cell marker PECAM-1 shows the presence of blood vessels that are perfused, partially perfused or not perfused with dextran. (E) Higher magnification of the (a) non-perfused and (b) hypo-perfused regions in panel D. Non-perfused blood vessels in (a) are only PECAM-1+ whereas, perfused blood vessels in (b) are double-labelled (Oregon Green+ and PECAM-1+).

To functionally define these three regions of perfusion, dextran-fluorochrome labelled blood vessels were counted within a 200 µm by 200 µm area placed within the non-perfused, hypo-perfused and perfused regions. Labelled blood vessels were counted in the three regions at 4, 8, 12, 24 and 72 hours following stroke or saline surgeries (Table 3.1). In both stroke and saline injuries, a region of non-perfusion was observed across all time points and was defined as having ≤5 fluorochrome-labelled blood vessels. The perfused region was defined by counting the number of labelled blood vessels in the contralateral hemisphere in a comparable location as the infarct. The perfused region was defined as having >10 labelled blood vessels. Around the perimeter of the non-perfused region of the infarct was the hypo-perfused region, which was defined as having >5 -10 labelled blood vessels within a 200 µm x 200 µm area (Fifield et al., 2019). In saline injuries, the transition from the non-perfused to the perfused was more rapid than that observed with ischemic infarcts resulting in a band around the perimeter that was too narrow for the 200 µm x 200 µm box and was therefore excluded from subsequent analysis. The number of labelled blood vessels within each region of perfusion was

similar across the different time points post-stroke. This suggests that following reperfusion the number of perfused blood vessels within each region is relatively stable.

3.3.3 Breakdown of the blood brain barrier is observed at 24 h post-stroke.

The large size of the 70 kDa dextran prevents it from leaking out of blood vessels in healthy, uninjured brains. Therefore, the presence of diffuse fluorochrome staining patterns within the brain parenchyma of the infarct was defined as breakdown of the BBB (Fig. 3.3 A, B). These diffuse fluorochrome staining patterns were not observed in naïve control brains or in the contralateral hemisphere of stroke brains. Therefore, to assess the severity of BBB breakdown, the number of diffuse fluorochrome staining incidences was counted within saline and ET-1 injuries from 4 to 72 h post-surgery. Breakdown of the BBB was affected by treatment [$F(1,30)=27.19$, $p<0.0001$], time [$F(4,30)=13.62$, $p<0.0001$] and the interaction between the two [$F(4,30)=5.095$, $p=0.003$]. There was a significant increase in the number of leaky blood vessels (patches of dextran) within the infarcts of ET-1 treated mice with 7.6 ± 1.9 compared to saline treated mice with 1.8 ± 1.0 at 24 h ($p<0.001$). By 72 h post-stroke, 3.7 ± 1.2 leaks were observed within the non-perfused core in saline injuries, whereas there were 7.9 ± 2.6 leaks in ET-1 infarcts ($p<0.01$) (Fig. 3.3 C). Due to the low number of dextran leaks quantified at 24 h and 72 h post-stroke, Cohen's d analysis was used to assess the effect size of increase in leaks between saline and ET-1. The effect size was 3.90 at 24 h and 2.10 at 72 h post-stroke indicating that the differences were separated by more than two standard deviations.

Astrocytes provide a crucial connection between the vasculature and the nervous system with astrocyte endfeet wrapping around blood vessels (Wang & Parpura, 2016). In

regions where the BBB was compromised, a lack of GFAP immunofluorescence was noted suggesting astrocyte endfeet lost their connection with the blood vessel (Fig. 3.3 B). By 72 h post-stroke, hypertrophic, GFAP+ astrocytes were observed wrapped around blood vessels along the border of the infarct (Fig. 3.3 D, E). Further evidence of BBB breakdown was observed with immunostaining for Ly6G, a marker of invading neutrophils at 24 h post-stroke (Fig. 3.3 F, G). Ly6G immunostaining was not observed in the uninjured contralateral hemisphere or in naïve brains with an intact BBB (data not shown).

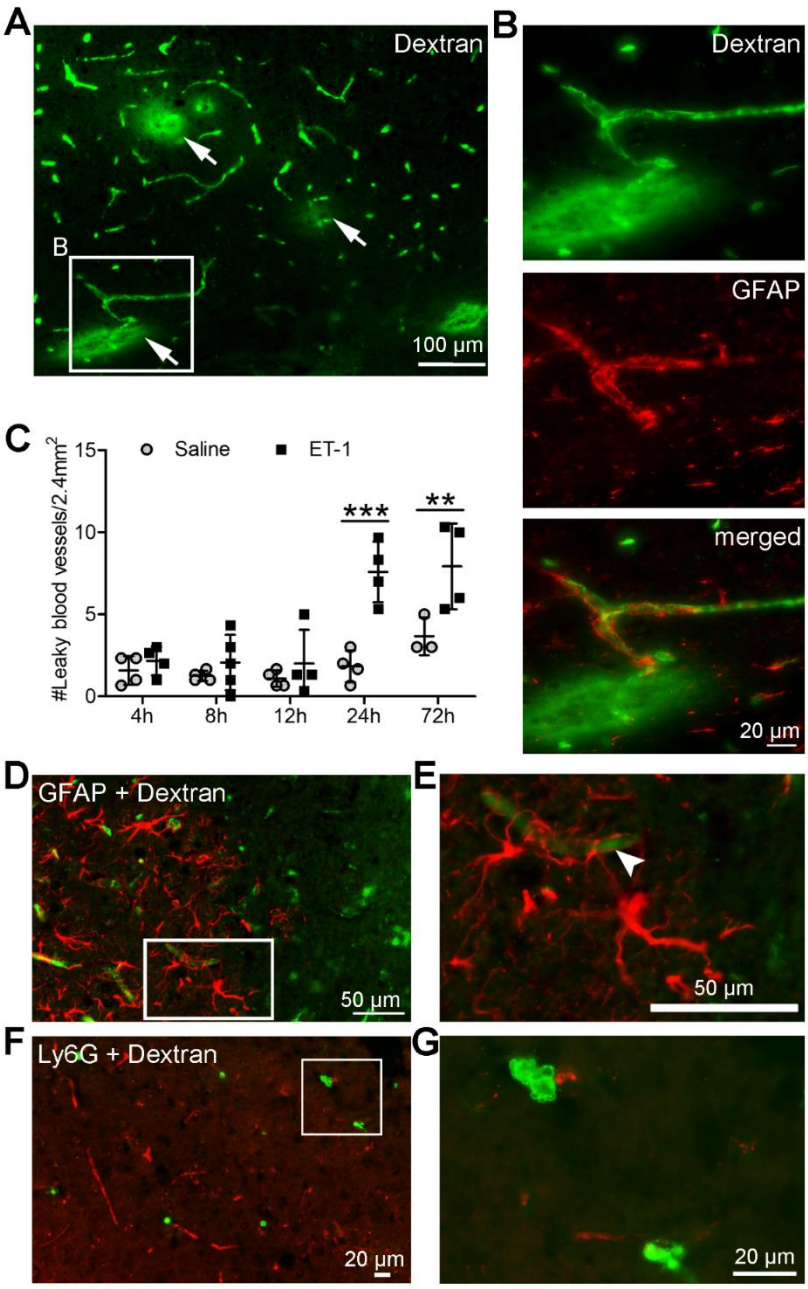

Figure 3.3: Blood brain barrier breakdown is observed as a leakage of dextran-conjugated Oregon Green into the brain parenchyma at 24 h and 72 h post-stroke.

(A) Leakage of dextran-conjugated Oregon Green within the infarcted cortex at 24 h post-stroke (arrows). (B) Higher magnification of the boxed region in B shows the astrocyte

marker GFAP co-localized with dextran-conjugated Oregon Green. (C) A significant increase in the number of leaks (patches of dextran) within a 2.4 mm^2 area is observed at 24 h and 72 h post-stroke (two-way ANOVA and Bonferroni post hoc, 4 h: *n*=4 Saline, *n*=4 ET-1; 8 h: *n*=4 Saline, *n*=5 ET-1; 12 h: *n*=4 Saline, *n*=4 ET-1; 24 h: *n*=4 Saline, *n*=4 ET-1; 72 h: *n*=3 Saline, *n*=4 ET-1). Data are expressed as mean +/- SD. ***p<0.01*, ****p<0.001* (D) An increase in GFAP immunopositivity is observed along the border of the infarct at 72 h post-stroke. (E) Higher magnification of boxed region shows astrocyte endfeet wrapping around a perfused Texas Red+ blood vessel (arrow head). (F, G) At 24 h post-stroke, Ly6G+ neutrophils were observed within the brain parenchyma, providing further evidence of a breakdown in the BBB.

3.3.4 Astrocyte reactivity is significantly elevated by 24 h post-stroke.

To examine the progression of astrogliosis, the relative density of GFAP was measured around the border of the injury for saline and ET-1 mice (Fig. 3.4 A). GFAP immunoreactivity was affected by treatment [$F(1,30)=45.59$, *p<0.0001*], time [$F(4,30)=72.56$, *p<0.0001*] and the interaction between the two [$F(4,30)=12.86$, *p<0.0001*]. When compared to saline controls, a significant increase in astrogliosis was observed in ET-1 mice at 24 h post-stroke (*p<0.05*) which increased further by 72 h (*p<0.001*) (Fig. 3.4 A, B).

Next, the astrogliosis response was compared across the different regions of perfusion at 72 h post-stroke. In both saline and ET-1 groups, few GFAP+ cells were observed within the non-perfused injury core (Fig. 3.4 C-F). In contrast, within both the perfused and hypo-perfused regions surrounding the saline and ET-1 injuries numerous GFAP+ cells were observed. At higher magnification, hypertrophic, highly ramified astrocytes were observed in both the perfused and hypo-perfused regions (Fig. 3.4 D, F).

These results demonstrate that astrogliosis surrounds the infarct and spreads outward, but not into the non-perfused region of the injury consistent with the role of astrocytes forming a protective barrier around the injury.

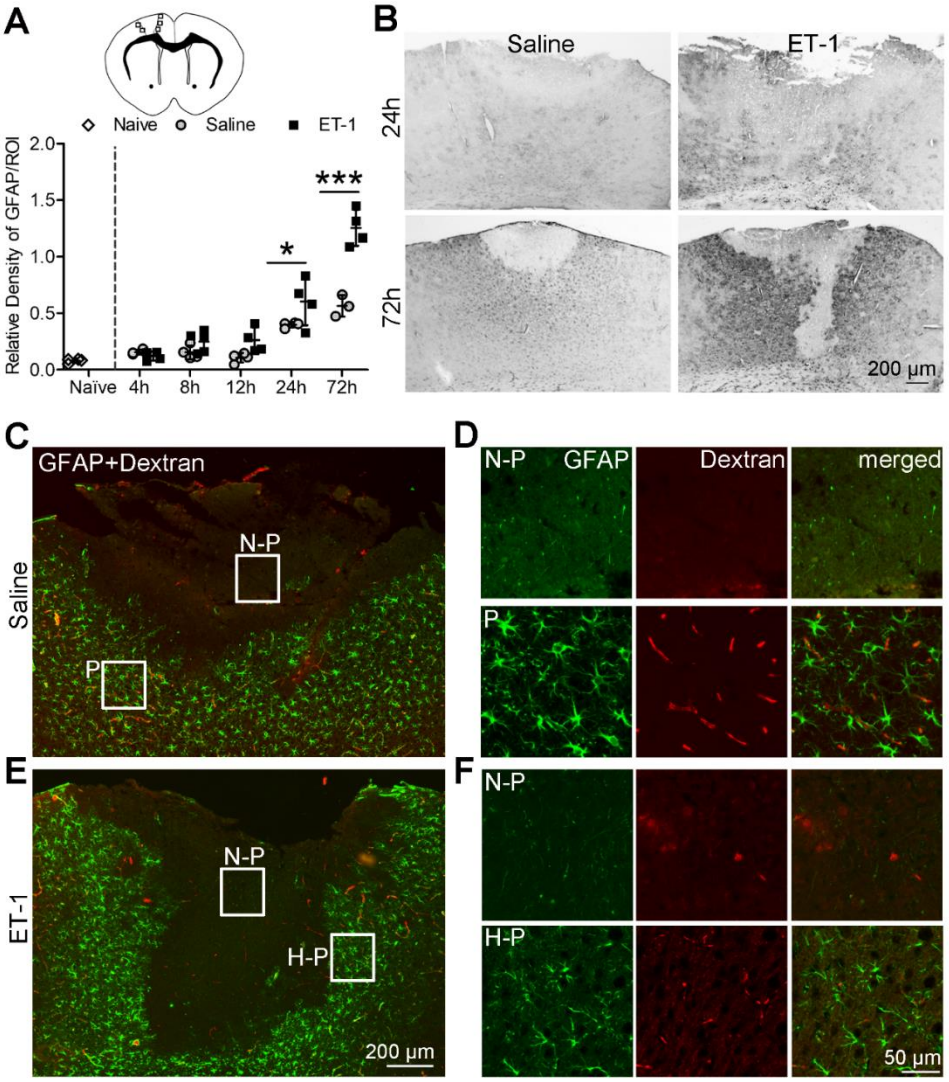

Figure 3.4: An increase in astrogliosis is observed at 24 h post-stroke.

(A) Schematic showing a coronal section of a mouse brain with the location of the stroke and areas of GFAP density measurements. Quantification of the relative density of GFAP shows a significant progressive increase in astrogliosis from 24 to 72 h in mice that received a stroke injury (ROI: 100 µm x 100 µm boxed area, two-way ANOVA and Bonferroni post hoc, Naïve: *n*=4; 4 h: *n*=3 Saline, *n*=4 ET-1; 8 h: *n*=4 Saline, *n*=4 ET-1; 12 h: *n*=4 Saline, *n*=5 ET-1; 24 h: *n*=4 Saline, *n*=4 ET-1; 72 h: *n*=3 Saline, *n*=4 ET-1). Data are expressed as mean +/- SD. (B) Representative low magnification photomicrographs of GFAP immunoreactivity around the infarct at 24 and 72 h post-

surgery. (C) GFAP immunofluorescence within the non-perfused and perfused regions at 72 h following saline injection. (D) Higher magnification of boxed regions in C showing GFAP+ astrocytes only within the perfused region around the injury. (E) GFAP immunofluorescence within the non-perfused and hypo-perfused regions that extends into the perfused region at 72 h post-stroke. (F) Higher magnification of boxed regions in E showing GFAP+ astrocytes within the hypo-perfused region. N-P= non-perfused, H-P= hypo-perfused, P= perfused *$p<0.05$, ***$p<0.001$

3.3.5 An increase in microglia/macrophages is observed at 24 h post-stroke with distinct localization within the infarct.

To examine the microglia/macrophage response during the acute time points post-surgery, immunohistochemistry for Iba-1 was performed. Iba-1+ microglia/macrophages were counted within the infarct and saline injuries. A two-way ANOVA of the cell counts revealed that the number of Iba-1+ cells was affected by treatment [$F(1,30)=21.69$, $p<0.0001$], time [$F(4,30)=72.24$, $p<0.0001$] and by the interaction between the two [$F(4,30)=3.59$, $p=0.016$]. A significant increase in Iba-1+ microglia/macrophages was observed within the stroke brain compared to saline controls at 24 h post-stroke ($p<0.05$) with a further increase observed at 72 h post-stroke ($p<0.001$) (Fig. 3. 5A, B).

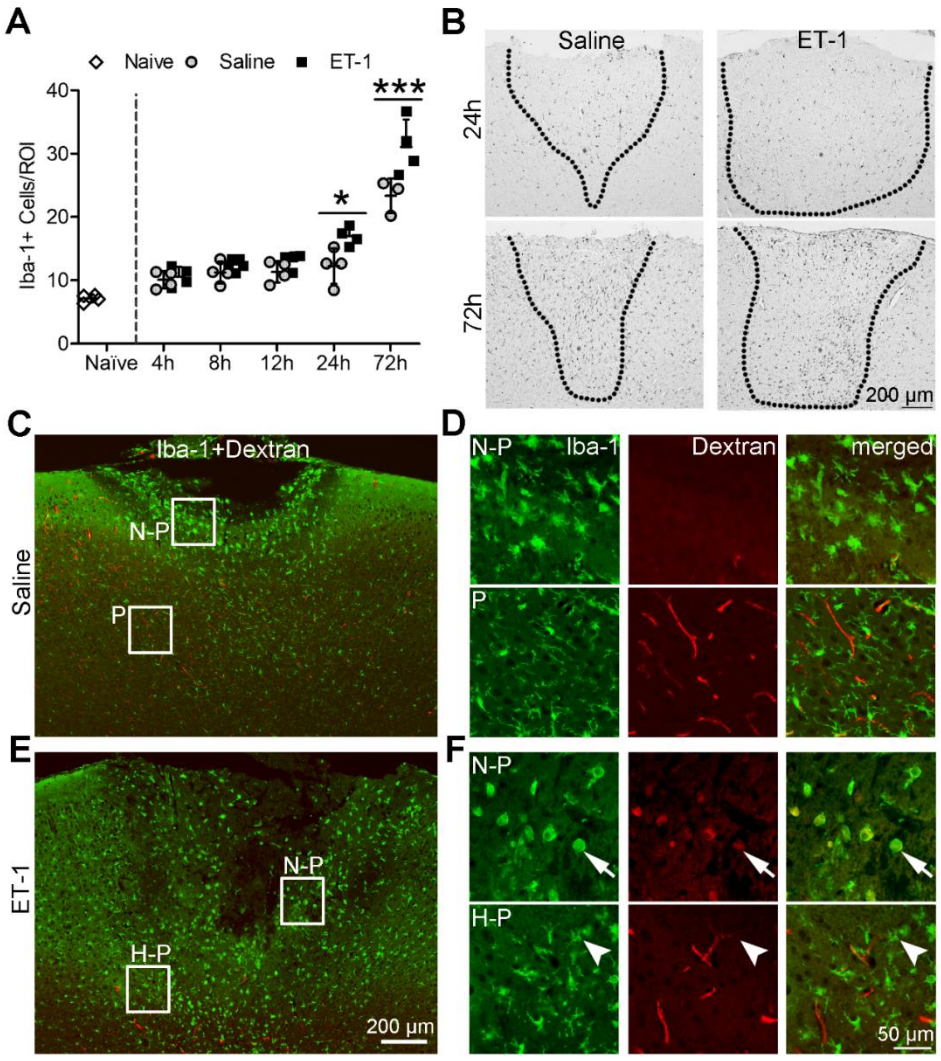

Figure 3.5: A significant increase in the microglia/macrophage response begins at 24 h post stroke and continues to increase up to 72 h.

(A) Quantification of the number of Iba-1+ cells within the ET-1 and saline injuries from 4 h to 72 h post-surgery. A significant increase in the number of Iba-1 positive cells was observed at 24 h and 72 h post-stroke (ROI: 200 µm x 200 µm boxed area, two-way ANOVA and Bonferroni post hoc, Naïve: *n*=4; 4 h: *n*=4 Saline, *n*=4 ET-1; 8 h: *n*=4 Saline, *n*=5 ET-1; 12 h: *n*=4 Saline, *n*=4 ET-1; 24 h: *n*=4 Saline, *n*=4 ET-1; 72 h: *n*=3 Saline, *n*=4 ET-1). Data are expressed as mean +/- SD. (B) Representative low magnification photomicrographs of Iba-1 immunohistochemistry labelling microglia and

macrophages within saline and stroke injuries at 24 and 72 h post-surgery. Dotted lines indicate the injury borders. (C) Iba-1 immunofluorescent images showing the location of Iba-1+ cells within the saline injury at 72 h post-surgery. (D) Higher magnification of boxed regions in C of Iba-1+ microglia/macrophages within the non-perfused and perfused regions. (E) Iba-1 immunofluorescent images showing the location of Iba-1+ cells within the infarct at 72 h post-stroke. (F) Higher magnification of boxed regions in panel E of Iba-1+ microglia/macrophages within the non-perfused and hypo-perfused regions. Arrowheads show ramified processes of Iba-1+ microglia/macrophages in the hypo-perfused region whereas, arrows show amoeboid shaped microglia/macrophages in the non-perfused region. N-P= non-perfused, H-P= hypo-perfused, P= perfused *$p<0.05$, ***$p<0.001$

The distribution of Iba-1+ microglia and macrophages within the non-perfused, hypo-perfused and perfused regions was examined at 72 h post-stroke. Iba-1+ microglia/macrophages were observed within each region of perfusion; however, distinct differences in morphology were observed (Fig. 3.5 C-F). Iba-1 expression was upregulated in microglial cells in the perfused region surrounding the saline injury; however, their morphology was comparable to microglia in the uninjured contralateral cortex (data not shown). Iba-1+ microglia and macrophages in the hypo-perfused region in ET-1 brains were hypertrophic with numerous ramified processes (Fig. 3.5 D, F). In contrast, Iba-1+ cells within the non-perfused regions of ET and saline brains were amoeboid in shape with few to no processes visible (Fig. 3.5 D-F). The amoeboid shape is indicative of a phagocytic phenotype and evidence of Texas Red was observed within some of these cells (Fig. 3.5 F). To verify the phagocytic phenotype, immunofluorescence for CD68, a phagocytic marker, was performed on brain sections at 24 and 72 h post-

stroke. At 24 h post-stroke, only a few CD68+ cells were observed within the infarct and appear to be associated with blood vessels. However, by 72 h post-stroke, numerous CD68+ cells were observed throughout the infarct with a similar amoeboid morphology as the Iba-1+ cells in the non-perfused injury core (Fig. 3.5 F, Fig. 3.6 A-B).

To further determine the immune cell profile within the infarct, double immunofluorescence for TMEM119, a specific microglia marker, and CD68 was performed at 72 h post-stroke. Within the non-perfused region, relatively few TMEM119+ microglia were observed. The majority of cells were TMEM119-/CD68+ suggesting infiltration of peripheral monocytes (Fig. 3.6 C). In contrast, TMEM119+ microglia were abundant within the hypo-perfused region and their processes expressed CD68 (Fig. 3.6 C). Few TMEM119-/CD68+ cells were observed in this region. This demonstrates distinct immune cell localization within both the ischemic core and hypo-perfused region of the infarct.

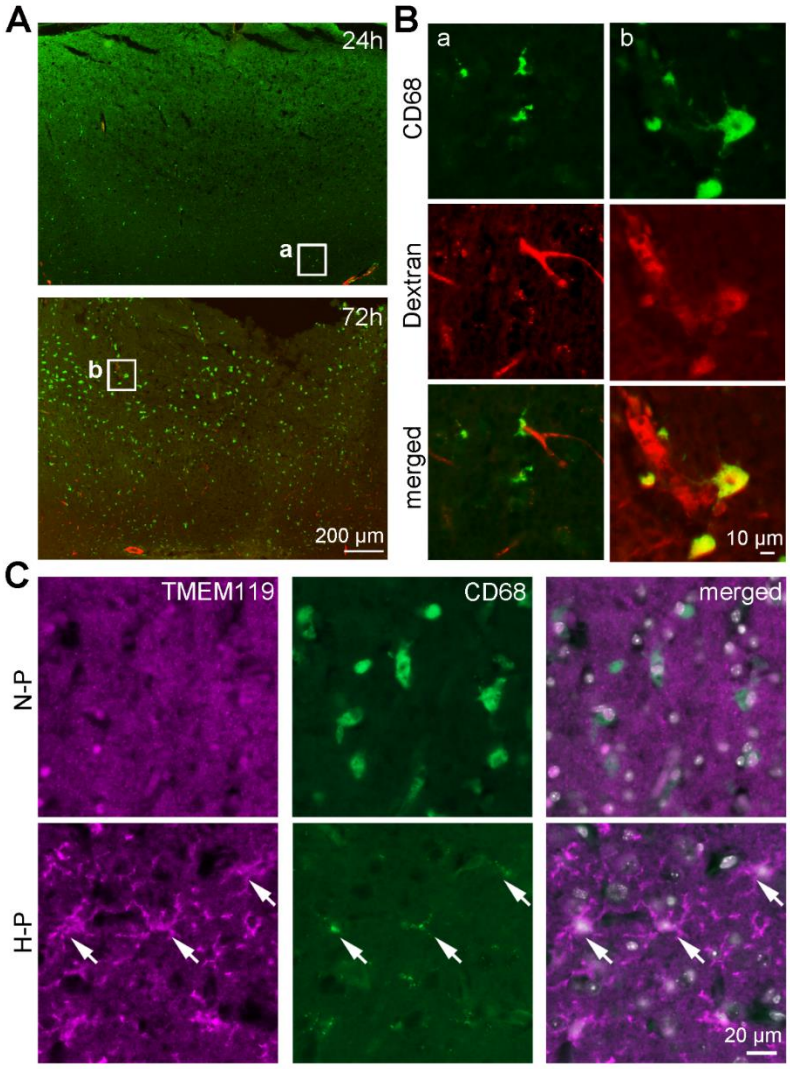

Figure 3.6: An increase in phagocytosis is observed from 24 to 72 h post-stroke with a distinct localization of immune cells within the infarct.

(A) Low magnification photomicrographs show CD68+ cells within the infarct at 24 h and 72 h post-stroke. (B) Higher magnification shows CD68+ cells near perfused blood vessels labelled with Texas Red within the infarct. (C) Double-labelling of TMEM119 and CD68 shows predominantly TMEM119-/CD68+ infiltrating monocytes within the non-perfused region at 72 h post-stroke. TMEM119+/CD68+ microglia are observed

within the hypo-perfused region. Arrows point to CD68+ staining within the processes of microglia. N-P= non-perfused, H-P= hypo-perfused

3.3.6 The majority of neuronal cell death occurs within the first 4 h post-stroke.

To examine the extent of neurodegeneration, brain sections were stained with FJC, an anionic fluorescent marker of degenerating neurons (Schmued et al., 2005). At 4 h post-stroke, numerous FJC+ neurons were observed throughout the infarct and even a few beyond the limits of the infarct. By 24 and 72 h post-stroke, FJC+ neurons were observed only within the infarct boundaries (Fig. 3.7 A, B).

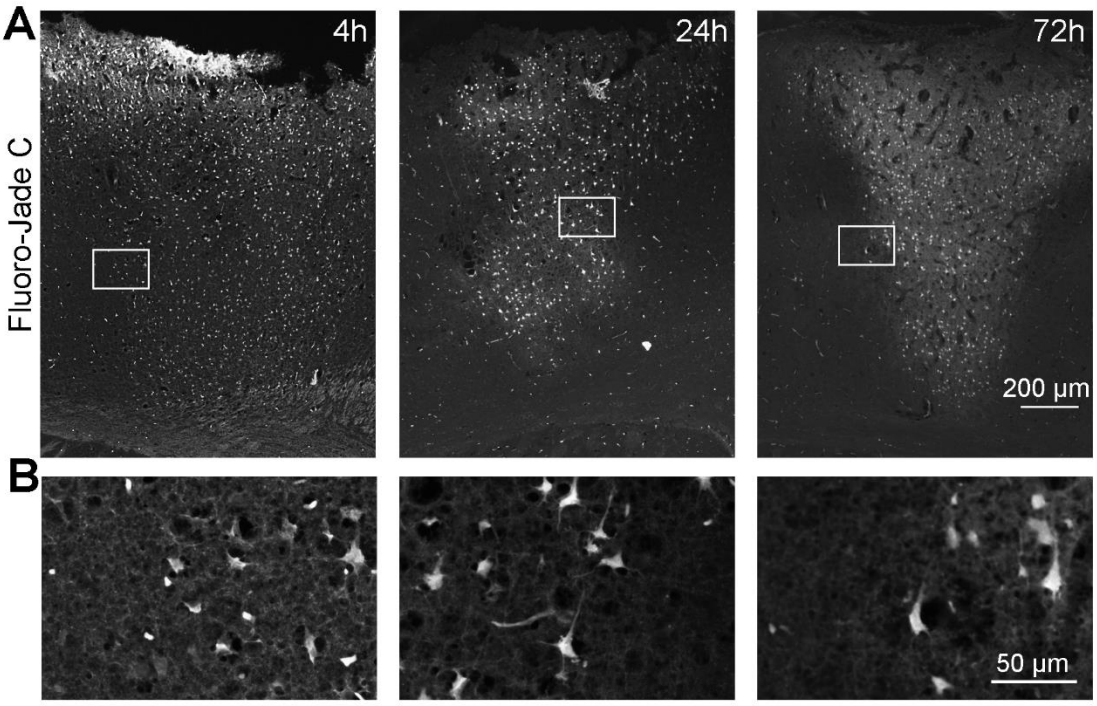

Figure 3.7: Extensive neuron degeneration is observed across the infarct during the initial 72 h post-stroke.

(A) Representative low magnification images of Fluoro-Jade C+ neurons within the infarct at 4 h, 24 h, and 72 h post-stroke. (B) Higher magnification of degenerating neurons along the border of the infarct.

To assess neuron survival within the non-perfused core and hypo-perfused region, NeuN immunofluorescence was performed and the number of NeuN+ neurons and Hoechst+ nuclei were quantified and compared to naïve (Fig. 3.8). For each animal that received an intra-cortical injection of saline or ET-1, the NeuN+ neurons within the contralateral cortex was considered the perfused region. Neurons in the contralateral perfused region appeared robust and healthy. Comparisons of NeuN+ neurons and Hoechst+ nuclei in the perfused region were not significantly different between saline and ET-1 brains at each time point (data not shown).

Within the non-perfused core, the surviving NeuN+ neurons appeared shrunken in both saline and ET-1 brains (Fig. 3.8 A). Neuron death was immediate. At 4 hours post-surgery, there were only 17.1 ± 6.5 NeuN+ neurons surviving in saline brains and 11.9 ± 11.5 NeuN+ neurons in ET-1 brains in comparison to 66.0 ± 3.2 NeuN+ within the same region in naïve brains (Fig. 3.8 B). Thus, ~80% of neurons died within the first 4 hours following stroke in the non-perfused core. The number of NeuN+ neurons within the non-perfused core was affected by treatment [$F(1,30) = 28.22$, $p<0.0001$]. Neuron loss occurred more rapidly in ET-1 brains than saline brains with further losses observed at 8 and 12 h post-stroke. By 12 h, only 3.9 ± 2.0 NeuN+ neurons survived in ET-1 brains versus 17.4 ± 1.7 in saline brains ($p<0.05$). Beyond 12 h further neuronal cell death did not occur within the infarct core as by 72 h there was only 2.9 ± 1.1 NeuN+ neurons corresponding to a 5% survival rate. In saline injured brains, after the initial reduction of NeuN+ neurons at 4 h, a further loss was observed at 24 h post-injury and by 72 h, there was only 11.3 ± 3.4 NeuN+ neurons corresponding to a 17% survival rate. Similarly, the number of Hoechst+ nuclei within the non-perfused core revealed a sharp loss at 4 h with

69.3 ± 10.3 Hoechst+ nuclei in ET-1 and 68.2 ± 15.4 Hoechst+ nuclei in saline brains versus 110.4 ± 3.0 in naïve brains. This represents a 40% loss of Hoechst+ nuclei compared to naïve control brains. A comparison of the number of Hoechst+ nuclei between saline and stroke injuries revealed there was no significant change in Hoechst+ nuclei with treatment [$F(1,30)=0.02428$, $p=0.8772$] or time [$F(4,30)=0.6838$, $p=0.6087$] (Fig. 3.8 C).

Significantly more neurons survived in the hypo-perfused region than in the infarct core (Fig. 3.8 D). Compared to naïve brains where 66.0 ± 3.2 cells are NeuN+ in the counting region, there were only 40.2 ± 6.0 NeuN+ neurons in ET-1 brains at 4 h post-stroke indicating a 40% loss of neurons. By 72 h post-stroke, only ~50% of NeuN+ neurons (32.3 ± 3.7) survived within the hypo-perfused region. A one-way ANOVA revealed a significant main effect of stroke [$F(5,24) = 31.10$, $p<0.0001$] on the survival of NeuN+ neurons in the hypo-perfused region. Dunnett's multiple comparison post hoc test revealed each time point was significantly different than naïve ($p<0.001$) (Fig. 3.8 E). Despite the reduction in neuron numbers within the hypo-perfused region, there was no significant difference in the number of Hoechst+ nuclei compared to naïve [$F(5,24)=1.590$, $p=0.2106$] (Fig. 3.8 F).

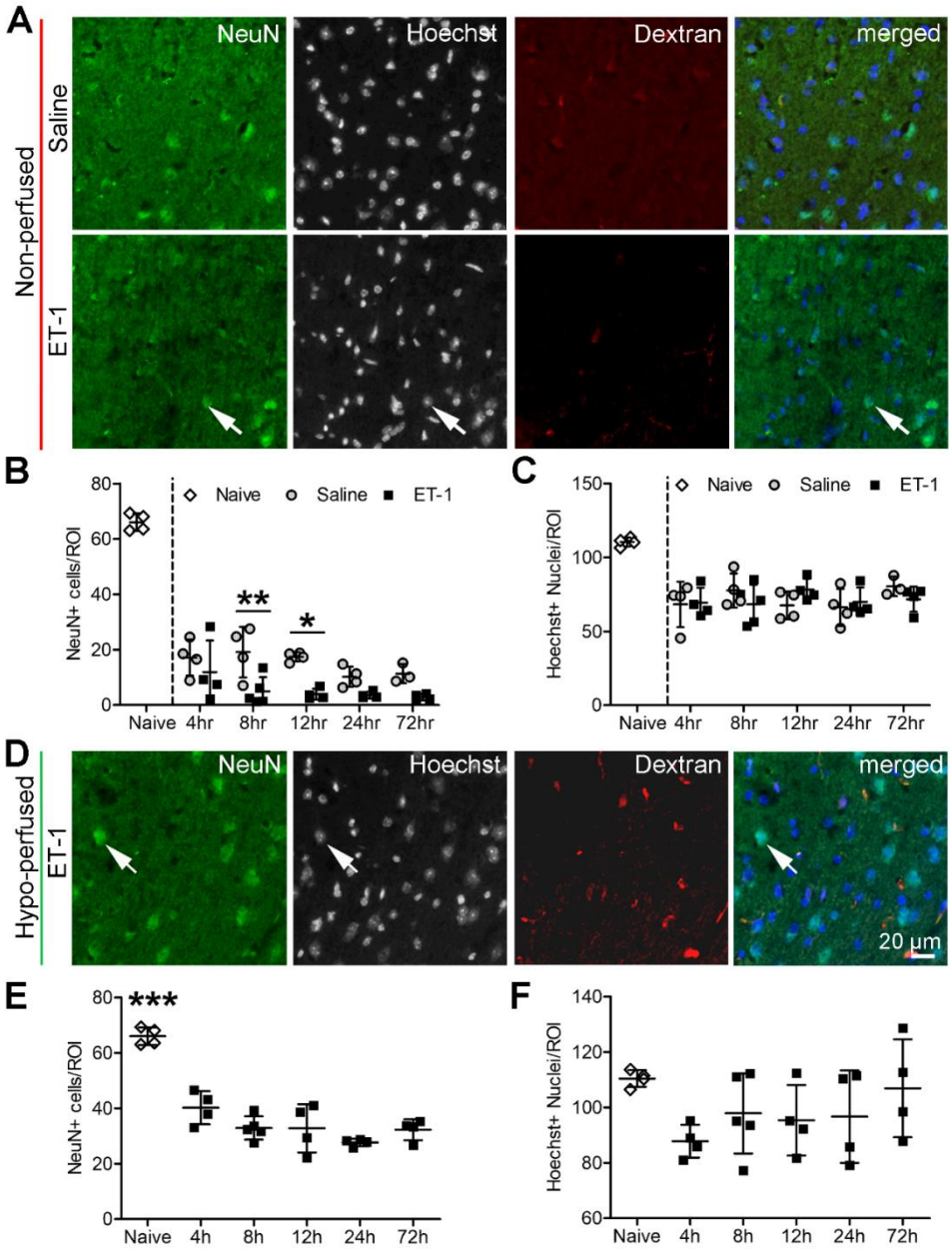

Figure 3.8: Neuronal loss occurs within the first 4 h post stroke.

(A) Representative images of NeuN+ neurons within the non-perfused injury core in saline and ET-1 brains. (B, C) NeuN+ cells and Hoechst+ nuclei were counted within the non-perfused, injury core in saline and ET-1 brains (ROI: 200 µm x 200 µm boxed area, two-way ANOVA and Bonferroni post hoc, Naïve: *n*=4; 4 h: *n*=4 Saline, *n*=4 ET-1; 8 h:

n=4 Saline, *n*=5 ET-1; 12 h: *n*=4 Saline, *n*=4 ET-1; 24 h: *n*=4 Saline, *n*=4 ET-1; 72 h: *n*=3 Saline, *n*=4 ET-1). (D) NeuN+ neurons in the hypo-perfused region of the infarct at 24 h post-stroke. Arrows point to NeuN+ neurons and nuclei labelled with Hoechst within each region. (E, F) NeuN+ cells and Hoechst+ nuclei were counted within the hypo-perfused region in ET-1 brains and compared to naïve brains (ROI: 200 µm x 200 µm boxed area, one-way ANOVA and Dunnett's post hoc, Naïve: *n*=4; 4 h: *n*=4 ET-1; 8 h: *n*=5 ET-1; 12 h: *n*=4 ET-1; 24 h: *n*=4 ET-1; 72 h: *n*=4 ET-1). *$p<0.05$, **$p<0.01$, ***$p<0.001$

The neuron cell counts were based on quantification of NeuN+ nuclei and do not relay information about the health of neuronal dendrites or axons, which are also susceptible to ischemic injury. To assess the state of dendrites, immunofluorescence for microtubule associated protein-2 (MAP-2) was performed. MAP-2 immunofluorescence labelled numerous dendrites spanning toward the pial surface in the uninjured, contralateral cortex (Fig. 3.9 A). At 4 h and 24 h post-stroke, the non-perfused infarct core was almost completely devoid of MAP-2+ dendrites. A closer examination of the hypo-perfused region at 4 h intervals within the acute 12 h period revealed widespread dendritic blebbing (Fig. 3.9 B). By 12 and 24 h post-stroke, degeneration of dendrites was visible with the discontinuous MAP-2 labelling of dendrites and an overall loss of MAP-2+ dendrites (Fig. 3.9 B). The number of intact MAP-2+ dendrites (50 µm in length or longer) were quantified within a 200 µm x 100 µm (w x h) boxed area. A one-way ANOVA revealed a main effect of stroke on reducing the number of intact dendrites within the hypo-perfused region [$F(2,11)= 36.19$, $p<0.0001$]. Dunnett's multiple comparison post hoc test revealed that the number of intact dendrites were significantly reduced at 4 h ($p<0.001$) and 24 h ($p<0.001$) in comparison to naïve (Fig. 3.9 C). Axons

within the hypo-perfused penumbra region, were visualized by immunofluorescence for SMI-312, a pan-neurofilament marker. In comparison to the healthy, contralateral cortex, SMI-312 immunofluorescence was only slightly reduced at 4 h post-stroke, however; by 24 h there was a clear loss of SMI-312 immunofluorescence with only a few axons visible (Fig. 3.9 D). Next, MAP-2 and NeuN double immunofluorescence of neurons in the hypo-perfused region at 24 h post-stroke was compared with the healthy neurons in the contralateral cortex. In contrast to healthy neurons, surviving neurons within the hypo-perfused region had an overall reduction of MAP-2 immunofluorescence in the cell soma, a loss of dendrites and shrunken nuclei that retained NeuN+ staining. (Fig. 3.9 E). Taken together, these results demonstrate that there is extensive degeneration of surviving neurons in the hypo-perfused region in the acute 24 h post-stroke.

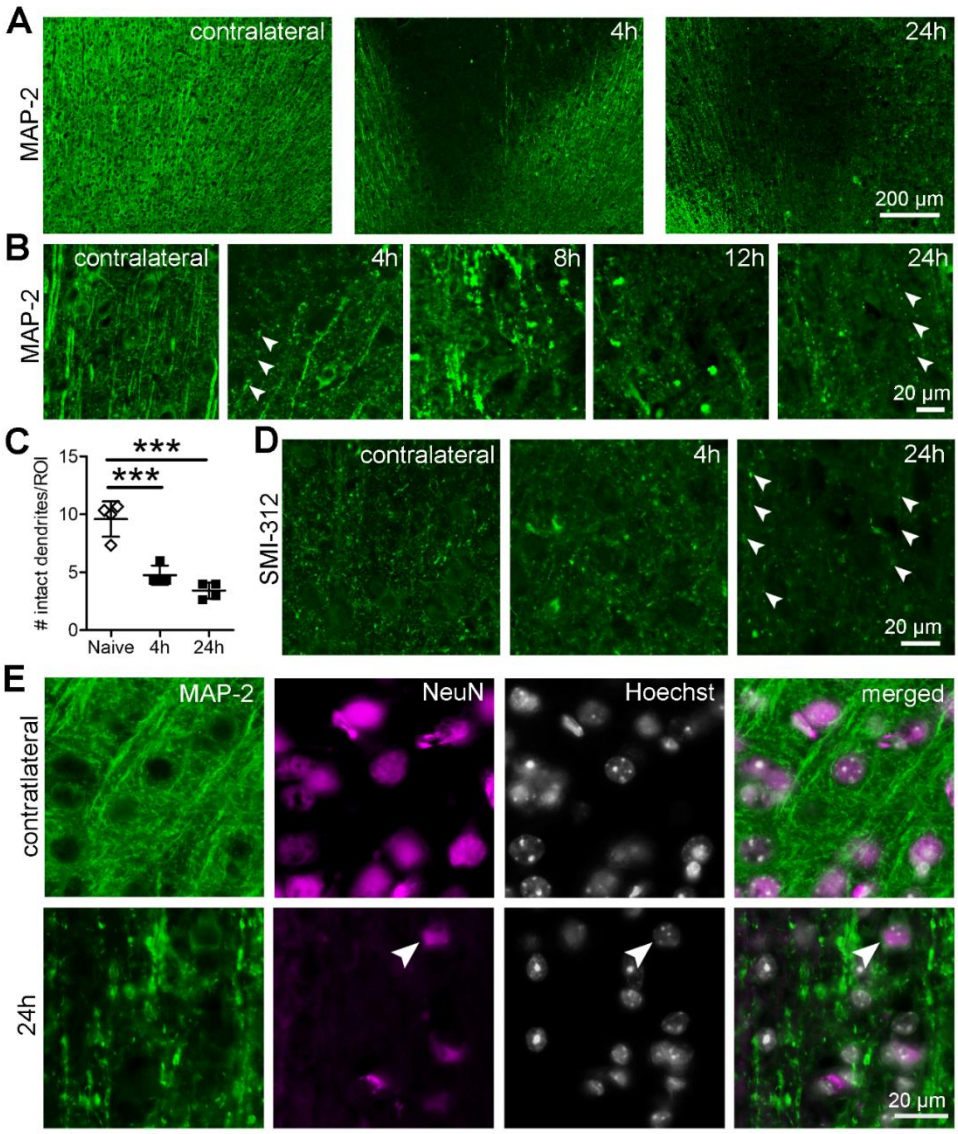

Figure 3.9: Degeneration of axons and dendrites occurs throughout the acute 24 h post-stroke period.

(A) Representative low magnification images of MAP-2 immunofluorescence labelling of dendrites in the contralateral hemisphere, and in ET-1 brains at 4 h and 24 h post-stroke. (B) Higher magnification images of MAP-2+ dendrites in the contralateral hemisphere and in the hypo-perfused region at 4, 8, 12 and 24 h post-stroke. Dendritic blebbing is observed by 4 h post-stroke and becomes extensive by 24 h (arrow heads). (C) The

number of intact MAP-2+ dendrites were quantified within the hypo-perfused region in ET-1 brains and compared to naïve (ROI: 200 µm wide x 100 µm high boxed area, one-way ANOVA and Dunnett's post hoc, Naïve: n=4; ET-1 4 h: n=4; ET-1 24 h, n=4, ***$p<0.001$). (D) SMI-312 immunolabelling of axons in the contralateral hemisphere and in the hypo-perfused regions at 4 h and 24 h post-stroke. SMI-312 immunofluorescent labelling of axons in the hypo-perfused region is lost in the initial 24 h post-stroke (arrow heads). (E) Representative images of MAP-2 and NeuN double immunolabelling of neurons in the contralateral hemisphere and the hypo-perfused region at 24 h post-stroke. The degeneration of surviving neurons within the hypo-perfused region is demonstrated by a loss in MAP-2 immunofluorescence, extensive dendritic blebbing and shrunken NeuN+ nuclei (arrowheads).

3.4 Discussion

In this study, the acute cellular response to a focal ischemic stroke within the infarct core was compared with the penumbra region. Dextran vascular labelling was used to distinguish the three zones of perfusion: the non-perfused, hypo-perfused and perfused regions. Our main findings show that following a small focal stroke: (i) significant disruption of the BBB occurred between 12 and 24 h post-stroke; (ii) the astroglial and microglia/macrophage responses were distinct in the infarct core versus the hypo-perfused, penumbra region; and (iii) neuron cell death occurred within the first 4 h post-stroke; however, degeneration of axons and dendrites continued throughout the hypo-perfused region in the acute 24 h period. The extensive degeneration of neuronal processes suggests that the health of surviving neurons within the penumbra region is in constant flux. Taken together, these findings demonstrate distinct spatiotemporal cell

responses to a focal ischemic stroke in the hypo-perfused, penumbra region versus the ischemic core.

3.4.1 Extensive BBB breakdown occurs during the acute post-stroke period.

Breakdown of the blood brain barrier occurs within hours following large ischemic strokes, such as MCAO and smaller focal strokes like photothrombosis. Occlusion of the MCA for two or three hours followed by 10 min reperfusion results in breakdown of the BBB as demonstrated by extensive leakage of dextran-conjugated fluorochromes into the brain (Jin et al., 2012). Using dimeglumine gadopenetate (590 Da) as an indicator of small molecule leakage and Evans Blue albumin (75.8 kDa) as an indicator of large molecule leakage from blood vessels, Strbian and colleagues showed that 90 min of MCAO followed by reperfusion resulted in breakdown of the BBB for both small and large molecules within 25 min of reperfusion (Strbian et al., 2008). Although other focal stroke models, such as photothrombosis, have shown breakdown of the BBB within the first 1-3 h following stroke (Nahirney et al., 2016; Schoknecht et al., 2014), less is known about the timing and extent of BBB breakdown following an ET-1 induced stroke.

In this study, dextran-conjugated fluorochrome labeling of blood vessels was used to identify open and perfused blood vessels because it adheres to the blood vessel walls and is retained in the tissue following processing for immunohistochemistry unlike Evans Blue. However, the leakage of dextran into the brain appeared patchy in contrast, to the diffuse staining of Evans Blue, which may be attributed to differences in the duration of application and adherent properties of dextran versus albumin. The protocol for Evans

Blue is to inject 30 min to 1 h prior to euthanasia allowing a longer time for the dye to diffuse through the brain, whereas in the current study dextran was injected 2 min prior to euthanasia which limited the time for diffusion of the dextran. Previous studies have similarly shown a patchy distribution of dextran when applied 10 min prior to euthanasia (Fernandez-Lopez et al., 2012; Jin et al., 2012). The 70 kDa dextran is a complex multi-branched glucan that may not diffuse as rapidly through brain tissue as Evans Blue.

Dextran leakage was not observed within the first 12 h post-stroke; however, by 24 h patches of dextran in the brain parenchyma were visible. This suggests that disruption of the BBB occurred between 12 and 24 h post-stroke. Due to the 70 kDa size of the dextran-conjugated fluorochrome, leakage into the brain parenchyma is consistent with significant disruption of the BBB. This is further supported by the observation of neutrophil infiltration in the brain at 24 h post-stroke. Although leakage of smaller molecules from the blood may occur earlier, our data shows that significant disruption of the BBB occurs between 12 and 24 h following an ET-1 induced stroke in mice. This is in sharp contrast to photothrombotic stroke models where the BBB breaks down within 3 h post-stroke (Nahirney et al., 2016; Schoknecht et al., 2014). However, there are differences in how ischemia is induced in each of the models. In photothrombotic stroke, photo activation of Rose Bengal causes the formation of oxygen free radicals, which results in platelet aggregation and the formation of thrombosis that block the blood vessel causing ischemia. Free radicals also cause cytotoxic damage to the vascular endothelial cells leading to rapid disruption of the BBB (Carmichael, 2005; Sommer, 2017; Watson et al., 1985). In contrast, cortical injections of ET-1 cause vasoconstriction of blood

vessels resulting in ischemia. Aside from ischemia, ET-1 does not directly damage endothelial cells.

Following an ET-1 stroke, the BBB remains compromised as dextran leaks were observed at 72 h post-stroke. This is consistent with other stroke models including photothrombotic and MCAO, where the BBB remains open for 3-4 weeks post-stroke (Abo-Ramadan et al., 2009; Nahirney et al., 2016; Reeson et al., 2015; Strbian et al., 2008). Similarly, BBB disruption has been observed in human patients at one month post-stroke (Liu et al., 2013). Whether the BBB is still compromised one month following an ET-1 stroke in mice has not been investigated; however, our data shows that significant disruptions in the BBB occurs between 12 and 24 h and remains open up to 72 h post-stroke.

3.4.2 Glial activation coincides with BBB breakdown

Glial cell activation coincided with breakdown of the BBB and infiltration of peripheral immune cells at 24 h post-stroke. Using upregulation of GFAP and Iba-1 as markers of activated astrocytes and microglia/macrophages respectively, significant activation was observed by 24 h post-stroke. GFAP+ reactive astrocytes were localized to the hypo-perfused and perfused region surrounding the infarct but were absent from the infarct core. This is consistent with previous studies that have shown a lack of reactive astrocytes in the infarct core that has been attributed to astroglial cell death (Fuxe et al., 1992). In contrast, Iba-1 immunoreactivity was observed throughout the non-perfused core and hypo-perfused, penumbra regions. Further analysis revealed that CD68+ amoeboid-shaped, macrophages were localized to the infarct core, whereas the more

ramified, double-labelled (TMEM119+ and CD68+) microglia were concentrated within the hypo-perfused region. Both GFAP and Iba-1 immunoreactivity were found to increase from 24 h to 72 h post-stroke. Immunoreactivity for both proteins has been shown to remain high up to 7 d post-stroke (Ahn et al., 2019; Fifield et al., 2019; Hughes et al., 2003; Sozmen et al., 2009). Although upregulation of GFAP and Iba-1 proteins are indicators of astrogliosis and activated microglia/macrophages, they are not markers of the initial stages of activation. These cells became fully activated within the initial 24 hours following a focal ET-1 induced stroke. Taken together, this demonstrates that the level of perfusion determines the location of astrogliosis and microglia/macrophage activation within the infarct.

3.4.3 Neuron survival is significantly reduced within 4 hours post-stroke

Cell death following large ischemic strokes such as MCAO has been well documented; however, the time-course of cell death following a small focal ischemic stroke such as an ET-1 stroke has not been well characterized. Early events such as chromatolysis of neurons is observed within 3 h of an ET-1 stroke (Fuxe et al., 1992). In previous studies, FJC labelling of degenerating neurons was found to be highest at 1 day and dropped by 4 days following an ET-1 stroke in mice or rats (Nguemeni et al., 2015; Nusrat et al., 2018). In this study, neuronal cell death was examined within the initial 24 h period. Counts of NeuN+ neurons within the non-perfused core and hypo-perfused region revealed that the largest reduction in neuron numbers occurred within the first 4 h post-stroke with ~80% loss of neurons in the non-perfused core and ~40% loss within the hypo-perfused region. Neuronal cell death is immediate and rapid in both regions and is

consistent with necrosis and excitotoxic injury, which is known to occur immediately following an ischemic insult (Fricker et al., 2018; Lo et al., 2005). From 8 to 72 h post-stroke, further reductions in the number of NeuN+ neurons was not observed within either the non-perfused core or the hypo-perfused region. However, numerous FJC+ neurons were observed throughout the infarct at 4, 24 and 72 h post-stroke indicating extensive neuron degeneration. This apparent mismatch may be attributed to a slow clearance rate of degenerating neurons and retention of the NeuN signal in some degenerating neurons. This is supported by our finding that at 24 h post-stroke, degenerating neurons within the hypo-perfused region still retained the NeuN+ signal despite the loss of MAP-2 immunofluorescence, significant dendritic blebbing, and shrunken nuclei. I have previously demonstrated that a small portion of FJC+ neurons co-label with NeuN+ following ischemic stroke (Fifield et al., 2019). This suggests that the NeuN+ signal does not provide information on the health of the neuron.

3.4.4 Surviving neurons undergo extensive degeneration from 4 to 24 hours post-stroke

The penumbra region surrounding the infarct core is a region where delayed neuron cell death occurs. The delayed cell loss following stroke involves apoptotic, excitotoxic and autophagic forms of cell death depending on the extent of cellular damage (Fricker et al., 2018; Lo et al., 2005). Because these forms of cell death can be blocked, the neurons in this region are considered “rescuable”. In our study, although neuronal cell death was not observed within the hypo-perfused penumbra region between 8 and 72 h post-stroke, extensive degeneration of neuronal dendrites and axons was observed. By 4 h post-stroke, there was a reduction in intact MAP-2+ dendrites and SMI-312+ axons and

by 24 h, the loss was extensive. Brown et al., showed that extensive dendritic spine loss occurs from 2-24 h following an ET-1 stroke, while surviving spines elongate within the penumbra region (Brown et al., 2008). Within 6 h of an ET-1 induced white matter stroke, numerous axons are immunopositive for amyloid precursor protein indicative of axonal damage (Gresle et al., 2006; Hughes et al., 2003). Similarly, at 24 h following an MCAO stroke, extensive dendritic degeneration is observed within the infarct (Hou et al., 2009). To some extent, axon and dendritic damage is reversible (Li & Murphy, 2008; Zhu et al., 2017). With two-photon microscopy to visualize axons and dendrites in real-time, axon blebbing was observed within minutes of a MCAO or bilateral common carotid artery occlusion as a result of ischemia initiated depolarization (Murphy et al., 2008). The reversal of dendritic blebbing depends on the duration of ischemia. One hour of ischemia or less resulted in almost full recovery of dendritic blebbing, whereas partial recovery was observed with 3 h of ischemia and no recovery after 6 h (Zhu et al., 2017). In contrast, the loss of MAP-2 and SMI-312 immunoreactivity in dendrites and axons from 4 to 24 h post-stroke is indicative of significant degeneration of the cytoskeleton within neural processes. Unlike MCAO and carotid ligation models of stroke, where reperfusion is immediate, reperfusion in the ET-1 stroke model is gradual - extending over several hours (Biernaskie et al., 2001). Our data shows that the reduced number of dextran-labelled blood vessels in the hypo-perfused region does not change over the 72 h post-stroke, indicating that fewer blood vessels were perfusing the tissue keeping it in a hypo-perfused state for an extended period of time. Without sufficient levels of oxygen and glucose to recover and restore essential cellular functions, degeneration ensues. Although there were no additional losses of NeuN+ neurons within the hypo-perfused region from 8 to 72 h

post-stroke, the extensive degeneration of axons and dendrites suggests that these "rescuable neurons" may have a much shorter survival time than previously anticipated.

The acute response to a focal stroke reveals that the initial ischemic insult is the most damaging to neurons. This resulted in rapid neuron cell death within the initial 4 h post-stroke (Fig. 3.10). Neurons that survived in the hypo-perfused, penumbra region showed extensive axon and dendrite degeneration from 4 h to 24 h post-stroke. Degeneration of the neuronal processes is likely a result of the initial excitotoxic injury to the neurons as it occurred prior to glial cell activation, BBB breakdown and peripheral immune cell infiltration, which was not observed until 24 h post-stroke (Fig. 3.10) (Murphy et al., 2008). Rescue of neurons and reversal of early dendritic blebbing and spine loss is feasible if tissue reperfusion is rapid. As the degeneration of neuronal processes occurs over the initial 12-24 h post-stroke, it remains to be shown whether combining reperfusion strategies with inhibitors to block axon and dendritic degeneration may improve stroke outcomes.

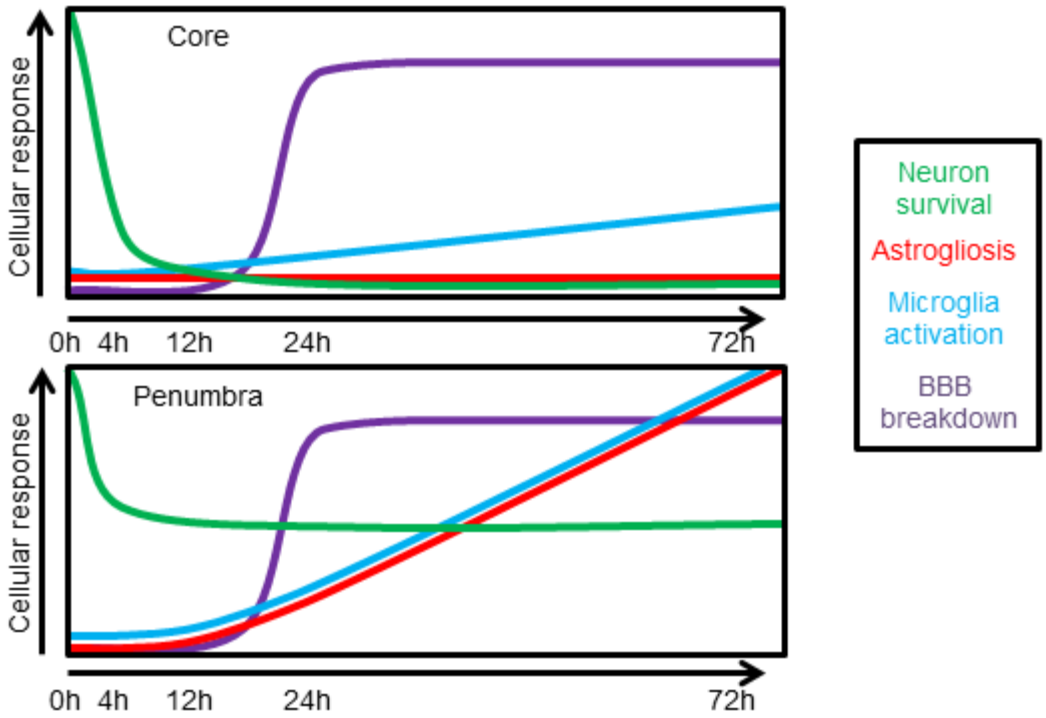

Figure 3.10: Comparison of the acute cellular responses to an ischemic stroke between the non-perfused infarct core and hypo-perfused penumbra region.

Distinct cellular responses were observed within the ischemic core and hypo-perfused, penumbra region during the acute post-stroke period. Neuron cell death occurred within the first 4 h post-stroke in both the infarct core and hypo-perfused region. Neuron numbers remained relatively constant within both regions from 4 h to 72 h. Blood brain barrier breakdown was observed from 24 h to 72 h post-stroke within both regions. The breakdown of the BBB coincided with the appearance of activated microglia in the hypo-perfused region and macrophages within the ischemic core at 24 h. Their numbers continued to increase up to 72 h post-stroke. The appearance of astrogliosis also coincided with breakdown of the BBB at 24 h. Astrogliosis was not observed within the infarct core, but progressively increased in the hypo-perfused region from 24 to 72 h.

3.5 Conclusions

In summary, these findings demonstrate that the acute cellular response to a small focal ischemic stroke changes over time and is dependent on the level of perfusion. Using vascular labelling to distinguish the hypo-perfused, penumbra region from the non-perfused ischemic core, the results show how the cellular responses in each region are distinct (Fig. 3.11). Astrogliosis and microglia were activated within the hypo-perfused region, whereas the non-perfused core contained primarily infiltrating monocytes. More neurons survived within the hypo-perfused region; however, they showed signs of extensive axon and dendrite degeneration in the acute 24 h post-stroke period indicating their precarious state. The rapid degeneration of surviving neurons within the penumbra region reveals an urgent need to develop acute therapies to inhibit neural degeneration within the first few hours post-stroke to rescue salvageable brain tissue.

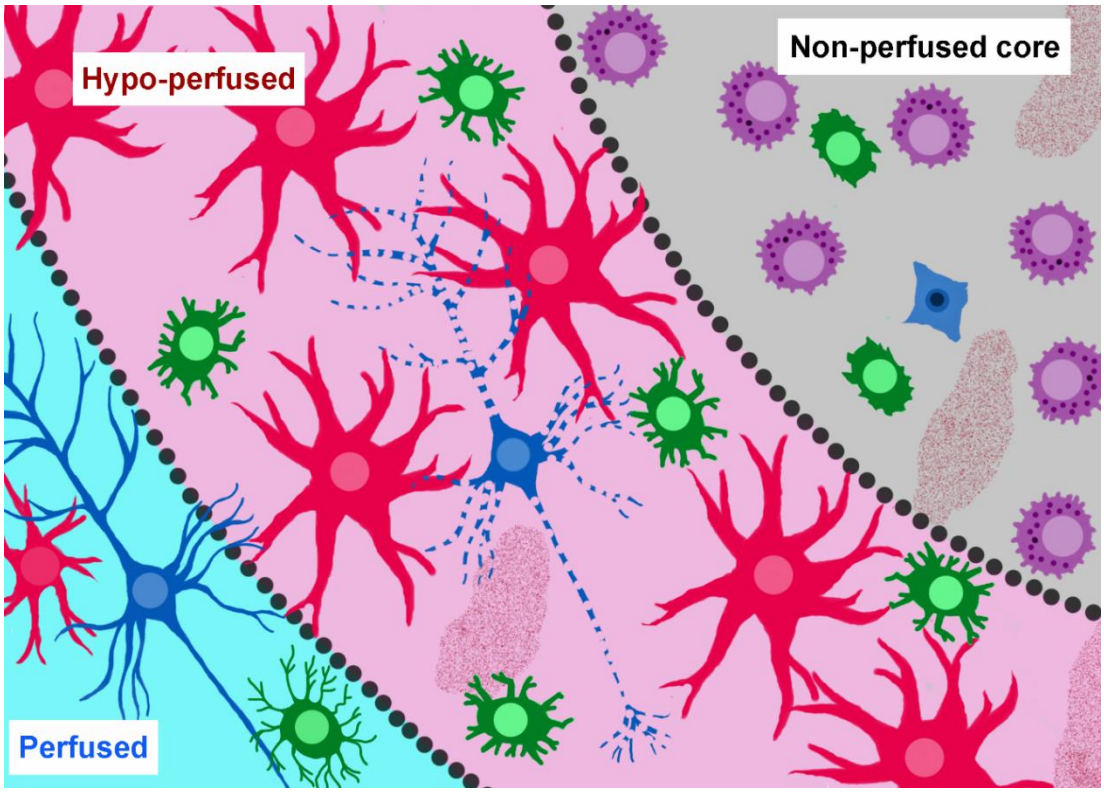

Figure 3.11: Distinct cellular responses are observed within the core, hypo-perfused penumbra and perfused region.

Within the core, extensive neuronal death (condensed nucleus) is observed with infiltrating macrophages, activated microglia and leakage of blood vessels. Within the hypo-perfused region, neuron degeneration is accompanied by activated microglia, astrogliosis and leaky blood vessels. Blue=neurons; pink= astrocytes; purple= macrophages; green= microglia; speckled red= leakage of blood vessels.

CHAPTER 4

DOCOSAHEXAENOIC ACID ATTENUATES BLOOD BRAIN BARRIER DISRUPTION WITHIN THE CORTEX OF LEAN MICE FOLLOWING ACUTE ISCHEMIC STROKE.

CO-AUTHORSHIP STATEMENT

I, Kathleen Fifield, designed the experiments with my supervisor Dr. Jacqueline Vanderluit. I performed all experiments and made all figures with edits from my supervisor.

4.1 Introduction

Ischemic stroke is a neurovascular disease that is associated with several independent risk factors, most notably diet-induced obesity (Meschia et al., 2014). Numerous studies have demonstrated a link between diets high in saturated fats leading to obesity and the increased risk of cardiovascular disease leading to ischemic stroke (Lee et al., 2018; Meschia et al., 2014; Strazzullo et al., 2010). However, the majority of animal research investigating ischemic stroke has neglected to include the obesity factor and instead used healthy, lean rodents. It is therefore not surprising that preclinical research has had challenges translating to the clinic (Haley & Lawrence, 2016).

The type of fat, whether it is a saturated or unsaturated fatty acid, can have a different effect on the development or prevention of ischemic stroke, respectively (Sun et al., 2018; Teng et al., 2014). Previous studies have shown that diets high in saturated fats lead to obesity, vascular dysfunction and an overall reduction in CBF within the brain (Ayata et al., 2013; Li et al., 2013). For instance, 8 weeks of 45% HFD reduced functional hyperemia within the rat barrel somatosensory cortex following whisker stimulation (Li et al., 2013). This indicates impaired cerebrovascular function with chronic HFD feeding. Furthermore, chronic low-grade inflammation within the periphery and CNS has been observed with prolonged diets high in saturated fats (Guillemot-Legris et al., 2016). This consistent inflammation has been shown to increase circulating cytokines that can cause neuroinflammation within the brain (Guillemot-Legris & Muccioli, 2017). Previous studies have also shown that prolonged HFD can intensify stroke severity (Cao et al., 2015; Fifield et al., 2019; Herz et al., 2015; Maysami et al., 2015). A 3-fold increase in infarct volume was observed following 30 minutes of MCAO

and 6 months of 60% HFD feeding (Maysami et al., 2015). Although this effect is dependent on the duration of stroke and HFD exposure.

An increase in inflammation is observed within the brain post-stroke with HFD. Studies have shown an increase in proinflammatory cytokines and chemokines with HFD, such as TNF-α, CXCL-1 and CCL3, that can exacerbate ischemic injury (Maysami et al., 2015; Terao et al., 2008). Furthermore, HFD increases adhesion molecules ICAM-1 and VCAM-1 within cerebral blood vessels which can increase leukocyte infiltration within the brain and also promote BBB disruption (Herz et al., 2014; Herz et al., 2015; Maysami et al., 2015; Terao et al., 2008). These studies indicate that prolonged HFD can modulate post-stroke inflammation increasing stroke severity.

To date, the most effective post-stroke treatments involve recanalization to restore blood flow during the immediate hours following ischemic stroke. These include the clot busting drug tPA or surgical removal of the clot via endovascular thrombectomy. These treatments are limited to a time frame of approximately 4.5 to 6.5 hours and not all patients are eligible (Nadeau et al., 2005). Furthermore, tPA has been shown to be damaging to the endothelial cells of blood vessels (Abu Fanne et al., 2010; Chevilley et al., 2015; Nicole et al., 2001; Wang et al., 2003). Therefore, post-stroke treatments that are less damaging and can be administered beyond the restrictive time frame are crucial. One potential candidate that has been shown to restore cardiovascular dysfunction following stroke is polyunsaturated fatty acids such as omega-3.

Current knowledge on omega-3 use following stroke is controversial, showing both beneficial and adverse impacts on outcomes (Belayev et al., 2018; Yang et al., 2007). Previous studies have shown that the omega-3 DHA can reduce stroke severity

when administered through diet or i.v./i.p. injection (Belayev et al., 2009; Eady et al., 2012; Lalancette-Hebert et al., 2011; Pu et al., 2016). Low to medium doses of DHA (3.5 to 35 mg/kg, i.v. injection) was shown to improve neurological deficits when given 3 hours following 60 min of MCAO (Belayev et al., 2009). Interestingly, the highest dose (70 mg/kg) was not effective in reducing neurological deficits. When infarct volume was measured, the lower DHA dose of 3.5 mg/kg was more effective in reducing infarct volume compared to higher doses of DHA. A n-3 PUFA diet given 5-28 days post stroke in combination with daily i.p. injections of DHA at 10 mg/kg for 14 days was shown to reduce infarct volume, while either treatment on its own was insufficient (Pu et al., 2016). Combining both treatments (diet and i.p. injections) significantly reduced ischemic injury and enhanced both neurogenesis and angiogenesis 28 days following MCAO. These studies suggests the dose and the route of administration can impact post-stroke improvements observed with DHA (Belayev et al., 2009). In contrast to these studies showing promising results, other studies have shown that DHA can be detrimental to stroke recovery (Yang et al., 2007). Both arachidonic acid (500 nmol) and DHA (500 nmol) increased infarct volume at 24 hours post-stroke when administered i.p. 60 min following 90 min occlusion of the right MCA and bilateral CCA (Yang et al., 2007). This study indicates that the effect of DHA on acute ischemic stroke is unclear. The majority of studies that examine DHA treatment on stroke outcome use chronic time points (i.e. out to 7 days to 28 days post-stroke) and the effect of DHA on the acute post-stroke brain has yet to be elucidated. Furthermore, the effect of DHA on acute ischemic stroke with obesity as a comorbidity remains unknown.

The goal of this study was to assess early DHA administration following acute focal ischemic stroke in lean and obese mice. A focal ischemic stroke was induced using intra-cortical injections of ET-1. Here, we show that acute administration of DHA reduces BBB breakdown and infiltration of peripheral immune cells into the infarcted cortex at 24 hours post-stroke.

4.2 Methods

4.2.1 Experimental design

A total of 26 male C57BL/6 mice were singly housed and assigned either a standard chow diet (Chow) (16% calories from fat; Teklad Diets, Envigo; Cat. # 2018) or a high fat diet (HFD) (60% of calories from fat, Research Diets, NJ, Cat. # D12492) beginning at the time of weaning. Food and water were provided *ad libitum*. Animals were weighed weekly for 12 weeks and then received intra-cortical injections of Endothelin-1 (ET-1) to induce ischemic stroke. Mice were randomly assigned to one of four groups: Ctl+Chow (n=6), Ctl+HFD (n=7), DHA+Chow (n=6) and DHA+HFD (n=7). Chow or HFD mice were given an intraperitoneal (i.p.) injection of saline (control (Ctl), 200 µl total volume) or DHA (20 mg/kg, 200 µl total volume) at 2, 4 and 6 hours following ET-1 stroke. This dose of DHA was determined based on our preliminary results using 10 mg/kg or 20 mg/kg doses injected at different time points post-stroke (data not shown). The 20 mg/kg dose at 24 hours post-stroke was chosen following observational analysis of the infarct using Cresyl violet staining and NeuN immunofluorescence. Based on observations, the ischemic injury appeared smaller with

more NeuN+ neurons with the higher 20 mg/kg dose in comparison to the 10 mg/kg dose, consequently the higher dose was chosen. Mice were euthanized at 24 hours post-stroke and tissue was processed for analysis. This 24-hour time point was chosen due to the results observed in Chapter 2 where BBB breakdown, immune cell infiltration and a heightened glial response coincided at this time. All experiments were conducted in compliance with ARRIVE (Animal Research: Reporting of *In Vivo* Experiments) guidelines (Kilkenny et al., 2010). Experiments were approved by Memorial University of Newfoundland's Institutional Animal Care Committee adhering to the Canadian Council on Animal Care guidelines.

4.2.2 Focal ischemic stroke surgical procedures

Stereotaxic surgery was performed on deeply anaesthetised animals using isoflurane as previously described in Chapter 2. A subcutaneous (s.c.) injection of Buprenorphine (0.02 mg/kg) was given for pain management. Body temperature was monitored using a rectal probe and maintained at $37^{o}C \pm 0.5^{0}C$ with a heat lamp and heating pad. During the surgery, two intra-cortical injections of ET-1 were administered at the following coordinates relative to bregma (i) +0.2 anterior-posterior (AP), +1.5 medial-lateral (ML), -1.0 dorsal-ventral (DV) and (ii) +1.0 AP, +1.5 ML, -1.0 DV. At each injection site, 1 µl of ET-1 (2 µg/µl, Cedarlane, Cat. # 05-23-3800) was injected over 5 minutes at a rate of 0.2 µl/min. To avoid backflow, the needle was left in place for 5 min after each injection. Following intra-cortical injections, mice were given a s.c. injection of saline (1 mL of 0.9%) for rehydration. Mice were placed back in their home cage following surgery with a heating pad underneath for approximately 2 hours.

Wellness was monitored until euthanasia. One animal died during surgery and was therefore excluded from the study (n=1, Ctl+HFD).

4.2.3 Tissue processing for histology and immunohistochemistry

Mice were anaesthetized with an intra-peritoneal injection of Euthanyl (250 mg/ml sodium pentobarbital, Vetoquinol, Cat. #IEUS001). Once unresponsive, an incision was made in the chest cavity to expose the heart and 250 µl of dextran-conjugated Texas Red (1 µg/µl, Invitrogen, Cat. # D1864) was injected into the left ventricle of the heart. Dissection began approximately 2 min following the intra-cardiac injection of dextran to ensure optimal labelling of blood vessels within the brain (Grade et al., 2013). Brains were extracted and blocked using a coronal 1 mm acrylic brain matrix, and brain slices were fixed in 4% paraformaldehyde for two days. Blocked brain sections were cryoprotected in increasing concentrations of sucrose (12%, 16% and 22%) over three days then frozen in isopentane cooled with dry ice. Frozen brains were sectioned with a cryostat microtome at 14 µm thickness in the coronal plane from the anterior to posterior extent of the stroke injury. Serial sections were collected across 6 slides such that, sections on each slide were 140 µm apart.

4.2.4 Cresyl Violet histology

To visualize the stroke within the cortex, slides containing sections throughout the injury were stained with cresyl violet. Slides were warmed at 37^{o}C for 20 minutes using a slide drying bench and transferred to filtered 0.1% w/v Cresyl Violet in water (Sigma, Cat. # C1791) for 30 minutes. Slides were placed in increasing concentrations of EtOH (50%, 70%, 90%, 95% and three times in 100% EtOH) for dehydration followed by

isopropanol and toluene for 30 seconds each. Slides were coverslipped using Permount (Fisher Scientific, Cat. # SP15-500) and dried overnight at room temperature.

4.2.5 Infarct volume and non-perfused region calculation

Infarct volume corrected for edema was conducted on cresyl violet stained sections throughout the rostral to caudal extent of the infarct as previously described in Chapter 2. Infarcts were mapped and those that were located within the anterior forelimb motor cortex were included in the study (Roome et al., 2014). This was to ensure that cell quantification and analysis was completed in similar regions within the brain. Two animals were excluded from infarct calculations due to incomplete sectioning of the entire stroke.

Dextran-conjugated Texas Red was used to label blood vessels that were open and perfusing at the time of euthanasia. The region of infarct that was void of Texas Red labelling indicated blood vessels that were not perfused and thus deemed the non-perfused region. The area (mm^2) of this region was quantified across three sections taken from the centre of the infarct per animal and averaged.

4.2.6 Immunohistochemistry

Immunohistochemistry was completed on slides of brain sections within the center of the infarct. The following primary antibodies were used: CD68 (1:400, AbD Serotec, Cat. # MCA1957, RRID: AB_322219), cyclooxygenase-2 (COX-2, 1:500, Cayman Chemical, Cat. # 160126, RRID: AB_327872), Ly6G (1:500, BD Pharmingen, Cat. # 551459, RRID: AB_394206), neuronal nuclei (NeuN, 1:100, Millipore, Cat. # MAB-377, RRID: AB_2298772) and TMEM119 (1:100, Abcam, Cat. # ab209064, RRID:

AB_2728083). Slides were incubated with the primary antibody overnight at room temperature and following three washes in PBS, incubated with the respective secondary antibody for 1 hour. The following secondary antibodies were used: goat anti-mouse Alexa Fluor 488 antibody (1:200, Invitrogen, Cat. # A21202, RRID: AB_2535788), goat anti-rat Alexa Fluor 488 antibody (1:200, Invitrogen, Cat. # A21208, RRID: AB_2535794) goat anti-rabbit Alexa Fluor 488 antibody (1:200, Invitrogen, Cat. # A21206, RRID: AB_2535792) and DyLight 649 goat anti-rabbit antibody (1:200, Jackson ImmunoResearch Lab Inc., Cat. # 111-496-144). After the 1 hour incubation, slides were washed in PBS and stained with Hoechst (Bisbenzimide H33258, Sigma Chemical Co., Cat. # 1155) to label nuclei. Slides were coverslipped with 1:3 glycerol: PBS solution and sealed with nail polish.

For albumin immunohistochemistry, slides were incubated overnight with albumin horse radish peroxidase (HRP)-conjugate (1:1000, GeneTex Inc., Cat. # GTX19195). After washes, slides were placed in hydrogen peroxide, methanol treatment for 10 min and then treated with the 3,3'-Diaminobenzidine (DAB) reaction according to the manufacturer's instructions (Cedarlane, Cat. # SK-4100, RRID: AB_2336382). Slides were dehydrated using ethanol solutions of increasing concentration followed with isopropanol and toluene and then coverslipped with Permount (Fisher Scientific, Cat. # SP15-500).

4.2.7 Fluoro Jade C staining

For FJC staining, slides were placed in solutions in the following order: 1% sodium hydroxide in 80% EtOH for 5 min, 70% EtOH for 2 min, water for 2 min, 0.06%

potassium permanganate solution for 10 min, water for 2 min, 0.0001% FJC working solution diluted in acetic acid solution for 30 min then followed by a wash in water for 2 min. Slides were dried on a slide warmer overnight at 35^{o}C in the dark. The following day, slides were cleared in xylene for 1 min and coverslipped with DPEX (Cedarlane, Cat. # 13514) (Fifield & Vanderluit, 2020).

4.2.8 Microscopy and cytometric analysis

Brain sections were imaged using a Zeiss Imager.Z1 upright microscope or a Zeiss Stemi-2000C dissecting microscope with an attached Zeiss Axiocam Mrm Rev3 camera (Carl Zeiss, Germany). Cytation 5 cell imaging multi-mode reader (Biotek, VT, USA) was used to image whole brains. Adobe Photoshop CS2 (San Jose, CA, USA) was used to compile figures with contrast and brightness adjusted equally for all images.

Cell counts were completed across a minimum of three sections per animal within the center of the infarct then averaged for each animal, using ImageJ software (https://imagej.nih.gov/ij/). TMEM119+, CD68+ and TMEM119+/CD68+ cells were counted within a 200 µm X 200 µm boxed area across the hypo-perfused, non-perfused and perfused (contralateral cortex) regions. The three perfusion regions were characterized based on blood vessel counts within a 200 µm X 200 µm boxed area and defined as follows: non-perfused core (≤ 5 BV), hypo-perfused penumbra (> 5 – 10 BV), and perfused region (> 10 BV) (Fifield et al., 2019). Total Ly6G+, COX-2+ and CD68+ cells were counted within the entire infarct. BBB breakdown was assessed by counting the total number of dextran-conjugated Texas Red leakages within the infarct in an area of 2.4 mm^2 (dimension 1.549 mm X 1.549 mm boxed region), at a 5x field of view. A

blood vessel was considered “leaky” if the size of the patch of dextran leakage was greater than 15 µm in diameter. Diffuse patches of dextran leakage meeting this criterion were included in the analysis whether or not it was associated with a visible blood vessel (Fifield & Vanderluit, 2020). Three sections were quantified per animal and the mean number of leaky blood vessels/section/animal were presented. The area of albumin extravasation was quantified as an assessment of BBB breakdown. Albumin+ staining appeared diffuse throughout the infarct and around the infarct border. The area containing the darkest albumin+ staining following DAB immunohistochemistry was measured across three sections per animal. Neuron survival was assessed by counting the number of NeuN+ cells within a 200 µm X 200 µm boxed area within the non-perfused and hypo-perfused regions as defined in Chapter 2. NeuN+ and Hoechst+ cells were quantified electronically using ImageJ software within the non-perfused and hypo-perfused regions. A macro in ImageJ was created with the following parameters: for NeuN+ cells, radius=50, size=30, infinity circularity=0.2 to 1.00; for Hoechst+ cells, radius=25, size=25, infinity circularity=0.3-1.00. The area of FJC+ degenerating neurons within the infarct, as well as the corresponding area of the non-perfused region lacking Texas Red labelling was quantified across three sections within the center of the infarct then averaged for each animal using AxioVision (AxioVision v4.8, Carl Zeiss, Germany).

4.2.9 Statistical Analysis

Statistical analysis was completed using GraphPad Prism 5 software (La Jolla, CA, USA). T-test, two-way ANOVA and repeated measures ANOVA followed by

Bonferroni post-hoc analysis was used for analysis and data were expressed as mean ± SD. Statistical significance level for all analysis was $p<0.05$.

4.3 Results

4.3.1 A significant increase in weight is observed following 12 weeks of high fat diet feeding.

To induce obesity, mice were fed either a HFD (n=13) or a standard chow diet (n=12) over 12 weeks beginning at the time of weaning. As expected, HFD feeding led to a greater increase in weight compared to chow-fed mice over the 12 week period (Fig. 4.1A). A two-way ANOVA revealed there was a significant increase in the percent weight gain over time [$F(11,253)=372.8$, $p<0.0001$], a significant increase in percent weight gain with HFD [$F(1,23)=34.34$, $p<0.0001$] and a significant interaction [$F(11,253)=40.1$, $p<0.0001$]. The percent increase in weight over baseline was significantly increased in mice fed HFD beginning at 5 weeks of feeding ($p<0.01$) in comparison to chow-fed controls and this continued up to 12 weeks ($p<0.0001$). Overall, Chow-fed mice weighed 31.6 g ± 4.5 g at the time of surgery, whereas HFD-fed mice weighed 44.0 g ± 4.0 g, approximately a 12 g increase in weight ($t(23)=7.3386$, $p<0.0001$) (Chow, n=12; HFD, n=13). These results are consistent with our previous study showing that 12 weeks of HFD is sufficient to cause a significant increase in weight and adipose tissue (Fifield et al., 2019).

4.3.2 The effect of post-stroke DHA treatment on infarct volume following acute focal ischemic stroke.

Previous data has shown that intra-cortical injections of ET-1 within the cortex results in a reproducible focal ischemic stroke with measurable behavioural deficits (Fifield et al., 2019; Roome et al., 2014). To determine whether post-stroke application of DHA affected infarct size, infarct volumes were compared across all experimental groups. Prolonged HFD feeding did not significantly increase infarct volume in the acute 24 h post-stroke period [$F(1,19)=0.765$, $p>0.05$] (Ctl+Chow 1.69 ± 0.31 mm^3 vs. Ctl+HFD 2.11 ± 0.76 mm^3). There was no significant difference in infarct volumes following DHA treatment [$F(1,19)=0.737$, $p>0.05$] (Ctl+Chow 1.69 ± 0.31 mm^3; Ctl+HFD 2.11 ± 0.76 mm^3; DHA+Chow, 1.68 ± 0.51 mm^3; DHA+HFD 1.69 ± 0.58 mm^3) (Fig 4.1B). We observed larger infarct volumes with HFD at 7 days post-stroke (Chapter 2), however; this was not observed at 24 hours. Furthermore, DHA did not reduce infarct volume at this time.

Dextran-conjugated Texas Red was used to label blood vessels that are open and perfusing at the time of euthanasia. The core of the infarct has few to none Texas Red+ blood vessels and corresponds to the area of reduced cresyl violet staining (Fig. 4.1C, D). To measure the perfusion deficit, the non-perfused area, void of Texas Red+ blood vessels was quantified. A two-way ANOVA revealed that neither diet [$F(1,21)=0.4506$, $p>0.05$] nor DHA [$F(1,21)=1.084$, $p>0.05$] treatment significantly affected the size of the non-perfused ischemic core (Fig. 4.1E).

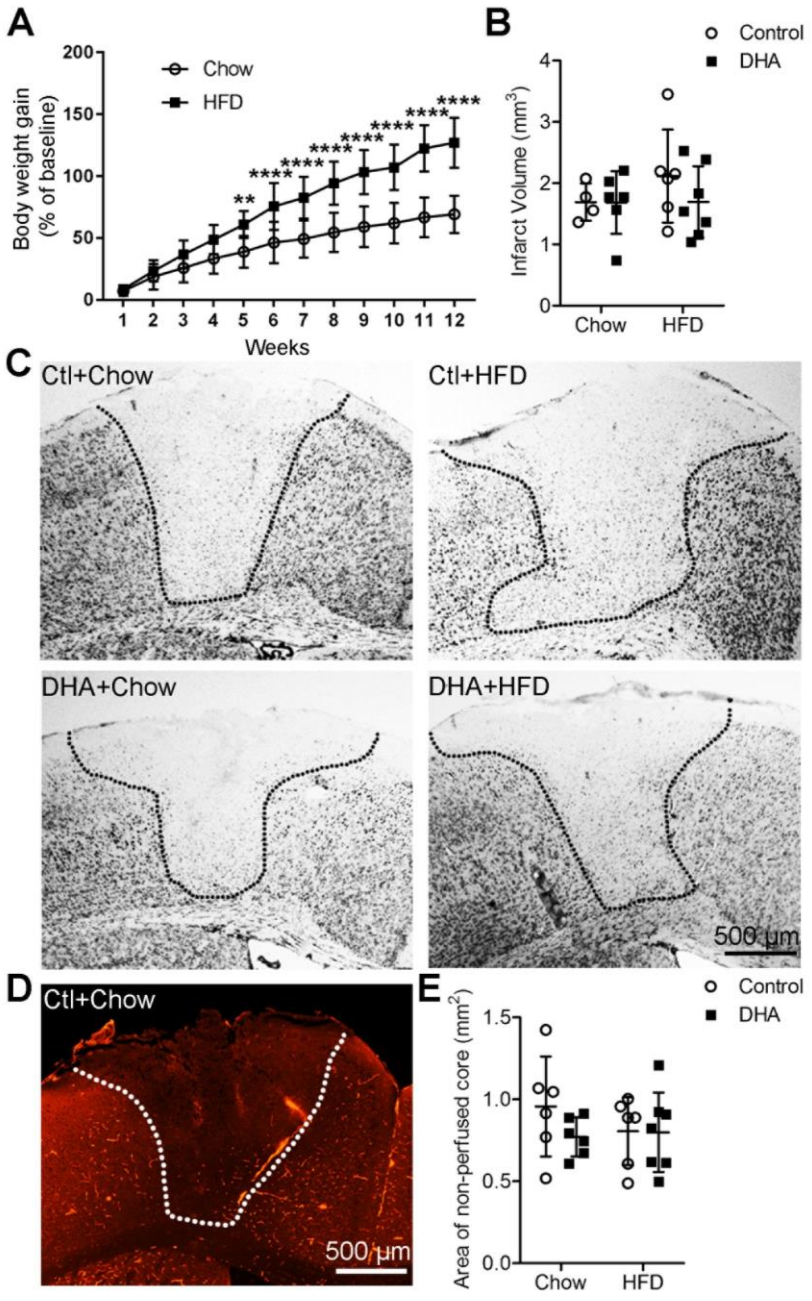

Figure 4.1: The effect of acute post-stroke DHA treatment on infarct size.

(A) Mice were fed a standard chow diet or HFD for 12 weeks and body weight was measured weekly. From 5 to 12 weeks of feeding, mice fed a HFD gained significantly more weight than Chow fed controls ($p<0.01$) ($p<0.0001$) (Chow, n=12, HFD, n=13). (B) The acute post-stroke application of DHA did not impact infarct volume in Chow fed

mice. Infarct volume was measured at 24 hours post-stroke (Ctl+Chow, *n*=4; Ctl+HFD, *n*=6; DHA+Chow, *n*=6; DHA+HFD, *n*=7). (C) Cresyl violet staining shows representative images of cortical infarcts at 24 hours post-stroke. (D) Dextran conjugated Texas Red labelling of perfused blood vessels shows a perfusion deficit within the infarct. (E) Quantification of the non-perfused ischemic core within the infarct at 24 hours post-stroke (Ctl+Chow, *n*=6; Ctl+HFD, *n*=6; DHA+Chow, *n*=6; DHA+HFD, *n*=7). Data are expressed as mean ± SD. ***p<0.01*, ****p<0.0001*.

4.3.3 DHA treatment reduced BBB breakdown however, this effect was reduced with HFD feeding.

Next, the effect of acute DHA treatment post-stroke on BBB breakdown within lean and obese mice was examined. Dextran-conjugated Texas Red extravasation was used to indicate the extent of breakdown of the BBB. This dextran has a molecular weight of approximately 70 kDa therefore, leakage of this large molecule would not be possible unless extensive breakdown of the blood brain barrier occurs (Fifield & Vanderluit, 2020). BBB breakdown was assessed by quantifying the number of diffuse patches of dextran with a minimum size of 15 µm in diameter within an area of 2.4 mm^2 (dimension 1.549 mm X 1.549 mm boxed region), at a 5x field of view (Fig. 4.2A). Dextran leakage was not observed at 12 hours post-stroke in ischemic brains (data not shown). However, extensive leakage within the non-perfused core and hypo-perfused penumbra was observed at 24 hours post-stroke (Fig. 4.2A). The patches of dextran leakage were often associated with a blood vessel, but not always (arrows in Fig. 2A). A two-way ANOVA revealed a main effect of DHA treatment on the number of leakages [$F(1,21)=21.59$, *p<0.001*], but no effect of diet was observed [$F(1,21)=0.007625$, *p>0.05*] (Fig. 4.2B).

Bonferroni post-hoc analysis showed that DHA treatment reduced dextran leakage within the brain of chow-fed mice following ischemic stroke (Ctl+Chow, 9.0 ± 2.4 vs. DHA+Chow, 4.6 ± 1.7, $p<0.01$) and to a lesser extent in HFD fed mice (Ctl+HFD, 8.4 ± 3.0 vs. DHA+HFD, 5.1 ± 0.8, $p<0.05$).

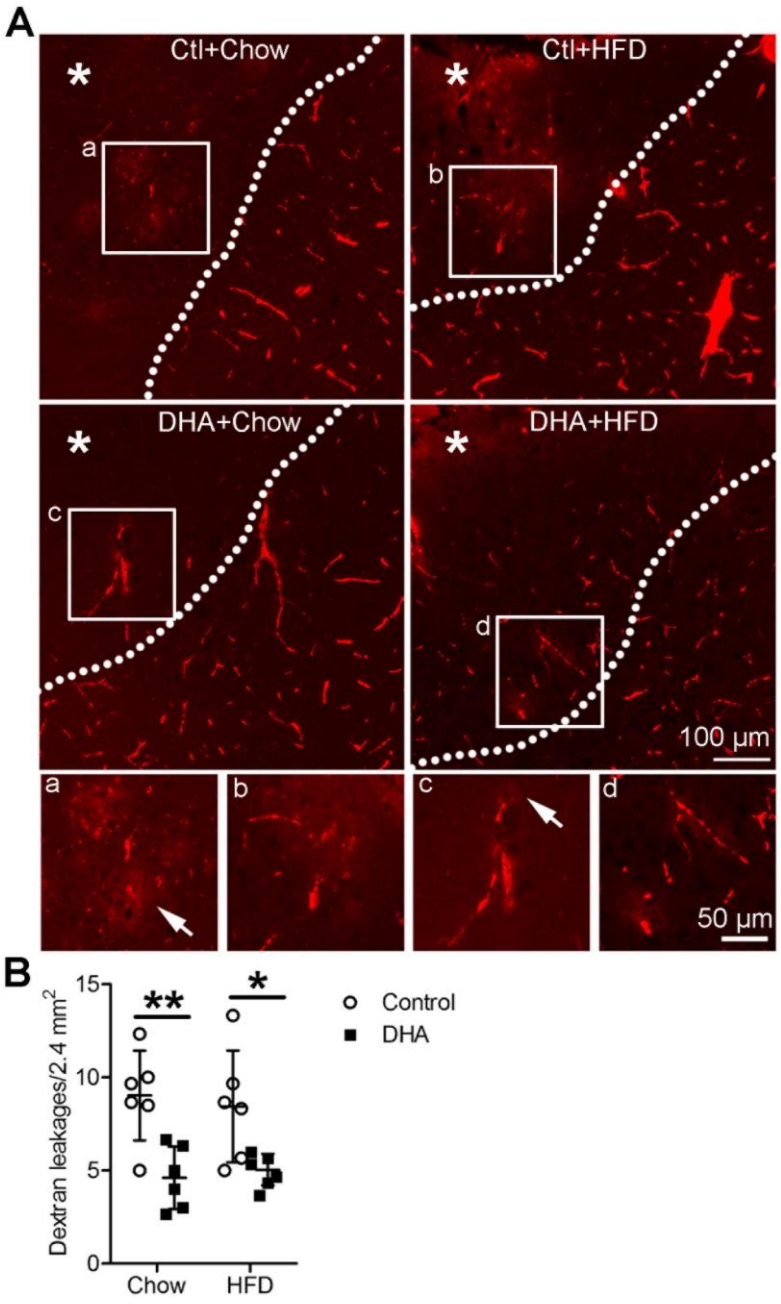

Figure 4.2: DHA treatment attenuated BBB breakdown.

(A) Low magnification images depict blood vessels labelled with dextran-conjugated Texas Red within the infarct at the time of euthanasia. Asterisks indicate location of the ischemic core and dotted lines demarcate the boundary of the ischemic core and penumbra. (a-d) Higher magnification of boxed regions in A shows dextran extravasation

(arrows) within the infarct. (B) At 24h post-stroke, DHA treatment significantly reduced the number of blood vessels leaking dextran-conjugated Texas Red. (Ctl+Chow, n=6; Ctl+HFD, n=6; DHA+Chow, n=6; DHA+HFD, n=7). Data are expressed as mean ± SD. *$p<0.05$, **$p<0.01$.

The injection of dextran at the point of euthanasia at 24 h post-stroke captures the state of the BBB at that specific time point. The circulating dextran labels perfused blood vessels within the infarct. Extravasation of the dextran from blood vessels is an indicator of vasculature injury specifically at 24 hours, when it is injected. To examine the extent of BBB breakdown over the first 24 hours post-stroke, the accumulation of albumin extravasation into the infarct was assessed (Fig. 4.3A, B). Extravasation of the albumin protein would occur from the initial ischemic injury up until 24 hours post-stroke. Using these two labelling techniques, BBB breakdown can be determined over the first 24 hour period with albumin staining and specifically at 24 hours with dextran labelling. Albumin staining appeared diffuse throughout the infarct with darker staining in the ischemic core (Fig. 4.3A). Albumin extravasation occurred with all treatment conditions (Fig. 4.3B). DHA treatment did not significantly reduce albumin staining within the cortex of Chow and HFD-fed mice [$F(1,21)=3.763$, $p=0.0659$] (Ctl+Chow, 2.68 ± 0.76 mm^2, vs DHA+Chow, 2.09 ± 0.45 mm^2), (Ctl+HFD, 2.60 ± 0.55 mm^2, vs DHA+HFD, 2.22 ± 0.70 mm^2) (Fig. 4.3C). There was no impact of diet [$F(1,21)=0.01164$, $p>0.05$].

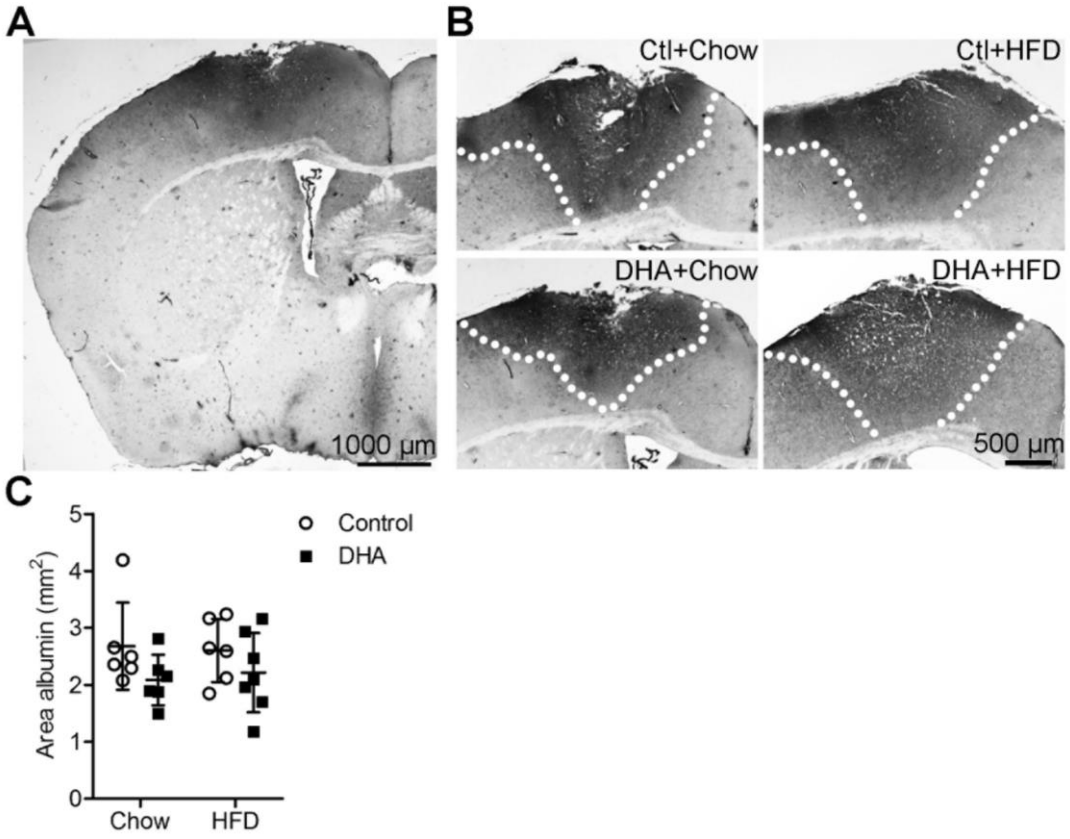

Figure 4.3: Albumin extravasation within the cortex 24 hours following a focal ischemic stroke.

(A) Low magnification image shows the accumulation of albumin extravasation within the cortex over the 24-hour post-stroke period. (B) Higher magnification images depict albumin+ staining for each condition. Dotted lines outline albumin+ staining. (C) Quantification of the area of albumin extravasation within the infarct (Ctl+Chow, *n*=6; Ctl+HFD, *n*=6; DHA+Chow, *n*=6; DHA+HFD, *n*=7). Data are expressed as mean ± SD.

Peripheral neutrophil infiltration in the brain is another indicator of the cumulative effect of BBB breakdown (Rosell et al., 2008). The number of infiltrating neutrophils were counted within the infarct. Neutrophil infiltration was not observed at 12 hours post-stroke (unpublished data); however, by 24 hours post-stroke, Ly6G+ neutrophils were observed within the infarcts of all experimental mice (Fig. 4.4A). A two-way ANOVA of the mean numbers of Ly6G+ cells revealed main effects for diet [$F(1,21)=8.178$, $p<0.01$] and DHA treatment [$F(1,21)=23.14$, $p<0.001$]. Regardless of treatment, there were significantly more Ly6G+ neutrophils within the infarcts of HFD fed mice. Bonferroni post-hoc analysis showed that DHA injections post-stroke reduced the number of infiltrating neutrophils in chow-fed animals from 49.9 ± 8.4 cells to 19.8 ± 3.6 cells (Ctl+Chow vs. DHA+Chow, $p<0.001$) and in HFD fed mice from 57.7 ± 2.3 cells to 40.2 ± 3.6 cells although the effect was attenuated (Ctl+HFD vs. DHA+HFD, $p<0.05$) (Fig. 4.4B). This shows that prolonged HFD feeding reduces the efficacy of DHA. Taken together, these results demonstrate that acute post-stroke application of DHA affects blood vessel integrity by reducing BBB breakdown.

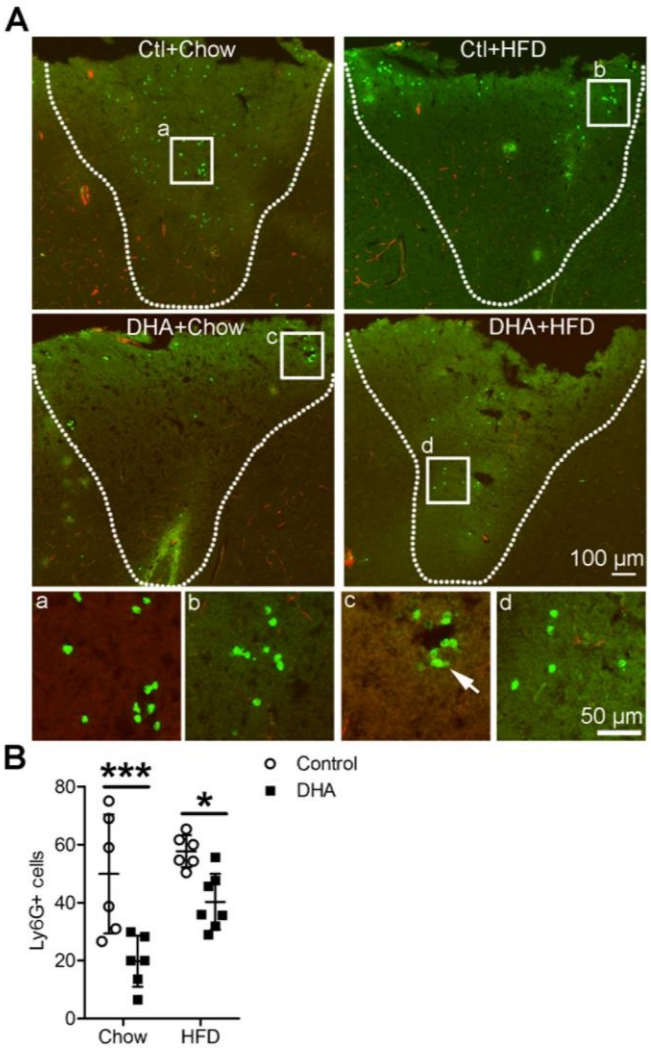

Figure 4.4: Infiltration of neutrophils within the infarct was reduced with DHA treatment.

(A) Low magnification images show neutrophils within the infarct at 24h post-stroke. Perfused blood vessels are labelled with dextran-conjugated Texas Red. (a-d) Higher magnification of boxed regions in A show Ly6G+ neutrophils infiltrating the stroke (arrow). (B) Quantification of Ly6G+ cells within the infarct reveals that DHA treatment reduced neutrophil infiltration within the brains in both chow-fed and HFD-fed animals (Ctl+Chow, n=6; Ctl+HFD, n=6; DHA+Chow, n=6; DHA+HFD, n=7). Data are expressed as mean ± SD. *$p<0.05$, ***$p<0.001$.

4.3.4 DHA alters the inflammatory response within the acute ischemic brain.

Inflammation within the brain following acute ischemic stroke was examined using antibodies against COX-2, an indicator of inflammation. Up-regulation of COX-2 leads to the production of prostanoids and reactive oxygen species that indirectly contributes to secondary stroke damage (Iadecola et al., 1999). This up-regulation of COX-2 is observed in neurons, endothelial cells and infiltrating immune cells such as neutrophils following stroke injury (Iadecola et al., 1999; Iadecola et al., 2001; Miettinen et al., 1997; Nogawa et al., 1997). Therefore, the number of double labelled COX-2+ and Hoechst+ cells were quantified within the infarct. COX-2+ cells were observed within the penumbra and ischemic core; however, the majority of these cells were located within the core (Fig 4.5A). Overall, there was an increase in COX-2+ cells within the infarct of HFD fed mice in comparison to Chow fed mice (Ctl+Chow, 57.3 ± 4.8 cells; Ctl+HFD, 70.0 ± 14.2 cells) ($t(10)= 2.629$, $p<0.05$). Furthermore, a two-way ANOVA analyzing the number of COX-2+ cell counts within the entire infarct revealed a main effect of DHA treatment [$F(1,21)=19.87$, $p<0.001$] (Fig. 4.5B). Bonferroni post-hoc analysis showed that DHA treatment significantly reduced COX-2+ cells within the infarct for both Chow and HFD conditions (Ctl+Chow 57.3 ± 4.8 cells vs. DHA+Chow 41.8 ± 11.3 cells, $p<0.05$; Ctl+HFD 70.0 ± 14.2 cells vs. DHA+HFD 45.7 ± 11.9 cells, $p<0.01$). DHA treatment resulted in a greater reduction in COX-2+ cells in HFD fed mice than Chow fed mice. DHA treatment therefore, reduces COX-2 expression within the infarct in the acute post-stroke period.

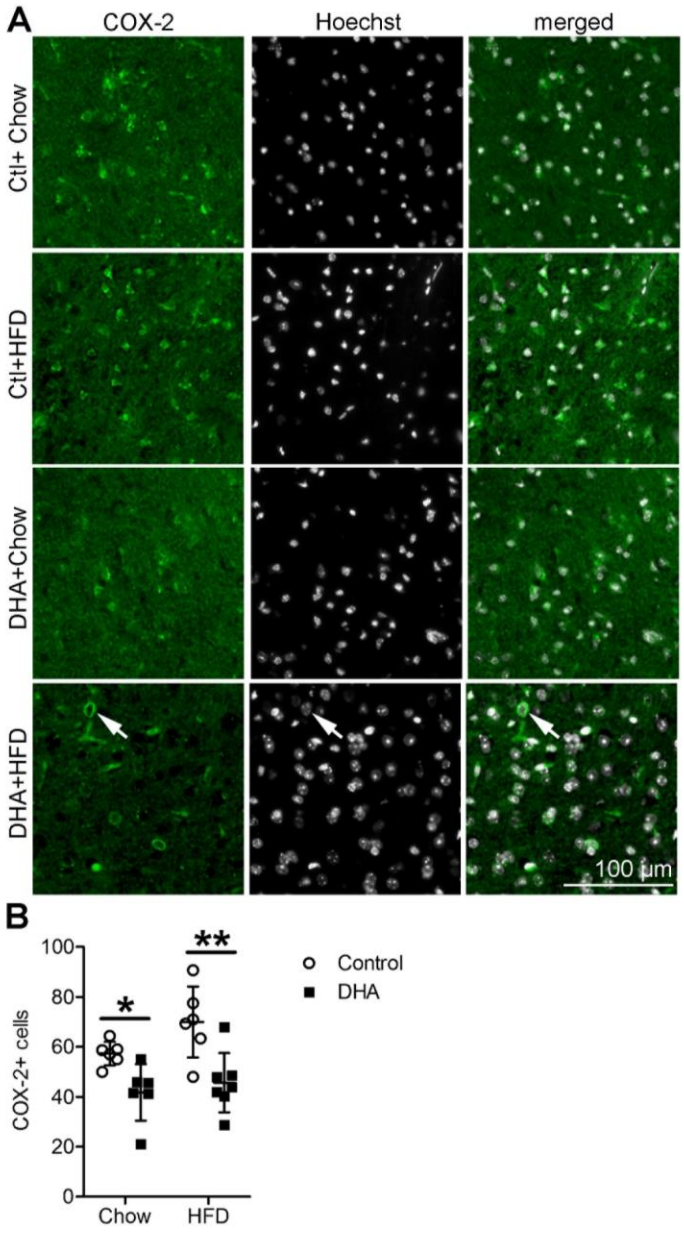

Figure 4.5: DHA reduced cyclooxygenase-2 expression within the infarct.

(A) Images of COX-2+ cells within the infarct at 24 hours post-stroke. Arrow indicates COX-2+ labelling within a Hoechst+ cell. (B) A significant reduction in COX-2+ cells within the infarct is observed with DHA treatment (Ctl+Chow, n=6; Ctl+HFD, n=6; DHA+Chow, n=6; DHA+HFD, n=7). Data are expressed as mean ± SD. *$p<0.05$, **$p<0.01$.

The number of CD68+ and TMEM119+ cells within the infarct, markers for phagocytosing cells and microglia respectively, were assessed. CD68+ cells were found within both the core and penumbra of the infarct for each condition (Fig. 4.6A, B). A two-way ANOVA analyzing the total CD68+ cell counts within the entire infarct revealed a significant main effect of diet indicating an overall increase in the number of inflammatory cells with HFD feeding [$F(1,21)=6.666$, $p<0.05$] (Fig. 4.6C). DHA treatment; however, did not have an impact on the total number of CD68+ immune cells within the infarct [$F(1,21)=0.5607$, $p>0.05$].

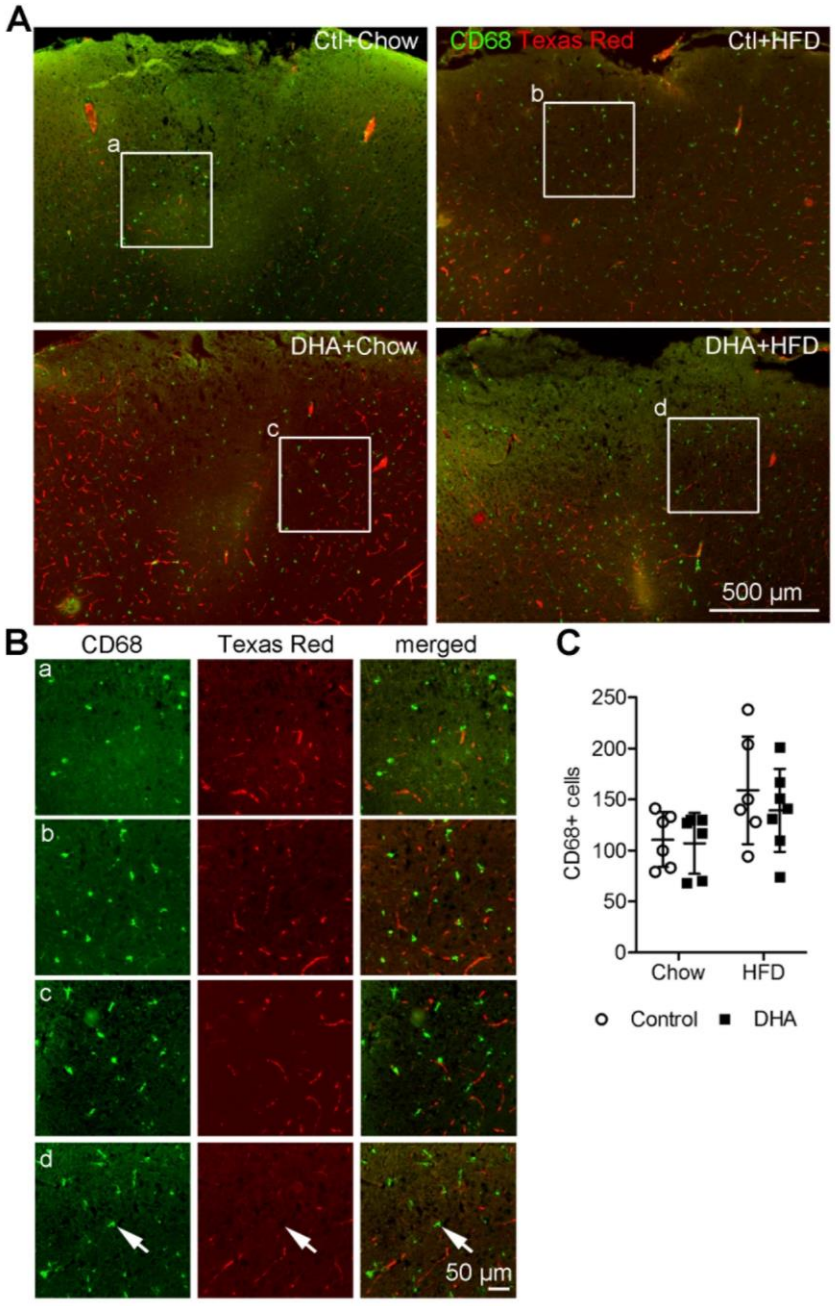

Figure 4.6: HFD led to an increase in microglia and macrophages within the infarct at 24 hours post-stroke.

(A) Images of CD68+ immune cells within the entire infarct at 24 h post-stroke. (B) Higher magnification images of boxed areas a-d in A show CD68+ cells. (C) Quantification revealed a significant increase in CD68+ cells within the infarct in HFD-

fed mice; however, DHA treatment did not affect the total number of CD68+ cells. Data are expressed as mean ± SD.

Microglia and macrophages specifically within the ischemic core and hypo-perfused penumbra were examined (Fig. 4.7). Within the ischemic core, the majority of cells were TMEM119-/CD68+ macrophages with few TMEM119+/CD68+ microglia (Fig. 4.7A). This is consistent with our previous study that showed that peripheral macrophages enter the brain at 24 hours post-stroke and are localised within the core (Fifield & Vanderluit, 2020) (Chapter 3). It was also previously shown that more CD68+ cells are located within the infarct in HFD fed mice in comparison to Chow fed mice at 7 days post-stroke (Fifield et al., 2019) (Chapter 2). When examining TMEM119-/CD68+ macrophages within the non-perfused core, a two-way ANOVA revealed a significant interaction between diet and DHA treatment [$F(1,21)=6.779$, $p<0.05$], but no main effect of diet [$F(1,21)=0.8070$, $p>0.05$] or DHA treatment [$F(1,21)=0.02805$, $p>0.05$] (Fig 4.7B). DHA treatment did not significantly reduce the number of TMEM119-/CD68+ macrophages infiltrating the core in Chow fed mice (Ctl+Chow: 6.0 ± 0.9 cells/ROI; DHA+Chow: 4.6 ± 1.3 cells/ROI) (Fig. 4.7B). Overall, there were similar numbers of TMEM119+/CD68+ microglia within the core regardless of diet [$F(1,21)=0.1528$, $p>0.05$] or DHA treatment [$F(1,21)=0.3439$, $p>0.05$] (Fig. 4.7B).

In contrast with the infarct core, there were few TMEM119-/CD68+ macrophages within the hypo-perfused penumbra and statistical analysis revealed no effect of diet [$F(1,21)=1.347$, $p>0.05$] or DHA treatment [$F(1,21)=1.694$, $p>0.05$] (Fig. 4.7C). Conversely, TMEM119+/CD68+ microglia were more numerous in the hypo-perfused

penumbra; however, once again, there was no effect of diet [$F(1,21)= 0.5849$, $p>0.05$] or DHA treatment [$F(1,21)=2.936$, $p>0.05$] (Fig. 4.7C). Overall, these results indicate that HFD or DHA treatment did not affect the ratio of microglia and macrophages within the core or penumbra.

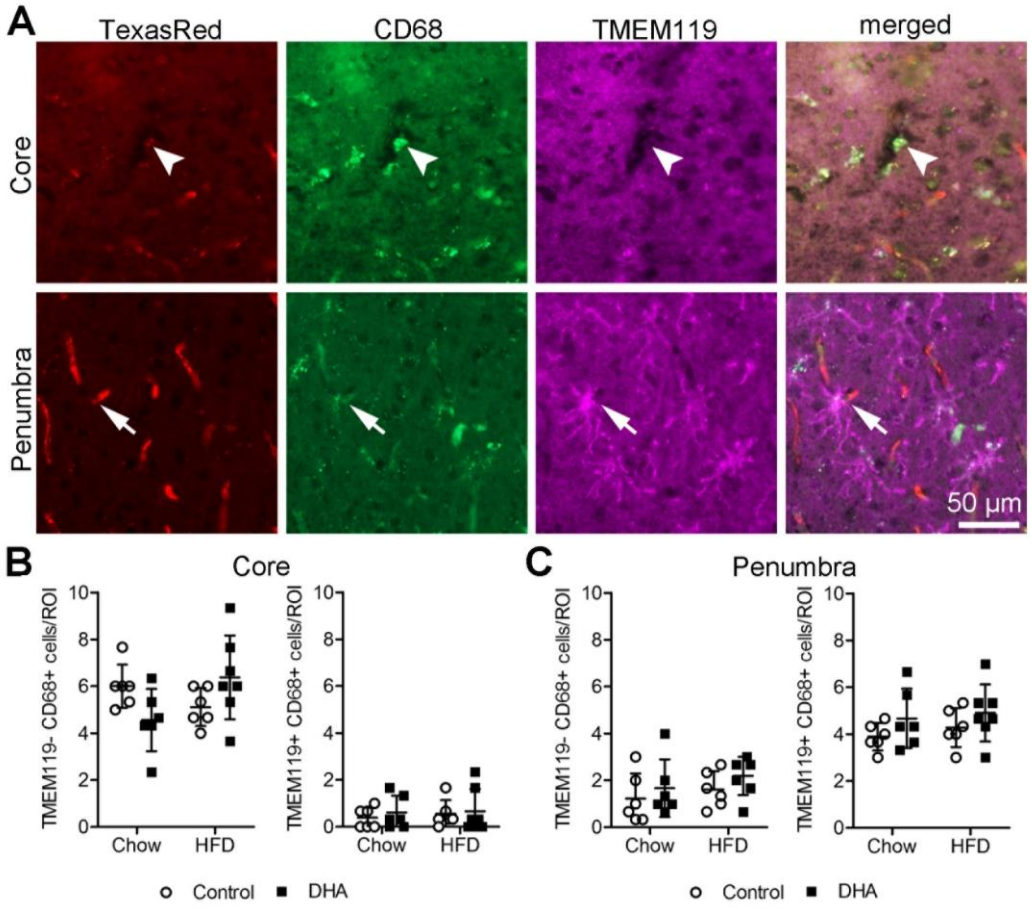

Figure 4.7: Macrophage/microglia location within the infarct following acute ischemic stroke.

(A) Images show the location of TMEM119- CD68+ macrophages (arrowhead) within the ischemic core and TMEM119+CD68+ microglia (arrow) within the penumbra 24 hours following stroke. (B) Quantification of TMEM119- CD68+ macrophages and TMEM119+ CD68+ microglia within the ischemic core. Analysis revealed no effect of diet or DHA treatment. (C) Quantification of TMEM119- CD68+ macrophages and TMEM119+ CD68+ microglia within the penumbra show no effect of diet or DHA treatment. ROI= 200 µm X 200 µm boxed area (Ctl+Chow, *n*=6; Ctl+HFD, *n*=6; DHA+Chow, *n*=6; DHA+HFD, *n*=7). Data are expressed as mean ± SD.

4.3.5 Acute DHA treatment promotes neuron survival within the core but not in the penumbra.

The effect of DHA on neurons was assessed within the non-perfused core and hypo-perfused penumbra by quantifying the number of NeuN+ neurons (Fig. 4.8). Compared to neurons within the penumbra, there were fewer NeuN+ neurons within the non-perfused core and they appeared smaller with condensed nuclei (Fig. 4.8A, arrow). Quantification of neurons within the non-perfused core revealed a main effect of DHA treatment on neuron survival at 24 hours post-stroke [$F(1,21)=7.063$, $p<0.05$] with no impact of diet [$F(1,21)=0.2451$, $p>0.05$]. Bonferroni post-hoc analysis revealed an increase in the number of neurons with DHA treatment in chow-fed mice (Ctl+Chow, 4.4 ± 1.6 neurons/ROI vs. DHA+Chow, 12.4 ± 8.2 neurons/ROI, $p<0.05$) however; this effect was not observed in HFD-fed mice (Fig. 4.8, B). There was no difference in the number of Hoechst+ nuclei across each of the conditions (Fig. 4.8C). Within the penumbra, NeuN+ neurons appeared healthier when compared to the ischemic core (Fig. 4.8A, D). A two-way ANOVA analysing the number of neurons within the penumbra showed comparable neuron survival across all conditions with no effect of DHA [$F(1,21)=0.7636$, $p>0.05$] or diet [$F(1,21)=0.05252$, $p>0.05$] (Fig. 4.8E). Similar to the ischemic core, there was no difference in the number of Hoechst+ nuclei across all conditions (Fig. 4.8F).

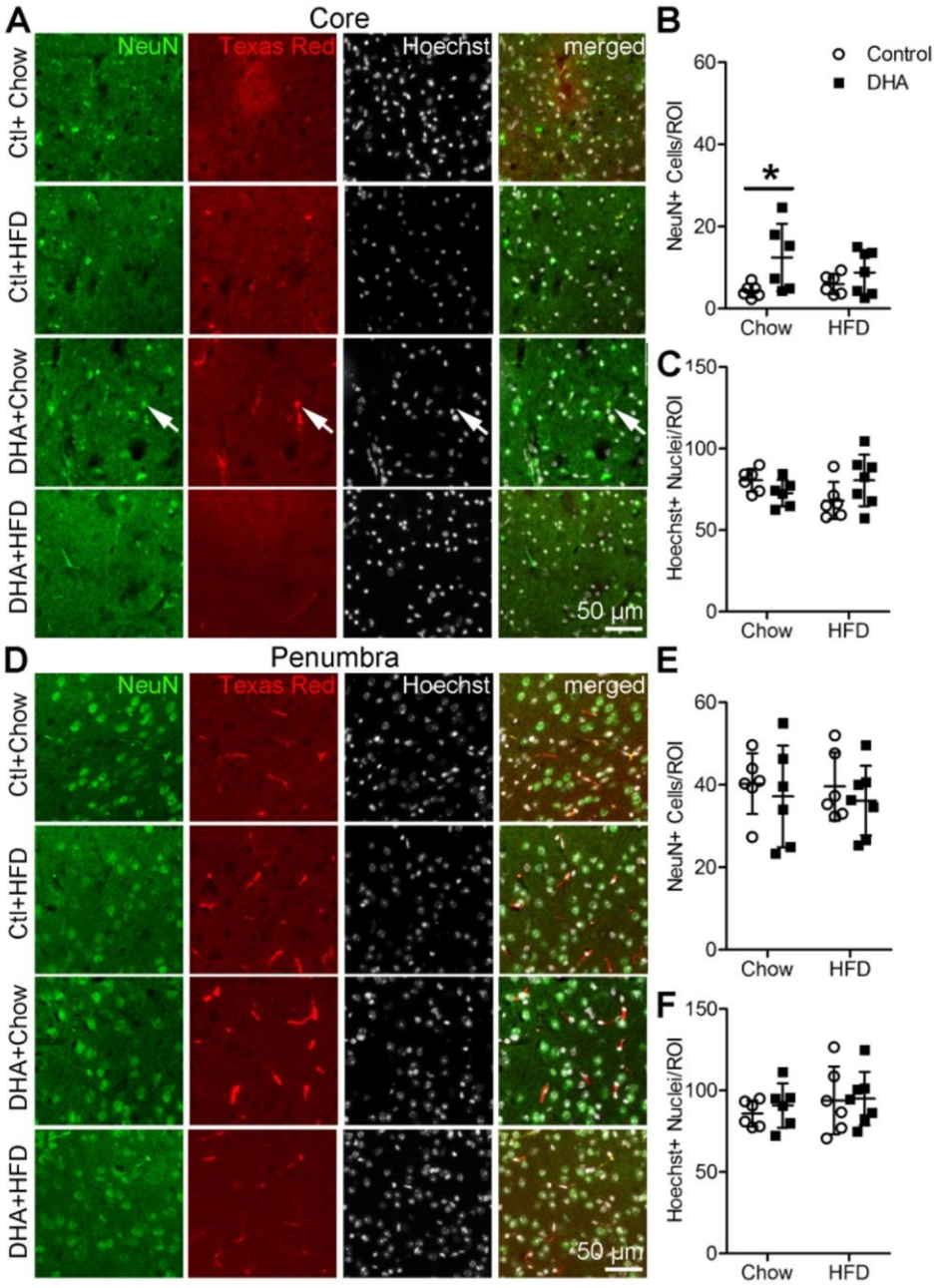

Figure 4.8: Effect of DHA on neuron survival within the ischemic core and penumbra.

(A) Images show NeuN+ neurons within the non-perfused core at 24 h post-stroke. Arrow indicates a NeuN+ neuron within the core with a condensed nucleus. (B) Quantification of NeuN+ neurons show a significant increase in survival following treatment with DHA

in chow-fed animals however; this effect is lost in HFD fed animals. (C) Quantification of Hoechst+ nuclei within the non-perfused core. (D) Images show NeuN+ neurons within the hypo-perfused penumbra at 24 h post-stroke. (E) Quantification of NeuN+ neurons within the penumbra shows no effect of DHA treatment on survival. (F) Quantification of Hoechst+ nuclei within the penumbra. ROI= 200 µm X 200 µm boxed area (Ctl+Chow, n=6; Ctl+HFD, n=6; DHA+Chow, n=6; DHA+HFD, n=7). Data are expressed as mean ± SD. *$p<0.05$.

Degeneration of neurons within the core and hypo-perfused penumbra was assessed using FJC staining. FJC+ neurons were observed within the ischemic core and hypo-perfused penumbra (Fig. 4.9A). Upon crude observation, the numbers of FJC+ cells appeared similar across all treatments (Fig. 4.9A). The area of FJC+ neurons was compared across all treatment. There was no effect of DHA treatment [$F(1,21)=1.057$, $p>0.05$] or diet [$F(1,21)=0.004881$, $p>0.05$] on neuron degeneration (Fig. 4.9B). The FJC staining shows extensive degeneration within the infarct independent of treatment. Although there were slightly more neurons within the core with DHA treatment, there was no effect on neuron survival within the penumbra and these neurons were undergoing extensive degeneration.

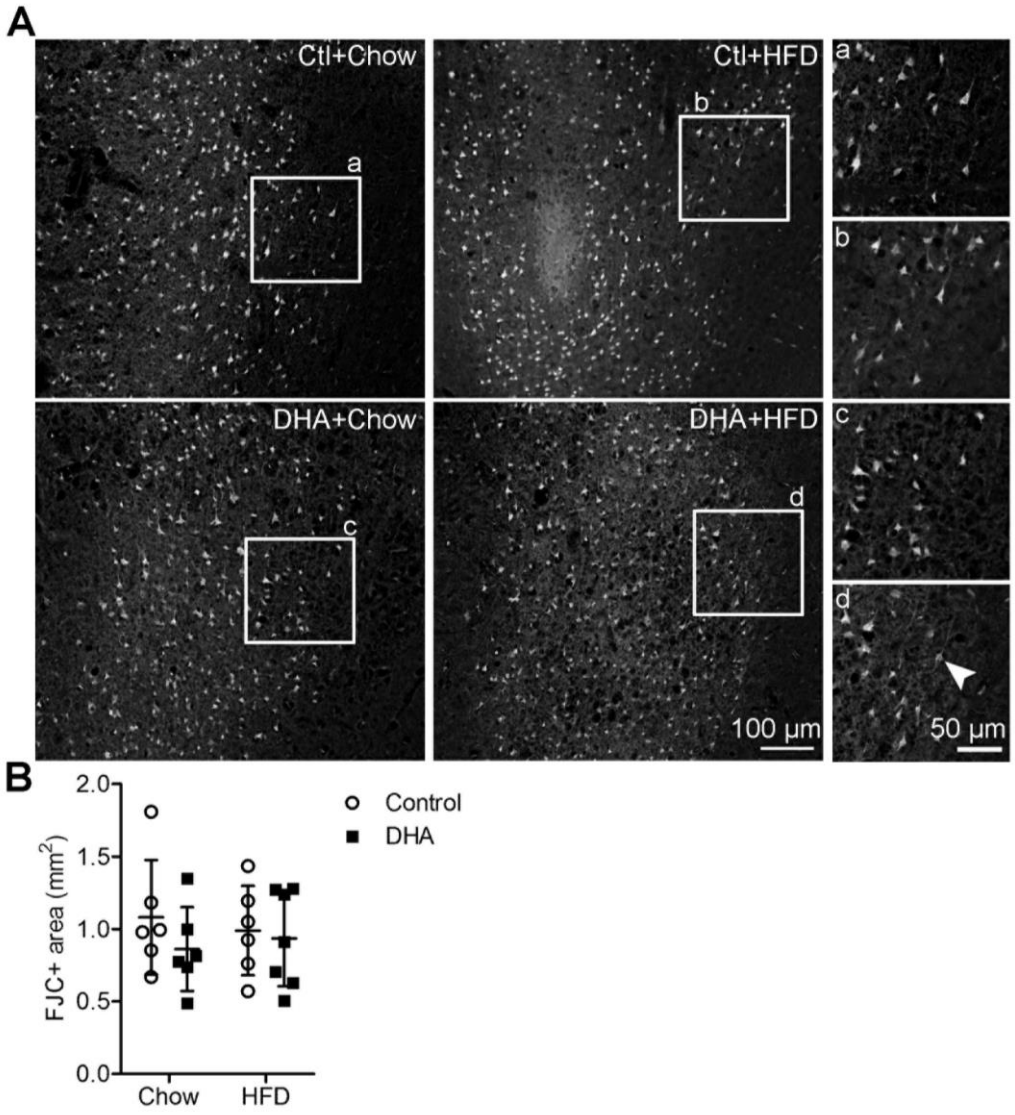

Figure 4.9: DHA treatment does not rescue neuron degeneration.

(A) Images show FJC+ neurons undergoing degeneration in the infarct at 24 h. (a-d) Higher magnification images show FJC+ neurons on the border of the infarct. (B) Quantification of the area of FJC+ staining shows no effect of DHA treatment on neuron degeneration post-stroke.

4.4 Discussion

This is the first study to examine DHA treatment on the cellular responses following ET-1 ischemic stroke in both lean and diet-induced obese mice. Overall, the main findings show that DHA reduces (i) BBB breakdown (ii) infiltration of peripheral immune cells such as neutrophils and macrophages within the brain and (iii) COX-2+ cells within the ischemic injury. Although overall infarct volumes were not affected, DHA reduced BBB damage and consequently reduced immune cell infiltration within the brain. This effect of DHA was diminished in obese mice fed HFD. Taken together, these findings demonstrate that DHA treatment reduces ischemic injury within the acute post-stroke period.

4.4.1 The effect of HFD and DHA on infarct size at 24 hours post-stroke

In comparison to other ischemic stroke models, ET-1 induced ischemic stroke produced small infarcts ranging from 0.74 mm^3 to 3.45 mm^3 across all conditions (Carmichael, 2005). Our data did not show larger infarcts in the HFD-fed mice at 24 hours. However, using the same HFD feeding protocol, we previously showed $\geq 50\%$ increase in infarct volume in HFD mice compared to chow controls at 7 days post-stroke (Chapter 2). This is in contrast to larger strokes where HFD does affect infarct size in the acute stroke period (Cao et al., 2015; Li et al., 2013). For instance, Li and colleagues show an approximately 20% increase in infarct volume following 3 hours of MCAO and 21 hours reperfusion in rats fed 45% HFD for 8 weeks (Li et al., 2013). There are differences in experimental techniques and low animal numbers that can contribute to this variation. These differences may be due to the length of HFD feeding, ischemic model

used or duration of ischemia and the method for calculating infarct volume (Maysami et al., 2015). Indeed, increases in infarct volume was only seen in mice fed HFD for 4 to 6 months and 30 min MCAO (Maysami et al., 2015). This was not observed when HFD was given for less than 4 months or if the ischemic duration was less than 30 minutes. These studies suggest that several factors may determine the effect of HFD on the size of infarction within the brain. Furthermore, the ET-1 stroke model used in the present study produced a small focal infarct, wherein the infarct is still expanding by 24 hours post-stroke. HFD may have a greater impact on the delayed expansion of the infarct. It is not until 7 days that the impact of HFD is observed on infarct volume as observed in Chapter 2.

In the present study, DHA was administered via i.p. injection at a dose of 20 mg/kg, 2-, 4- and 6-hours following ischemic stroke. This dose was chosen based on preliminary observations testing the time of injection after stroke and dosage (10 mg/kg versus 20 mg/kg). A higher dose was also chosen because DHA was applied by i.p. which would presumably take longer than intravenous administration to enter into the circulatory system. However, both the method of DHA administration and the dose given can affect the size of infarct volume. In a study conducted by Belayev and colleagues, the i.v. dose of DHA was compared in rats given 60 min of MCAO with 3 hours of reperfusion (Belayev et al., 2009). The lower dose of 3.5 mg/kg reduced infarct volume by 72% compared to the control condition, a greater effect compared to higher DHA doses (7 mg/kg reduced infarct volume 51%, 14 mg/kg reduced to 59% and 35 mg/kg reduced to 63%) (Belayev et al., 2009). Using i.p injection to administer DHA in the present study may not have been as effective as using i.v. injection, in which DHA is

directly introduced into vascular circulation. Furthermore, DHA i.p. injection in combination with a DHA enriched diet has been shown to reduce atrophy volume post-stroke (Pu et al., 2016). In a study conducted by Pu and colleagues, mice received one of three treatments: 1) mice were fed an omega-3 diet beginning at 5 days post-stroke up to 28 days post-stroke, 2) were given a 10 mg/kg i.p. injection at 2 hours post-stroke and then daily for 14 days, or 3) received both combined treatments. Atrophy volume, as quantified by multiplying the area lacking MAP-2+ staining by the thickness of the evaluated area, was significantly reduced only when both treatments were combined (Pu et al., 2016). These studies suggest that the mode of administration, dose of DHA and timing of DHA administration (i.e., acute application versus long term application) can affect total infarct size which may account for the findings in the present study.

4.4.2 DHA reduces BBB breakdown at 24 hours post-stroke

The BBB is compromised following ischemic stroke leading to extravasation of immune cells and molecules into the brain (Daneman, 2015). Studies have shown contradictory evidence on the effect of DHA to reduce BBB breakdown (Hong et al., 2015; Pan et al., 2009; Yang et al., 2007). A single i.p. DHA injection 1 hour prior to 90 minute ischemia (occlusion of MCA and bilateral CCAs) reduced extravasation of Evans Blue within the cortex of rats when assessed at 24 hours reperfusion (Pan et al., 2009). In contrast, when DHA was administered 60 minutes after reperfusion, Evans Blue extravasation within the cortex was increased (Yang et al., 2007). Evans Blue was injected via tail vein following 24-hour reperfusion and allowed to diffuse throughout the brain for 3 hours. The variable timing of DHA injection and the 3-hour diffusion time for

Evans Blue post-stroke could lead to different results. In the current study, BBB disruption was determined by the leakage of Dextran (70 kDa) injected 2 min prior to euthanasia thus limiting the time for diffusion within the brain. Albumin staining was also performed to verify BBB disruption and demonstrated the accumulation of albumin (66.5 kDa) extravasation into the cortex over the first 24 hours post-stroke. DHA administration significantly reduced the number of dextran leakages in both Chow and HFD-fed mice. BBB disruption was further determined by examining peripheral neutrophil infiltration within the brain. DHA significantly reduced neutrophils within the infarct by 60% in Chow fed mice and by 30% in HFD-fed mice. This is consistent with a previous study conducted by Cai and colleagues that showed approximately 50% reduced infiltration of neutrophils within the brain with DHA (i.p., 10 mg/kg) for 3 consecutive days following 1 hour MCAO (Cai et al., 2018). Indeed, DHA diet has been shown to reduce expression of adhesion molecules ICAM-1 and VCAM-1, thereby limiting leukocyte adhesion and infiltration into the brain (Baker et al., 2018). HFD feeding significantly increased the number of infiltrating neutrophils post-stroke in comparison to controls. Although this HFD effect was not observed with dextran leakage or albumin extravasation, it does suggest that the BBB disruption is exacerbated with HFD, thereby accounting for the reduced efficacy of DHA in HFD fed mice. These results suggest that DHA attenuates BBB breakdown during acute ischemic stroke; however, prolonged HFD may reduce this effect.

4.4.3 DHA reduces inflammation within the ischemic brain

The anti-inflammatory effect of DHA has been well documented; however, these effects during the acute period in small strokes is unclear (Lalancette-Hebert et al., 2011; Pan et al., 2009; Ren et al., 2019; Zendedel et al., 2015). DHA has been shown to reduce pro-inflammatory mediators, including TNF-α, IL-1β and COX-2 (Lalancette-Hebert et al., 2011; Pan et al., 2009; Zendedel et al., 2015). Mice fed an enriched DHA diet for 3 months prior, had a 32% reduction in COX-2 levels 48 hours following 1 hour MCAO (Lalancette-Hebert et al., 2011). In the current study, DHA reduced the number of cells expressing COX-2 by 26% in Chow fed mice and by 34% in HFD fed mice compared to saline injected controls. Furthermore, prolonged HFD significantly increased the number of cells expressing COX-2. This is consistent with previous studies that show an increase in COX-2 expression with prolonged HFD feeding (Dhungana et al., 2013; Zhang et al., 2005). COX-2 metabolises arachidonic acid producing prostanoids such as prostaglandins that can induce inflammation and ROS (Smith et al., 2000). This can damage the BBB leading to leukocyte infiltration within the brain (Candelario-Jalil et al., 2007). Indeed, inhibition of COX-2 via application of nimesulide, a non-steroidal anti-inflammatory drug, immediately or 6 hours post-stroke has been shown to reduce Evans Blue leakage within the cortex 48 hours following ischemic stroke (Candelario-Jalil et al., 2007). In the current study, DHA reduced COX-2 expression within the infarct, which may account for the reduced BBB disruption that was observed within the brain.

Prolonged HFD feeding increased the number of CD68+ immune cells within the ischemic injury at 24 hours post-stroke. This is consistent with our previous data that show an increase in CD68+ macrophages at 7 days post-stroke with 12 weeks HFD feeding (Chapter 2) (Fifield et al., 2019). The increased infiltration of CD68+ immune

cells within the infarct may account for the reduced efficacy of DHA to attenuate BBB disruption in HFD fed mice. Indeed, studies have shown that immune cells release pro-inflammatory mediators and MMPs that can increase BBB breakdown (del Zoppo et al., 2007; Deng et al., 2014; Maysami et al., 2015). For instance, Deng and colleagues show reduced IgG extravasation in MMP-9 -/- mice fed HFD for 10 weeks that received 90 min MCAO (Deng et al., 2014). In the current study, microglia and macrophages were examined specifically within the core and penumbra. Overall, macrophages were located within the core and microglia were observed in the penumbra. Cai and colleagues show reduced infiltration of macrophages, neutrophils and T and B lymphocytes when DHA (10 mg/kg, i.p.) was administered after reperfusion and daily for 3 days following 1 hour MCAO (Cai et al., 2018). Furthermore, DHA polarized $CD45^{high}CD11b^{+}$ macrophages toward a M2 ($CD206^{+}$ $CD16^{-}$) anti-inflammatory phenotype. Although microglia or macrophage phenotype (M1 vs. M2) was not assessed in the current study at 24 hours, it is possible that DHA could polarize these immune cells toward an anti-inflammatory (M2) phenotype.

4.4.4 DHA does not affect the immediate survival of neurons in the penumbra

It has previously been shown that DHA reduces neuron cell death following ischemic stroke *in vivo* and *in vitro* (Belayev et al., 2018; Cai et al., 2018; Luo et al., 2018; Shi et al., 2016; Zhang et al., 2014). We therefore assessed acute neuron survival and degeneration within the core and penumbra at 24 hours post-stroke. Overall, there was a slight increase in neuron survival within the core of Chow fed mice with DHA; however, DHA did not affect neuron survival within the penumbra. Furthermore, DHA

did not reduce neuronal degeneration. This is different from previous studies that show increased neuron survival with DHA treatment and may be due to the mode of DHA administration or when neuron survival was assessed post-stroke. The present study administered DHA (20 mg/kg) via intraperitoneal injection at 2, 4 and 6 hours post-stroke and assessed acute survival at 24 hours. DHA was administered based on weight (20 mg/kg, 200 µl) which could be a potential confounding factor. It is possible that applying DHA via intravenous injection and assessing the delayed death of neurons over an extended post-stroke period may lead to different results. Indeed, DHA reduced BBB disruption and inflammation at 24 hours which may affect the delayed death and degeneration of neurons beyond this time point. This is supported by a study conducted by Eady and colleagues that assessed the effect of DHA on neuron survival following 2 hour MCAO (Eady et al., 2012). DHA (5 mg/kg, i.v.) that was administered 3 hours after stroke onset, increased the number of NeuN+ neurons within the penumbra at 7 days post-stroke, and not before this time (Eady et al., 2012). Furthermore, DHA upregulated AKT p473 and AKT p308 phosphorylation in NeuN+ neurons at 4 hours. This activation of the AKT signaling pathway, a pathway involved in cell survival, may account for the enhanced neuron survival and reduced infarct volume observed at 7 days post-stroke (Eady et al., 2012). DHA can convert to neuroprotectin D1(NPD1), a neuroprotective derivative that increases cell survival by inhibiting apoptosis (Bazan, 2005). The neuroprotective properties of DHA may attenuate delayed cell death, such as apoptosis. Indeed, 2 hour pre-treatment with DHA has been shown to reduce the percent of apoptotic cells undergoing 2 hours of OGD *in vitro* (Ren et al., 2019). DHA pre-treatment inhibits ERK phosphorylation and increases AKT phosphorylation, pathways involved in

cell survival, proliferation and anti-apoptotic effects (Ren et al., 2019). Although we did not observe an impact on the immediate survival of neurons within the penumbra at 24 hours, it is possible that DHA could attenuate the delayed neuronal death out to 7 days and beyond through inhibiting apoptosis.

4.5 Conclusions

In summary, these findings demonstrate that DHA attenuates BBB disruption following acute ischemic stroke. Specifically, DHA reduced dextran leakage and neutrophil infiltration, indicators of BBB disruption. DHA decreased BBB disruption and inflammation; however, this effect was attenuated with HFD feeding. Although DHA did not affect immediate neuron survival within the penumbra, it is possible that DHA could attenuate delayed cell death beyond 24 hours post-stroke. Taken together, acute administration of DHA has the potential to ameliorate ischemic injury of small infarcts.

CHAPTER 5

DISCUSSION

5.1 The impact of diet on infarct volume

This thesis used ET-1 to induce a small focal ischemic stroke that mimics covert stroke; however, the change in size of these smaller strokes overtime is unknown. In rats following an ET-1 stroke, infarct volumes peak at 24 hours and then remain stable out to 7 days post-stroke (Nguemeni et al., 2015). Here, we show that infarct volume induced by ET-1 intra-cortical injections in the mouse brain is relatively stable over the first 12 hours to 72 hours post-stroke Although infarct volumes are smaller in our ischemic stroke model ranging from 1.42 mm^3 to 3.60 mm^3, a consistent infarct volume over time is also observed out to 7 days post-stroke (Fig. 5.1).

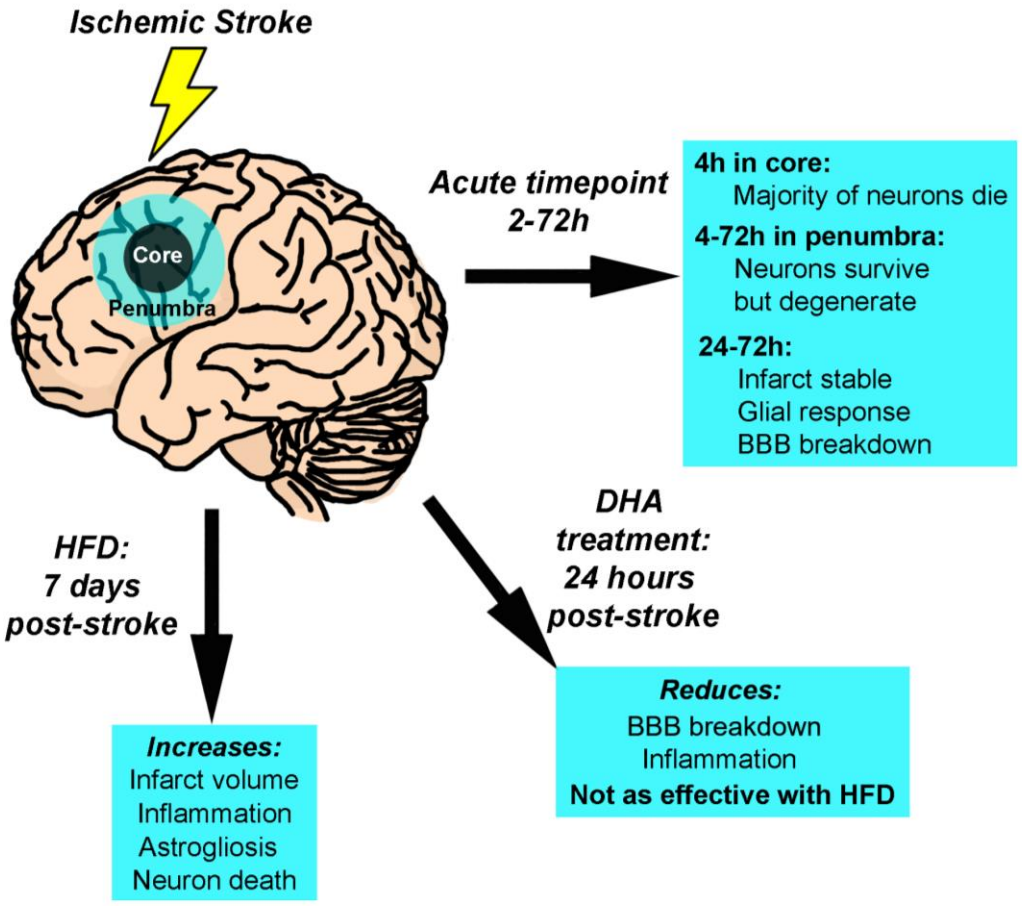

Figure 5.1: Summary of main findings.

Overall, 12 weeks of HFD worsened cellular responses at 7 days post-stroke. This included an increase in inflammation, astrogliosis and neuron cell death within the stroke. Analysis following acute ischemic stroke (2 to 72h), revealed that the majority of neurons within the core died by 4 hours in the core. Surviving neurons within the penumbra were undergoing degeneration. Glial responses and BBB breakdown was observed from 24 to 72 hours. DHA reduced both BBB breakdown and inflammation at 24 hours post stroke, however; this effect was attenuated with prolonged HFD feeding.

In the present studies, mice fed a HFD had larger infarcts than Chow-fed mice (Fig. 5.1). At 24 hours post-stroke, similar infarct size was observed in HFD-fed mice and Chow controls; however, by 7 days post-stroke, HFD fed mice had infarct volumes that were ≥ 50% larger than in Chow-fed mice (Chapter 2). The implications of this study are that chronic HFD intensifies ischemic injury even in smaller strokes. The greater difference in infarct size between HFD-fed mice versus Chow-fed mice at 7 days versus 24 hours suggests that HFD affects the secondary/delayed cell death resulting in a greater expansion of the infarct. Previous studies have shown greater delayed cell death post-stroke in the form of apoptosis with HFD feeding (Cao et al., 2015; Herz et al., 2015; Tulsulkar et al., 2016; Wu et al., 2016). Rats fed western diet for 3 months show an increase in TUNEL+ adiponectin containing neurons following 1 hour MCAO and 72 hours post-stroke (Wu et al., 2016). To attempt to attenuate the effect of HFD, we examined DHA treatment during the acute post-stroke period. DHA did not affect infarct size in Chow-fed animals. Furthermore, DHA did not affect the infarct size in HFD-fed mice, which could be due to a lack of significant HFD effect on the infarct size at 24 hours post-stroke. Nonetheless, it is possible that DHA would show a significant protective effect at later time points when HFD exacerbates the infarct size.

5.2 Vascular responses and injury of the BBB

We found that prolonged HFD leads to smaller blood vessel lumen and reduced contractile properties of cerebral arterioles within the cortex (Chapter 2). This narrowing of the arteries may account for the larger infarcts observed with HFD as reperfusion

would be reduced. If reperfusion is diminished, this may cause greater damage to vascular endothelial cells and further disrupt the BBB.

Extensive BBB breakdown was assessed using extravasation of a dextran conjugated to a fluorochrome (70 kDa), however; this technique does not show the initial injury of the BBB at the tight junction level. For instance, Jiao and colleagues show reduced mRNA expression of the tight junction proteins claudin-5, occludin and ZO-1 as early as 3 hours following 2 hour MCAO, coinciding with permeability of Evans Blue (Jiao et al., 2011). Here, we show extensive BBB breakdown, as visualized with extravasation of the large dextran molecule, not until 12 to 24 hours after the initial ischemic injury (Fig. 5.1). This delay in BBB may be due to the size of the injury. Larger strokes such as MCAO cause greater damage and BBB breakdown within hours (Carmichael, 2005; Knowland et al., 2014). Furthermore, the MCAO ischemic model induces reperfusion by removal of the suture occluding the MCA (Carmichael, 2005). This rapid reperfusion of blood flow can cause additional damage to the blood vessels due to oxidative damage (Sun et al., 2018). In contrast, the ET-1 stroke model causes a smaller stroke by reversibly occluding blood vessels localised around the injection site, limiting the area of blood supply loss. Reperfusion occurs gradually over hours, potentially reducing reperfusion injury that is typically seen with MCAO (Biernaskie et al., 2001; Nguemeni et al., 2015).

Acute DHA treatment reduced BBB breakdown in lean and obese conditions at 24 hours post-stroke, resulting in less extravasation of dextran labelled Texas Red and neutrophil infiltration (Fig. 5.1). DHA may attenuate blood vessel injury through direct interaction or indirectly by reducing MMPs that mediate BBB disruption (Thota et al.,

2018; Zhang et al., 2016). Persistent constriction of blood vessels causes injury to vascular endothelial cells causing BBB breakdown (Kwon et al., 2009). DHA has been shown to dilate blood vessels by modulating NO production, which could counteract ET-1-induced vasoconstriction (Limbu et al., 2018; Yamagata, 2017). Interestingly, DHA had a greater effect on BBB breakdown in Chow-fed mice than HFD-fed mice. Our data showed that HFD resulted in a narrowing of cerebral arterioles and reduced contractile properties, which suggests that the blood vessels are likely impaired in HFD-fed mice. This pre-existing vasculature damage may impair DHA mediated relaxation of blood vessels and account for the reduced efficacy of DHA to prevent BBB disruption in HFD-fed mice.

5.3 Distinction of the ischemic core from the penumbra

Ischemic stroke results in a non-perfused ischemic core and hypo-perfused penumbra, and the challenge for stroke models is assessing cellular responses specifically within these regions. Typically, the ischemic core and penumbra can be distinguished based on the CBF within the brain (Moskowitz et al., 2010). Previous studies have used various imaging techniques, such as positron emission tomography, MRI or Mass Spectrometry Imaging, to distinguish the core and penumbra in animal stroke models (Mulder et al., 2019; Qian et al., 2016; Saita et al., 2004). Following photothrombotic stroke in mice, Qian and colleagues used MRI to overlay PWI of low perfused areas and DWI of hypointense areas to create a mismatch representing the penumbra (Qian et al., 2016). With this technique, the evolution of the infarct and the penumbra can be observed over the first 24 hours post-stroke. A unique feature of this thesis was delineating the non-

perfused ischemic core and hypo-perfused penumbra and assessing cellular responses in these regions using immunofluorescent microscopy. To distinguish the infarct core from the penumbra in the ET-1 stroke model, I injected dextran-conjugated Texas Red into the bloodstream to label open and perfused blood vessels at the time of euthanasia. The ischemic core and penumbra were defined based on the number of blood vessels labeled with dextran-conjugated Texas Red. In the core, the lack of Texas Red labelled blood vessels indicated minimal reperfusion. Using this technique, distinct cellular responses were observed within the non-perfused core and hypo-perfused penumbra within the acute period. Although this technique has limitations, it can provide valuable information pertaining to the unique cellular responses occurring within each region over time.

5.4 Glial Response and inflammation

We found significant astrogliosis and immune cell infiltration within the infarct by 24 hours post-stroke (Fig. 5.1). Extensive BBB disruption occurred prior to astrogliosis and immune cell infiltration. We show that these glial responses are distinct within the core and penumbra. Reactive astrocytes are located within the penumbra; however, few astrocytes are located within the core from 24 hours up to 7 days post-stroke. In contrast, the majority of infiltrating macrophages are located within the core during this time. Astrogliosis within the penumbra and surrounding perfused brain is more prominent with HFD at 7 days post-stroke. Furthermore, HFD increased peripheral macrophage infiltration within the ischemic brain.

Previous studies have shown increased BBB disruption post-stroke with chronic HFD (Heiss, 2012). This may account for the increased infiltration of peripheral

macrophages within the infarct. For instance, extravasation of IgG within the brain is increased with 10 weeks and 6 months of HFD following 90 minute and 20 minute MCAO, respectively (Deng et al., 2014; Maysami et al., 2015). This is also associated with an increase in pro-inflammatory cytokines and chemokines as well as MMP activity that can damage the BBB. Therefore, it is likely that the increased immune cells within the infarct shown in this thesis were due to augmented BBB disruption with HFD. Interestingly, using a 12-week HFD feeding regime did not significantly increase the expression of the adhesion molecule VCAM-1 in larger basilar arteries. This is in contrast with previous studies showing an upregulation of both ICAM-1 and VCAM-1 within cerebral blood vessels following prolonged HFD (Cao et al., 2015; Herz et al., 2015). Therefore, it is possible that VCAM-1 may be upregulated within smaller cerebral arterioles in the current study, which could contribute to the increase in macrophage infiltration with HFD.

We found that DHA reduces inflammation within the infarct of both Chow-fed and HFD-fed mice with a greater effect on COX-2 reduction in HFD-fed animals (Fig. 5.1). This may be a result of the greater number of CD68+ immune cells in HFD-fed mice, indicating there was more inflammation within the HFD infarct in comparison to controls. This may provide an environment for DHA to have a greater anti-inflammatory effect (Sun et al., 2018). Furthermore, the anti-inflammatory properties of DHA may account for the reduced BBB disruption. Upregulation of COX-2 has been shown to induce BBB breakdown following ischemic stroke, therefore reducing COX-2 with DHA treatment could potentially diminish BBB injury (Candelario-Jalil et al., 2007;

Frankowski et al., 2015). Overall, these results indicate that post-stroke application of DHA can reduce inflammation within small strokes.

5.5 Neuronal survival following ischemic stroke

The majority of neuron death occurs acutely within the first 4 hours post-stroke (Fig. 5.1). Within the first 4 hours, ~80% of neurons die within the core and ~40% of neurons die within the penumbra. Neurons that survive within the hypo-perfused region beyond 4 hours display extensive degeneration of both dendrites and axons that extend out to 24 hours post-stroke. This suggests that surviving neurons within the penumbra are in a vulnerable state.

An examination of the acute response at 24 hours post-stroke revealed that HFD did not impact neuron survival within the penumbra and there was a trend towards a larger infarct. However, at 7 days post-stroke, fewer surviving neurons were observed in the core and penumbra with prolonged HFD (Fig. 5.1). Furthermore, there was a trend towards increased FJC+ neurons within the penumbra with HFD compared to controls. This indicates that the surviving neurons in HFD-fed mice are less healthy and undergoing degeneration. This demonstrates that in the ET-1 model, prolonged HFD has a small impact on the acute ischemic injury but primarily affects delayed cell death beyond 24 hours post-stroke. Extensive BBB breakdown, astrogliosis and immune cell infiltration all coincide with the 12-to-24-hour period following stroke and can reduce neuron survival. Therefore, it is not surprising that HFD did not affect neuron survival within the penumbra at 24 hours, since this is a time point when secondary damage is just beginning to occur. Reactive immune cells release pro-inflammatory cytokines, such as

TNF-α, as well as ROS and MMPs that reduce neuron survival post-stroke (Xu et al., 2020). Furthermore, activated microglia can induce reactive astrogliosis (Joshi et al., 2019). We observe an increase in astrogliosis and macrophages post-stroke with HFD. Reactive astrocytes contribute to neuron degeneration which may account for the reduced neuron survival with HFD at 7 days (Xu et al., 2020). Although the glial scar prevents the spread of immune cells post-stroke, reactive astrocytes release pro-inflammatory cytokines and free radicals such as NO and superoxide that can damage neurons (Xu et al., 2020). It is possible that neurons are more vulnerable within this region due to the toxic inflammatory milieu observed with HFD.

Here we show that DHA slightly increased neuron survival in the ischemic core in Chow-fed mice, albeit no effects were observed within the penumbra. DHA had a minimal effect on reducing neuron death within the immediate hours post-stroke. Our data suggests that DHA affects multiple cellular responses post-stroke, which appear to be interrelated. DHA attenuated inflammation and BBB breakdown at 24 hours post-stroke. However, these benefits did not improve neuron survival within the penumbra at this 24 hour time point. It is possible that DHA application at later time points could prevent delayed neuron death by reducing inflammation and BBB breakdown. Secondary injury caused by immune cell infiltration, inflammation and BBB breakdown is beginning to occur from 12 hours to 24 hours post-stroke (as shown in Chapter 3). DHA reduces this secondary damage and therefore could potentially reduce neuron death beyond this time. Indeed, studies have shown that DHA can inhibit apoptosis when pretreated 2 hours prior to OGD *in vitro* and when treated 1 hour following MCAO *in vivo* (Eady et al., 2012; Ren et al., 2019). Therefore, application of DHA after the 2 to 6 hour post-stroke period

applied in the present study may prevent delayed cell death and expansion of the ischemic injury.

5.6 Future directions

The work in this thesis establishes a framework for the ET-1 ischemic stroke model in producing small focal strokes that mimic covert-stroke. However, several questions remain that require future experimentation. Ischemic stroke is a multifaceted neurovascular disease with several interacting cells that become disrupted. The ET-1 ischemic stroke model produces a small stroke in which cellular responses can be examined at various time points post-stroke. However, it is difficult to examine these responses and cell-cell interactions using immunofluorescence microscopy where static 2D images are obtained. Using a two-photon microscope, time lapse images of cellular interactions can be viewed following stroke *in vivo*. A study using this imaging procedure examined damage to dendrites and spines following 6 to 8 minutes of bilateral CCA occlusion. Reperfusion for 3 to 5 minutes rapidly restored synaptic structures which occurred up to 60 minutes (Murphy et al., 2008). Using these techniques, degeneration of dendrites and axons within the penumbra can be observed over time within minutes to hours following ET-1 injection. Pharmacological treatments can then be applied during various time points post-stroke and the health of neurons can be observed within the penumbra in real time. This would allow therapeutic interventions to be tested and observed at the cellular level over the first 24 hours following stroke.

It is unclear what intracellular processes are initiated when neurons begin to degenerate. Previous studies have suggested that an increase in autophagy is initiated

within neuronal structures following stroke; however, whether autophagy is beneficial or detrimental to stroke recovery is still in debate (Chen et al., 2014; Sun et al., 2019; Wang et al., 2018; Wei et al., 2013). Examining the expression of autophagy proteins such as Beclin-1 and microtubule-associated protein light-chain II (LC3-II) within the acute post-stroke period may elucidate this process within degenerating neurons. Furthermore, using an autophagy inhibitor such as 3-MA when neuronal degeneration occurs may indicate whether or not this process is harmful or beneficial post-stroke (Wei et al., 2013). Elucidating the intracellular processes that occur within dying neurons may help to develop pharmacological agents that can inhibit cell death and degeneration.

This thesis demonstrates that prolonged HFD increases stroke severity. However, it remains unclear whether cellular disruption is exacerbated directly due to the saturated fatty acid interaction with cells, or indirectly due to the chronic inflammation resulting from obesity affecting the vasculature. This can be examined by inducing stroke in mice with increasing degree of weight gain during the HFD feeding regiment. Grouping mice according to their degree of weight gain at different time points (i.e., 1 week HFD versus 12 weeks HFD) could determine the effect of the diet only versus diet-induced obesity. Alternatively, this can be examined by inducing stroke in transgenic mice that are either prone to diet-induced obesity or resistant to diet-induced obesity despite increased HFD food intake. For instance, *ob*/*ob* mice become obese even without HFD feeding due to the inability to produce leptin, whereas melanin-concentrating hormone receptor 1 (MCHR1) knockout mice are resistant to becoming obese due to the lack of MCH signalling (Chen et al., 2002; Pelleymounter et al., 1995). With these transgenic mice, the impact of saturated fatty acids versus excessive adipose tissue on stroke severity can be compared

in vivo. Metabolic measurements, such as glucose metabolism, were not examined in the current studies. It is possible that metabolic disturbances could affect stroke severity. It has been shown that 3-day consumption of HFD disrupts glucose metabolism and chronic HFD consumption increases blood triglycerides (Haley et al., 2017). Therefore, examining these parameters in future experiments could control any confounding metabolic effects.

In the current study, i.p. injections of DHA were administered following 2, 4 and 6 hours post-stroke. However, the dose, method applied (i.p. versus i.v.) and time of injection post-stroke could alter the effectiveness of DHA. Our results showed that i.p. application of DHA had an impact on BBB disruption and inflammation; however, less of an impact on infarct volume at 24 hours post-stroke. Future experiments should test using i.v. application of DHA to test whether this would further reduce ischemic injury. Therefore, the optimal method for DHA treatment should be determined. Furthermore, DHA treatment at later time points may reduce the delayed cell death and therefore, is important to examine.

There are other factors that could affect stroke outcome, such as age and sex, which is a limitation to this thesis. Ischemic stroke typically occurs in older population, however; the mice used in the current studies to model ischemic stroke were young (less than 6 months old) (Kissela et al., 2012). Furthermore, it has been previously shown that sex can impact stroke recovery in both animal and human studies (Ahnstedt et al., 2020; Demeestere et al., 2021). Future studies should address age (young versus old) and sex (male versus female) as a potential factor affecting the progression of ischemic stroke injury.

5.7 Implications of findings

The focus of this thesis was to examine the effect of small ischemic strokes during the acute period and how they are influenced by diet. I present evidence that diet can exacerbate the cellular responses to covert ischemic stroke and acute DHA treatment can ameliorate ischemic injury. Overall findings demonstrate that in the ET-1 stroke model, HFD exacerbates cell death and expansion of the infarct over time which is likely due to the early increase in BBB breakdown, infiltration of immune cells and glial response. This thesis demonstrates the importance of obesity as a comorbidity that should be considered when treating stroke, and that there may be a window of opportunity to minimize tissue damage following covert strokes in obese patients.

Since the majority of neurons die within the first 4 hours, it is within this time that therapeutic interventions are most effective to salvage the penumbra (Nadeau et al., 2005). Whether the penumbra can be salvaged out to 24 hours post-stroke using pharmacological agents remains unclear (Pena et al., 2017; Tan et al., 2015). Therapeutic intervention aimed at reperfusion within the acute time points (i.e. 4 to 6 hours) may reduce neuron death; however, we show that further degeneration still occurs. Therefore, acute therapeutic interventions should aim to inhibit axon and dendritic degeneration with the goal to prevent delayed death of this vulnerable neuron population. As inflammation and BBB breakdown can potentially lead to delayed cell death of neurons within the penumbra, the effect of DHA to reduce inflammation and BBB breakdown shown in this thesis could be beneficial following strokes in the clinic. Treatments past 6 hours post-stroke are limited and alternative treatments are needed to reduce ischemic injury beyond this time (Pena et al., 2017). It is possible that the beneficial vascular and anti-

inflammatory effects of DHA could reduce ischemic injury within the acute period, making it a potential candidate for therapeutic application (Milligan et al., 2017).

5.8 Conclusions

In summary, this thesis provides valuable insight into the impact of diet on small focal ischemic strokes that mimic clinical covert strokes and demonstrates the need for effective treatments during acute ischemic stroke. The results show that the cellular responses to covert strokes are not identical to overt strokes, and may be amenable to different treatment strategies. We found that HFD worsens ischemic injury following these small covert-like strokes by affecting delayed cell death, suggesting that treatments targeting delayed responses may be effective for these conditions. The acute period following ischemic stroke is crucial for implementing therapeutic interventions as the majority of cells within the penumbra are vulnerable to further damage during this time. However, the only treatments currently available for ischemic stroke are tPA and EVT, which must be implemented during the first hours post-stroke and not all patients are eligible. Therefore, other treatment options, such as DHA, must be explored. Taken together, this thesis provides critical scientific evidence that could inform future therapeutic developments and public health policies on healthy diet recommendations.

References

Abo-Ramadan, U., Durukan, A., Pitkonen, M., Marinkovic, I., Tatlisumak, E., Pedrono, E., . . . Tatlisumak, T. (2009). Post-ischemic leakiness of the blood-brain barrier: a quantitative and systematic assessment by Patlak plots. *Exp Neurol, 219*(1), 328-333. doi:10.1016/j.expneurol.2009.06.002

Abu Fanne, R., Nassar, T., Yarovoi, S., Rayan, A., Lamensdorf, I., Karakoveski, M., . . . Higazi, A. A. (2010). Blood-brain barrier permeability and tPA-mediated neurotoxicity. *Neuropharmacology, 58*(7), 972-980. doi:10.1016/j.neuropharm.2009.12.017

Adams, H. P., Jr., Bendixen, B. H., Kappelle, L. J., Biller, J., Love, B. B., Gordon, D. L., & Marsh, E. E., 3rd. (1993). Classification of subtype of acute ischemic stroke. Definitions for use in a multicenter clinical trial. TOAST. Trial of Org 10172 in Acute Stroke Treatment. *Stroke, 24*(1), 35-41. doi:10.1161/01.str.24.1.35

Ahn, J. H., Song, M., Kim, H., Lee, T. K., Park, C. W., Park, Y. E., . . . Park, J. H. (2019). Differential regional infarction, neuronal loss and gliosis in the gerbil cerebral hemisphere following 30 min of unilateral common carotid artery occlusion. *Metab Brain Dis, 34*(1), 223-233. doi:10.1007/s11011-018-0345-9

Ahnstedt, H., Patrizz, A., Chauhan, A., Roy-O'Reilly, M., Furr, J. W., Spychala, M. S., . . . McCullough, L. D. (2020). Sex differences in T cell immune responses, gut permeability and outcome after ischemic stroke in aged mice. *Brain Behav Immun, 87*, 556-567. doi:10.1016/j.bbi.2020.02.001

Albers, G. W. (1999). Expanding the window for thrombolytic therapy in acute stroke. The potential role of acute MRI for patient selection. *Stroke, 30*(10), 2230-2237. doi:10.1161/01.str.30.10.2230

Albers, G. W., Thijs, V. N., Wechsler, L., Kemp, S., Schlaug, G., Skalabrin, E., . . . Investigators, D. (2006). Magnetic resonance imaging profiles predict clinical response to early reperfusion: the diffusion and perfusion imaging evaluation for understanding stroke evolution (DEFUSE) study. *Ann Neurol, 60*(5), 508-517. doi:10.1002/ana.20976

Arnoldussen, I. A., Kiliaan, A. J., & Gustafson, D. R. (2014). Obesity and dementia: adipokines interact with the brain. *Eur Neuropsychopharmacol, 24*(12), 1982-1999. doi:10.1016/j.euroneuro.2014.03.002

Artal-Sanz, M., & Tavernarakis, N. (2005). Proteolytic mechanisms in necrotic cell death and neurodegeneration. *FEBS Lett, 579*(15), 3287-3296. doi:10.1016/j.febslet.2005.03.052

Arvidsson, A., Collin, T., Kirik, D., Kokaia, Z., & Lindvall, O. (2002). Neuronal replacement from endogenous precursors in the adult brain after stroke. *Nat Med, 8*(9), 963-970. doi:10.1038/nm747

Asghar, A., & Sheikh, N. (2017). Role of immune cells in obesity induced low grade inflammation and insulin resistance. *Cell Immunol, 315*, 18-26. doi:10.1016/j.cellimm.2017.03.001

Astrup, J., Siesjo, B. K., & Symon, L. (1981). Thresholds in cerebral ischemia - the ischemic penumbra. *Stroke, 12*(6), 723-725.

Ayata, C., Shin, H. K., Dilekoz, E., Atochin, D. N., Kashiwagi, S., Eikermann-Haerter, K., & Huang, P. L. (2013). Hyperlipidemia disrupts cerebrovascular reflexes and worsens ischemic perfusion defect. *J Cereb Blood Flow Metab, 33*(6), 954-962. doi:10.1038/jcbfm.2013.38

Back, T., Hemmen, T., & Schuler, O. G. (2004). Lesion evolution in cerebral ischemia. *Journal of Neurology, 251*(4), 388-397. doi:10.1007/s00415-004-0399-y

Baker, E. J., Yusof, M. H., Yaqoob, P., Miles, E. A., & Calder, P. C. (2018). Omega-3 fatty acids and leukocyte-endothelium adhesion: Novel anti-atherosclerotic actions. *Mol Aspects Med, 64*, 169-181. doi:10.1016/j.mam.2018.08.002

Bandera, E., Botteri, M., Minelli, C., Sutton, A., Abrams, K. R., & Latronico, N. (2006). Cerebral blood flow threshold of ischemic penumbra and infarct core in acute ischemic stroke - A systematic review. *Stroke, 37*(5), 1334-1339. doi:10.1161/01.Str.0000217418.29609.22

Bandera, E., Botteri, M., Minelli, C., Sutton, A., Abrams, K. R., & Latronico, N. (2006). Cerebral blood flow threshold of ischemic penumbra and infarct core in acute ischemic stroke: a systematic review. *Stroke, 37*(5), 1334-1339. doi:10.1161/01.STR.0000217418.29609.22

Barreto, G., White, R. E., Ouyang, Y., Xu, L., & Giffard, R. G. (2011). Astrocytes: targets for neuroprotection in stroke. *Cent Nerv Syst Agents Med Chem, 11*(2), 164-173. doi:10.2174/187152411796011303

Barros, L. F., Brown, A., & Swanson, R. A. (2018). Glia in brain energy metabolism: A perspective. *Glia, 66*(6), 1134-1137. doi:10.1002/glia.23316

Bazan, N. G. (2005). Neuroprotectin D1 (NPD1): a DHA-derived mediator that protects brain and retina against cell injury-induced oxidative stress. *Brain Pathol., 15*, 159-166. doi:10.1111/j.1750-3639.2005.tb00513.x

Bejot, Y., Catteau, A., Caillier, M., Rouaud, O., Durier, J., Marie, C., . . . Giroud, M. (2008). Trends in incidence, risk factors, and survival in symptomatic lacunar stroke in Dijon, France, from 1989 to 2006: a population-based study. *Stroke, 39*(7), 1945-1951. doi:10.1161/STROKEAHA.107.510933

Belanger, M., Allaman, I., & Magistretti, P. J. (2011). Brain energy metabolism: focus on astrocyte-neuron metabolic cooperation. *Cell Metab, 14*(6), 724-738. doi:10.1016/j.cmet.2011.08.016

Belayev, L., Busto, R., Zhao, W., & Ginsberg, M. D. (1996). Quantitative evaluation of blood-brain barrier permeability following middle cerebral artery occlusion in rats. *Brain Res, 739*(1-2), 88-96. doi:10.1016/s0006-8993(96)00815-3

Belayev, L., Hong, S. H., Menghani, H., Marcell, S. J., Obenaus, A., Freitas, R. S., . . . Bazan, N. G. (2018). Docosanoids Promote Neurogenesis and Angiogenesis, Blood-Brain Barrier Integrity, Penumbra Protection, and Neurobehavioral Recovery After Experimental Ischemic Stroke. *Mol Neurobiol, 55*(8), 7090-7106. doi:10.1007/s12035-018-1136-3

Belayev, L., Khoutorova, L., Atkins, K. D., & Bazan, N. G. (2009). Robust docosahexaenoic acid-mediated neuroprotection in a rat model of transient, focal cerebral ischemia. *Stroke, 40*(9), 3121-3126. doi:10.1161/STROKEAHA.109.555979

Benjamin, E. J., Muntner, P., Alonso, A., Bittencourt, M. S., Callaway, C. W., Carson, A. P., . . . Stroke Statistics, S. (2019). Heart Disease and Stroke Statistics-2019 Update: A Report From the American Heart Association. *Circulation, 139*(10), e56-e528. doi:10.1161/CIR.0000000000000659

Benjamin, E. J., Virani, S. S., Callaway, C. W., Chamberlain, A. M., Chang, A. R., Cheng, S., . . . Epidemi, A. H. A. C. (2018). Heart Disease and Stroke Statistics-2018 Update A Report From the American Heart Association. *Circulation, 137*(12), E67-E492. doi:10.1161/Cir.0000000000000558

Beray-Berthat, V., Croci, N., Plotkine, M., & Margaill, I. (2003). Polymorphonuclear neutrophils contribute to infarction and oxidative stress in the cortex but not in the striatum after ischemia-reperfusion in rats. *Brain Res, 987*(1), 32-38. doi:10.1016/s0006-8993(03)03224-4

Berkhemer, O. A., Fransen, P. S., Beumer, D., van den Berg, L. A., Lingsma, H. F., Yoo, A. J., . . . Investigators, M. C. (2015). A randomized trial of intraarterial treatment for acute ischemic stroke. *N Engl J Med, 372*(1), 11-20. doi:10.1056/NEJMoa1411587

Bernhardt, J., Hayward, K. S., Kwakkel, G., Ward, N. S., Wolf, S. L., Borschmann, K., . . . Cramer, S. C. (2017). Agreed Definitions and a Shared Vision for New Standards in Stroke Recovery Research: The Stroke Recovery and Rehabilitation Roundtable Taskforce. *Neurorehabil Neural Repair, 31*(9), 793-799. doi:10.1177/1545968317732668

Berretta, A., Gowing, E. K., Jasoni, C. L., & Clarkson, A. N. (2016). Sonic hedgehog stimulates neurite outgrowth in a mechanical stretch model of reactive-astrogliosis. *Sci Rep, 6*, 21896. doi:10.1038/srep21896

Biernaskie, J., Chernenko, G., & Corbett, D. (2004). Efficacy of rehabilitative experience declines with time after focal ischemic brain injury. *J Neurosci, 24*(5), 1245-1254. doi:10.1523/JNEUROSCI.3834-03.2004

24/5/1245 [pii]

Biernaskie, J., Corbett, D., Peeling, J., Wells, J., & Lei, H. (2001). A serial MR study of cerebral blood flow changes and lesion development following endothelin-1-induced ischemia in rats. *Magn Reson Med, 46*(4), 827-830. doi:10.1002/mrm.1263

Birenbaum, D., Bancroft, L. W., & Felsberg, G. J. (2011). Imaging in acute stroke. *West J Emerg Med, 12*(1), 67-76.

Brown, C. E., Wong, C., & Murphy, T. H. (2008). Rapid morphologic plasticity of peri-infarct dendritic spines after focal ischemic stroke. *Stroke, 39*(4), 1286-1291. doi:10.1161/STROKEAHA.107.498238

Buetefisch, C. M. (2015). Role of the Contralesional Hemisphere in Post-Stroke Recovery of Upper Extremity Motor Function. *Front Neurol, 6*, 214. doi:10.3389/fneur.2015.00214

Cai, W., Liu, S., Hu, M., Sun, X., Qiu, W., Zheng, S., . . . Lu, Z. (2018). Post-stroke DHA Treatment Protects Against Acute Ischemic Brain Injury by Skewing Macrophage

Polarity Toward the M2 Phenotype. *Transl Stroke Res, 9*(6), 669-680. doi:10.1007/s12975-018-0662-7

Candelario-Jalil, E., Gonzalez-Falcon, A., Garcia-Cabrera, M., Leon, O. S., & Fiebich, B. L. (2007). Post-ischaemic treatment with the cyclooxygenase-2 inhibitor nimesulide reduces blood-brain barrier disruption and leukocyte infiltration following transient focal cerebral ischaemia in rats. *J Neurochem, 100*(4), 1108-1120. doi:10.1111/j.1471-4159.2006.04280.x

Cao, X. L., Du, J., Zhang, Y., Yan, J. T., & Hu, X. M. (2015). Hyperlipidemia exacerbates cerebral injury through oxidative stress, inflammation and neuronal apoptosis in MCAO/reperfusion rats. *Exp Brain Res, 233*(10), 2753-2765. doi:10.1007/s00221-015-4269-x

Carmichael, S. T. (2005). Rodent models of focal stroke: size, mechanism, and purpose. *NeuroRx, 2*(3), 396-409. doi:10.1602/neurorx.2.3.396

Chang, C. Y., Kuan, Y. H., Li, J. R., Chen, W. Y., Ou, Y. C., Pan, H. C., . . . Chen, C. J. (2013). Docosahexaenoic acid reduces cellular inflammatory response following permanent focal cerebral ischemia in rats. *J Nutr Biochem, 24*(12), 2127-2137. doi:10.1016/j.jnutbio.2013.08.004

Chen, A. Q., Fang, Z., Chen, X. L., Yang, S., Zhou, Y. F., Mao, L., . . . Hu, B. (2019). Microglia-derived TNF-alpha mediates endothelial necroptosis aggravating blood brain-barrier disruption after ischemic stroke. *Cell Death Dis, 10*(7), 487. doi:10.1038/s41419-019-1716-9

Chen, W., Sun, Y., Liu, K., & Sun, X. (2014). Autophagy: a double-edged sword for neuronal survival after cerebral ischemia. *Neural Regen Res, 9*(12), 1210-1216. doi:10.4103/1673-5374.135329

Chen, Y., Hu, C., Hsu, C. K., Zhang, Q., Bi, C., Asnicar, M., . . . Shi, Y. (2002). Targeted disruption of the melanin-concentrating hormone receptor-1 results in hyperphagia and resistance to diet-induced obesity. *Endocrinology, 143*(7), 2469-2477. doi:10.1210/endo.143.7.8903

Chen, Z., & Trapp, B. D. (2016). Microglia and neuroprotection. *J Neurochem, 136 Suppl 1*, 10-17. doi:10.1111/jnc.13062

Cheon, S. H., Yan, B. C., Chen, B. H., Park, J. H., Ahn, J. H., Kim, I. H., . . . Won, M. H. (2014). Accelerated and exacerbated effects of high dietary fat on neuronal damage induced by transient cerebral ischemia in the gerbil septum. *Endocrinol Metab (Seoul), 29*(3), 328-335. doi:10.3803/EnM.2014.29.3.328

Chevilley, A., Lesept, F., Lenoir, S., Ali, C., Parcq, J., & Vivien, D. (2015). Impacts of tissue-type plasminogen activator (tPA) on neuronal survival. *Front Cell Neurosci, 9*, 415. doi:10.3389/fncel.2015.00415

Chistiakov, D. A., Killingsworth, M. C., Myasoedova, V. A., Orekhov, A. N., & Bobryshev, Y. V. (2017). CD68/macrosialin: not just a histochemical marker. *Lab Invest, 97*(1), 4-13. doi:10.1038/labinvest.2016.116

Chu, D. T., Malinowska, E., Jura, M., & Kozak, L. P. (2017). C57BL/6J mice as a polygenic developmental model of diet-induced obesity. *Physiol Rep, 5*(7), 1-20. doi:10.14814/phy2.13093

Cipolla, M. J. (2009). In *The Cerebral Circulation.* San Rafael (CA).

Clarkson, A. N., Lopez-Valdes, H. E., Overman, J. J., Charles, A. C., Brennan, K. C., & Thomas Carmichael, S. (2013). Multimodal examination of structural and functional remapping in the mouse photothrombotic stroke model. *J Cereb Blood Flow Metab, 33*(5), 716-723. doi:10.1038/jcbfm.2013.7

Cordner, Z. A., & Tamashiro, K. L. (2015). Effects of high-fat diet exposure on learning & memory. *Physiol Behav, 152*(Pt B), 363-371. doi:10.1016/j.physbeh.2015.06.008

Cornell-Bell, A. H., Finkbeiner, S. M., Cooper, M. S., & Smith, S. J. (1990). Glutamate induces calcium waves in cultured astrocytes: long-range glial signaling. *Science, 247*(4941), 470-473. doi:10.1126/science.1967852

Coutts, S. B., Wein, T. H., Lindsay, M. P., Buck, B., Cote, R., Ellis, P., . . . Stroke Foundation Canada Canadian Stroke Best Practices Advisory, C. (2015). Canadian Stroke Best Practice Recommendations: secondary prevention of stroke guidelines, update 2014. *Int J Stroke, 10*(3), 282-291. doi:10.1111/ijs.12439

Cozzolino, O., Marchese, M., Trovato, F., Pracucci, E., Ratto, G. M., Buzzi, M. G., . . . Santorelli, F. M. (2018). Understanding Spreading Depression from Headache to Sudden Unexpected Death. *Front Neurol, 9*, 19. doi:10.3389/fneur.2018.00019

Csige, I., Ujvarosy, D., Szabo, Z., Lorincz, I., Paragh, G., Harangi, M., & Somodi, S. (2018). The Impact of Obesity on the Cardiovascular System. *J Diabetes Res, 2018*, 3407306. doi:10.1155/2018/3407306

Daneman, R. (2015). Regulation of the Blood-Brain Barrier in Health and Disease. *Faseb Journal, 29*. doi: https://doi.org/10.1096/fasebj.29.1_supplement.216.1

Daneman, R., & Prat, A. (2015). The blood-brain barrier. *Cold Spring Harb Perspect Biol, 7*(1), a020412. doi:10.1101/cshperspect.a020412

Davalos, D., Grutzendler, J., Yang, G., Kim, J. V., Zuo, Y., Jung, S., . . . Gan, W. B. (2005). ATP mediates rapid microglial response to local brain injury in vivo. *Nat Neurosci, 8*(6), 752-758. doi:10.1038/nn1472

Davis, S., & Donnan, G. A. (2014). Time is Penumbra: imaging, selection and outcome. The Johann jacob wepfer award 2014. *Cerebrovasc Dis, 38*(1), 59-72. doi:10.1159/000365503

de Pablo, Y., Nilsson, M., Pekna, M., & Pekny, M. (2013). Intermediate filaments are important for astrocyte response to oxidative stress induced by oxygen-glucose deprivation and reperfusion. *Histochem Cell Biol, 140*(1), 81-91. doi:10.1007/s00418-013-1110-0

del Zoppo, G. J., Milner, R., Mabuchi, T., Hung, S., Wang, X., Berg, G. I., & Koziol, J. A. (2007). Microglial activation and matrix protease generation during focal cerebral ischemia. *Stroke, 38*(2 Suppl), 646-651. doi:10.1161/01.STR.0000254477.34231.cb

Demeestere, J., Christensen, S., Mlynash, M., Federau, C., Albers, G. W., Lemmens, R., & Lansberg, M. G. (2021). Effect of Sex on Clinical Outcome and Imaging after Endovascular Treatment of Large-Vessel Ischemic Stroke. *J Stroke Cerebrovasc Dis, 30*(2), 105468. doi:10.1016/j.jstrokecerebrovasdis.2020.105468

Denes, A., Thornton, P., Rothwell, N. J., & Allan, S. M. (2010). Inflammation and brain injury: acute cerebral ischaemia, peripheral and central inflammation. *Brain Behav Immun, 24*(5), 708-723. doi:10.1016/j.bbi.2009.09.010

Deng, J., Zhang, J., Feng, C., Xiong, L., & Zuo, Z. (2014). Critical role of matrix metalloprotease-9 in chronic high fat diet-induced cerebral vascular remodelling and increase of ischaemic brain injury in mice. *Cardiovasc Res, 103*(4), 473-484. doi:10.1093/cvr/cvu154

Deng, J., Zhang, J., Feng, C., Xiong, L., & Zuo, Z. (2014). Critical role of matrix metalloprotease-9 in chronic high fat diet-induced cerebral vascular remodelling and increase of ischaemic brain injury in micedagger. *Cardiovasc Res, 103*(4), 473-484. doi:10.1093/cvr/cvu154

Deng, P., & Xu, Z. C. (2009). Four-Vessel Occlusion Model in Rats. In: Chen J., Xu Z.C., Xu XM., Zhang J.H. (eds) Animal Models of Acute Neurological Injuries. . *Springer Protocols Handbooks. Humana Press.*, pp 65-76.

Deutsch, C., Portik-Dobos, V., Smith, A. D., Ergul, A., & Dorrance, A. M. (2009). Diet-induced obesity causes cerebral vessel remodeling and increases the damage caused by ischemic stroke. *Microvasc Res, 78*(1), 100-106. doi:10.1016/j.mvr.2009.04.004

Dhungana, H., Rolova, T., Savchenko, E., Wojciechowski, S., Savolainen, K., Ruotsalainen, A. K., . . . Malm, T. (2013). Western-type diet modulates inflammatory responses and impairs functional outcome following permanent middle cerebral artery occlusion in aged mice expressing the human apolipoprotein E4 allele. *J Neuroinflammation, 10*, 102. doi:10.1186/1742-2094-10-102

Dirnagl, U., & Endres, M. (2014). Found in translation: preclinical stroke research predicts human pathophysiology, clinical phenotypes, and therapeutic outcomes. *Stroke, 45*(5), 1510-1518. doi:10.1161/STROKEAHA.113.004075

Dirnagl, U., Iadecola, C., & Moskowitz, M. A. (1999). Pathobiology of ischaemic stroke: an integrated view. *Trends Neurosci, 22*(9), 391-397. doi:10.1016/s0166-2236(99)01401-0.

Dojo Soeandy, C., Salmasi, F., Latif, M., Elia, A. J., Suo, N. J., & Henderson, J. T. (2019). Endothelin-1-mediated cerebral ischemia in mice: early cellular events and the role of caspase-3. *Apoptosis, 24*(7-8), 578-595. doi:10.1007/s10495-019-01541-z

Domingo, Z., Bradley, J. K., Blamire, A. M., Brindle, K., Styles, P., & Rajagopalan, B. (2000). Diffusion weighted imaging and magnetic resonance spectroscopy in a low flow ischaemia model due to endothelin induced vasospasm. *NMR Biomed, 13*(3), 154-162. doi:10.1002/1099-1492(200005)13:3<154::aid-nbm620>3.0.co;2-w.

Donkor, E. S. (2018). Stroke in the 21(st) Century: A Snapshot of the Burden, Epidemiology, and Quality of Life. *Stroke Res Treat, 2018*, 3238165. doi:10.1155/2018/3238165

Dorrance, A. M., Matin, N., & Pires, P. W. (2014). The effects of obesity on the cerebral vasculature. *Curr Vasc Pharmacol, 12*(3), 462-472. doi:10.2174/15701611126661404232224l1

Dudvarski Stankovic, N., Teodorczyk, M., Ploen, R., Zipp, F., & Schmidt, M. H. H. (2016). Microglia-blood vessel interactions: a double-edged sword in brain pathologies. *Acta Neuropathol, 131*(3), 347-363. doi:10.1007/s00401-015-1524-y

Durukan, A., Marinkovic, I., Strbian, D., Pitkonen, M., Pedrono, E., Soinne, L., . . . Tatlisumak, T. (2009). Post-ischemic blood-brain barrier leakage in rats: one-week follow-up by MRI. *Brain Res, 1280,* 158-165. doi:10.1016/j.brainres.2009.05.025

Eady, T. N., Belayev, L., Khoutorova, L., Atkins, K. D., Zhang, C., & Bazan, N. G. (2012). Docosahexaenoic acid signaling modulates cell survival in experimental ischemic stroke penumbra and initiates long-term repair in young and aged rats. *PLoS One, 7*(10), e46151. doi:10.1371/journal.pone.0046151

Ebinger, M., De Silva, D. A., Christensen, S., Parsons, M. W., Markus, R., Donnan, G. A., & Davis, S. M. (2009). Imaging the penumbra - strategies to detect tissue at risk after ischemic stroke. *J Clin Neurosci, 16*(2), 178-187. doi:10.1016/j.jocn.2008.04.002

Edinger, A. L., & Thompson, C. B. (2004). Death by design: apoptosis, necrosis and autophagy. *Curr Opin Cell Biol, 16*(6), 663-669. doi:10.1016/j.ceb.2004.09.011

Falkowska, A., Gutowska, I., Goschorska, M., Nowacki, P., Chlubek, D., & Baranowska-Bosiacka, I. (2015). Energy Metabolism of the Brain, Including the Cooperation between Astrocytes and Neurons, Especially in the Context of Glycogen Metabolism. *Int J Mol Sci, 16*(11), 25959-25981. doi:10.3390/ijms161125939

Fanning, J. P., Wesley, A. J., Wong, A. A., & Fraser, J. F. (2014). Emerging spectra of silent brain infarction. *Stroke, 45*(11), 3461-3471. doi:10.1161/STROKEAHA.114.005919

Fern, R., & Moller, T. (2000). Rapid ischemic cell death in immature oligodendrocytes: a fatal glutamate release feedback loop. *J Neurosci, 20*(1), 34-42.

Fernandez-Lopez, D., Faustino, J., Daneman, R., Zhou, L., Lee, S. Y., Derugin, N., . . . Vexler, Z. S. (2012). Blood-brain barrier permeability is increased after acute adult stroke but not neonatal stroke in the rat. *J Neurosci, 32*(28), 9588-9600. doi:10.1523/JNEUROSCI.5977-11.2012

Fifield, K. E., Rowe, T. M., Raman-Nair, J. B., Hirasawa, M., & Vanderluit, J. L. (2019). Prolonged high fat diet worsens the cellular response to a small, covert-like ischemic stroke. *Neuroscience*. doi:10.1016/j.neuroscience.2019.01.050

Fifield, K. E., Rowe, T. M., Raman-Nair, J. B., Hirasawa, M., & Vanderluit, J. L. (2019). Prolonged High Fat Diet Worsens the Cellular Response to a Small, Covert-like Ischemic Stroke. *Neuroscience, 406*, 637-652. doi:10.1016/j.neuroscience.2019.01.050

Fifield, K. E., & Vanderluit, J. L. (2020). Rapid degeneration of neurons in the penumbra region following a small, focal ischemic stroke. *Eur J Neurosci*. doi:10.1111/ejn.14678

Fluri, F., Schuhmann, M. K., & Kleinschnitz, C. (2015). Animal models of ischemic stroke and their application in clinical research. *Drug Design Development and Therapy, 9*, 3445-3454. doi:10.2147/Dddt.S56071

Fluri, F., Schuhmann, M. K., & Kleinschnitz, C. (2015). Animal models of ischemic stroke and their application in clinical research. *Drug Design Development and Therapy, 9*, 3445-3454. doi:10.2147/Dddt.S56071

Fotis, L., Agrogiannis, G., Vlachos, I. S., Pantopoulou, A., Margoni, A., Kostaki, M., . . . Perrea, D. (2012). Intercellular adhesion molecule (ICAM)-1 and vascular cell adhesion molecule (VCAM)-1 at the early stages of atherosclerosis in a rat model. *In Vivo, 26*(2), 243-250.

Frankowski, J. C., DeMars, K. M., Ahmad, A. S., Hawkins, K. E., Yang, C., Leclerc, J. L., . . . Candelario-Jalil, E. (2015). Detrimental role of the EP1 prostanoid receptor in blood-brain barrier damage following experimental ischemic stroke. *Sci Rep, 5*, 17956. doi:10.1038/srep17956

Fransen, P. S., Beumer, D., Berkhemer, O. A., van den Berg, L. A., Lingsma, H., van der Lugt, A., . . . Investigators, M. C. (2014). MR CLEAN, a multicenter randomized clinical trial of endovascular treatment for acute ischemic stroke in the Netherlands: study protocol for a randomized controlled trial. *Trials, 15*, 343. doi:10.1186/1745-6215-15-343

Fricker, M., Tolkovsky, A. M., Borutaite, V., Coleman, M., & Brown, G. C. (2018). Neuronal Cell Death. *Physiol Rev, 98*(2), 813-880. doi:10.1152/physrev.00011.2017

Fumagalli, S., Fiordaliso, F., Perego, C., Corbelli, A., Mariani, A., De Paola, M., & De Simoni, M. G. (2019). The phagocytic state of brain myeloid cells after ischemia revealed by superresolution structured illumination microscopy. *Journal of Neuroinflammation, 16*. doi:Artn 9

10.1186/S12974-019-1401-Z

Furlan, A., Higashida, R., Wechsler, L., Gent, M., Rowley, H., Kase, C., . . . Rivera, F. (1999). Intra-arterial prourokinase for acute ischemic stroke. The PROACT II study: a randomized controlled trial. Prolyse in Acute Cerebral Thromboembolism. *JAMA, 282*(21), 2003-2011. doi:10.1001/jama.282.21.2003

Fuxe, K., Kurosawa, N., Cintra, A., Hallstrom, A., Goiny, M., Rosen, L., . . . Ungerstedt, U. (1992). Involvement of local ischemia in endothelin-1 induced lesions of the neostriatum of the anaesthetized rat. *Exp Brain Res, 88*(1), 131-139.

Ganjehei, L., Massumi, A., Razavi, M., & Rasekh, A. (2011). Stroke prevention in nonvalvular atrial fibrillation. *Tex Heart Inst J, 38*(4), 350-352.

Ghanta, R. K., LaPar, D. J., Zhang, Q., Devarkonda, V., Isbell, J. M., Yarboro, L. T., . . . Ailawadi, G. (2017). Obesity Increases Risk-Adjusted Morbidity, Mortality, and Cost Following Cardiac Surgery. *J Am Heart Assoc, 6*(3), 1-9. doi:10.1161/JAHA.116.003831

Gonzalez-Amaro, R., Diaz-Gonzalez, F., & Sanchez-Madrid, F. (1998). Adhesion molecules in inflammatory diseases. *Drugs, 56*(6), 977-988. doi:10.2165/00003495-199856060-00003

Gordon, G. R., Howarth, C., & MacVicar, B. A. (2011). Bidirectional control of arteriole diameter by astrocytes. *Exp Physiol, 96*(4), 393-399. doi:10.1113/expphysiol.2010.053132

Gordon, G. R., Mulligan, S. J., & MacVicar, B. A. (2007). Astrocyte control of the cerebrovasculature. *Glia, 55*(12), 1214-1221. doi:10.1002/glia.20543

Gorelick, P. B. (2004). Epidemiology of transient ischemic attack and ischemic stroke in patients with underlying cardiovascular disease. *Clin Cardiol, 27*(5 Suppl 2), II4-11. doi:10.1002/clc.4960271403

Grade, S., Weng, Y. C., Snapyan, M., Kriz, J., Malva, J. O., & Saghatelyan, A. (2013). Brain-derived neurotrophic factor promotes vasculature-associated migration of neuronal precursors toward the ischemic striatum. *PLoS One, 8*(1), e55039. doi:10.1371/journal.pone.0055039

Gresle, M. M., Jarrott, B., Jones, N. M., & Callaway, J. K. (2006). Injury to axons and oligodendrocytes following endothelin-1-induced middle cerebral artery occlusion in conscious rats. *Brain Res, 1110*(1), 13-22. doi:10.1016/j.brainres.2006.06.111

Grysiewicz, R. A., Thomas, K., & Pandey, D. K. (2008). Epidemiology of ischemic and hemorrhagic stroke: incidence, prevalence, mortality, and risk factors. *Neurol Clin, 26*(4), 871-895, vii. doi:10.1016/j.ncl.2008.07.003

Gu, P., & Xu, A. (2013). Interplay between adipose tissue and blood vessels in obesity and vascular dysfunction. *Rev Endocr Metab Disord, 14*(1), 49-58. doi:10.1007/s11154-012-9230-8

Guan, Y., Wang, Y., Yuan, F., Lu, H., Ren, Y., Xiao, T., . . . Yang, G. Y. (2012). Effect of suture properties on stability of middle cerebral artery occlusion evaluated by synchrotron radiation angiography. *Stroke, 43*(3), 888-891. doi:10.1161/STROKEAHA.111.636456

Guillemot-Legris, O., Masquelier, J., Everard, A., Cani, P. D., Alhouayek, M., & Muccioli, G. G. (2016). High-fat diet feeding differentially affects the

development of inflammation in the central nervous system. *J Neuroinflammation, 13*(1), 206. doi:10.1186/s12974-016-0666-8

Guillemot-Legris, O., & Muccioli, G. G. (2017). Obesity-Induced Neuroinflammation: Beyond the Hypothalamus. *Trends Neurosci, 40*(4), 237-253. doi:10.1016/j.tins.2017.02.005

Gupta, Farrell, & Mittal. (2014). Transient ischemic attacks: predictability of future ischemic stroke or transient ischemic attack events. *Ther Clin Risk Manag, 10*, 27-35. doi:10.2147/TCRM.S54810

Gupta, A., Giambrone, A. E., Gialdini, G., Finn, C., Delgado, D., Gutierrez, J., . . . Kamel, H. (2016). Silent Brain Infarction and Risk of Future Stroke: A Systematic Review and Meta-Analysis. *Stroke, 47*(3), 719-725. doi:10.1161/STROKEAHA.115.011889

Haley, M. J., Krishnan, S., Burrows, D., de Hoog, L., Thakrar, J., Schiessl, I., . . . Lawrence, C. B. (2017). Acute high-fat feeding leads to disruptions in glucose homeostasis and worsens stroke outcome. *J Cereb Blood Flow Metab*, 271678X17744718. doi:10.1177/0271678X17744718

Haley, M. J., & Lawrence, C. B. (2016). Obesity and stroke: Can we translate from rodents to patients? *J Cereb Blood Flow Metab, 36*(12), 2007-2021. doi:10.1177/0271678X16670411

Haley, M. J., & Lawrence, C. B. (2017). The blood-brain barrier after stroke: Structural studies and the role of transcytotic vesicles. *J Cereb Blood Flow Metab, 37*(2), 456-470. doi:10.1177/0271678X16629976

Hatakeyama, M., Ninomiya, I., & Kanazawa, M. (2020). Angiogenesis and neuronal remodeling after ischemic stroke. *Neural Regen Res, 15*(1), 16-19. doi:10.4103/1673-5374.264442

Heart&Stroke. (2019). (Dis)connected: How unseen links are putting us at risk, 2019 Report on Heart, Stroke and Vascular Cognitive Impairment.

Heiss, W. D. (2012). The ischemic penumbra: how does tissue injury evolve? *Ann N Y Acad Sci, 1268*, 26-34. doi:10.1111/j.1749-6632.2012.06668.x

Henshall, D. C., Butcher, S. P., & Sharkey, J. (1999). A rat model of endothelin-3-induced middle cerebral artery occlusion with controlled reperfusion. *Brain Res, 843*(1-2), 105-111. doi:10.1016/s0006-8993(99)01896-x

Herz, J., Hagen, S. I., Bergmuller, E., Sabellek, P., Gothert, J. R., Buer, J., . . . Doeppner, T. R. (2014). Exacerbation of ischemic brain injury in hypercholesterolemic mice is associated with pronounced changes in peripheral and cerebral immune responses. *Neurobiol Dis, 62*, 456-468. doi:10.1016/j.nbd.2013.10.022

Herz, J., Sabellek, P., Lane, T. E., Gunzer, M., Hermann, D. M., & Doeppner, T. R. (2015). Role of Neutrophils in Exacerbation of Brain Injury After Focal Cerebral Ischemia in Hyperlipidemic Mice. *Stroke, 46*(10), 2916-2925. doi:10.1161/STROKEAHA.115.010620

Hofmeijer, J., & van Putten, M. J. (2012). Ischemic cerebral damage: an appraisal of synaptic failure. *Stroke, 43*(2), 607-615. doi:10.1161/STROKEAHA.111.632943

Hong, S. H., Khoutorova, L., Bazan, N. G., & Belayev, L. (2015). Docosahexaenoic acid improves behavior and attenuates blood-brain barrier injury induced by focal

cerebral ischemia in rats. *Exp Transl Stroke Med, 7*(1), 3. doi:10.1186/s13231-014-0012-0

Hou, K., Xu, D., Li, F., Chen, S., & Li, Y. (2019). The progress of neuronal autophagy in cerebral ischemia stroke: Mechanisms, roles and research methods. *J Neurol Sci, 400*, 72-82. doi:10.1016/j.jns.2019.03.015

Hou, S. T., Jiang, S. X., Aylsworth, A., Ferguson, G., Slinn, J., Hu, H., . . . Kaibuchi, K. (2009). CaMKII phosphorylates collapsin response mediator protein 2 and modulates axonal damage during glutamate excitotoxicity. *J Neurochem, 111*(3), 870-881. doi:10.1111/j.1471-4159.2009.06375.x

Hu, X., Li, P., Guo, Y., Wang, H., Leak, R. K., Chen, S., . . . Chen, J. (2012). Microglia/macrophage polarization dynamics reveal novel mechanism of injury expansion after focal cerebral ischemia. *Stroke, 43*(11), 3063-3070. doi:10.1161/STROKEAHA.112.659656

Huang, H., Chen, Y. M., Zhu, F., Tang, S. T., Xiao, J. D., Li, L. L., & Lin, X. J. (2015). Down-regulated Na(+)/K(+)-ATPase activity in ischemic penumbra after focal cerebral ischemia/reperfusion in rats. *Int J Clin Exp Pathol, 8*(10), 12708-12717.

Hughes, P. M., Anthony, D. C., Ruddin, M., Botham, M. S., Rankine, E. L., Sablone, M., . . . Perry, V. H. (2003). Focal lesions in the rat central nervous system induced by endothelin-1. *J Neuropathol Exp Neurol, 62*(12), 1276-1286. doi:10.1093/jnen/62.12.1276

Iadecola, C. (2017). The Neurovascular Unit Coming of Age: A Journey through Neurovascular Coupling in Health and Disease. *Neuron, 96*(1), 17-42. doi:10.1016/j.neuron.2017.07.030

Iadecola, C., Forster, C., Nogawa, S., Clark, H. B., & Ross, M. E. (1999). Cyclooxygenase-2 immunoreactivity in the human brain following cerebral ischemia. *Acta Neuropathol, 98*(1), 9-14. doi:10.1007/s004010051045

Iadecola, C., Niwa, K., Nogawa, S., Zhao, X., Nagayama, M., Araki, E., . . . Ross, M. E. (2001). Reduced susceptibility to ischemic brain injury and N-methyl-D-aspartate-mediated neurotoxicity in cyclooxygenase-2-deficient mice. *Proc Natl Acad Sci U S A, 98*(3), 1294-1299. doi:10.1073/pnas.98.3.1294

Innes, J. K., & Calder, P. C. (2018). Omega-6 fatty acids and inflammation. *Prostaglandins Leukot Essent Fatty Acids, 132*, 41-48. doi:10.1016/j.plefa.2018.03.004

Jain, A. P., Aggarwal, K. K., & Zhang, P. Y. (2015). Omega-3 fatty acids and cardiovascular disease. *Eur Rev Med Pharmacol Sci, 19*(3), 441-445.

Jiang, S. Z., Lu, W., Zong, X. F., Ruan, H. Y., & Liu, Y. (2016). Obesity and hypertension. *Exp Ther Med, 12*(4), 2395-2399. doi:10.3892/etm.2016.3667

Jiang, X., Andjelkovic, A. V., Zhu, L., Yang, T., Bennett, M. V. L., Chen, J., . . . Shi, Y. (2018). Blood-brain barrier dysfunction and recovery after ischemic stroke. *Prog Neurobiol, 163-164*, 144-171. doi:10.1016/j.pneurobio.2017.10.001

Jiao, H., Wang, Z., Liu, Y., Wang, P., & Xue, Y. (2011). Specific role of tight junction proteins claudin-5, occludin, and ZO-1 of the blood-brain barrier in a focal cerebral ischemic insult. *J Mol Neurosci, 44*(2), 130-139. doi:10.1007/s12031-011-9496-4

Jickling, G. C., Liu, D., Stamova, B., Ander, B. P., Zhan, X., Lu, A., & Sharp, F. R. (2014). Hemorrhagic transformation after ischemic stroke in animals and humans. *J Cereb Blood Flow Metab, 34*(2), 185-199. doi:10.1038/jcbfm.2013.203

Jickling, G. C., & Sharp, F. R. (2015). Improving the translation of animal ischemic stroke studies to humans. *Metab Brain Dis, 30*(2), 461-467. doi:10.1007/s11011-014-9499-2

Jin, X., Liu, J., Yang, Y., Liu, K. J., & Liu, W. (2012). Spatiotemporal evolution of blood brain barrier damage and tissue infarction within the first 3h after ischemia onset. *Neurobiol Dis, 48*(3), 309-316. doi:10.1016/j.nbd.2012.07.007

Jones, K. A., Maltby, S., Plank, M. W., Kluge, M., Nilsson, M., Foster, P. S., & Walker, F. R. (2018). Peripheral immune cells infiltrate into sites of secondary neurodegeneration after ischemic stroke. *Brain Behav Immun, 67*, 299-307. doi:10.1016/j.bbi.2017.09.006

Joshi, A. U., Minhas, P. S., Liddelow, S. A., Haileselassie, B., Andreasson, K. I., Dorn, G. W., 2nd, & Mochly-Rosen, D. (2019). Fragmented mitochondria released from microglia trigger A1 astrocytic response and propagate inflammatory neurodegeneration. *Nat Neurosci, 22*(10), 1635-1648. doi:10.1038/s41593-019-0486-0

Kalichman, L., Alperovitch-Najenson, D., & Treger, I. (2016). The impact of patient's weight on post-stroke rehabilitation. *Disabil Rehabil, 38*(17), 1684-1690. doi:10.3109/09638288.2015.1107640

Kannangara, T. S., Carter, A., Xue, Y., Dhaliwal, J. S., Beique, J. C., & Lagace, D. C. (2018). Excitable Adult-Generated GABAergic Neurons Acquire Functional

Innervation in the Cortex after Stroke. *Stem Cell Reports, 11*(6), 1327-1336. doi:10.1016/j.stemcr.2018.10.011

Keaney, J., & Campbell, M. (2015). The dynamic blood-brain barrier. *FEBS J, 282*(21), 4067-4079. doi:10.1111/febs.13412

Kernan, W. N., Inzucchi, S. E., Sawan, C., Macko, R. F., & Furie, K. L. (2013). Obesity: a stubbornly obvious target for stroke prevention. *Stroke, 44*(1), 278-286. doi:10.1161/STROKEAHA.111.639922

Kidwell, C. S., Jahan, R., Gornbein, J., Alger, J. R., Nenov, V., Ajani, Z., . . . Investigators, M. R. (2013). A trial of imaging selection and endovascular treatment for ischemic stroke. *N Engl J Med, 368*(10), 914-923. doi:10.1056/NEJMoa1212793

Kilkenny, C., Browne, W., Cuthill, I. C., Emerson, M., & Altman, D. G. (2010). Animal research: reporting in vivo experiments: the ARRIVE guidelines. *Br J Pharmacol, 160*(7), 1577-1579. doi:10.1111/j.1476-5381.2010.00872.x

Kim, E., Tolhurst, A. T., & Cho, S. (2014). Deregulation of inflammatory response in the diabetic condition is associated with increased ischemic brain injury. *J Neuroinflammation, 11*, 83. doi:10.1186/1742-2094-11-83

Kim, K. A., Shin, D., Kim, J. H., Shin, Y. J., Rajanikant, G. K., Majid, A., . . . Bae, O. N. (2018). Role of Autophagy in Endothelial Damage and Blood-Brain Barrier Disruption in Ischemic Stroke. *Stroke, 49*(6), 1571-1579. doi:10.1161/STROKEAHA.117.017287

Kissela, B. M., Khoury, J. C., Alwell, K., Moomaw, C. J., Woo, D., Adeoye, O., . . . Kleindorfer, D. O. (2012). Age at stroke: temporal trends in stroke incidence in a

large, biracial population. *Neurology, 79*(17), 1781-1787. doi:10.1212/WNL.0b013e318270401d

Knowland, D., Arac, A., Sekiguchi, K. J., Hsu, M., Lutz, S. E., Perrino, J., . . . Agalliu, D. (2014). Stepwise recruitment of transcellular and paracellular pathways underlies blood-brain barrier breakdown in stroke. *Neuron, 82*(3), 603-617. doi:10.1016/j.neuron.2014.03.003

Krueger, H., Koot, J., Hall, R. E., O'Callaghan, C., Bayley, M., & Corbett, D. (2015). Prevalence of Individuals Experiencing the Effects of Stroke in Canada: Trends and Projections. *Stroke, 46*(8), 2226-2231. doi:10.1161/STROKEAHA.115.009616

Kunz, A., Dirnagl, U., & Mergenthaler, P. (2010). Acute pathophysiological processes after ischaemic and traumatic brain injury. *Best Pract Res Clin Anaesthesiol, 24*(4), 495-509. doi:10.1016/j.bpa.2010.10.001

Kuroiwa, T., Ting, P., Martinez, H., & Klatzo, I. (1985). The biphasic opening of the blood-brain barrier to proteins following temporary middle cerebral artery occlusion. *Acta Neuropathol, 68*(2), 122-129. doi:10.1007/BF00688633

Kwon, I., Kim, E. H., del Zoppo, G. J., & Heo, J. H. (2009). Ultrastructural and temporal changes of the microvascular basement membrane and astrocyte interface following focal cerebral ischemia. *J Neurosci Res, 87*(3), 668-676. doi:10.1002/jnr.21877

Lake, E. M., Chaudhuri, J., Thomason, L., Janik, R., Ganguly, M., Brown, M., . . . Stefanovic, B. (2015). The effects of delayed reduction of tonic inhibition on

ischemic lesion and sensorimotor function. *J Cereb Blood Flow Metab, 35*(10), 1601-1609. doi:10.1038/jcbfm.2015.86

Lake, E. M. R., Bazzigaluppi, P., Mester, J., Thomason, L. A. M., Janik, R., Brown, M., . . . Stefanovic, B. (2017). Neurovascular unit remodelling in the subacute stage of stroke recovery. *Neuroimage, 146*, 869-882. doi:10.1016/j.neuroimage.2016.09.016

Lalancette-Hebert, M., Julien, C., Cordeau, P., Bohacek, I., Weng, Y. C., Calon, F., & Kriz, J. (2011). Accumulation of dietary docosahexaenoic acid in the brain attenuates acute immune response and development of postischemic neuronal damage. *Stroke, 42*(10), 2903-2909. doi:10.1161/STROKEAHA.111.620856

Lansberg, M. G., O'Brien, M. W., Tong, D. C., Moseley, M. E., & Albers, G. W. (2001). Evolution of cerebral infarct volume assessed by diffusion-weighted magnetic resonance imaging. *Arch Neurol, 58*(4), 613-617. doi:10.1001/archneur.58.4.613

LeDoux, J. E., Thompson, M. E., Iadecola, C., Tucker, L. W., & Reis, D. J. (1983). Local cerebral blood flow increases during auditory and emotional processing in the conscious rat. *Science, 221*(4610), 576-578. doi:10.1126/science.6867731

Lee, H. J., Choi, E. K., Lee, S. H., Kim, Y. J., Han, K. D., & Oh, S. (2018). Risk of ischemic stroke in metabolically healthy obesity: A nationwide population-based study. *PLoS One, 13*(3), e0195210. doi:10.1371/journal.pone.0195210

Lee, J. Y., Sohn, K. H., Rhee, S. H., & Hwang, D. (2001). Saturated fatty acids, but not unsaturated fatty acids, induce the expression of cyclooxygenase-2 mediated through Toll-like receptor 4. *J Biol Chem, 276*(20), 16683-16689. doi:10.1074/jbc.M011695200

Lee, V. M., Burdett, N. G., Carpenter, A., Hall, L. D., Pambakian, P. S., Patel, S., . . . James, M. F. (1996). Evolution of photochemically induced focal cerebral ischemia in the rat. Magnetic resonance imaging and histology. *Stroke, 27*(11), 2110-2118; discussion 2118-2119. doi:10.1161/01.str.27.11.2110

Lees, K. R., Bluhmki, E., von Kummer, R., Brott, T. G., Toni, D., Grotta, J. C., . . . Byrnes, G. (2010). Time to treatment with intravenous alteplase and outcome in stroke: an updated pooled analysis of ECASS, ATLANTIS, NINDS, and EPITHET trials. *Lancet, 375*(9727), 1695-1703. doi:10.1016/S0140-6736(10)60491-6

Leigh, R., Knutsson, L., Zhou, J., & van Zijl, P. C. (2018). Imaging the physiological evolution of the ischemic penumbra in acute ischemic stroke. *J Cereb Blood Flow Metab, 38*(9), 1500-1516. doi:10.1177/0271678X17700913

Leys, D. (2001). Atherothrombosis: a major health burden. *Cerebrovasc Dis, 11 Suppl 2*, 1-4. doi:10.1159/000049137

Li, Prakash, R., Chawla, D., Du, W., Didion, S. P., Filosa, J. A., . . . Ergul, A. (2013). Early effects of high-fat diet on neurovascular function and focal ischemic brain injury. *Am J Physiol Regul Integr Comp Physiol, 304*(11), R1001-1008. doi:10.1152/ajpregu.00523.2012

Li, L., Lundkvist, A., Andersson, D., Wilhelmsson, U., Nagai, N., Pardo, A. C., . . . Pekny, M. (2008). Protective role of reactive astrocytes in brain ischemia. *J Cereb Blood Flow Metab, 28*(3), 468-481. doi:10.1038/sj.jcbfm.9600546

Li, P., & Murphy, T. H. (2008). Two-photon imaging during prolonged middle cerebral artery occlusion in mice reveals recovery of dendritic structure after reperfusion. *J Neurosci, 28*(46), 11970-11979. doi:10.1523/JNEUROSCI.3724-08.2008

Liang, D., Bhatta, S., Gerzanich, V., & Simard, J. M. (2007). Cytotoxic edema: mechanisms of pathological cell swelling. *Neurosurg Focus, 22*(5), E2. doi:10.3171/foc.2007.22.5.3

Liddelow, S. A., Guttenplan, K. A., Clarke, L. E., Bennett, F. C., Bohlen, C. J., Schirmer, L., . . . Barres, B. A. (2017). Neurotoxic reactive astrocytes are induced by activated microglia. *Nature, 541*(7638), 481-487. doi:10.1038/nature21029

Limbu, R., Cottrell, G. S., & McNeish, A. J. (2018). Characterisation of the vasodilation effects of DHA and EPA, n-3 PUFAs (fish oils), in rat aorta and mesenteric resistance arteries. *PLoS One, 13*(2), e0192484. doi:10.1371/journal.pone.0192484

Linn, F. H., Rinkel, G. J., Algra, A., & van Gijn, J. (1996). Incidence of subarachnoid hemorrhage: role of region, year, and rate of computed tomography: a meta-analysis. *Stroke, 27*(4), 625-629. doi:10.1161/01.str.27.4.625

Liu, H. S., Chung, H. W., Chou, M. C., Liou, M., Wang, C. Y., Kao, H. W., . . . Chen, C. Y. (2013). Effects of microvascular permeability changes on contrast-enhanced T1 and pharmacokinetic MR imagings after ischemia. *Stroke, 44*(7), 1872-1877. doi:10.1161/STROKEAHA.113.001558

Liu, X., Liu, J., Zhao, S., Zhang, H., Cai, W., Cai, M., . . . Hu, X. (2016). Interleukin-4 Is Essential for Microglia/Macrophage M2 Polarization and Long-Term Recovery

After Cerebral Ischemia. *Stroke, 47*(2), 498-504. doi:10.1161/STROKEAHA.115.012079

Lo, E. H. (2008). A new penumbra: transitioning from injury into repair after stroke. *Nat Med, 14*(5), 497-500. doi:10.1038/nm1735

Lo, E. H., Moskowitz, M. A., & Jacobs, T. P. (2005). Exciting, radical, suicidal: how brain cells die after stroke. *Stroke, 36*(2), 189-192. doi:10.1161/01.STR.0000153069.96296.fd

Longstreth, W. T., Jr. (2005). Brain vascular disease overt and covert. *Stroke, 36*(10), 2062-2063. doi:https://doi.org/10.1161/01.STR.0000179040.36574.99

Loscalzo, J., & Braunwald, E. (1988). Tissue plasminogen activator. *N Engl J Med, 319*(14), 925-931. doi:10.1056/NEJM198810063191407

Luo, C., Ren, H., Yao, X., Shi, Z., Liang, F., Kang, J. X., . . . Su, H. (2018). Enriched Brain Omega-3 Polyunsaturated Fatty Acids Confer Neuroprotection against Microinfarction. *EBioMedicine, 32*, 50-61. doi:10.1016/j.ebiom.2018.05.028

Ma, Y., Wang, J., Wang, Y., & Yang, G. Y. (2017). The biphasic function of microglia in ischemic stroke. *Prog Neurobiol, 157*, 247-272. doi:10.1016/j.pneurobio.2016.01.005

Mabuchi, T., Kitagawa, K., Ohtsuki, T., Kuwabara, K., Yagita, Y., Yanagihara, T., . . . Matsumoto, M. (2000). Contribution of microglia/macrophages to expansion of infarction and response of oligodendrocytes after focal cerebral ischemia in rats. *Stroke, 31*(7), 1735-1743. doi:10.1161/01.str.31.7.1735

Mangia, S., Giove, F., & Dinuzzo, M. (2012). Metabolic pathways and activity-dependent modulation of glutamate concentration in the human brain. *Neurochem Res, 37*(11), 2554-2561. doi:10.1007/s11064-012-0848-4

Marques, B. L., Carvalho, G. A., Freitas, E. M. M., Chiareli, R. A., Barbosa, T. G., Di Araujo, A. G. P., . . . Pinto, M. C. X. (2019). The role of neurogenesis in neurorepair after ischemic stroke. *Semin Cell Dev Biol, 95*, 98-110. doi:10.1016/j.semcdb.2018.12.003

Martin, A., Mace, E., Boisgard, R., Montaldo, G., Theze, B., Tanter, M., & Tavitian, B. (2012). Imaging of perfusion, angiogenesis, and tissue elasticity after stroke. *J Cereb Blood Flow Metab, 32*(8), 1496-1507. doi:10.1038/jcbfm.2012.49

Matsumoto, H., Kumon, Y., Watanabe, H., Ohnishi, T., Shudou, M., Chuai, M., . . . Tanaka, J. (2008). Accumulation of macrophage-like cells expressing NG2 proteoglycan and Iba1 in ischemic core of rat brain after transient middle cerebral artery occlusion. *Journal of Cerebral Blood Flow and Metabolism, 28*(1), 149-163. doi:10.1038/sj.jcbfm.9600519

Maysami, S., Haley, M. J., Gorenkova, N., Krishnan, S., McColl, B. W., & Lawrence, C. B. (2015). Prolonged diet-induced obesity in mice modifies the inflammatory response and leads to worse outcome after stroke. *J Neuroinflammation, 12*, 140. doi:10.1186/s12974-015-0359-8

McCabe, C., Arroja, M. M., Reid, E., & Macrae, I. M. (2018). Animal models of ischaemic stroke and characterisation of the ischaemic penumbra. *Neuropharmacology, 134*(Pt B), 169-177. doi:10.1016/j.neuropharm.2017.09.022

McColl, B. W., Carswell, H. V., McCulloch, J., & Horsburgh, K. (2004). Extension of cerebral hypoperfusion and ischaemic pathology beyond MCA territory after intraluminal filament occlusion in C57Bl/6J mice. *Brain Res, 997*(1), 15-23. doi:10.1016/j.brainres.2003.10.028

McColl, B. W., Rose, N., Robson, F. H., Rothwell, N. J., & Lawrence, C. B. (2010). Increased brain microvascular MMP-9 and incidence of haemorrhagic transformation in obese mice after experimental stroke. *J Cereb Blood Flow Metab, 30*(2), 267-272. doi:10.1038/jcbfm.2009.217

Meschia, J. F., Bushnell, C., Boden-Albala, B., Braun, L. T., Bravata, D. M., Chaturvedi, S., . . . Council on, H. (2014). Guidelines for the primary prevention of stroke: a statement for healthcare professionals from the American Heart Association/American Stroke Association. *Stroke, 45*(12), 3754-3832. doi:10.1161/STR.0000000000000046

Miettinen, S., Fusco, F. R., Yrjanheikki, J., Keinanen, R., Hirvonen, T., Roivainen, R., . . . Koistinaho, J. (1997). Spreading depression and focal brain ischemia induce cyclooxygenase-2 in cortical neurons through N-methyl-D-aspartic acid-receptors and phospholipase A2. *Proc Natl Acad Sci U S A, 94*(12), 6500-6505. doi:10.1073/pnas.94.12.6500

Milligan, G., Alvarez-Curto, E., Hudson, B. D., Prihandoko, R., & Tobin, A. B. (2017). FFA4/GPR120: Pharmacology and Therapeutic Opportunities. *Trends Pharmacol Sci, 38*(9), 809-821. doi:10.1016/j.tips.2017.06.006

Mind the Connection: Preventing stroke and dementia. (2016). *2016 Stroke Report, 2016*.

Miyamoto, N., Tanaka, Y., Ueno, Y., Tanaka, R., Hattori, N., & Urabe, T. (2012). Benefits of prestroke use of angiotensin type 1 receptor blockers on ischemic stroke severity. *J Stroke Cerebrovasc Dis, 21*(5), 363-368. doi:10.1016/j.jstrokecerebrovasdis.2010.09.011

Moskowitz, M. A., Lo, E. H., & Iadecola, C. (2010). The science of stroke: mechanisms in search of treatments. *Neuron, 67*(2), 181-198. doi:10.1016/j.neuron.2010.07.002

Mulder, I. A., Ogrinc Potocnik, N., Broos, L. A. M., Prop, A., Wermer, M. J. H., Heeren, R. M. A., & van den Maagdenberg, A. (2019). Distinguishing core from penumbra by lipid profiles using Mass Spectrometry Imaging in a transgenic mouse model of ischemic stroke. *Sci Rep, 9*(1), 1090. doi:10.1038/s41598-018-37612-5

Murata, Y., Rosell, A., Scannevin, R. H., Rhodes, K. J., Wang, X., & Lo, E. H. (2008). Extension of the thrombolytic time window with minocycline in experimental stroke. *Stroke, 39*(12), 3372-3377. doi:10.1161/STROKEAHA.108.514026

Murphy, T. H., & Corbett, D. (2009). Plasticity during stroke recovery: from synapse to behaviour. *Nat Rev Neurosci, 10*(12), 861-872. doi:10.1038/nrn2735

Murphy, T. H., Li, P., Betts, K., & Liu, R. (2008). Two-photon imaging of stroke onset in vivo reveals that NMDA-receptor independent ischemic depolarization is the major cause of rapid reversible damage to dendrites and spines. *J Neurosci, 28*(7), 1756-1772. doi:10.1523/JNEUROSCI.5128-07.2008

Nadarajan, V., Perry, R. J., Johnson, J., & Werring, D. J. (2014). Transient ischaemic attacks: mimics and chameleons. *Pract Neurol, 14*(1), 23-31. doi:10.1136/practneurol-2013-000782

Nadeau, J. O., Shi, S., Fang, J., Kapral, M. K., Richards, J. A., Silver, F. L., . . . Investigators for the Registry of the Canadian Stroke, N. (2005). TPA use for stroke in the Registry of the Canadian Stroke Network. *Can J Neurol Sci, 32*(4), 433-439. doi:10.1017/s0317167100004418

Nahirney, P. C., Reeson, P., & Brown, C. E. (2016). Ultrastructural analysis of blood-brain barrier breakdown in the peri-infarct zone in young adult and aged mice. *J Cereb Blood Flow Metab, 36*(2), 413-425. doi:10.1177/0271678X15608396

Nguemeni, C., Gomez-Smith, M., Jeffers, M. S., Schuch, C. P., & Corbett, D. (2015). Time course of neuronal death following endothelin-1 induced focal ischemia in rats. *J Neurosci Methods, 242*, 72-76. doi:10.1016/j.jneumeth.2015.01.005

Nicole, O., Docagne, F., Ali, C., Margaill, I., Carmeliet, P., MacKenzie, E. T., . . . Buisson, A. (2001). The proteolytic activity of tissue-plasminogen activator enhances NMDA receptor-mediated signaling. *Nat Med, 7*(1), 59-64. doi:10.1038/83358

Nogawa, S., Zhang, F., Ross, M. E., & Iadecola, C. (1997). Cyclo-oxygenase-2 gene expression in neurons contributes to ischemic brain damage. *J Neurosci, 17*(8), 2746-2755. doi:10.1523/JNEUROSCI.17-08-02746.1997

Nogueira, R. G., Jadhav, A. P., Haussen, D. C., Bonafe, A., Budzik, R. F., Bhuva, P., . . . Investigators, D. T. (2018). Thrombectomy 6 to 24 Hours after Stroke with a

Mismatch between Deficit and Infarct. *N Engl J Med, 378*(1), 11-21. doi:10.1056/NEJMoa1706442

Nudo, R. J. (2003). Functional and structural plasticity in motor cortex: implications for stroke recovery. *Phys Med Rehabil Clin N Am, 14*(1 Suppl), S57-76. doi:10.1016/s1047-9651(02)00054-2

Nusrat, L., Livingston-Thomas, J. M., Raguthevan, V., Adams, K., Vonderwalde, I., Corbett, D., & Morshead, C. M. (2018). Cyclosporin A-Mediated Activation of Endogenous Neural Precursor Cells Promotes Cognitive Recovery in a Mouse Model of Stroke. *Front Aging Neurosci, 10*, 93. doi:10.3389/fnagi.2018.00093

O'Collins, V. E., Macleod, M. R., Donnan, G. A., Horky, L. L., van der Worp, B. H., & Howells, D. W. (2006). 1,026 experimental treatments in acute stroke. *Ann Neurol, 59*(3), 467-477. doi:10.1002/ana.20741

Oesch, L., Tatlisumak, T., Arnold, M., & Sarikaya, H. (2017). Obesity paradox in stroke - Myth or reality? A systematic review. *PLoS One, 12*(3), e0171334. doi:10.1371/journal.pone.0171334

Osmond, J. M., Mintz, J. D., Dalton, B., & Stepp, D. W. (2009). Obesity increases blood pressure, cerebral vascular remodeling, and severity of stroke in the Zucker rat. *Hypertension, 53*(2), 381-386. doi:10.1161/HYPERTENSIONAHA.108.124149

Overgaard, K., Rasmussen, R. S., & Johansen, F. F. (2010). The site of embolization related to infarct size, oedema and clinical outcome in a rat stroke model - further translational stroke research. *Exp Transl Stroke Med, 2*(1), 17. doi:10.1186/2040-7378-2-17

Pan, H. C., Kao, T. K., Ou, Y. C., Yang, D. Y., Yen, Y. J., Wang, C. C., . . . Chen, C. J. (2009). Protective effect of docosahexaenoic acid against brain injury in ischemic rats. *J Nutr Biochem, 20*(9), 715-725. doi:10.1016/j.jnutbio.2008.06.014

Patel, A. R., Ritzel, R., McCullough, L. D., & Liu, F. (2013). Microglia and ischemic stroke: a double-edged sword. *Int J Physiol Pathophysiol Pharmacol, 5*(2), 73-90.

Pekny, M., Wilhelmsson, U., & Pekna, M. (2014). The dual role of astrocyte activation and reactive gliosis. *Neurosci Lett, 565*, 30-38. doi:10.1016/j.neulet.2013.12.071

Pelleymounter, M. A., Cullen, M. J., Baker, M. B., Hecht, R., Winters, D., Boone, T., & Collins, F. (1995). Effects of the obese gene product on body weight regulation in ob/ob mice. *Science, 269*(5223), 540-543. doi:10.1126/science.7624776

Pena, I. D., Borlongan, C., Shen, G., & Davis, W. (2017). Strategies to Extend Thrombolytic Time Window for Ischemic Stroke Treatment: An Unmet Clinical Need. *J Stroke, 19*(1), 50-60. doi:10.5853/jos.2016.01515

Peters, O., Schipke, C. G., Hashimoto, Y., & Kettenmann, H. (2003). Different mechanisms promote astrocyte Ca2+ waves and spreading depression in the mouse neocortex. *J Neurosci, 23*(30), 9888-9896. doi:https://doi.org/10.1523/JNEUROSCI.23-30-09888.2003

Phillips, S. J., & Whisnant, J. P. (1992). Hypertension and the brain. The National High Blood Pressure Education Program. *Arch Intern Med, 152*(5), 938-945.

Pickering, M., Cumiskey, D., & O'Connor, J. J. (2005). Actions of TNF-alpha on glutamatergic synaptic transmission in the central nervous system. *Exp Physiol, 90*(5), 663-670. doi:10.1113/expphysiol.2005.030734

Pontarelli, F., Ofengeim, D., Zukin, R. S., & Jonas, E. A. (2012). Mouse Transient Global Ischemia Two-Vessel Occlusion Model. *Bio Protoc, 2*(18). doi:10.21769/bioprotoc.262

Poppendieck, S., Kapapa, M., Haas, P., & Kielstein, H. (2013). Prolonged postsurgical recovery period and adverse effects of a leptin application in endotoxemic obese rodents. *Life Sci, 93*(5-6), 247-256. doi:10.1016/j.lfs.2013.06.015

Powers, W. J., Derdeyn, C. P., Biller, J., Coffey, C. S., Hoh, B. L., Jauch, E. C., . . . American Heart Association Stroke, C. (2015). 2015 American Heart Association/American Stroke Association Focused Update of the 2013 Guidelines for the Early Management of Patients With Acute Ischemic Stroke Regarding Endovascular Treatment: A Guideline for Healthcare Professionals From the American Heart Association/American Stroke Association. *Stroke, 46*(10), 3020-3035. doi:10.1161/STR.0000000000000074

Pu, H., Jiang, X., Hu, X., Xia, J., Hong, D., Zhang, W., . . . Shi, Y. (2016). Delayed Docosahexaenoic Acid Treatment Combined with Dietary Supplementation of Omega-3 Fatty Acids Promotes Long-Term Neurovascular Restoration After Ischemic Stroke. *Transl Stroke Res, 7*(6), 521-534. doi:10.1007/s12975-016-0498-y

Qian, C., Li, P. C., Jiao, Y., Yao, H. H., Chen, Y. C., Yang, J., . . . Teng, G. J. (2016). Precise Characterization of the Penumbra Revealed by MRI: A Modified Photothrombotic Stroke Model Study. *PLoS One, 11*(4), e0153756. doi:10.1371/journal.pone.0153756

Quintana, F. J. (2017). Astrocytes to the rescue! Glia limitans astrocytic endfeet control CNS inflammation. *J Clin Invest, 127*(8), 2897-2899. doi:10.1172/JCI95769

Razinia, T., Saver, J. L., Liebeskind, D. S., Ali, L. K., Buck, B., & Ovbiagele, B. (2007). Body mass index and hospital discharge outcomes after ischemic stroke. *Arch Neurol, 64*(3), 388-391. doi:10.1001/archneur.64.3.388

Reeson, P., Tennant, K. A., Gerrow, K., Wang, J., Weiser Novak, S., Thompson, K., . . . Brown, C. E. (2015). Delayed inhibition of VEGF signaling after stroke attenuates blood-brain barrier breakdown and improves functional recovery in a comorbidity-dependent manner. *J Neurosci, 35*(13), 5128-5143. doi:10.1523/JNEUROSCI.2810-14.2015

Regenhardt, R. W., Das, A. S., Ohtomo, R., Lo, E. H., Ayata, C., & Gurol, M. E. (2019). Pathophysiology of Lacunar Stroke: History's Mysteries and Modern Interpretations. *J Stroke Cerebrovasc Dis, 28*(8), 2079-2097. doi:10.1016/j.jstrokecerebrovasdis.2019.05.006

Ren, Z., Chen, L., Wang, Y., Wei, X., Zeng, S., Zheng, Y., . . . Liu, H. (2019). Activation of the Omega-3 Fatty Acid Receptor GPR120 Protects against Focal Cerebral Ischemic Injury by Preventing Inflammation and Apoptosis in Mice. *J Immunol, 202*(3), 747-759. doi:10.4049/jimmunol.1800637

Ritzel, R. M., Patel, A. R., Grenier, J. M., Crapser, J., Verma, R., Jellison, E. R., & McCullough, L. D. (2015). Functional differences between microglia and monocytes after ischemic stroke. *Journal of Neuroinflammation, 12*. doi:Artn 106

10.1186/S12974-015-0329-1

Ronaldson, P. T., & Davis, T. P. (2012). Blood-Brain Barrier Integrity and Glial Support: Mechanisms that can be Targeted for Novel Therapeutic Approaches in Stroke. *Curr Pharm Des*, *18*(25), 3624-3644.

Roome, R. B., Bartlett, R. F., Jeffers, M., Xiong, J., Corbett, D., & Vanderluit, J. L. (2014). A reproducible Endothelin-1 model of forelimb motor cortex stroke in the mouse. *J Neurosci Methods*, *233*, 34-44. doi:10.1016/j.jneumeth.2014.05.014

Roome, R. B., & Vanderluit, J. L. (2015). Paw-dragging: a novel, sensitive analysis of the mouse cylinder test. *J Vis Exp*(98), e52701. doi:10.3791/52701

Rosell, A., Cuadrado, E., Ortega-Aznar, A., Hernandez-Guillamon, M., Lo, E. H., & Montaner, J. (2008). MMP-9-positive neutrophil infiltration is associated to blood-brain barrier breakdown and basal lamina type IV collagen degradation during hemorrhagic transformation after human ischemic stroke. *Stroke*, *39*(4), 1121-1126. doi:10.1161/STROKEAHA.107.500868

Sacco, S., Marini, C., Toni, D., Olivieri, L., & Carolei, A. (2009). Incidence and 10-year survival of intracerebral hemorrhage in a population-based registry. *Stroke*, *40*(2), 394-399. doi:10.1161/STROKEAHA.108.523209

Saita, K., Chen, M., Spratt, N. J., Porritt, M. J., Liberatore, G. T., Read, S. J., . . . Howells, D. W. (2004). Imaging the ischemic penumbra with 18F-fluoromisonidazole in a rat model of ischemic stroke. *Stroke*, *35*(4), 975-980. doi:10.1161/01.STR.0000121647.01941.ba

Sandoval, K. E., & Witt, K. A. (2008). Blood-brain barrier tight junction permeability and ischemic stroke. *Neurobiol Dis*, *32*(2), 200-219. doi:10.1016/j.nbd.2008.08.005

Saver, J. L., Goyal, M., van der Lugt, A., Menon, B. K., Majoie, C. B., Dippel, D. W., . . . Collaborators, H. (2016). Time to Treatment With Endovascular Thrombectomy and Outcomes From Ischemic Stroke: A Meta-analysis. *JAMA, 316*(12), 1279-1288. doi:10.1001/jama.2016.13647

Schaeffler, A., Gross, P., Buettner, R., Bollheimer, C., Buechler, C., Neumeier, M., . . . Falk, W. (2009). Fatty acid-induced induction of Toll-like receptor-4/nuclear factor-kappaB pathway in adipocytes links nutritional signalling with innate immunity. *Immunology, 126*(2), 233-245. doi:10.1111/j.1365-2567.2008.02892.x

Schallert, T., Fleming, S. M., Leasure, J. L., Tillerson, J. L., & Bland, S. T. (2000). CNS plasticity and assessment of forelimb sensorimotor outcome in unilateral rat models of stroke, cortical ablation, parkinsonism and spinal cord injury. *Neuropharmacology, 39*(5), 777-787. doi:10.1016/S0028-3908(00)00005-8

Schlaug, G., Benfield, A., Baird, A. E., Siewert, B., Lovblad, K. O., Parker, R. A., . . . Warach, S. (1999). The ischemic penumbra: operationally defined by diffusion and perfusion MRI. *Neurology, 53*(7), 1528-1537. doi:10.1212/wnl.53.7.1528

Schmidt-Kastner, R., Paschen, W., Ophoff, B. G., & Hossmann, K. A. (1989). A modified four-vessel occlusion model for inducing incomplete forebrain ischemia in rats. *Stroke, 20*(7), 938-946. doi:10.1161/01.str.20.7.938

Schmued, L. C., Stowers, C. C., Scallet, A. C., & Xu, L. (2005). Fluoro-Jade C results in ultra high resolution and contrast labeling of degenerating neurons. *Brain Res, 1035*(1), 24-31. doi:10.1016/j.brainres.2004.11.054

Schoknecht, K., Prager, O., Vazana, U., Kamintsky, L., Harhausen, D., Zille, M., . . . Friedman, A. (2014). Monitoring stroke progression: in vivo imaging of cortical

perfusion, blood-brain barrier permeability and cellular damage in the rat photothrombosis model. *J Cereb Blood Flow Metab, 34*(11), 1791-1801. doi:10.1038/jcbfm.2014.147

Seidel, J. L., Escartin, C., Ayata, C., Bonvento, G., & Shuttleworth, C. W. (2016). Multifaceted roles for astrocytes in spreading depolarization: A target for limiting spreading depolarization in acute brain injury? *Glia, 64*(1), 5-20. doi:10.1002/glia.22824

Sekerdag, E., Solaroglu, I., & Gursoy-Ozdemir, Y. (2018). Cell Death Mechanisms in Stroke and Novel Molecular and Cellular Treatment Options. *Curr Neuropharmacol, 16*(9), 1396-1415. doi:10.2174/1570159X16666180302115544

Shabir, O., Berwick, J., & Francis, S. E. (2018). Neurovascular dysfunction in vascular dementia, Alzheimer's and atherosclerosis. *BMC Neurosci, 19*(1), 62. doi:10.1186/s12868-018-0465-5

Shen, J., Hafeez, A., Stevenson, J., Yang, J., Yin, C., Li, F., . . . Ding, Y. (2016). Omega-3 fatty acid supplement prevents development of intracranial atherosclerosis. *Neuroscience, 334*, 226-235. doi:10.1016/j.neuroscience.2016.08.013

Shi, Z., Ren, H., Luo, C., Yao, X., Li, P., He, C., . . . Su, H. (2016). Enriched Endogenous Omega-3 Polyunsaturated Fatty Acids Protect Cortical Neurons from Experimental Ischemic Injury. *Mol Neurobiol, 53*(9), 6482-6488. doi:10.1007/s12035-015-9554-y

Simard, J. M., Chen, M., Tarasov, K. V., Bhatta, S., Ivanova, S., Melnitchenko, L., . . . Gerzanich, V. (2006). Newly expressed SUR1-regulated NC(Ca-ATP) channel

mediates cerebral edema after ischemic stroke. *Nat Med, 12*(4), 433-440. doi:10.1038/nm1390

Simard, J. M., Sahuquillo, J., Sheth, K. N., Kahle, K. T., & Walcott, B. P. (2011). Managing malignant cerebral infarction. *Curr Treat Options Neurol, 13*(2), 217-229. doi:10.1007/s11940-010-0110-9

Smith. (2011). Reducing the global burden of ischemic heart disease and stroke: a challenge for the cardiovascular community and the United Nations. *Circulation, 124*(3), 278-279. doi:10.1161/CIRCULATIONAHA.111.040170

Smith, W. L., DeWitt, D. L., & Garavito, R. M. (2000). Cyclooxygenases: structural, cellular, and molecular biology. *Annu Rev Biochem, 69*, 145-182. doi:10.1146/annurev.biochem.69.1.145

Smith, W. S., Sung, G., Starkman, S., Saver, J. L., Kidwell, C. S., Gobin, Y. P., . . . Investigators, M. T. (2005). Safety and efficacy of mechanical embolectomy in acute ischemic stroke: results of the MERCI trial. *Stroke, 36*(7), 1432-1438. doi:10.1161/01.STR.0000171066.25248.1d

Snelling, B., McCarthy, D. J., Chen, S., Sur, S., Elwardany, O., Sheinberg, D. L., . . . Starke, R. M. (2019). Extended Window for Stroke Thrombectomy. *J Neurosci Rural Pract, 10*(2), 294-300. doi:10.4103/jnrp.jnrp_365_18

Sofroniew, M. V. (2015). Astrocyte barriers to neurotoxic inflammation. *Nat Rev Neurosci, 16*(5), 249-263. doi:10.1038/nrn3898

Sommer, C. J. (2017). Ischemic stroke: experimental models and reality. *Acta Neuropathol, 133*(2), 245-261. doi:10.1007/s00401-017-1667-0

Sorop, O., Olver, T. D., van de Wouw, J., Heinonen, I., van Duin, R. W., Duncker, D. J., & Merkus, D. (2017). The microcirculation: a key player in obesity-associated cardiovascular disease. *Cardiovasc Res, 113*(9), 1035-1045. doi:10.1093/cvr/cvx093

Soylu, H., Zhang, D., Buist, R., Martin, M., Albensi, B. C., & Parkinson, F. E. (2012). Intracortical injection of endothelin-1 induces cortical infarcts in mice: effect of neuronal expression of an adenosine transporter. *Exp Transl Stroke Med, 4*(1), 4. doi:10.1186/2040-7378-4-4

Sozmen, E. G., Kolekar, A., Havton, L. A., & Carmichael, S. T. (2009). A white matter stroke model in the mouse: axonal damage, progenitor responses and MRI correlates. *J Neurosci Methods, 180*(2), 261-272. doi:10.1016/j.jneumeth.2009.03.017

Stadtmann, A., & Zarbock, A. (2012). CXCR2: From Bench to Bedside. *Front Immunol, 3*, 263. doi:10.3389/fimmu.2012.00263

Stankowski, J. N., & Gupta, R. (2011). Therapeutic targets for neuroprotection in acute ischemic stroke: lost in translation? *Antioxid Redox Signal, 14*(10), 1841-1851. doi:10.1089/ars.2010.3292

StatisticsCanada. (2008). Ten leading causes of death, by sex and geography, 2008 — Newfoundland and Labrador. https://www150.statcan.gc.ca/n1/pub/84-215-x/2011001/tbl/t014-eng.htm

Stokum, J. A., Gerzanich, V., & Simard, J. M. (2016). Molecular pathophysiology of cerebral edema. *J Cereb Blood Flow Metab, 36*(3), 513-538. doi:10.1177/0271678X15617172

Strazzullo, P., D'Elia, L., Cairella, G., Garbagnati, F., Cappuccio, F. P., & Scalfi, L. (2010). Excess body weight and incidence of stroke: meta-analysis of prospective studies with 2 million participants. *Stroke, 41*(5), e418-426. doi:10.1161/STROKEAHA.109.576967

Strbian, D., Durukan, A., Pitkonen, M., Marinkovic, I., Tatlisumak, E., Pedrono, E., . . . Tatlisumak, T. (2008). The blood-brain barrier is continuously open for several weeks following transient focal cerebral ischemia. *Neuroscience, 153*(1), 175-181. doi:10.1016/j.neuroscience.2008.02.012

Su, Z., Yuan, Y., Cao, L., Zhu, Y., Gao, L., Qiu, Y., & He, C. (2010). Triptolide promotes spinal cord repair by inhibiting astrogliosis and inflammation. *Glia, 58*(8), 901-915. doi:10.1002/glia.20972

Sun, G. Y., Simonyi, A., Fritsche, K. L., Chuang, D. Y., Hannink, M., Gu, Z., . . . Beversdorf, D. Q. (2018). Docosahexaenoic acid (DHA): An essential nutrient and a nutraceutical for brain health and diseases. *Prostaglandins Leukot Essent Fatty Acids, 136*, 3-13. doi:10.1016/j.plefa.2017.03.006

Sun, M. S., Jin, H., Sun, X., Huang, S., Zhang, F. L., Guo, Z. N., & Yang, Y. (2018). Free Radical Damage in Ischemia-Reperfusion Injury: An Obstacle in Acute Ischemic Stroke after Revascularization Therapy. *Oxid Med Cell Longev, 2018*, 3804979. doi:10.1155/2018/3804979

Sun, Y., Zhu, Y., Zhong, X., X., C., Wang, J., & Ying, G. (2019). Crosstalk Between Autophagy and Cerebral Ischemia. *Front. Neurosci.* doi:doi: 10.3389/fnins.2018.01022

Szydlowska, K., & Tymianski, M. (2010). Calcium, ischemia and excitotoxicity. *Cell Calcium, 47*(2), 122-129. doi:10.1016/j.ceca.2010.01.003

Takatsuru, Y., Fukumoto, D., Yoshitomo, M., Nemoto, T., Tsukada, H., & Nabekura, J. (2009). Neuronal circuit remodeling in the contralateral cortical hemisphere during functional recovery from cerebral infarction. *J Neurosci, 29*(32), 10081-10086. doi:10.1523/JNEUROSCI.1638-09.2009

Tan, Z., Lucke-Wold, B. P., Logsdon, A. F., Turner, R. C., Tan, C., Li, X., . . . Huber, J. D. (2015). Bryostatin extends tPA time window to 6 h following middle cerebral artery occlusion in aged female rats. *Eur J Pharmacol, 764*, 404-412. doi:10.1016/j.ejphar.2015.07.035

Teng, K. T., Chang, C. Y., Chang, L. F., & Nesaretnam, K. (2014). Modulation of obesity-induced inflammation by dietary fats: mechanisms and clinical evidence. *Nutr J, 13*, 12. doi:10.1186/1475-2891-13-12

Terao, S., Yilmaz, G., Stokes, K. Y., Ishikawa, M., Kawase, T., & Granger, D. N. (2008). Inflammatory and injury responses to ischemic stroke in obese mice. *Stroke, 39*(3), 943-950. doi:10.1161/STROKEAHA.107.494542

Thaler, J. P., Yi, C. X., Schur, E. A., Guyenet, S. J., Hwang, B. H., Dietrich, M. O., . . . Schwartz, M. W. (2012). Obesity is associated with hypothalamic injury in rodents and humans. *J Clin Invest, 122*(1), 153-162. doi:10.1172/JCI59660

Thota, R. N., Ferguson, J. J. A., Abbott, K. A., Dias, C. B., & Garg, M. L. (2018). Science behind the cardio-metabolic benefits of omega-3 polyunsaturated fatty acids: biochemical effects vs. clinical outcomes. *Food Funct, 9*(7), 3576-3596. doi:10.1039/c8fo00348c

Tulsulkar, J., Nada, S. E., Slotterbeck, B. D., McInerney, M. F., & Shah, Z. A. (2016). Obesity and hyperglycemia lead to impaired post-ischemic recovery after permanent ischemia in mice. *Obesity (Silver Spring), 24*(2), 417-423. doi:10.1002/oby.21388

Uesugi, M., Kasuya, Y., Hama, H., Yamamoto, M., Hayashi, K., Masaki, T., & Goto, K. (1996). Endogenous endothelin-1 initiates astrocytic growth after spinal cord injury. *Brain Res, 728*(2), 255-259. doi:10.1016/0006-8993(96)00524-0

Uesugi, M., Kasuya, Y., Hayashi, K., & Goto, K. (1998). SB209670, a potent endothelin receptor antagonist, prevents or delays axonal degeneration after spinal cord injury. *Brain Res, 786*(1-2), 235-239. doi:10.1016/s0006-8993(97)01431-5

Uzdensky, A. B. (2018). Photothrombotic Stroke as a Model of Ischemic Stroke. *Transl Stroke Res, 9*(5), 437-451. doi:10.1007/s12975-017-0593-8

van Strien, M. E., van den Berge, S. A., & Hol, E. M. (2011). Migrating neuroblasts in the adult human brain: a stream reduced to a trickle. *Cell Res, 21*(11), 1523-1525. doi:10.1038/cr.2011.101

Verhaar, M. C., Strachan, F. E., Newby, D. E., Cruden, N. L., Koomans, H. A., Rabelink, T. J., & Webb, D. J. (1998). Endothelin-A receptor antagonist-mediated vasodilatation is attenuated by inhibition of nitric oxide synthesis and by endothelin-B receptor blockade. *Circulation, 97*(8), 752-756. doi:10.1161/01.cir.97.8.752

Vermeer, S. E., Hollander, M., van Dijk, E. J., Hofman, A., Koudstaal, P. J., Breteler, M. M., & Rotterdam Scan, S. (2003). Silent brain infarcts and white matter lesions

increase stroke risk in the general population: the Rotterdam Scan Study. *Stroke, 34*(5), 1126-1129. doi:10.1161/01.STR.0000068408.82115.D2

Vermeer, S. E., Longstreth, W. T., Jr., & Koudstaal, P. J. (2007). Silent brain infarcts: a systematic review. *Lancet Neurol, 6*(7), 611-619. doi:10.1016/S1474-4422(07)70170-9

Wake, H., Moorhouse, A. J., Jinno, S., Kohsaka, S., & Nabekura, J. (2009). Resting microglia directly monitor the functional state of synapses in vivo and determine the fate of ischemic terminals. *J Neurosci, 29*(13), 3974-3980. doi:10.1523/JNEUROSCI.4363-08.2009

Wang, P., Shao, B. Z., Deng, Z., Chen, S., Yue, Z., & Miao, C. Y. (2018). Autophagy in ischemic stroke. *Prog Neurobiol, 163-164*, 98-117. doi:10.1016/j.pneurobio.2018.01.001

Wang, X., Lee, S. R., Arai, K., Lee, S. R., Tsuji, K., Rebeck, G. W., & Lo, E. H. (2003). Lipoprotein receptor-mediated induction of matrix metalloproteinase by tissue plasminogen activator. *Nat Med, 9*(10), 1313-1317. doi:10.1038/nm926

Wang, Y. F., & Parpura, V. (2016). Central Role of Maladapted Astrocytic Plasticity in Ischemic Brain Edema Formation. *Front Cell Neurosci, 10*, 129. doi:10.3389/fncel.2016.00129

Watson, B. D., Dietrich, W. D., Busto, R., Wachtel, M. S., & Ginsberg, M. D. (1985). Induction of reproducible brain infarction by photochemically initiated thrombosis. *Ann Neurol, 17*(5), 497-504. doi:10.1002/ana.410170513

Wei, L., Ying, D. J., Cui, L., Langsdorf, J., & Yu, S. P. (2004). Necrosis, apoptosis and hybrid death in the cortex and thalamus after barrel cortex ischemia in rats. *Brain Res, 1022*(1-2), 54-61. doi:10.1016/j.brainres.2004.06.080

Wei, N., Yu, S. P., Gu, X. H., Chen, D. D., Whalin, M. K., Xu, G. L., . . . Wei, L. (2013). The involvement of autophagy pathway in exaggerated ischemic brain damage in diabetic mice. *CNS Neurosci Ther, 19*(10), 753-763. doi:10.1111/cns.12123

Wiley, K. E., & Davenport, A. P. (2004). Endothelin receptor pharmacology and function in the mouse: comparison with rat and man. *J Cardiovasc Pharmacol, 44 Suppl 1*, S4-6. doi:10.1097/01.fjc.0000166204.89426.20

Willing, A. E. (2009). Experimental models: help or hindrance. *Stroke, 40*(3 Suppl), S152-154. doi:10.1161/STROKEAHA.108.533505

Windle, V., Szymanska, A., Granter-Button, S., White, C., Buist, R., Peeling, J., & Corbett, D. (2006). An analysis of four different methods of producing focal cerebral ischemia with endothelin-1 in the rat. *Exp Neurol, 201*(2), 324-334. doi:S0014-4886(06)00268-8 [pii]

10.1016/j.expneurol.2006.04.012

Winkler, L., Blasig, R., Breitkreuz-Korff, O., Berndt, P., Dithmer, S., Helms, H. C., . . . Haseloff, R. F. (2020). Tight junctions in the blood-brain barrier promote edema formation and infarct size in stroke - Ambivalent effects of sealing proteins. *J Cereb Blood Flow Metab*, 271678X20904687. doi:10.1177/0271678X20904687

Witt, K. A., Mark, K. S., Sandoval, K. E., & Davis, T. P. (2008). Reoxygenation stress on blood-brain barrier paracellular permeability and edema in the rat. *Microvasc Res, 75*(1), 91-96. doi:10.1016/j.mvr.2007.06.004

Woo, M. S., Yang, J., Beltran, C., & Cho, S. (2016). Cell Surface CD36 Protein in Monocyte/Macrophage Contributes to Phagocytosis during the Resolution Phase of Ischemic Stroke in Mice. *J Biol Chem, 291*(45), 23654-23661. doi:10.1074/jbc.M116.750018

Wu, M. H., Chio, C. C., Tsai, K. J., Chang, C. P., Lin, N. K., Huang, C. C., & Lin, M. T. (2016). Obesity Exacerbates Rat Cerebral Ischemic Injury through Enhancing Ischemic Adiponectin-Containing Neuronal Apoptosis. *Mol Neurobiol, 53*(6), 3702-3713. doi:10.1007/s12035-015-9305-0

Xing, C., Arai, K., Lo, E. H., & Hommel, M. (2012). Pathophysiologic cascades in ischemic stroke. *Int J Stroke, 7*(5), 378-385. doi:10.1111/j.1747-4949.2012.00839.x

Xu, M., Wang, M. M., Gao, Y., Keep, R. F., & Shi, Y. (2019). The effect of age-related risk factors and comorbidities on white matter injury and repair after ischemic stroke. *Neurobiol Dis, 126*, 13-22. doi:10.1016/j.nbd.2018.07.008

Xu, M., & Zhang, H. L. (2011). Death and survival of neuronal and astrocytic cells in ischemic brain injury: a role of autophagy. *Acta Pharmacol Sin, 32*(9), 1089-1099. doi:10.1038/aps.2011.50

Xu, S., Lu, J., Shao, A., Zhang, J. H., & Zhang, J. (2020). Glial Cells: Role of the Immune Response in Ischemic Stroke. *Front Immunol, 11*, 294. doi:10.3389/fimmu.2020.00294

Xu, W. W., Zhang, Y. Y., Su, J., Liu, A. F., Wang, K., Li, C., . . . Jiang, W. J. (2018). Ischemia Reperfusion Injury after Gradual versus Rapid Flow Restoration for Middle Cerebral Artery Occlusion Rats. *Sci Rep, 8*(1), 1638. doi:10.1038/s41598-018-20095-9

Yaegashi, M., Jean, R., Zuriqat, M., Noack, S., & Homel, P. (2005). Outcome of morbid obesity in the intensive care unit. *J Intensive Care Med, 20*(3), 147-154. doi:10.1177/0885066605275314

Yamagata, K. (2017). Docosahexaenoic acid regulates vascular endothelial cell function and prevents cardiovascular disease. *Lipids Health Dis, 16*(1), 118. doi:10.1186/s12944-017-0514-6

Yamashita, T., Kamiya, T., Deguchi, K., Inaba, T., Zhang, H., Shang, J., . . . Abe, K. (2009). Dissociation and protection of the neurovascular unit after thrombolysis and reperfusion in ischemic rat brain. *J Cereb Blood Flow Metab, 29*(4), 715-725. doi:10.1038/jcbfm.2008.164

Yan, B. C., Park, J. H., Ahn, J. H., Kim, I. H., Lee, J. C., Yoo, K. Y., . . . Won, M. H. (2014). Effects of high-fat diet on neuronal damage, gliosis, inflammatory process and oxidative stress in the hippocampus induced by transient cerebral ischemia. *Neurochem Res, 39*(12), 2465-2478. doi:10.1007/s11064-014-1450-8

Yang, C., Hawkins, K. E., Dore, S., & Candelario-Jalil, E. (2019). Neuroinflammatory mechanisms of blood-brain barrier damage in ischemic stroke. *Am J Physiol Cell Physiol, 316*(2), C135-C153. doi:10.1152/ajpcell.00136.2018

Yang, D. Y., Pan, H. C., Yen, Y. J., Wang, C. C., Chuang, Y. H., Chen, S. Y., . . . Chen, C. J. (2007). Detrimental effects of post-treatment with fatty acids on brain injury

in ischemic rats. *Neurotoxicology, 28*(6), 1220-1229. doi:10.1016/j.neuro.2007.08.003

Yang, J., Weimer, R. M., Kallop, D., Olsen, O., Wu, Z., Renier, N., . . . Tessier-Lavigne, M. (2013). Regulation of axon degeneration after injury and in development by the endogenous calpain inhibitor calpastatin. *Neuron, 80*(5), 1175-1189. doi:10.1016/j.neuron.2013.08.034

Yang, Y., Salayandia, V. M., Thompson, J. F., Yang, L. Y., Estrada, E. Y., & Yang, Y. (2015). Attenuation of acute stroke injury in rat brain by minocycline promotes blood-brain barrier remodeling and alternative microglia/macrophage activation during recovery. *J Neuroinflammation, 12*, 26. doi:10.1186/s12974-015-0245-4

Ye, D., Zhang, D., Oltman, C., Dellsperger, K., Lee, H. C., & VanRollins, M. (2002). Cytochrome p-450 epoxygenase metabolites of docosahexaenoate potently dilate coronary arterioles by activating large-conductance calcium-activated potassium channels. *J Pharmacol Exp Ther, 303*(2), 768-776. doi:10.1124/jpet.303.2.768

Yilmaz, G., & Granger, D. N. (2008). Cell adhesion molecules and ischemic stroke. *Neurol Res, 30*(8), 783-793. doi:10.1179/174313208X341085

Yuan, J. (2009). Neuroprotective strategies targeting apoptotic and necrotic cell death for stroke. *Apoptosis, 14*(4), 469-477. doi:10.1007/s10495-008-0304-8

Zendedel, A., Habib, P., Dang, J., Lammerding, L., Hoffmann, S., Beyer, C., & Slowik, A. (2015). Omega-3 polyunsaturated fatty acids ameliorate neuroinflammation and mitigate ischemic stroke damage through interactions with astrocytes and microglia. *J Neuroimmunol, 278*, 200-211. doi:10.1016/j.jneuroim.2014.11.007

Zhang, L., Zhang, R. L., Jiang, Q., Ding, G., Chopp, M., & Zhang, Z. G. (2015). Focal embolic cerebral ischemia in the rat. *Nat Protoc, 10*(4), 539-547. doi:10.1038/nprot.2015.036

Zhang, M., Wang, S., Mao, L., Leak, R. K., Shi, Y., Zhang, W., . . . Zhang, F. (2014). Omega-3 fatty acids protect the brain against ischemic injury by activating Nrf2 and upregulating heme oxygenase 1. *J Neurosci, 34*(5), 1903-1915. doi:10.1523/JNEUROSCI.4043-13.2014

Zhang, R. L., Chopp, M., Chen, H., & Garcia, J. H. (1994). Temporal profile of ischemic tissue damage, neutrophil response, and vascular plugging following permanent and transient (2H) middle cerebral artery occlusion in the rat. *J Neurol Sci, 125*(1), 3-10. doi:10.1016/0022-510x(94)90234-8

Zhang, W., Zhang, H., Mu, H., Zhu, W., Jiang, X., Hu, X., . . . Gao, Y. (2016). Omega-3 polyunsaturated fatty acids mitigate blood-brain barrier disruption after hypoxic-ischemic brain injury. *Neurobiol Dis, 91*, 37-46. doi:10.1016/j.nbd.2016.02.020

Zhang, X., Dong, F., Ren, J., Driscoll, M. J., & Culver, B. (2005). High dietary fat induces NADPH oxidase-associated oxidative stress and inflammation in rat cerebral cortex. *Exp Neurol, 191*(2), 318-325. doi:10.1016/j.expneurol.2004.10.011

Zheng, Y., He, R., Wang, P., Shi, Y., Zhao, L., & Liang, J. (2019). Exosomes from LPS-stimulated macrophages induce neuroprotection and functional improvement after ischemic stroke by modulating microglial polarization. *Biomater Sci, 7*(5), 2037-2049. doi:10.1039/c8bm01449c

Zhou, T., Huang, Z., Sun, X., Zhu, X., Zhou, L., Li, M., . . . He, C. (2017). Microglia Polarization with M1/M2 Phenotype Changes in rd1 Mouse Model of Retinal Degeneration. *Front Neuroanat, 11*, 77. doi:10.3389/fnana.2017.00077

Zhu, L., Wang, L., Ju, F., Khan, A., Cheng, X., & Zhang, S. (2017). Reversible recovery of neuronal structures depends on the degree of neuronal damage after global cerebral ischemia in mice. *Exp Neurol, 289*, 1-8. doi:10.1016/j.expneurol.2016.12.002

Zonta, M., Angulo, M. C., Gobbo, S., Rosengarten, B., Hossmann, K. A., Pozzan, T., & Carmignoto, G. (2003). Neuron-to-astrocyte signaling is central to the dynamic control of brain microcirculation. *Nat Neurosci, 6*(1), 43-50. doi:10.1038/nn980

Appendix

Animal Ethics Approval Documentation

Vanderluit, Jacqueline

From:	ambakwe@mun.ca
Sent:	May 9, 2018 10:19 AM
To:	Dr. Jacqueline Vanderluit (Principal Investigator)
Cc:	ambakwe@mun.ca
Subject:	Your Animal Use Protocol has been renewed

MEMORIAL UNIVERSITY

Institutional Animal Care Committee (IACC)
St. John's, NL, Canada A1C 5S7
Tel: 709 777-6620 acs@mun.ca
www.mun.ca/research/about/acs/

Dear: Dr. Jacqueline Vanderluit, Associate Professor/Faculty of Medicine\Division of BioMedical Sciences

Researcher Portal File No.: 20190114
Animal Care File: 18-01-JV
Entitled: (18-01-JV) Effect of obesity on behavioral and cellular responses to ischemic stroke.
Status: Active
Related Awards:

Approval Date: May 01, 2018
Annual Report Due: May 01, 2019
Ethics Clearance Expires: May 1, 2021

Your Animal Use Protocol has been renewed for a three-year term. This file replaces previous File ID [[40005182]] and Animal Care ID [[15-04-JV]] as the active ethics clearance associated with this project. Please note the new file ID and Animal Care ID when referring to this protocol.

This ethics clearance includes the following Team Members: Dr. Jacqueline Vanderluit (Principal Investigator)

An Event [Annual Report] will be required following each year of protocol activity.

Should you encounter an unexpected incident that negatively affects animal welfare or the research project relating to animal use, please submit an Event [Incident Report].

Any alterations to the protocol requires prior submission and approval of an Event [Amendment].

Sincerely,

ANULIKA MBAKWE | IACC COORDINATOR
Department of Animal Care Services
Memorial University of Newfoundland
Health Sciences Centre | Room H1848
P: 709-777-6621
E-Mail: ambakwe@mun.ca
www.mun.ca/acs

1

Diet Composition

	Chow	HFD
Protein	26	20
Carbohydrate	59.1	20
Fat	14.9	60
Total (kcal%)	100	100
Cholesterol (mg)/kg	199	279.6

14% Chow obtained from Lab Diet (Product #0001495)

60% HFD (from lard) obtained from Research Diets (Product #D12492)